

**EROSION OF PLASMA TORCH ELECTRODES**

by

**Roberto Nunes Szente**

A Thesis submitted to the Faculty of Graduate Studies  
and Research in Partial Fulfillment of the  
Requirements for the Degree of  
Doctor of Philosophy

Department of Chemical Engineering  
McGill University  
Montreal, Canada

October 1989

**EROSION  
OF  
PLASMA TORCH ELECTRODES**

## ABSTRACT

The erosion of copper electrodes in a concentric cylinder geometry with magnetically driven arcs was studied at steady state for currents up to 250 A in a variety of gases and gas mixtures, magnetic field strengths and gas flow rates. The effects of arc velocity, gas composition, current density and heat transfer to the cathode on erosion rates were examined.

The arc velocity varied with the magnetic field strength and arc current accordingly to a newly developed equation,  $V \propto B^{0.60} I^{0.56}$ , when the cathode surface was slightly contaminated with C, Cl, O or N. The composition of the surfaces was found using Auger and ESCA spectroscopy. A surface drag force, a new force opposing to the arc motion was proposed. In the case of clean and heavily contaminated surfaces (contaminant layers thicker than 10 microns), the surface drag becomes the major force opposing the arc movement. Work function measurements showed that surface drag increased as electron emission became more difficult.

A novel technique was developed to determine the current distribution of the arc foot on the electrodes. A correlation between the arc foot current density and erosion rate was proposed. The effects of the surface composition, magnetic field and arc velocity on the arc current distribution were also examined.

A conceptual model was developed for electrode erosion; the model was supported by experimental results and by the results of simulations using macroscopic and microscopic heat transfer models.

## Résumé

Cette étude porte sur l'érosion d'électrodes en cuivre de géométrie cylindrique par un arc soufflé par un champ magnétique; les conditions d'opération sont stables pour des courants d'arc allant jusqu'à 250 A et une gamme de valeurs de champ magnétique et de débit gazeux dans différents gaz et mélanges gazeux. Les effets sur le taux d'érosion de la vitesse de l'arc, de la composition du gaz, de la densité du courant et du transfert de chaleur à la cathode ont été examinés.

Quand l'électrode est légèrement contaminée avec C, Cl, O ou N la vitesse de l'arc varie avec les valeurs du champ magnétique et du courant d'arc selon une loi déterminée au cours de ce travail:  $V \propto B^{0.60} I^{0.56}$ . La composition de la surface a été déterminée en utilisant la spectroscopie Auger et ESCA. Pour expliquer le mouvement de l'arc il a fallu introduire l'existence d'une "force de friction" de l'arc sur la surface de l'électrode. Dans le cas de surface propre ou fortement contaminée la force de friction contrôle le mouvement de l'arc; des mesures de potentiel d'extraction ont montré que dans ce cas le potentiel est également plus élevé.

Une nouvelle technique a été mise au point pour la détermination de la distribution du courant d'arc à la surface de l'électrode. Une corrélation entre la densité de courant et la taux d'érosion a été établie. Les effets de la composition de la surface, des valeurs du champ magnétique et de la vitesse de l'arc sur la distribution du courant ont été déterminés.

Un modèle conceptuel de l'érosion d'électrode en présence d'un arc a été proposé; ce modèle est supporté par les résultats expérimentaux et par les résultats de simulations basées sur des modèles macroscopique et microscopique de transfert de chaleur.

## ACKNOWLEDGMENTS

A Ph.D. is made of:

3 years of fun; 1080 boxes of 0.5 l of chocolate milk; 157 books and 512 articles from the library (to carry these books around, you need milk); 430 movies in cinemas; \$ 12 500 in telephone bills (Bell loves us, Mom and Dad); 135 letters from Mom; learning how to enjoy chocolate mint ice cream...

This is my favourite part of the thesis. Here I have the chance to say at least once how much I appreciated the help, the friendship, the trust and the support that so many people gave me in the past years... Thank you all!! Really!!

Well, a thesis starts (and finishes) with the supervisors. In my case, I am happy to say it started and finished in the best possible way... Dr. R. Munz and Dr. M. Drouet, you two were just fabulous!! I know sometimes (to not say most of the times!) it was very hard to avoid saying something when you were interrupted in the middle of meetings by someone screaming "It works!" ; just for half an hour later to be interrupted again by the same someone saying "It doesn't work!"... I wish I could say here how much I enjoyed these years working for you two... Well, I guess I can say now that, at the end, .... it worked!!

I was a member of an extremely exciting and funny plasma group. These people, Dr. Gauvin, Dr. Berk, Dr. Meunier, Jan, G.Q., Bogdan, Maysa, Paul P., Mario, Paul S., Murray, made me feel part of a big family (and what a family!). And let's not mention the parties...

In the Chemical Engineering Department, the secretaries, Anne, Pat, Louise, Valerie, were always trying to make some sense out of my messes... The people in the Mechanical Work Shop, Mr. Krish, Alain, Walter, Charlie, these guys are just out of this world!! They do not just build things from nothing, they also reconstruct things from nothing (well, I destroyed my equipment not more than 3 times. Ok, four times tops)!! Lou, in charge of the Electronic Work Shop, the person who could understand even my "fantastic" circuit diagrams... And Mr. Dumont, the store keeper who knows everything about anything that is important to know, who can even read minds...

Some professors of the Department had always time for my most of the time unusual questions (I wonder if the sign at their door "in, except for Roberto" has anything to do with me...); Dr. Kamal, Dr. Vera, Dr. Rey, Dr. Patterson, thank you for all the help!

I guess in life no one can accomplish anything if he doesn't have friends... A friend is one of those marvellous inventions that make life so incredible (another of those inventions is mint tea). Mazen (Irina and monopoly with russians), Vincent (To the optimism!), Earle (Chicken noodles Friday night), Liz (What a dress!), Omar (CKAD news in the morning), Rani (Hi honey!), Peter P. (Mary talked to you?), John M. (we haven't talked about..), Sassan (Where is the secretary?), Hasan (Man, where is the soccer ball?); I see friends shaking hands...

It is hard to put in words how much my family is important to me... My father and mother, who taught me how to fly; my brother and sister, who encouraged me in the flights; my brother in law and sister in law, who gave colours to the flights; my uncle and aunt, who kept in close contact during the flights; meuses, who prayed during the flights; my turtles, who can't fly (yet!)... I hope that one day I can return to you at least a little of all the happiness you have given me..... And I think to myself, what a wonderful world...

**TABLE OF CONTENTS**

	Page
<b>Abstract</b>	
<b>Resume</b>	
<b>Acknowledgements</b> .....	i
<b>Table of Contents</b> .....	iii
<b>List of Figures</b> .....	xii
<b>List of Tables</b> .....	xx

**CHAPTER I. INTRODUCTION**

1) GENERALITIES .....	1
2) THE IMPORTANCE OF ELECTRODE EROSION IN PLASMA TORCHES .....	2
3) UNRESOLVED PROBLEMS .....	3
4) ORGANIZATION OF THE THESIS .....	4

**CHAPTER II. EQUIPMENT - EXPERIMENTAL PROCEDURES**

1) INTRODUCTION	
A) Chapter Guideline .....	6
2) TEST CHAMBER .....	6

## CHAPTER II. EQUIPMENT - EXPERIMENTAL PROCEDURES

### 3) AUXILIARY EQUIPMENT

A) Rotameters .....	9
B) Rectifiers .....	10
C) Arc Velocity Measurement .....	10
D) Probe Connections .....	10
E) Arc Current/Voltage Measurements .....	11

4) EXPERIMENTAL PROCEDURES .....	11
----------------------------------	----

REFERENCES .....	12
------------------	----

## CHAPTER III. ARC MOVEMENT

### 1) INTRODUCTION

A) Chapter Guideline .....	13
B) Choice of Equipment .....	14

2) LORENTZ FORCE .....	15
------------------------	----

3) AERODYNAMIC DRAG FORCE .....	17
---------------------------------	----

4) BALANCE BETWEEN LORENTZ AND AERODYNAMIC FORCES .....	18
--	----

5) RESULTS FROM THE LITERATURE .....	19
--------------------------------------	----

### CHAPTER III. ARC MOVEMENT

6) MODIFICATION OF THE AERODYNAMIC DRAG FORCE COMPONENT .....	22
7) ADDITION OF SURFACE DRAG FORCE .....	24
8) EXPERIMENTAL RESULTS - ARC VELOCITY	
A) External Magnetic Field .....	25
B) Arc Current .....	33
C) Self Magnetic Field .....	35
9) ARC MOVEMENT - SURFACE DRAG .....	36
10) HIGH SPEED MOVIES	
A) Qualitative Description .....	46
B) Qualitative Analysis .....	51
C) Quantitative Analysis - Histograms .....	53
11) ARC CURRENT AND VOLTAGE FLUCTUATIONS	
A) Description of the Technique .....	58
B) Results .....	61
12) CONCLUSIONS .....	71
REFERENCES .....	74

## CHAPTER IV. SURFACE ANALYSIS

1) INTRODUCTION	
A) Chapter Guideline .....	78
B) Why Contamination? .....	78
2) GAS CONTAMINATION - SURFACE CONTAMINATION .....	79
3) AUGER AND ESCA .....	83
4) AES - ESCA RESULTS	
A) Experiments With Pure Ar and He .....	85
B) Experiments With Ar+0.3%N <sub>2</sub> and He+0.4%N <sub>2</sub> .....	92
C) Ar+0.3%N <sub>2</sub> and He+0.4%N <sub>2</sub> - Kinetics of Contaminant Removal .....	97
5) WORK FUNCTION .....	103
6) SEM	
A) Helium .....	107
B) Ar+0.3%N <sub>2</sub> .....	110
C) Ar+0.3%CO .....	110
D) Ar+10%CO .....	114
7) CONCLUSIONS .....	114
REFERENCES .....	119

## CHAPTER V. CURRENT DENSITY

1) INTRODUCTON	
A) Chapter Guideline .....	123
B) Why Current Density? .....	123
2) DESCRIPTION OF THE PREVIOUS METHODS	
A) Optical Technique .....	124
B) Erosion Tracks .....	124
C) Voltage Induced in a Probe .....	125
3) NOVEL TECHNIQUE	
A) Description .....	131
B) Fourier Analysis .....	131
C) Calibration of the No Slit System .....	133
4) RESULTS	
A) Pure Ar and Ar+0.3%CO .....	137
B) Ar+0.3%CO and He+0.4%CO .....	140
C) Pure Helium .....	145
D) Pure CO .....	145
E) N <sub>2</sub> and He+0.4%N <sub>2</sub> .....	148
F) Anode .....	148
G) Summary .....	153
H) Cathode Spot - Signal Splitting .....	153
5) CONCLUSIONS .....	
REFERENCES .....	158

## CHAPTER VI. EROSION ANALYSIS

1) INTRODUCTION	
A) Chapter Guideline .....	161
B) Cathode Erosion Results in the Literature .....	162
2) RESULTS .....	162
3) CONCEPTUAL CATHODE EROSION MODEL	
A) Model .....	162
B) Applicability and Physical Evidences for the Model .....	167
C) Understanding the Model .....	172
4) QUALITATIVE ANALYSIS OF EROSION RATES	
A) Residence Time (Arc Velocity) - Arc Attach. Splitting .....	177
B) Current Density .....	186
C) Residence Time .....	189
D) Residence Time and Current Density .....	190
E) Residence Time, Current Density, Arc Attachment Diameter .....	191
5) OTHER ASPECTS OF CATHODE EROSION	
A) Power Input to the Cathode .....	192
B) Cathode Spots - Similarities With Vacuum Arcs .....	192
C) Electron Emission .....	194
D) Anode Erosion Rate .....	195
E) Arc Movement in Pure Helium .....	195

## CHAPTER VI. EROSION ANALYSIS

6) CONCLUSIONS .....	198
REFERENCES .....	201

## CHAPTER VII. HEAT TRANSFER ANALYSIS

1) INTRODUCTION	
A) Chapter Guideline .....	205
B) Heat Source and Losses .....	206
2) IDEAL HEAT TRANSFER STUDY .....	
208	
3) THREE DIMENSIONAL CYLINDRICAL GEOMETRY .....	
210	
4) PARAMETERS FOR THE 3D APPROACH .....	
213	
5) RESULTS FOR THE 3D APPROACH	
A) Comparison with the Literature .....	214
B) Heat Flux Input .....	215
C) Arc Velocity - Results and Discussion .....	216
D) Arc Attachment Diameter - Results and Discussion .....	222
E) Wall Thickness - Results and Discussion .....	222
F) Erosion Rate - Results and Discussion .....	226
G) Overall Discussion of the 3D Simulation .....	231

## CHAPTER VII. HEAT TRANSFER ANALYSIS

6) TWO DIMENSIONAL GEOMETRY - FIXED HEAT SOURCE .....	232
7) PARAMETERS FOR THE 2D APPROACH .....	235
8) RESULTS FOR THE 2D MODEL	
A) Comparison with the 3D Approach - Spot Lifetime .....	235
B) Cathode Spot Diameter - Results and Discussion .....	238
C) Multiple Spots - Results and Discussion .....	240
D) Cathode Erosion - Results and Discussion .....	242
E) Overall Discussion of the 2D Simulation Results - Summary .....	246
9) CONCLUSIONS	
A) 3D Approach - Macroscopic Model .....	247
B) 2D Approach - Microscopic Model .....	247
REFERENCES .....	249

## CHAPTER VIII. CONCLUSIONS

1) CONCLUSIONS .....	250
2) RECOMMENDATIONS FOR FUTURE WORK .....	253
3) CONTRIBUTIONS TO KNOWLEDGE .....	254

**APPENDICES**

A) Three Dimensional Model .....	257
B) Grid System for the 3D Model .....	259
C) Two Dimensional Model .....	259
D) Grid System for the 2D Model .....	260

**NOMENCLATURE**

.....	262
-------	-----

## LIST OF FIGURES

Page

### CHAPTER II. EQUIPMENT - EXPERIMENTAL PROCEDURES

2.1 - Schematic representation of the test chamber .....	7
2.2 - Detailed diagram of the electrode arrangement .....	8

### CHAPTER III. ARC MOVEMENT

3.1 - Schematic geometry of the electrodes and the B, E, F vectors ....	16
3.2 - Arc velocity vs magnetic field	
Results from the literature .....	21
3.3 - Arc velocity vs magnetic field	
Results for Ar+0.3%CO, He+0.4%CO, He+0.4%N <sub>2</sub> , N <sub>2</sub> .....	26
3.4 - Arc velocity vs magnetic field	
Current normalized curves .....	28
3.5 - Arc velocity vs magnetic field. Density correction	
Results for Ar+0.3%CO and He+0.4%CO .....	30
3.6 - Arc velocity vs magnetic field. Density correction	
Results for He+0.4%N <sub>2</sub> and N <sub>2</sub> .....	32
3.7 - Arc velocity vs magnetic field	
a) Argon    b) Helium .....	38
3.8 - Tracings of high speed photographs	
a) He        b) He+0.4%N <sub>2</sub> .....	42

### CHAPTER III. ARC MOVEMENT

3.9 - Tracings of high speed photographs	
a) Ar+0.3%CO    b) Ar .....	43
3.10 - Arc velocity vs concentration of CO in argon .....	44
3.11 - Geometry of the central electrode used in the high speed filming .....	47
3.12 - Characteristics tracings of high speed filming	
a) Argon    b) Ar+0.3%CO    c) Ar+0.3%N <sub>2</sub>	
d) Helium (1 000 G)    e) Helium (100 G)	
f) He+0.4%N <sub>2</sub> g) Nitrogen .....	48
3.13 - Histograms from the high speed filming	
Results for argon and Ar+0.3%CO .....	54
3.14 - Histograms from the high speed filming	
Results for argon and Ar+0.3%N <sub>2</sub> .....	56
3.15 - Residence time of the arc attachment at the cathode	
Jumping distance zero - results for Ar and Ar+0.3%N <sub>2</sub> .....	57
3.16 - Histograms from the high speed filming	
Results for helium at 1 000 G and 100 G .....	59
3.17 - Histograms from the high speed filming	
Results for He+0.4%N <sub>2</sub> and N <sub>2</sub> .....	60
3.18 - Arc current fluctuations tracing for argon .....	62
3.19 - Arc current fluctuations tracing for Ar+0.3%CO .....	64
3.20 - Arc current fluctuations tracing for Ar+0.3%N <sub>2</sub> .....	66
3.21 - Arc current fluctuations tracing for Ar+>4%CO .....	67

### CHAPTER III. ARC MOVEMENT

3.22 - Arc current fluctuations tracings for nitrogen	
a) 1 000 G    b) 400 G .....	69
3.23 - Arc current fluctuations tracings for helium	
a) 1 000 G    b) 700 G    c) 400 G .....	70

### CHAPTER IV. SURFACE ANALYSIS

4.1 - Arc voltage and velocity variations with time	
a) Ar        b) He .....	80
4.2 - Carbon concentration profiles - Auger analysis .....	86
4.3 - Oxygen concentration profiles - Auger analysis .....	89
4.4 - Chlorine concentration profile	
a) Clean cathode and 1 min Ar    b) 1 min Ar and 5 min Ar .....	90
4.5 - Chlorine concentration profile for He	
Two regions on the same cathode .....	91
4.6 - Carbon concentration profile	
Pure Ar and He; Ar+0.3%N <sub>2</sub> ; He+0.4%N <sub>2</sub> .....	93
4.7 - Nitrogen concentration profile for Ar+0.3%N <sub>2</sub>	
and He+0.4%N <sub>2</sub> .....	95
4.8 - Nitrogen concentration profile	
Kinetics of nitrogen removal by a helium arc .....	98
4.9 - Arc velocity and nitrogen concentration changes with time	
After stopping nitrogen addition in helium .....	100

## CHAPTER IV. SURFACE ANALYSIS

4.10 - Nitrogen concentration profile Kinetics of nitrogen removal by an argon arc .....	101
4.11 - SEM photograph of a cathode after an experiment using helium a) center b) intermediate region between center and edge .....	108
4.12 - SEM photograph of a cathode a) after an experiment with helium - edge of the cathode b) prior to the experiment .....	109
4.13 - SEM photograph of a cathode after an experiment using Ar+0.3%N <sub>2</sub> a) center b) edge .....	111
4.14 - SEM photograph of a cathode after an experiment using Ar+0.3%CO a) center b) center - higher magnification .....	112
4.15 - SEM photograph of a cathode after an experiment using Ar+0.3%CO a) carbon island b) back scattering photograph of similar region .....	113
4.16 - SEM photograph of a cathode after an experiment using Ar+10%CO a) center b) center - higher magnification .....	115
4.17 - SEM photograph of a cathode after an experiment using Ar+10%CO a) edge b) back scattering photograph of similar region .....	116

## CHAPTER V. CURRENT DENSITY

5.1 - Schematic representation of the slit current density probe .....	126
5.2 - Schematic representation of the cylindrical cathode a) with copper ring    b) with copper ring and solder .....	129
5.3 - Impedance of cavity-coil system vs frequency a) with copper ring    b) with copper ring and solder .....	130
5.4 - Signal obtained using He and He+0.4%CO at 160 m/s a) slit system            b) no slit system .....	134
5.5 - Signal obtained from the no slit system using CO at 95 m/s Before and after calibration with the transfer function .....	136
5.6 - Linear current distribution Ar and Ar+0.3%CO at similar arc velocities .....	138
5.7 - Linear current distribution for Ar+0.3%CO a) 75 m/s; 1 000 G    b) 43 m/s; 370 G .....	141
c) 26 m/s; 160 G      d) 4 m/s; 10 G .....	142
5.8 - Linear current distribution for He+0.4%CO a) 230 m/s; 1 000 G    b) 70 m/s; 120 G    c) 44 m/s; 60 G .....	143
5.9 - Linear current distribution for pure He 1 000 G and 120 G at similar arc velocities .....	146
5.10 - Linear current distribution for pure CO at 1 000 G and 90 m/s ....	147
5.11 - Linear current distribution for pure nitrogen a) 100 m/s; 1 000 G    b) 21 m/s; 100 G .....	149
5.12 - Linear current distribution for He+0.4%N <sub>2</sub> a) 180 m/s; 800 G    b) 130 m/s; 480 G    c) 65 m/s; 120 G .....	150

## CHAPTER V. CURRENT DENSITY

5.13 - Linear current distribution for He+0.4%N <sub>2</sub> and He (2 minutes after stopping the addition of nitrogen) at similar magnetic fields .....	151
5.14 - Linear current distribution for anode Argon at 1 000 G and 27 m/s .....	152
5.15 - Signal for Ar+0.3%CO at 4 m/s and 10 G Splitting of the signal .....	155

## CHAPTER VI. EROSION ANALYSIS

6.1 - Alignment of cathode spots in the direction of the magnetic field .....	170
6.2 - Cathode erosion rate vs arc velocity for pure nitrogen arcs .....	178
6.3 - Log plot of cathode erosion rate vs arc velocity for nitrogen arcs .....	179
6.4 - Cathode erosion rate vs arc velocity He+0.4%CO, He+0.4%N <sub>2</sub> , Ar+0.3%CO .....	182
6.5 - Cathode erosion rate vs magnetic field He+0.4%CO, He+0.4%N <sub>2</sub> , Ar+0.3%CO .....	183
6.6 - Cathode erosion rate vs arc velocity for Ar at different gas flow rates .....	185

## CHAPTER VII. HEAT TRANSFER ANALYSIS

7.1 - Geometry for the 3D simulations .....	211
7.2 - Maximum temperature profile of the cathode at the center of the arc attachment Power = 1 000 W; Arc attach. diameter = 1 mm; Wall thickness = 2.5 mm .....	217
7.3 - Two dimensional cathode temperature Power = 1 000 W; Arc attach. diameter = 1 mm a) Arc velocity = 0 m/s .....	218
b) Arc velocity = 2 m/s .....	219
7.4 - Maximum cathode temperature for different input powers Arc attach. diameter = 1 mm; Wall thickness = 2.5 mm .....	223
7.5 - Maximum cathode temperature for different arc attachment diameters Power = 1 000 W; Vel = 2 m/s; Wall thickness = 2.5 mm .....	224
7.6 - Two dimensional cathode temperature Power = 1 000 W; Vel = 2 m/s; Arc attach. diameter = 0.1 mm .....	225
7.7 - Maximum temperature of the cathode for different wall thicknesses Power = 1 000 W; Vel = 2 m/s; Arc attach. diameter = 1 mm ..	228
7.8 - Schematic representation of the cathode boiling region .....	233
7.9 - Geometry for the 2D simulations	
7.10 - Maximum cathode temperatures for different spot lifetimes Power = 1 000 W; spot diameter = 1 mm; cathode radius = 5 cm .....	236

**CHAPTER VII. HEAT TRANSFER ANALYSIS**

7.11 - Cathode temperature profile for the 1 $\mu\text{m}$ cathode spot diameter Power = 20 W; cathode radius = 5 cm; spot lifetime = 1 ms .....	239
7.12 - Maximum temperature of the cathode for different cathode radii, cathode spot diameters and cathode spot lifetime .....	241
7.13 - Cathode temperature profile Cathode radius = 100 $\mu\text{m}$ ; spot diameter = 10 $\mu\text{m}$ ; spot lifetime = 1 ms .....	244
7.14 - Cathode temperature profile Cathode radius = 5 cm; cathode spot diameter = 1 $\mu\text{m}$ ; spot lifetime = 0.001 ms .....	245

## LIST OF TABLES

	Page
<b>CHAPTER III. ARC MOVEMENT</b>	
3.1 - Operating Conditions for Data in Figure 3.2 .....	20
3.2 - Arc Velocities for Different Arc Currents .....	34
3.3 - Arc Current, Velocity and Voltage for Different Plasma Gases .....	40
3.4 - Arc Operating Conditions for High Speed Movies .....	49
<b>CHAPTER IV. SURFACE ANALYSIS</b>	
4.1 - Gas Contamination Concentration .....	83
4.2 - Transient Times for Removal of Contamination .....	103
4.3 - Work Function Measurements .....	105
<b>CHAPTER V. CURRENT DENSITY</b>	
5.1 - Operating Conditions for Signal from the System With Slit .....	133
5.2 - Operating Conditions for Figure 5.6 .....	137
5.3 - Minimum Equivalent Diameter for Ar+0.3%CO and He+0.4%CO .....	144
5.4 - Summary of Results Obtained with the No Slit System .....	154

**CHAPTER VI. EROSION ANALYSIS**

6.1 - Copper Cathode Erosion Results Using Air at Atmospheric Conditions .....	163
6.2 - Erosion Results and Operating Conditions for This Work .....	164
6.3 - Erosion Rates and Arc Velocities for Argon and Helium Mixtures .....	188
6.4 - Arc Velocity and Voltage for Different Magnetic Field Strengths in He .....	197

**CHAPTER VII. HEAT TRANSFER ANALYSIS**

7.1 - Comparison Between Results from this Simulation and the Literature .....	215
7.2 - Erosion Rates for the 3D Simulations .....	230
7.3 - Cathode Maximum Temperature for Different Cathode Spot Diameter .....	238
7.4 - Cathode Radii Used to Simulate Multiple Cathode Spots .....	242

*To*

*my father and my mother*

*(my lifelong teachers and supporters).*

# I. INTRODUCTION

## I. INTRODUCTION

### 1) GENERALITIES

*London. Beginning of the century. Saturday morning...*

*Watson is reading the newspaper, drinking his favourite tea, sitting on his favourite chair at the office of his best friend, Sherlock Holmes...*

*Watson raises his eyes from the news for a moment and looks at Holmes... He seems to be in one of those "thinking periods", when no one can possibly talk to him. His eyes are closed, his hands clasped on his lap, his pipe in his mouth, and showing no signs of being alive... Watson recalls how many times he has seen Holmes in this position. It has certainly been an exciting 15 years since he met Holmes for the first time... Watson thinks about all the adventures, mysteries and excitement of those years.. He wouldn't change them for anything in the world...*

*And suddenly, as Watson is lost in his thoughts, the door bell rings. Holmes opens his eyes, but doesn't move. Two minutes later, Miss Campbell, the good lady who has been working for Holmes since, well, since Watson can remember, brings a parcel to Holmes.*

*- It's for you, Mr. Holmes. The messenger didn't wait for an answer. Actually, he seemed quite anxious to leave...*

*She hands to Holmes a small parcel, the size of a book, wrapped in a dark brown paper. Holmes holds the parcel for some time, he seems to be intrigued with something...*

*- Holmes, for God' sake, aren't you going to open the parcel?*

*- Oh, I'm sorry Watson, I was just thinking... This wrapping paper hasn't been sold for at least 25 years; I know it because my mother used to wrap old bread with this kind of paper. They stopped making this type of paper years ago; it seems it was too heavy and expensive. And then suddenly we receive a parcel with this paper... It is very odd... But you are right, let's open the parcel!*

*Holmes carefully unwraps the parcel. Inside it he finds a small book, a kind of note book, the type you find in a laboratory, and a letter...*

*Holmes reads the letter. After three minutes, he drops it on the floor and his face is pale... Watson can't imagine what is happening.*

*- Holmes, are you all right? What does the letter say? Holmes, are you listening to me? Holmes??*

*- I'm fine Watson, I'm fine.. It is just that this is so incredible! Here, see for yourself! Holmes picks up the letter and gives it to his friend while he himself starts to read the note book..*

*Watson reads the letter...*

*It is addressed to Holmes. A certain scientist, Dr. Bergman, was doing research on a new form of matter, almost pure energy, he called it "plasma". He believed that it could solve all the problems of the chemical industries, from manufacturing to dumping byproducts in the rivers.. The only problem was with the equipment to generate the plasma; it wouldn't last long enough... There was a problem with some sort of electrodes. Dr. Bergman had some ideas how to solve the problem, but he didn't have enough time to test his theories. He was dying... It seems he was poisoned in his lab, he had just few days left... He had heard about the almost magical logic of Holmes and he decided to send his personal notes to him, hoping that with his logic Holmes could find the solution for the problem. Dr. Bergman was afraid that his discoveries could drop into the wrong hands, to people that would use it for their own benefit and not the whole of mankind... His only hope now was Holmes...*

*Watson can't believe what he read. He turns to Holmes, who seems to be completely absorbed by the notes.*

*- Holmes, this can't be serious! You are not a scientist; he shouldn't have sent this to you.. We have to give this to someone at the Royal Institute and...*

*Watson realizes that his friend cannot hear him. He is reading the notes, he seems hypnotized by the book.*

*After almost 2 hours in the most complete silence except for the noise of Holmes turning the pages of the note book, and during which Watson keeps reading and rereading the letter, Holmes suddenly says:*

*- Watson, are you still reading the letter!*

*Watson suprised with the sudden question, takes few seconds to recover.*

*- I still cannot believe in this whole story, Holmes... But I can see from the expression on your face that you are not taking this too serious...*

*- Au contraire, mon ami, au contraire! This is most exciting! We cannot waste one single moment more! We have to start immediatly this project; after all, the fate of many people could be depending on us... This is it, Watson, the ultimate work, the Electrode Erosion Journey!*

*And saying this, Holmes moves towards his bookshelves. Watson is in complete shock with all this and cannot even close his mouth...*

Coming back to 1989,

## 2) THE IMPORTANCE OF ELECTRODE EROSION IN PLASMA TORCHES

The application of thermal plasma technology to industrial processes is becoming a reality. Plasmas are starting to have an important role in the production of new

materials, in the destruction of toxic wastes, and in the development of safer and more efficient processes.

One of the remaining problems inhibiting the further industrial application of plasmas is related to the plasma generator or plasma torch. Short electrode lifetimes, unreliable torch performance and lack of flexibility in torch operation are all directly or indirectly due to lack of fundamental knowledge on the role of the electrodes in the plasma generating process.

This work is aimed at understanding the phenomena governing electrode erosion at copper cathodes. It is hoped that with this fundamental understanding, erosion rates can be decreased, increasing the electrode lifetime, and more flexibility in torch operation can be achieved.

### 3) UNRESOLVED PROBLEMS

The role of the electrodes in generating plasma has fascinated many researchers for the past 50 years. Many electrode studies have been conducted, enlarging tremendously our understanding in this area. However, many questions have been raised in these studies, and unsatisfactory answers are a reality. Most of the data in the literature unfortunately cannot be extrapolated to different systems or operating conditions. The importance of more than 20 different parameters on the electrode phenomena has been suggested but little support has been found for most of these suggestions. A more fundamental understanding of electrode phenomena has also been delayed by the lack of appropriate instruments to analyse both the plasma and the electrode surface in the older studies. Finally some of the findings and techniques could not be used at an industrial level as well.

This work was an attempt to partially resolve some of the problems mentioned above. The work was developed in both experimental and theoretical manners. Both these two different approaches were used during the research. The need for reliable data in one hand, and the analysis of these data in the light of well established theories on the other hand, directed the research towards its goals. Diagnostic techniques had to be developed along the work in order to obtain more information on the electrode phenomena.

#### 4) ORGANIZATION OF THE THESIS

Chapter II describes the equipment and experimental procedures. Chapter III is concerned with the fundamental study of the arc (and plasma) movement. The electrode surface is then examined as a function of chemistry and operating conditions in Chapter IV. The development of a new probe and its use to measure linear current density at the electrode surface are described in Chapter V. Chapter VI then uses the information of Chapters III to V to formulate a general conceptual model for electrode erosion in plasma torches and uses it to explain the erosion rate measurement results. Chapter VII, on the heat transfer analysis, is purely theoretical in nature and develops two heat transfer models of the electrode and electrode surface to examine some of the hypotheses and predictions of the erosion model. Chapter VIII is the summary of the conclusions made within the thesis and recommends the direction of future work in electrode phenomena.

An extensive literature review was conducted during this research; this has been incorporated directly into the appropriate chapters so that relevant results from the literature can be immediately compared to the present work. A list of the nomenclature used is given at the end of thesis.

**II. EQUIPMENT - EXPERIMENTAL PROCEDURES**

## II. EQUIPMENT - EXPERIMENTAL PROCEDURES

### 1) INTRODUCTION

*Watson is tired. He seems to be at point of collapsing; sweat comes out from every pore of his body, his legs refuse to move any further... He decides to stop for a while to catch his breath. He's been carrying the copper rod for almost half an hour now... He still has another 10 minutes until he reaches his destination. He wonders more and more why Holmes would ask him to pick up this rod at the Atica & Sons Copper Refinery and take it to Holmes' office. Watson is very tired, but his curiosity is stronger than himself and he bends slowly, lifts the rod and starts walking again... Fifteen minutes later he is at Holmes' door, ringing the bell... He hears strange and loud noises coming from upstairs. He waits for one minute, rings the bell again, and decides to try the door... To his surprise, the door is unlocked and Watson forgetting the weight of the rod rushes upstairs. He opens the office's door and shocked with what he sees, drops the rod on the floor... Holmes, in the middle of the room, jumps at the sound of the heavy metal hitting the ground..*

- *Watson! Good Lord, it's you! You almost killed me!*
- *Holmes, what are you doing? Are you all right?*
- *Of course I'm all right, Watson, what's the problem with you?*
- *But Holmes, you look, you look... awful!*

*Holmes looks at himself and realizes what his friend means... He is covered by dust, and his hands are black; he bleeds from small cuts along his arms; his clothes are almost totally tore apart...*

*- Oh, don't worry about my appearance, Watson! I've just been working in our erosion project. And I see that you brought the copper... Good, good, we will be starting in less than a week...*

*- Starting what Holmes?*

*- The experiments, of course... Come, come here Watson, I want to show you something...*

*And grabbing Watson's arm, Holmes pulls his friend to the corner of the office. He uncovers a sheet, and reveals a small metal vessel connected to all sorts of tubes and pipes...*

*- This is our test chamber, Watson! It's perfect for our experiments! With the copper you brought, we are going to make the electrodes and then everything is ready!!*

*- Holmes, this certainly looks impressive, but I still don't understand why you..*

*- Well, my dear friend, let's first take a look at the copper and then I'll explain what I have in mind...*

And coming back to this work...

#### A) Chapter Guideline

The equipment used for the experimental part of this work is described in this Chapter. The description covers the test chamber, the electrodes and the auxiliary equipment. The Chapter ends with the description of the experimental procedures.

#### 2) TEST CHAMBER

A chamber used for the first part of the erosion studies (Szente (1)) was modified for this work. A schematic diagram of the modified chamber is shown in Figure 2.1; a more detailed diagram of the electrode arrangement is given in Figure 2.2. In these figures the external electrode is indicated as the cathode. The electrode geometry simulates a tubular plasma torch. The chamber is gas tight and during the experiments the pressure inside the chamber is always kept slightly above one atmosphere (1.1 atm) to assure the gas purity inside the vessel. The chamber is made of stainless steel and other nonmagnetic materials. The walls of the chamber and the electrodes were water cooled. The dimensions of the chamber were chosen in order to have fully developed flow in the electrode region; the dimensions are indicated in Figures 2.1 and 2.2.

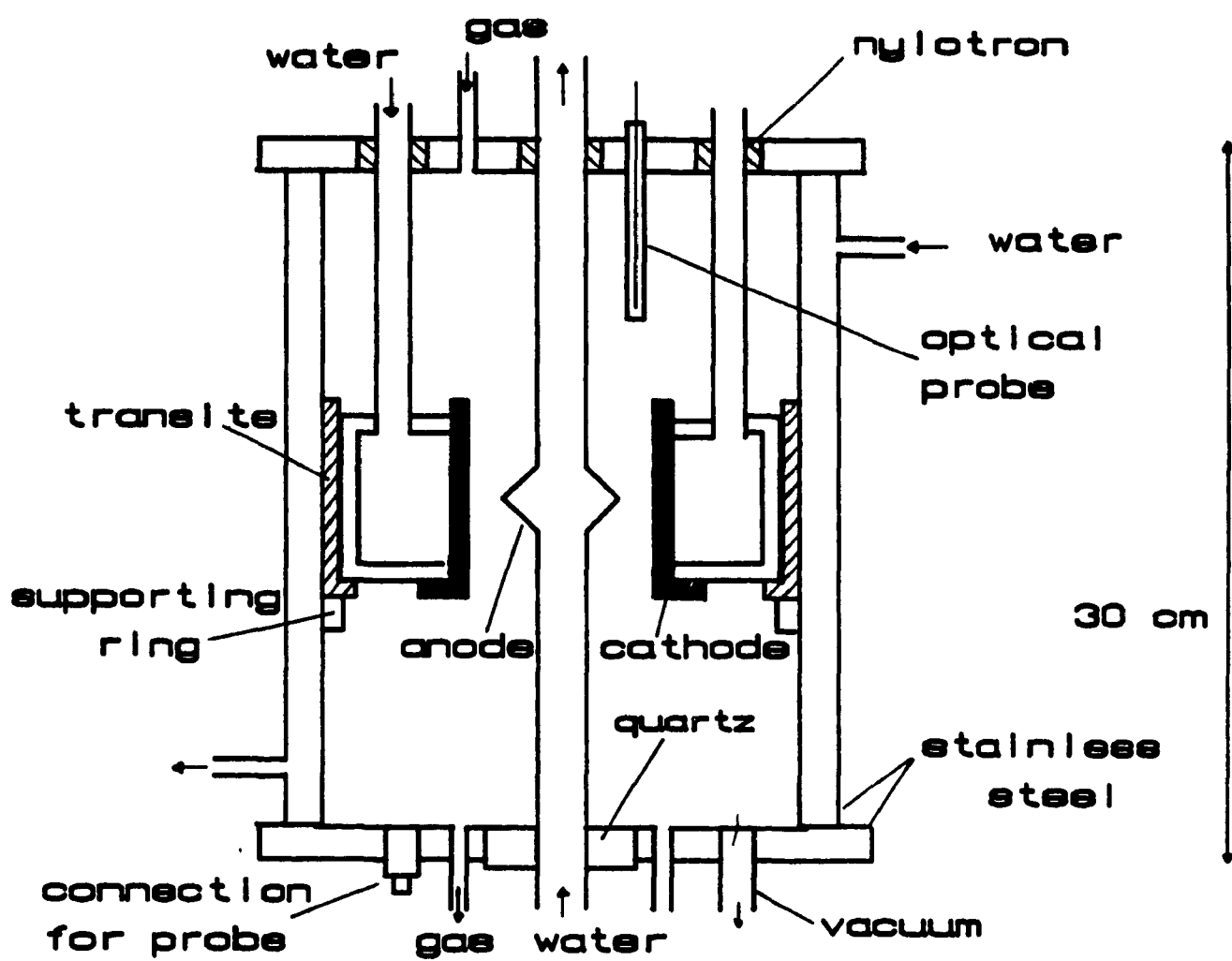


Figure 2.1 - Schematic representation of the test chamber

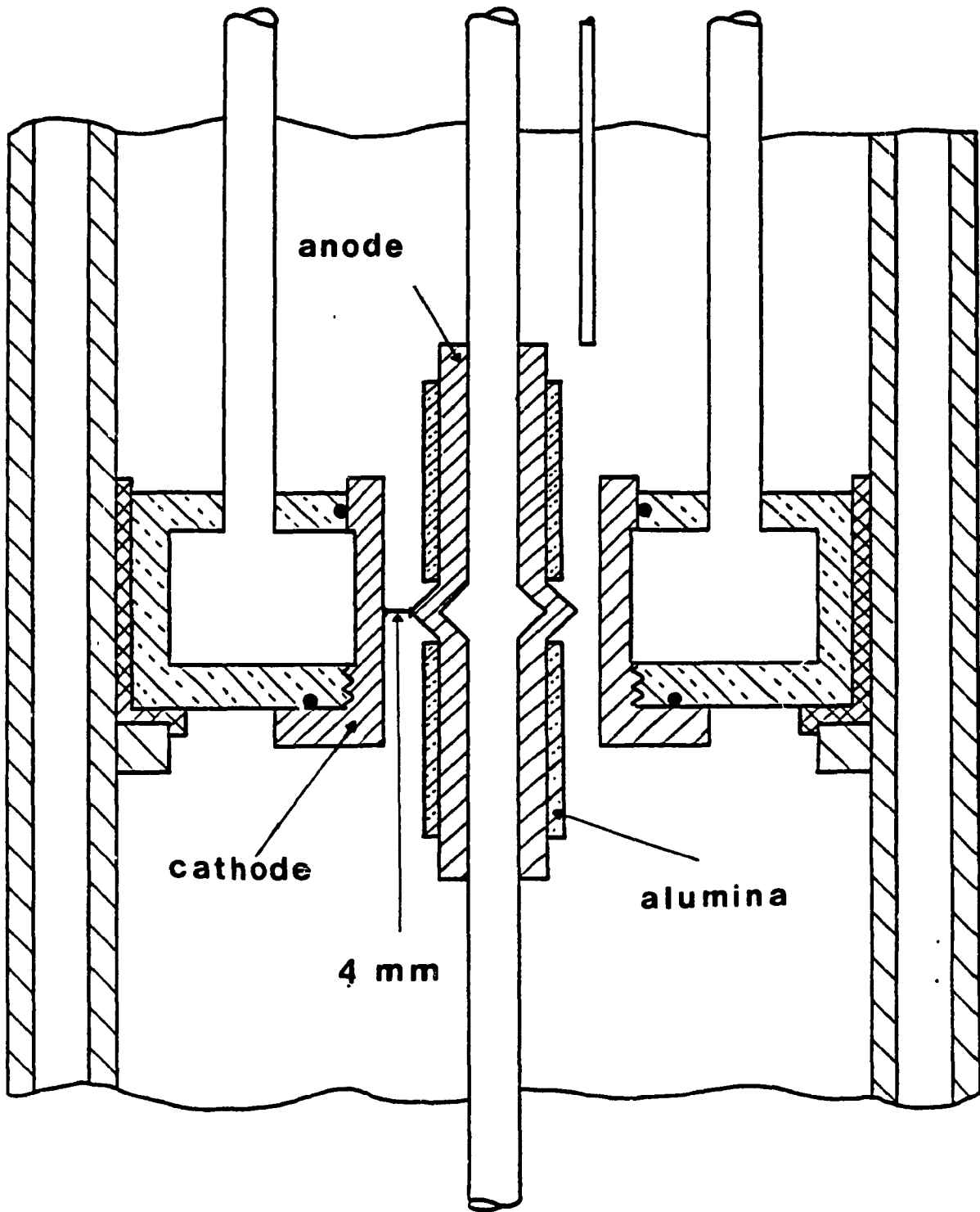


Figure 2.2 - Detailed diagram of the electrode arrangement

The external electrode was designed to be easily removed. The erosion analyses (weight loss, electron microscopy, current density probe, etc) were always done on this external electrode. Both electrodes were electrically insulated from the chamber; in this way the polarity of the electrodes could be inverted easily and therefore anodic and cathodic studies could be conducted. The electrodes were water cooled through separate water lines and thermocouples were installed in these lines to allow heat balances to be carried out in the electrodes. The electrodes in this work were made of electrolytic copper, with a minimum purity of 99.95% (major contaminants are oxygen, silver and sulfur).

An external coil concentric to the chamber generated a magnetic field transverse to the electric arc. The interaction of this magnetic field with the electric arc forced the latter to rotate within the annulus formed by the two electrodes. The magnetic field is essentially uniform within the interelectrode space.

### 3) AUXILIARY EQUIPMENT

#### A) Rotameters

Rotameters were installed in the gas and water lines to control and measure the gas and water flow rates. The mixture of contaminant and main gases was accomplished well before the chamber in order to assure a well mixed gas. The total flow rate was 20 l/min for the experiments (except for few experiments where the influence of the gas flow rate on the erosion phenomena was examined). The gases used in these experiments were industrial grade (minimum purity of 99.98%) and comparisons were also made using ultra pure gases (purity higher than 99.999%). The compositions of the gases can be found in Szente (1).

### B) Rectifiers

Two separate rectifiers were used to generate the D.C. current for the electric arc and for the coil. A Thermal Dynamics rectifier, model TDC 1A40 was used for the arc. The maximum power output of this rectifier is 75 kW; the open voltage circuit is 320 V. A Syntron rectifier, model P 0063 was used for the coil. It had a maximum output voltage of 40 V, corresponding to a current of 130 A in the coil. The electric arc was initiated using a Miller HF 250-1 model high frequency unit connected in series with the rectifier.

### C) Arc Velocity Measurement

The arc velocity was measured using an optical fiber probe installed inside the reactor perpendicular to the arc motion (see Figure 2.1). Each time the arc passed below the probe, light was conducted through the fiber to a photodiode connected to an electronic circuit; the electrical signal was filtered and displayed on an oscilloscope. The arc velocity at the external electrode was calculated from the frequency of rotation and the dimensions of the cathode. The arc velocity mentioned throughout the thesis refers always to the velocity calculated at the external electrode.

### D) Probe Connections

The connections for the current density probe (the probe is described in Chapter V) were installed in the bottom flange as indicated in Figure 2.1. They were teflon insulated coaxial connections. For the current density experiments the external electrode was grounded to avoid secondary currents into the probe signal.

### E) Arc Current/Voltage Measurements

### E) Arc Current/Voltage Measurements

The arc current was monitored during the experiments using a shunt connected in series with the cathode power line. The arc voltage was measured between the cathode and anode power lines approximately one meter away from the cathode and anode (the resistance of the power lines is less than 0.1 ohm/meter). A special shunt (short-circuit coaxial cable) was used for the current fluctuation measurements and is discussed in Chapter III.

## 4) EXPERIMENTAL PROCEDURES

Before an experiment the electrodes were cleaned using  $\text{CCl}_4$  and dilute nitric acid (see also Chapter IV for more details) and rinsed with distilled water. The electrodes were weighed (for erosion rate measurements) using a digital scale with a precision of 0.0001 g. The erosion rates reported in this work were obtained considering the difference in weight of the electrodes before and after the experiments (and after cleaning the electrodes again after the experiments, to remove any contaminant layer that was formed during the experiment). The error involved in the weighting procedure was less than 1%. The units of erosion rate are  $\mu\text{g}/\text{C}$ . The weight loss, measured in  $\mu\text{g}$ , is a function of the duration time of an experiment and the current used in the experiment. The product of the duration time (in seconds) and current (in amperes) gives C (Coulomb).

After installing the test electrode, the chamber was evacuated to a pressure of approximately 0.001 Torr for 5 minutes. The chamber was then purged with argon (or helium) for 5 minutes. The electric arc was initiated in argon, helium or mixtures of these inert gases with polyatomic gases (see Chapter IV). The pressure inside the

chamber was kept at 1.1 atm throughout the experiment.

The arc current used in these experiments varied between 80 and 250 A; most experiments were conducted at 100 A. The arc voltage was a function of the plasma gas used, as well as the operating conditions (see Chapters III and IV). Individual experiments lasted up to 4 hours; steady state was always reached much before the end of an experiment.

#### REFERENCE

- 1) Szente, R.N.; " Cathode Erosion in Magnetically Rotated Arcs", Master Thesis, Chemical Engineering Department., McGill Univ., Montreal, 1986.

### III. ARC MOVEMENT

### III. ARC MOVEMENT

#### 1) INTRODUCTION

- *But my dear Holmes, why should we study the movement of the electric arc? Holmes, lost in his thoughts, takes some time to realize that Watson was talking to him.*
- *I am sorry, Watson, but what were you saying ?*
- *Holmes, I was just wondering why we have to examine this "arc movement" if what we really want to do is to find what causes the electrode erosion..*
- *But that is precisely what we are doing, Watson! See if you do not agree with my logic... Intuitively, it is easy to visualize that the more time the electric arc spends over the same region of the electrodes, the more that region will have its temperature increased and consequently, more material will be volatilized and the higher will be the erosion rate. But now, if we can decrease the residence time of the arc over the same spot, the heat will be much better dissipated, since the area covered by the arc will be much larger...*
- *That is fascinating, Holmes... So, how do we start?*
- *Well, dear friend, the first thing is to decide about the method we are going to use to move the arc. Then we have to think about the diagnostics, then how to compare our results with the theoretical ones, then we should...*

We leave our friends at this point...

#### A) Chapter Guideline

In this chapter the fundamentals of the arc movement are examined. The forces moving the arc forward, the Lorentz force, and resisting the arc movement, the aerodynamic drag force, are presented. Experimental results from the literature are shown to be in disagreement with the previously proposed equilibrium between those two forces. A modification in the aerodynamic force is then proposed and a new force, the surface drag force, is introduced. Experimental results from this work show very good agreement with the new theory. The arc movement is then analyzed for different plasma gases using high speed photography and cine-photography. The

effect of surface contamination is highlighted and arc current fluctuations obtained during an experiment prove to be a valuable diagnostic tool for arc studies. The Chapter ends with a summary of the most important findings of this part of the work.

### B) Choice of Equipment

There are different ways of moving the electric arc in plasma torches; the two most common use either a gas vortex or an external magnetic field. Industrial torches normally use a combination of the two.

The gas vortex method is based on tangential injection of gas between the electrodes (tubular geometry). The vortex forces the electric arc and surrounding plasma to rotate within the tubes. The magnetic method uses a magnetic field perpendicular to the electric arc in order to move the arc and the surrounding plasma.

It was decided to use the magnetic field because it is more flexible in operation. The use of the gas vortex to change the arc velocity also requires changes in the gas flow rate or injection velocity. This affects not only the arc velocity but other operating conditions as well.

The magnetic field profile for this chamber was obtained previously (Szente (1)); it is very uniform in the area where the arc strikes, varying by less than 2 % from the axis of the chamber (which coincides with the axis of the magnetic field) to the inside wall of the cathode. The magnetic lines are thus considered to be parallel to the axis of the chamber in this central part of the reactor. The calculated values of the magnetic field agree extremely well with the experimental ones (Szente (1)). It is therefore assumed that the magnetic field strength,  $B$ , is uniform and well determined in the experiments.

As mentioned previously (Chapter II), the mean arc velocity was measured throughout the experiments using a light probe. The values obtained using this probe were periodically checked using two other independent methods (high speed film and magnetic probe).

## 2) LORENTZ FORCE

The magnetic field created by the coil located outside the reactor interacts with the electric arc and plasma, resulting in the movement of the arc and surrounding plasma. The theoretical aspects of this interaction are as follows:

- the equation of motion for charged particles in electric/magnetic fields is given by

$$m \frac{d\vec{v}}{dt} = e (\vec{E} + \vec{v} \times \vec{B}) \quad 3.1$$

where

$m$  = particle mass

$\vec{v}$  = particle velocity

$t$  = time

$e$  = particle charge

$\vec{E}$  = external electric field

$\vec{B}$  = external magnetic field

In the case of these experiments, the electric field  $\vec{E}$  will accelerate the particle  $e$  (electron) from the cathode to the anode. The electron will therefore have a velocity  $v$  in the same direction as  $\vec{E}$ , which is perpendicular to  $\vec{B}$ . Therefore  $\vec{v} \times \vec{B} = |v| \cdot |B|$  in a direction perpendicular to both  $\vec{E}$  and  $\vec{B}$ . Figure 3.1 illustrates this. Furthermore it is possible to consider the electric arc as a current-carrying conductor. Equation 3.1

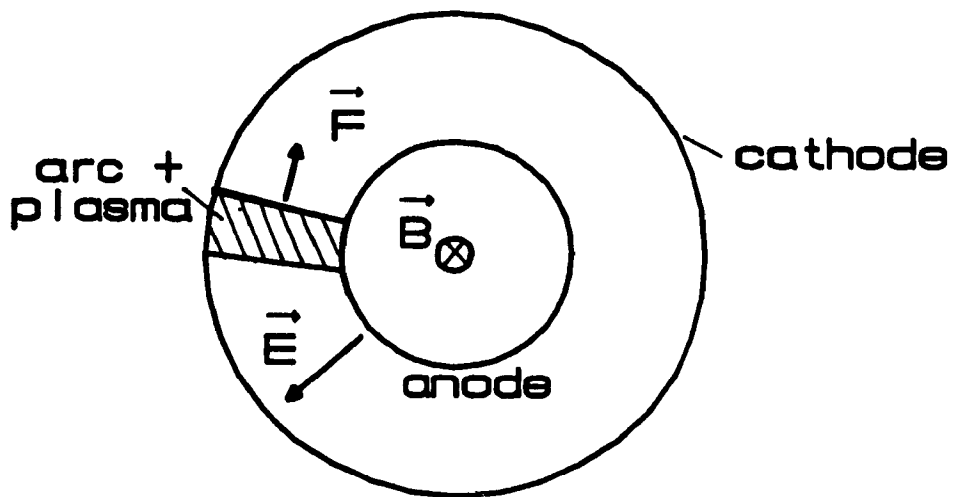


Figure 3.1 - Schematic geometry of the electrodes and the  $\vec{B}$ ,  $\vec{E}$  and  $\vec{F}$  vectors

becomes for an element  $dl$  of the conductor (Reitz and Milford (2)):

$$dF_i = N A dl e (\vec{v} \times \vec{B}) \quad 3.2$$

where

$F_i$  = Lorentz force

$N$  = charge carriers per unit volume

$A$  = cross sectional area of the conductor

Since  $N A e v = I$ , where  $I$  = arc current, it is possible to integrate eq. 3.2 to obtain

$$F_i = B I d \quad 3.3$$

where  $d$  = total length of the conductor in the direction of  $\vec{E}$

Therefore there will be a force  $\vec{F}_i$  (Lorentz force) moving the electric arc / plasma in the direction perpendicular to both  $\vec{B}$  and  $\vec{E}$ .

### 3) AERODYNAMIC DRAG FORCE

The electric arc plus the plasma surrounding it form a region in the space where temperatures are in excess of 5 000 K, reaching values as high as 20 000 K. The viscosity of the gas (plasma) is therefore extremely high and the whole region can be considered to be a rigid body (Roman and Myers (3); Fisher and Uhlenbush (4)). This seems to be a valid assumption for Reynolds number,  $Re$ , greater than 10 (Malghan and Benenson (5)), as it is the case in the experiments in this work ( $Re > 1\ 000$ ). The  $Re$  is defined in this and in the other works as:

$$Re = (Vel D \rho) / \mu$$

where     $Vel$  = arc velocity (relative to the cathode)  
            $D$     = arc column diameter  
            $\rho$     = gas density (in front of the arc)  
            $\mu$     = gas viscosity (in front of the arc)

Whenever a fluid moves relative to a rigid boundary, it exerts a dynamic force on the boundary. The component of this force in the opposite direction of the relative flow is called drag (Daily and Harleman (6)). The drag force is given by :

$$F_d = 0.5 C_d D d \rho Vel^2 \quad 3.4$$

where  $F_d$  = aerodynamic drag force  
         $C_d$  = drag coefficient  
         $D$  = arc diameter  
         $d$  = arc length  
         $\rho$  = gas density  
         $Vel$  = arc velocity

#### 4) BALANCE BETWEEN LORENTZ AND AERODYNAMIC FORCES

The summation of forces acting on the arc should be equal to zero for an arc moving at constant velocity, i.e.,

$$\Sigma \text{ forces} = 0$$

$$F_l = F_d$$

$$B I d = 0.5 C_d D d \rho \text{ Vel}^2 \quad 3.5$$

and further

$$\text{Vel} \propto B^{0.5} \quad 3.6a$$

$$\text{Vel} \propto I^{0.5} \quad 3.6b$$

if the other terms are independent of Vel. This relation has been proposed by different authors (Kopainsky and Schade (7); Alferov et al (8); Guile and Naylor (9)); in the next section, these equations are examined in more detail.

## 5) RESULTS FROM THE LITERATURE

The results shown in Figure 3.2 are for the variation of the arc velocity with the magnetic field. They include different electrode materials, geometries and arc currents. These conditions are described in Table 3.1. Since the results involve a large range of arc current (100 - 850 A), the arc velocities presented in Figure 3.2 were normalized for comparison using eq. 3.6b, i.e.,

$$\text{Vel} = \text{Vel}_0 (100/I_0)^{0.5} \quad 3.6c$$

where  $\text{Vel}$  = arc velocity normalized to 100 A

$\text{Vel}_0$  = arc velocity at a current  $I_0$

It can be seen in Figure 3.2 that the arc velocity did not show the expected variation with the magnetic field given by equation 3.6a. Most of the data could be correlated in the form of  $\text{Vel} \propto B^{0.7}$ , although the large scatter of the data makes this value questionable.

**TABLE 3.1**

Operating Conditions for Data in Figure 3.2  
(Air plasmas were used in all cases)

Reference	I (A)	Gap (mm)	Material	Geometry
Secker and Guile (10)	500	3.2	Copper	Rail Elec.
Guile and Adams (11)	200	12.7	Brass	Rail Elec.
Harry (12)	200	8.0	Copper	Conc. Cyl.
Sharakovskii (13)	850	5.0	Copper	Conc. Cyl.
Winsor (14)	109	3.0	Copper	Rail Elec.

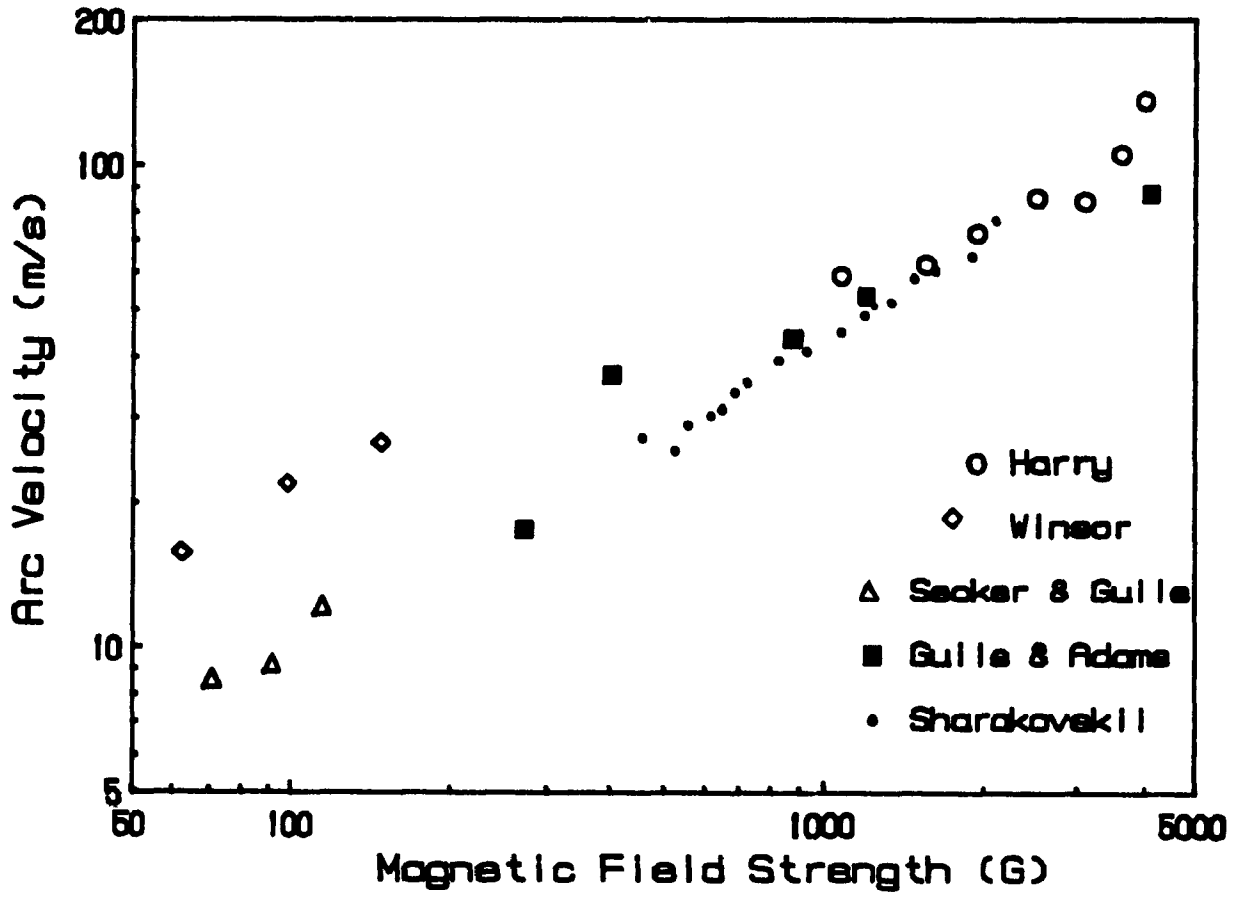


Figure 3.2 - Arc velocity vs magnetic field  
Results from the literature

Yas'ko (15) and Guile and Naylor (9) used dimensional analysis to determine the dependence of the arc velocity on arc current and magnetic field. After examining a large amount of data, Guile and Naylor proposed a relationship in the form of  $Vel \propto B^{0.6}I^{0.4}$  with a reported scatter of  $\pm 50 \%$ ; Yas'ko proposed  $Vel \propto B^{0.55}I^{0.45}$  with scatter of  $\pm 35 \%$ .

It was decided at this point to further investigate this problem of the dependence of arc velocity on magnetic field and arc current. This is presented in the next section.

## 6) MODIFICATION OF THE AERODYNAMIC DRAG FORCE COMPONENT

To develop equation 3.5 and the corresponding relations 3.6a and 3.6b it was assumed by the other researchers that the other terms in the drag force side of the equation were independent of the arc velocity. It will be shown here that this is not the case.

The term corresponding to the length of the arc in the direction perpendicular to the arc movement,  $d$ , is obviously constant for all  $Vel$ , since this is a geometric factor, depending only on the gap between the electrodes (the plane of the arc motion is characterized by the vectors  $\vec{E}$  and  $\vec{F}$  - see Figure 3.1).

The drag coefficient  $C_d$  is a function of  $Re$  for rigid cylinders. However it can be assumed constant for cylinders in cross flow at  $Re$  between 1 000 and 100 000 (Perry and Chilton (16)). In all the experiments in this work, the  $Re$  was between these two limit values. Kopainsky and Schade (7) also calculated  $C_d$  for a similar system and found that  $C_d$  was constant.

The diameter of the arc,  $D$ , is not independent of the arc velocity. It has been observed by different authors (Roman and Myers (3), Malghan and Benenson (5), Benenson and Baker (17)) that with zero arc velocity (or for stationary arcs, with no moving gas) the cross section of the arc column is circular. For increasing arc velocities (or increasing gas velocities for stationary arcs) the cross section of the arc column becomes an ellipse, with the major axis perpendicular to the direction of arc motion. Using the Roman and Myers (3) data, it was possible to establish the following relation for changes in  $D$  with arc velocity:

$$D = D_0 (Vel/Vel_0)^{0.11} \quad 3.7$$

where the subscript 0 refers to any reference condition.

In the case of continuous operation between concentric electrodes, the gas density in front of the moving arc is affected by the previous arc passage at the same space region, i.e., the arc burns in its own tail. This has been observed by Kopainsky and Schade (7). Using their data the gas density can be correlated with the arc velocity as follows (a similar correlation was also proposed by Sharakhovskii (13));

$$\rho = \rho_0 (Vel/Vel_0)^{0.5} \quad 3.8$$

where the subscript 0 refers to any reference condition.

These are the changes to be incorporated into equation 3.5 when the arc current is kept constant and just the magnetic field is varied. If the arc current is also varied, another correction should be included, since the arc diameter  $D$  increases for increasing currents. Lowke (18) studied the variation of arc diameter with arc current for stationary arcs, obtaining for the range of  $1 < I < 10\,000$  A,

$$D = D_0 (I/I_0)^{0.15} \quad 3.9$$

where the subscript 0 refers to any reference condition

### 7) ADDITION OF SURFACE DRAG FORCE

Up to this point, the arc velocity was analyzed by considering the forces acting on the arc column. There is another force affecting the arc movement; this force is related to the electrodes, and as it will be seen, specifically to the cathode surface. This force, which will henceforth be called the "surface drag force", is a function of the electronic state of the cathode surface, being independent of the magnetic field strength and arc current. This subject will be extensively covered in the following sections and in the next Chapters.

Incorporating all these considerations to equation 3.5 we have for steady state (i.e., for an arc moving at constant velocity);

$$\Sigma \text{ forces} = 0$$

$$B I d + 0.5 C_d d D(f(I, \text{Vel})) \rho(f(\text{Vel})) \text{Vel}^2 + S = 0 \quad 3.10$$

where  $S$  = surface drag force  
and the other terms as defined before

And from equation 3.10,

$$\text{Vel} \propto B^{0.62} \quad 3.11a$$

$$\text{Vel} \propto I^{0.56} \quad 3.11b$$

## 8) EXPERIMENTAL RESULTS - ARC VELOCITY

### A) External Magnetic Field

Experiments were performed using different plasma gases. The magnetic field was varied from 10 to 1 700 Gauss (0.001 to 0.17 T) and the arc velocity was measured using the optical probe. The arc velocities are shown as a function of the magnetic field strength in Figure 3.3. The exact composition of the plasma gases is discussed in the next Chapter. The following points can be raised from these results:

#### a) Scatter of data

The scatter in the four sets of data ( $N_2$ , He+0.4%CO, He+0.4% $N_2$ , Ar+0.3%CO) is very small for the whole range of magnetic field strength used. The lines in Figure 3.3 were obtained using linear regression of  $\log \text{Vel}$  vs  $\log B$ ; the equations and respective linear regression coefficients ( $r$ ) are:

He+0.4%CO	-	$\text{Vel} \propto B^{0.601}$	$r = 0.999$
He+0.4% $N_2$	-	$\text{Vel} \propto B^{0.599}$	$r = 0.999$
$N_2$	-	$\text{Vel} \propto B^{0.603}$	$r = 0.997$
Ar+0.3%CO	-	$\text{Vel} \propto B^{0.600}$	$r = 0.999$

The relation found for the four lines,  $\text{Vel} \propto B^{0.60}$  compares very well with equation 3.11a developed in the last section.

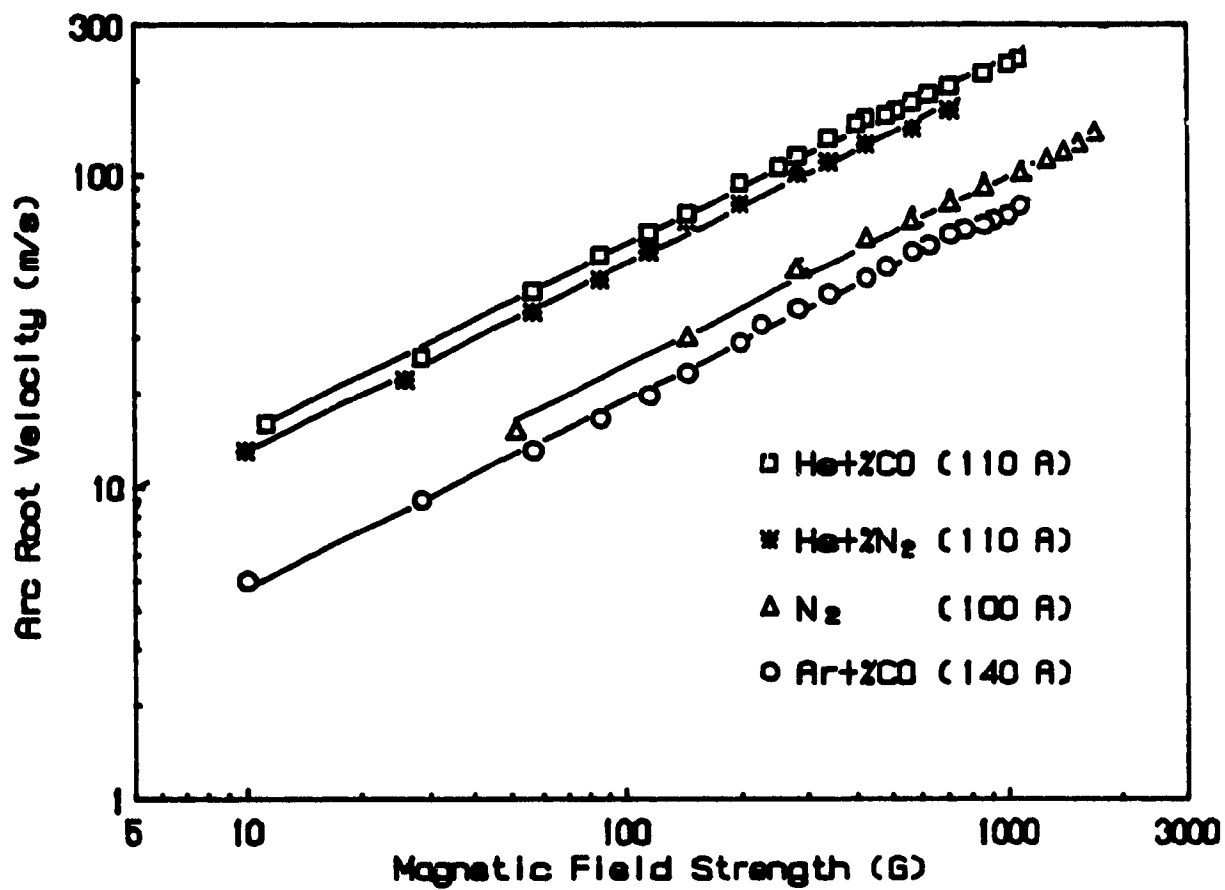


Figure 3.3 - Arc velocity vs magnetic field

Results for Ar+0.3%CO; He+0.4%CO; He+0.4%N<sub>2</sub>; N<sub>2</sub>

b) Different arc velocities

The differences among the four lines must be explained in more detail. These differences are discussed below, where two gases were compared at each time. Since the arc currents were different for the experiments (due to limitations of the power supply), the results were "normalized" to 100 A using equation 3.11b. The results of the normalization are presented in Figure 3.4.

$$\text{Vel}' = \text{Vel} (I/100)^{0.56} \quad 3.12$$

where Vel is the velocity for arc current I.

Vel' is the arc velocity plotted in Figure 3.4.

i) Ar+0.3%CO and He+0.4%CO

For reasons which will become clearer in the next section, it was necessary to contaminate Ar and He with small amounts (less than 1% in volume; see next Chapter) of CO (or some other contaminant; see next section) in order to have the arc moving according to equation 3.11a. The CO minimized the effect of the surface drag term for these two gases (this is discussed throughout the thesis).

To explain the differences in arc velocity at the same B, it is necessary to concentrate just on the aerodynamic drag force of equation 3.10. In this equation,  $C_d$  is considered constant and the same for both. The density of the gas in front of the arc,  $\rho$  in equation 3.10, has been corrected for changes in the arc velocity but not for density differences due to different atomic masses. Since the level of contamination (CO) of the inert gases is small, the densities can safely be assumed to be the values for the pure inert gases. Thus  $\rho_{\text{He}} / \rho_{\text{Ar}} = 4 / 40$  and using equation 3.8, the arc velocities become:

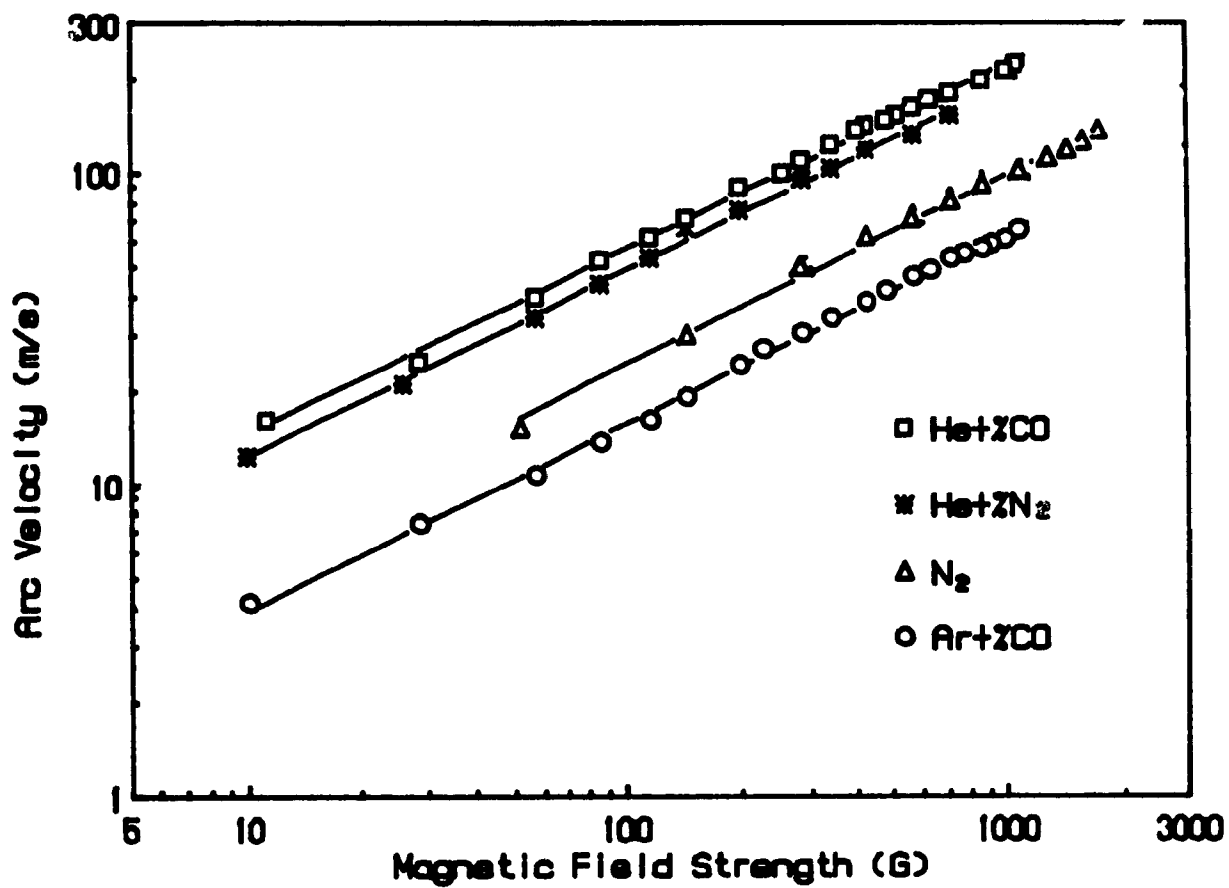


Figure 3.4 - Arc velocity vs magnetic field  
Current normalized curves

$$Vel''_{He+0.4\%CO} = Vel_{He+0.4\%CO} (4/40)^{0.60} \quad 3.12$$

where  $Vel''$  is the corrected  $Vel$

The corrections bring the two curves to within 8 % of each other as shown in Figure 3.5. This small difference can be due to different plasma temperatures; this is better explained when He+0.4%N<sub>2</sub> and N<sub>2</sub> curves are compared.

The diameter of the arc column for the two gases was considered in the above analysis to be the same for both gases. The diameter of the arc transverse to the direction of the arc movement has never been accurately measured, but it should not be very different.

ii) He+0.4%CO and He+0.4%N<sub>2</sub>

Small amounts of CO and N<sub>2</sub> (less than 1% in volume in both cases) were added to helium in order to have the arc moving according to equation 3.11a. No correction of gas density for different atomic masses is necessary, since the main gas is helium in both cases. The differences in these arc velocities can be understood when the surface drag term is examined. There is some evidence that the electron emission characteristics of the surface when CO is used as the contaminant are better than when N<sub>2</sub> is used (see section 9 and 10 in this Chapter and also work function measurements in Chapter IV). This would cause a higher value for the surface drag force for He+0.4%N<sub>2</sub> than for He+0.4%CO, although a quantification of this term is not possible at the present stage. This higher surface drag was also verified when Ar instead of He was used as the main gas.

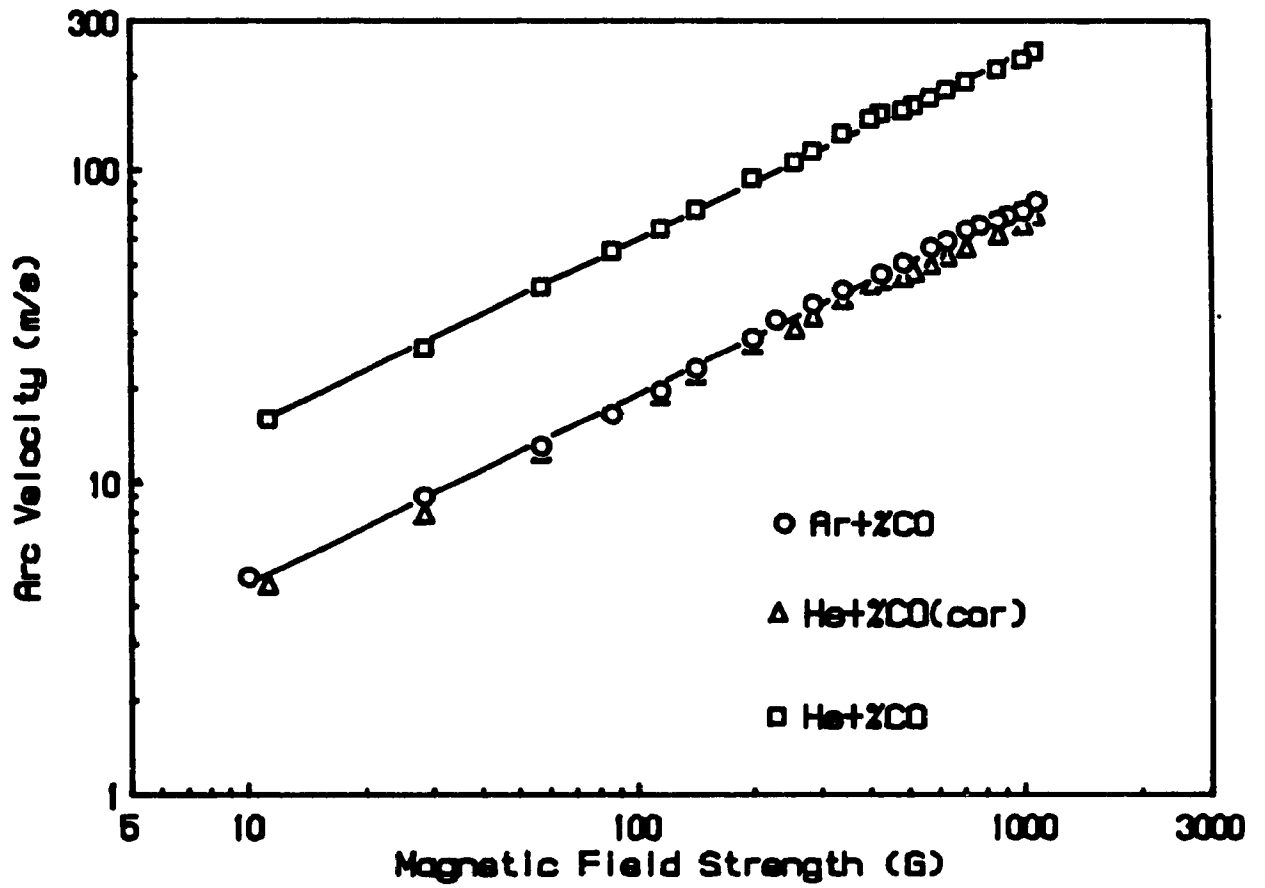


Figure 3.5 - Arc velocity vs magnetic field. Density correction.

Results for Ar+0.3%CO and He+0.4%CO

iii) He+0.4%N<sub>2</sub>, and N<sub>2</sub>

In this case it is necessary to consider the difference in densities of the two main gases (He and N<sub>2</sub>). Using the same relation as before,

$$Vel''_{N_2} = Vel_{N_2} (28/4)^{0.60} \quad 3.13$$

results in the curve N<sub>2</sub> corrected shown in Figure 3.6.

This density correction was insufficient to bring the two curves together and so other aspects should be investigated. It is likely that the surface drag in both cases was similar (see next Chapter) and therefore this term cannot be the cause of the difference in the two curves.

Two possible causes can explain the differences in the two curves: σ) different plasma gas temperature and ρ) different arc column diameter.

σ) The different plasma gas temperature would cause different gas densities, changing the overall aerodynamic drag force. Temperatures of the gas in the region in which the arc travels are extremely difficult to obtain, since this region is not hot enough for spectroscopic analysis and a thermocouple or probe inserted in this region would tremendously affect the arc movement. Circumstantial evidence suggests that He and N<sub>2</sub> do in fact have different temperatures: the outlet gas temperature for N<sub>2</sub> is much higher than for He and the ceramic protecting the anode melted in the N<sub>2</sub> experiments. Also Johnson et al (19) found higher temperatures for N<sub>2</sub> plasmas than for He. The higher N<sub>2</sub> temperature can therefore explain the apparently faster arcs for N<sub>2</sub>, since the aerodynamic drag would be smaller (lower gas density).

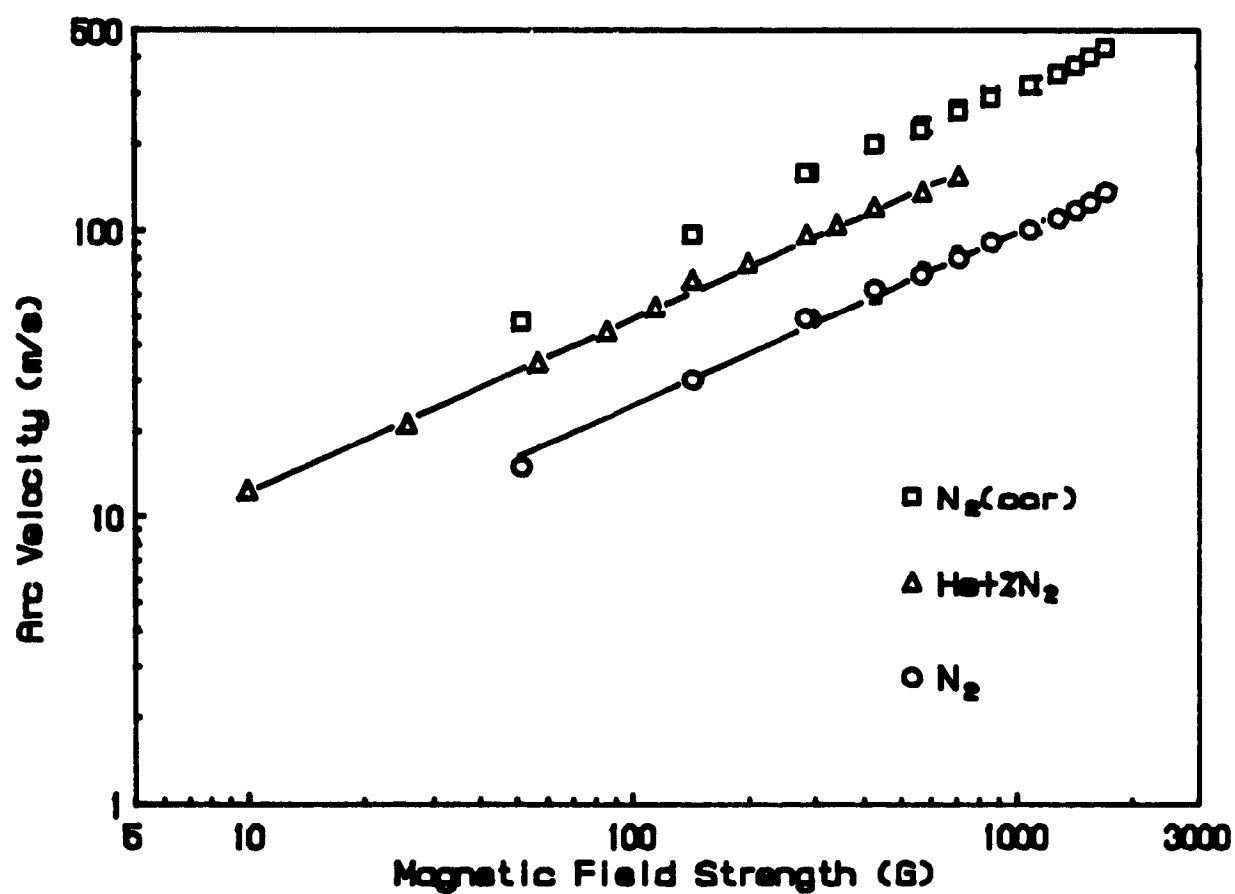


Figure 3.6 - Arc velocity vs magnetic field. Density correction.

Results for He+0.4% $N_2$  and  $N_2$

9) There is also some evidence that the diameter of the arc for polyatomic gases is smaller than for inert gases. This is caused by the larger energy needed to maintain an arc using polyatomic gases (dissociation energy plus ionization potential of the atoms) than for inert gases (ionization potential of the atoms only). Johnson et al (19) showed photographs illustrating the smaller arc column for nitrogen than for helium. It is however extremely difficult to estimate the arc diameter using optical measurements since the visual arc diameter does not necessarily reflect the aerodynamic drag diameter.

In conclusion, although no direct measurement is possible to verify which of the above explanations is the correct one, both suggest that the aerodynamic drag force for nitrogen arcs is smaller than for helium arcs for the same operating conditions and after correcting for the effect of different intrinsic gas densities. Similar analyses can be made for Ar+0.3%CO and He+0.4%CO. The 8 % difference in their arc velocities after correcting for the different atomic weight could be explained by a higher gas temperature for Ar than for He. This seems to be the case, although the temperature difference here is much smaller than that for N<sub>2</sub> and He (Johnson et al (19)).

#### B) Arc Current

Since the variation of the arc current in the experiments in this work was small (100-140 A) due to limitations of the power supply, it was not possible to check equation 3.11b, i.e.,

$$Vel \propto I^{0.56}$$

However a comparison was made between our results and those of different authors working at the same conditions of plasma gas, magnetic field strength and geometry. The results are presented in Table 3.2; the arc velocities were "corrected" for 100 A

using equation 3.11b for 100 A, i.e.,

$$\text{Vel}' = \text{Vel} (100/I)^{0.56} \quad 3.14$$

The magnetic field strength was 1 000 G and the geometry was the same for all the results.

**TABLE 3.2**  
Arc Velocities for Different Arc Currents  
(air plasmas were used in all cases)

Author	Arc Current (A)	Arc Veloc. (m/s)	Arc Veloc. correc. (m/s)
This work	100	60	60
Harry (12)	200	86	58
Sharakovskii (13)	850	170	52

The arc velocities corrected using equation 3.11b are reasonably close. The value of Sharakhovskii is lower than expected; this may be due to the higher gas flow rates he used. This would give a lower temperature and thus a higher gas density (Shabol'tas and Yas'ko (20)). It is concluded that equation 3.11b can be used safely within at least the range 100-850 A.

### C) Self Magnetic Field

One last point should be considered before leaving this section; this is the effect of the a) arc self-magnetic field and the b) magnetic field generated by the passage of current in the electrodes. These fields could, in principle, affect the arc velocity.

a) Using the Ampere's circuital law, the arc self magnetic field was calculated to be 50 Gauss; however in this case it produces no net force affecting the arc movement. This field is important only for the "pinch effect" and the formation of "kinks" in the arc column (Bittencourt (21)).

b) The magnetic field generated in the electrodes is very difficult to calculate due to the geometry used; it should also be very small because the current is collected symmetrically from the cathode as explained by Secker and Guile (10)).

Two simple experimental tests were performed to examine the importance of this field on the arc movement. Firstly the direction of the magnetic field was inverted by reversing the current in the coil, forcing the arc to move in the reverse direction. Since the magnetic field generated by the current in the electrodes is always in the same direction, a difference in the arc velocity between the two experiments would indicate the presence of an electrode magnetic field. The arc velocity was identical in both experiments, for magnetic fields higher than 15 G. The minimum magnetic field used in these experiments was 10 G due to limitations in the coil power supply. A 10 % difference between the arc velocities in the two experiments was detected when a magnetic field of 10 G was used. The use of equation 3.11a to explain this difference would result in an "electrode" magnetic field of approximately 1 G.

In the second test, the external magnetic field was cut off when using contaminated Ar with small amounts of CO. The arc still moved with a velocity of 1.5 m/s. Using equation 3.11a, this gives a magnetic field strength of 1.5 G, confirming the previous value. Since this value was very small, it did not significantly influence the arc movement, especially for magnetic fields higher than 10 G.

### 9) ARC MOVEMENT - SURFACE DRAG

It was shown in the last section that changing the plasma gas from air (used by other researchers) to N<sub>2</sub> (or Ar and He contaminated with small amounts of polyatomic gases) produced much less scatter of arc velocity data, allowing a better understanding of the aerodynamic drag force. In this section, it is proposed that the reasons for this are related to the surface drag.

Firstly it is necessary to understand how the arc moves. In the case where an external magnetic field is applied, the arc column interacts with this magnetic field, "producing" the Lorentz force, equation 3.3. However, it has been suggested by some authors that the electrode arc attachment movement could control the overall arc movement (Secker and Guile (10)); this was more extensively studied for vacuum arcs (see for example Rakhovskii (22) and Sherman et al (23)). The control of the arc movement by the arc attachment on the cathode is referred to in this work as surface drag by analogy with the aerodynamic drag experienced by the arc moving in the gas. The surface drag is related to the local capacity of the cathode to emit electrons. Overall the macroscopic arc movement and the surface drag can be understood as:

- the arc column moves from one discrete arc attachment to another on the cathode, depending on favourable voltage drop and cathode electron emission characteristics,

i.e., the arc will move to the next site if the combined voltage drop due to the arc column and electrodes are less than those at the present site. The column voltage is increased by the stretching of the arc by the magnetic field (Lorentz force applied to the arc column) so that at some point, the arc is forced to move to a new site. Thus the ease with which a cathode emits electrons affects the speed at which the arc can move and an apparent "surface drag" increases for increasingly difficult electron emission. These ideas were extensively examined in this study. In reality the arc attachment is made of a finite number of microscopic arc cathode spots; this is the microscopic view of the arc movement and it is discussed in Chapter VI.

When pure Ar and He were used as the plasma gases, the arc velocity was almost independent of the magnetic field (Ar) or showed a step function decrease at a threshold magnetic field (He) as shown in Figures 3.7a and 3.7b respectively. These behaviors cannot be explained by the effect of the aerodynamic drag force alone. When the inert gases were contaminated with polyatomic gases (CO, N<sub>2</sub>, etc), the changes of the arc velocity with magnetic field could be predicted by equation 3.11b. The conclusion was that for pure inert gases, the surface drag was high (poor electron emission) and that it "controlled" the overall arc movement; when the gases were contaminated, the surface drag decreased (ease of electron emission) and the arc velocity was "controlled" by the aerodynamic drag. Cheng and Xie (24) showed experimental results consistent with these explanations. The changes in the values of surface drag with different contaminants and the concentration of these contaminants will be covered in the next Chapter, Surface Analysis.

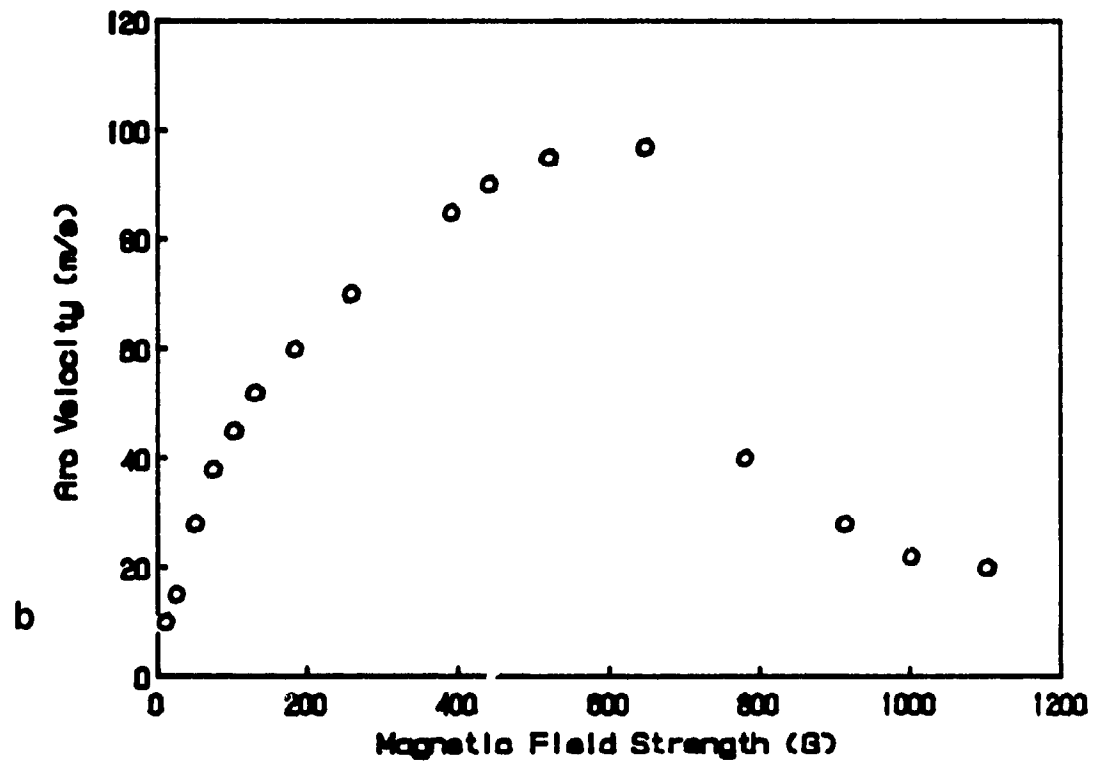
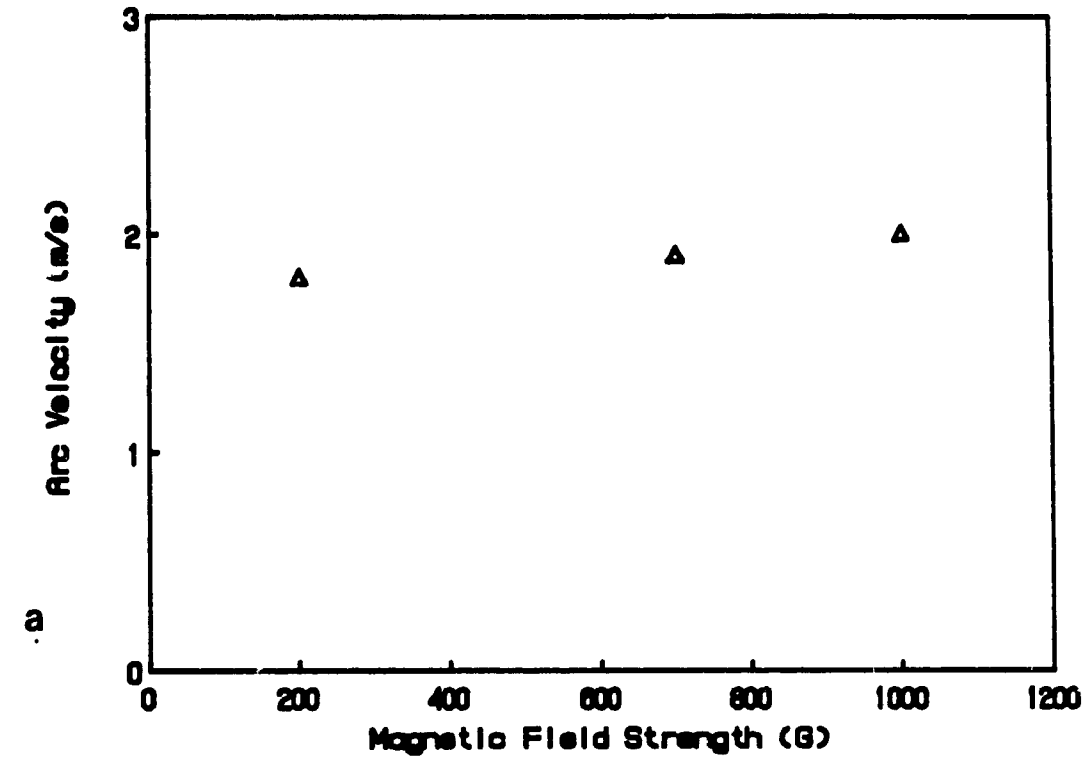


Figure 3.7 - Arc velocity vs magnetic field

a) Argon

b) Helium

The addition of contaminants, for example CO in He, caused changes in the arc velocity as well as in the arc voltage. These changes can be explained as follows: electron emission from a clean copper surface is difficult and thus surface drag "retards" the movement (low velocity). The magnetic field stretches the arc, increasing its length and thus its voltage. When the electrode surface is contaminated (using contaminated inert gases or polyatomic gases - see next Chapter), electron emission is easier, allowing faster movement of the arc root (giving higher velocities) and less stretching (lower voltages).

Values for arc velocity and arc voltage are presented in Table 3.3 for pure Ar and He as well for both gases contaminated with different polyatomic gases. The gas flow rate for all experiments was 20 liters per minute and the magnetic field strength was 1 000 G. The concentrations of the polyatomic gases in the inert gases are less than 1 % in volume.

It can be seen from this Table that the addition of O<sub>2</sub> and N<sub>2</sub> produced smaller changes in arc velocity than CO, CH<sub>4</sub>, H<sub>2</sub>S and Cl<sub>2</sub>. This suggests that the surface drag is highest for pure inert gases, intermediate with N<sub>2</sub> and O<sub>2</sub> as contaminants, and lowest for the rest of the contaminants listed above. The reasons for the different behaviors depending on the contaminant used and correlations with the electron emissivity of the surface are discussed further in the next Chapter.

TABLE 3.3

Arc Current, Velocity and Voltage for Different Plasma Gases

GAS	ARC CURRENT (A)	ARC VELOCITY (m/s)	ARC VOLTAGE (V)
Ar	100	2	44
Ar+0.3%N <sub>2</sub>	100	33	37
Ar+0.04%O <sub>2</sub>	100	37	32
Ar+0.3%CO	140	75	22
Ar+0.3%Cl <sub>2</sub>	140	75	22
Ar+0.3%CH <sub>4</sub>	140	75	22
Ar+0.3%H <sub>2</sub> S	140	70	23
He	110	20	105
He+0.4%N <sub>2</sub>	110	180	52
He+0.04%O <sub>2</sub>	110	190	50
He+0.4%CO	110	240	46
He+0.3%Cl <sub>2</sub>	110	230	48

An electronic camera (IMACON) was used to take photographs of the arc during the different operating conditions. Figures 3.8a and b show tracings of high speed photographs of the arc when He was contaminated with  $N_2$  and for pure He. Figures 3.9a and b show the tracings for Ar+0.3%CO and pure Ar respectively.

It can be seen from these figures that the arc is much shorter for the contaminated gases (less "magnetic stretching"), explaining the lower voltage. It also can be seen that the arc attachment at the cathode lags behind the arc column for the pure inert gases. This confirms the idea that surface drag is caused by the condition of the cathode surface. It will be shown in Chapter VI that the ease of electron emission also influences the cathode erosion rates.

The above discussion has been limited to experimental conditions where the degree of contamination was small, resulting in a "thin" contaminant layer on the cathode surface. Guile et al (25,26), Poeffel (27) and also Cheng et al (28) suggested that the thickness of the contaminating layer could affect the electron emission. This subject will also be examined in Chapter IV, but for now it will only be shown that "thick" layers also affect the arc movement. The definition of a "thick" layer is somewhat arbitrary, and varies for each author. In general, a layer more than 10  $\mu\text{m}$  in thickness is considered to be "thick".

Figure 3.10 shows the variations in arc velocity for increasing concentrations of CO in Ar (similar results were obtained with  $Cl_2$ ) for constant magnetic field (1 000 G) and similar arc currents (140 for Ar contaminated with less than 1 % of CO, 100 A for concentrations of CO above 1 % and for pure Ar). For concentrations up to 1 %, the arc velocity increases with increasing contaminant concentration. Around 4 %, there is a sudden drop in arc velocity and after this, the arc velocity increases for higher concentrations of CO.

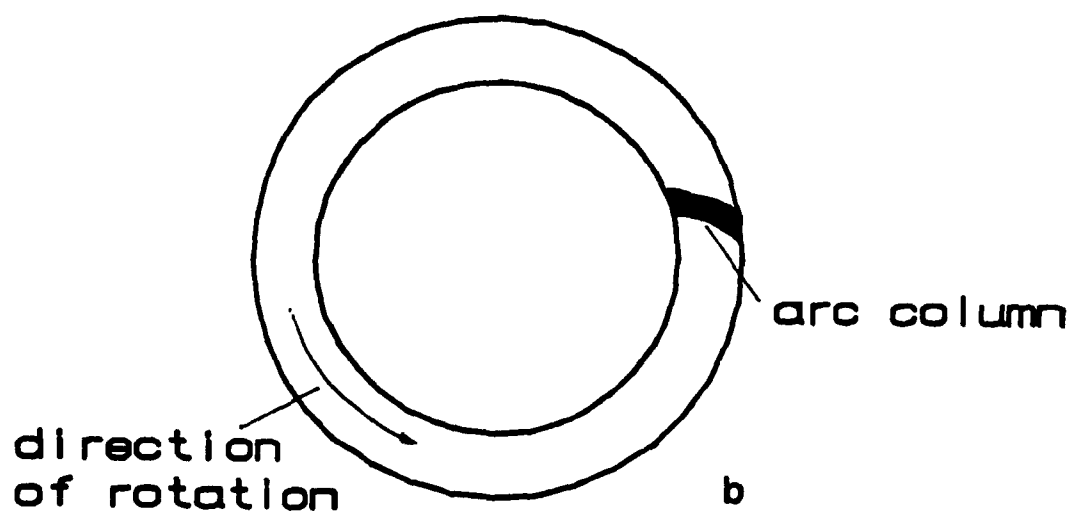
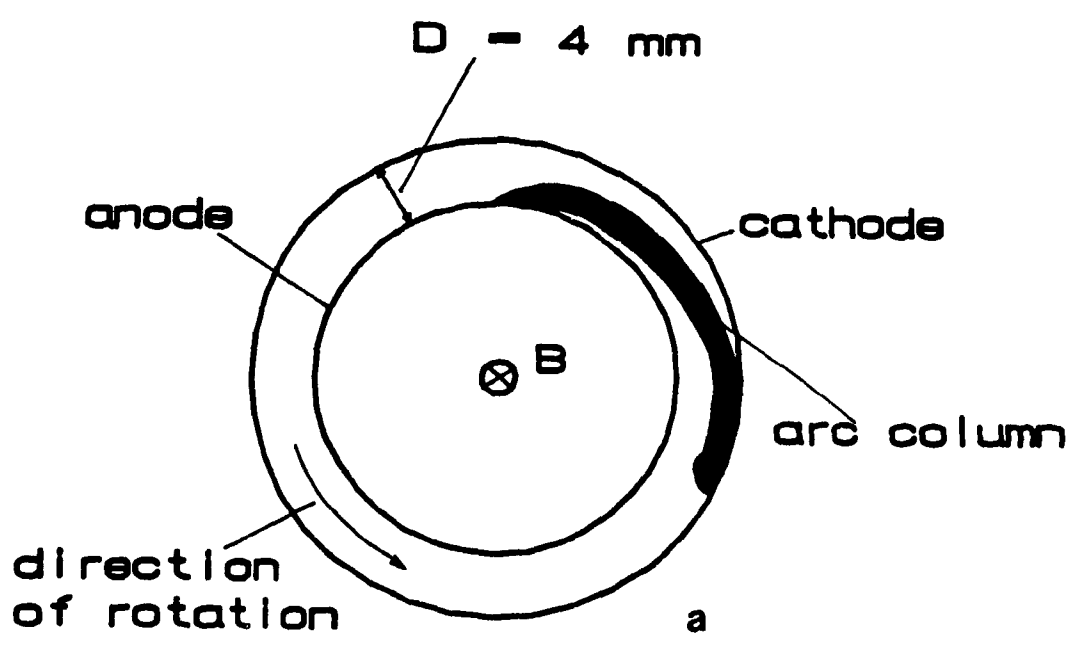


Figure 3.8 - Tracings of high speed photographs  
a) He                      b) He+0.4%N<sub>2</sub>

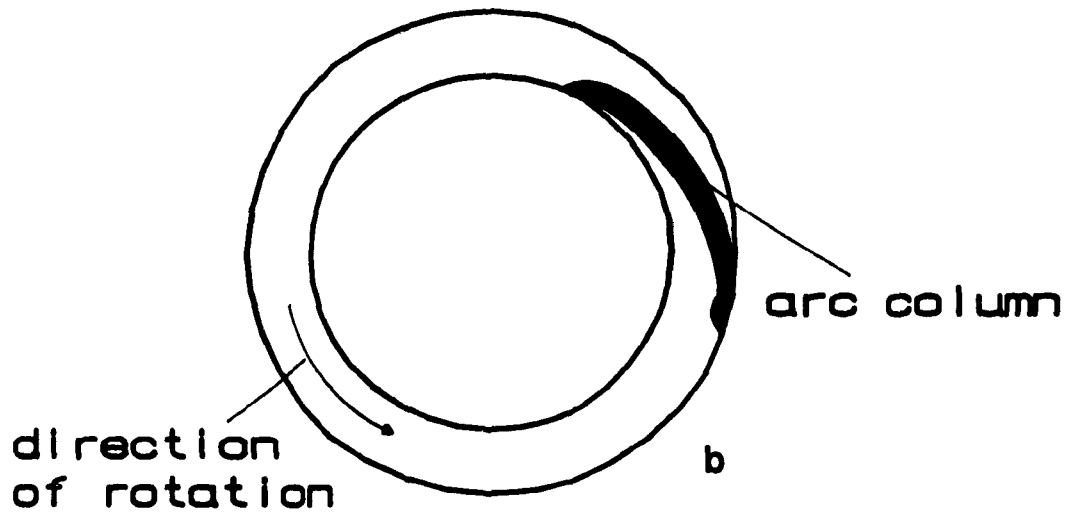
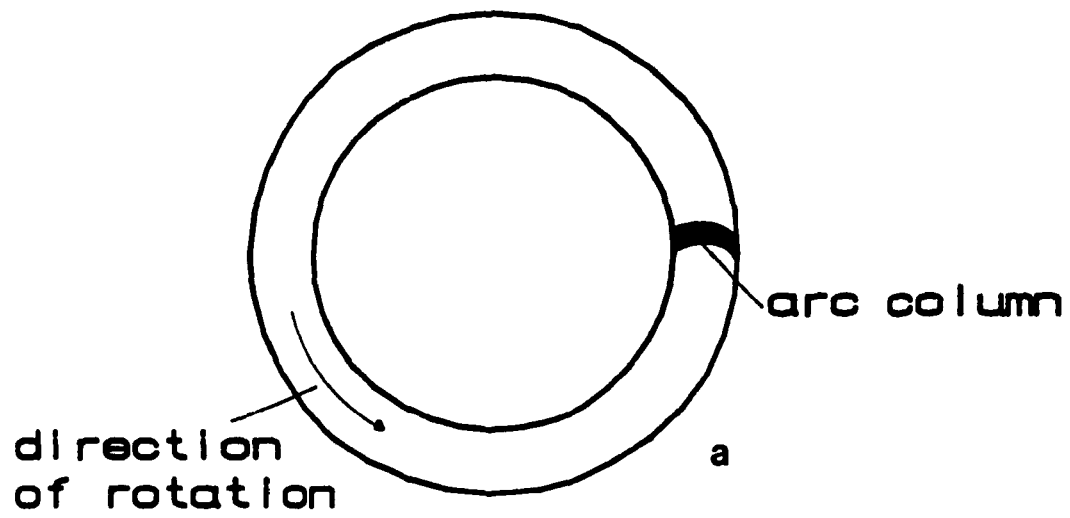


Figure 3.9 - Tracings of high speed photographs

a) Ar+0.3%CO

b) Ar

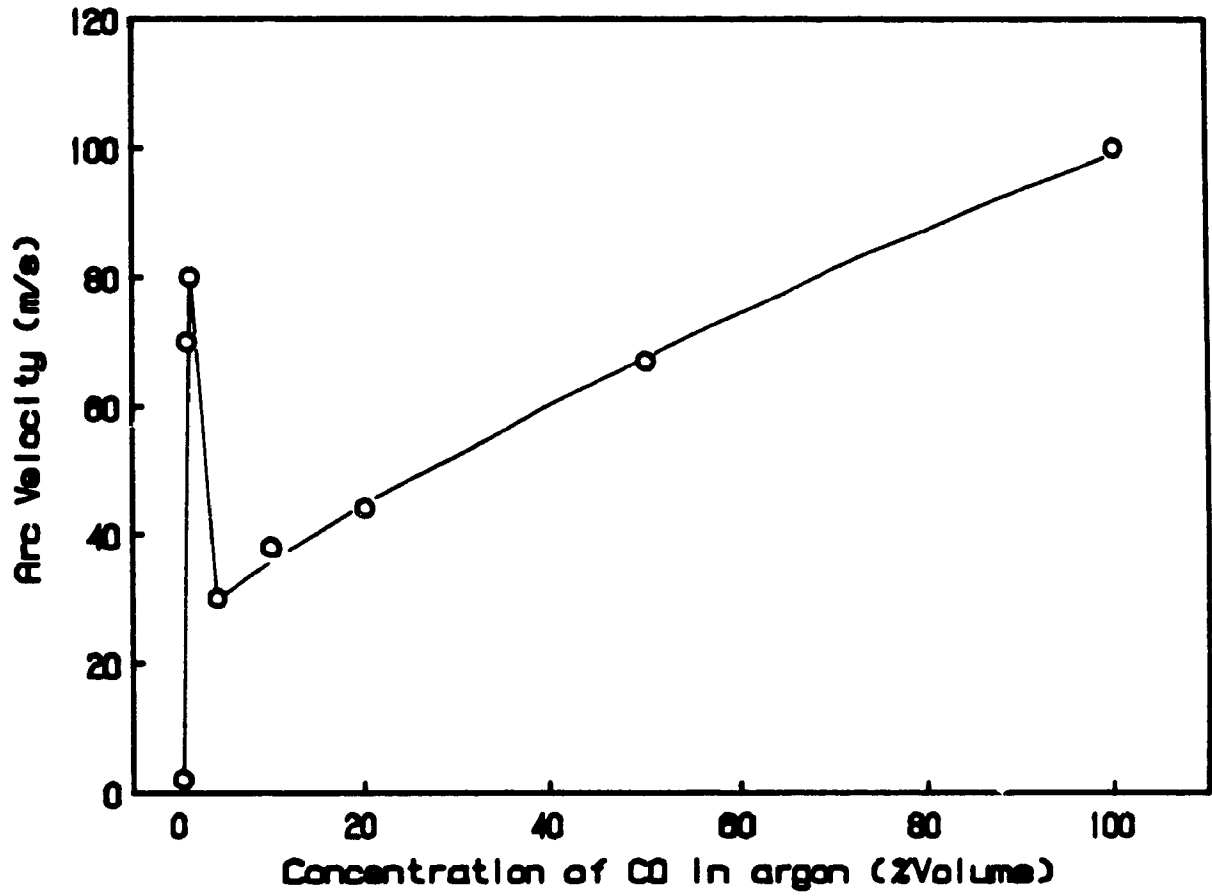


Figure 3.10 - Arc velocity vs concentration of CO in argon

These changes can be explained as follows: for pure Ar, the surface drag is highest. When less than 1 % CO is added to Ar, the surface drag reduces dramatically, and the arc velocity is "controlled" by the aerodynamic drag (Figure 3.3). Around 3-4 %, the surface drag increases to a value between a "clean" and "slightly" contaminated surface, decreasing the overall velocity. When the surface of the electrodes was visually examined after the experiments, no visible layer was found on the copper surface for less than 1 % CO. A "thick" layer was found for 4 % CO and above. For concentrations of CO above 4 %, the increase in the arc velocity with increasing concentrations of CO is probably due to changes in the arc column characteristics (density, temperature, arc diameter) rather than on the surface. These changes can be explained by the aerodynamic drag term. Similar changes in arc velocity for increasing concentrations of the contaminant were also observed with nitrogen as the contaminant.

It is now possible to understand the scatter of data for arc velocity versus magnetic field found in the literature when air was used as the plasma gas. Air will oxidize the copper (or brass) cathode surface, forming films that have different thicknesses depending on the duration of the experiments (some of the reported experiments were very short ( $< 1$  s) or in the case of rail electrodes, not continuous), on the arc power (surface temperature) and on the gas flow rate (surface temperature, gas mixing). Therefore, it is likely that for some operating conditions, the layers had different thicknesses, giving different values of surface drag force, generating the arc velocity scatter. Experiments with pure dry air also generated a higher scatter of the arc velocity in this work than when low levels of contaminants (including dry air) were added to the inert gases. The use of small amounts of contaminants produced a more uniform layer (minimum thickness) resulting in more uniform surface drag and arc velocity.

## 10) HIGH SPEED MOVIES

The arc movement and arc characteristics for different plasma gases and operating conditions were also studied using a high speed movie camera. The experimental set up was similar to that for the IMACON. An important difference was that instead of having water flowing from the top to the bottom of the central anode, this electrode was redesigned to incorporate an internal circulation of water, as shown in a schematic diagram in Figure 3.11. This allowed the full view of the arc to be photographed, avoiding the obstruction caused by the lower cooling channel. Calibration tests showed that the new arrangement caused no changes in the arc velocity, voltage, erosion rate or heat transferred to the electrodes.

The filming was done at 5 000 frames/second, calibrated by a fiber optics/oscilloscope arrangement and the exposure time per frame was 80  $\mu$ s. Table 3.4 summarizes the operating conditions used for the filming.

A characteristic tracing of the arc for each experiment is shown in Figure 3.12. A) qualitative description of the films, followed by B) qualitative analysis and C) quantitative analysis, is presented in the following pages.

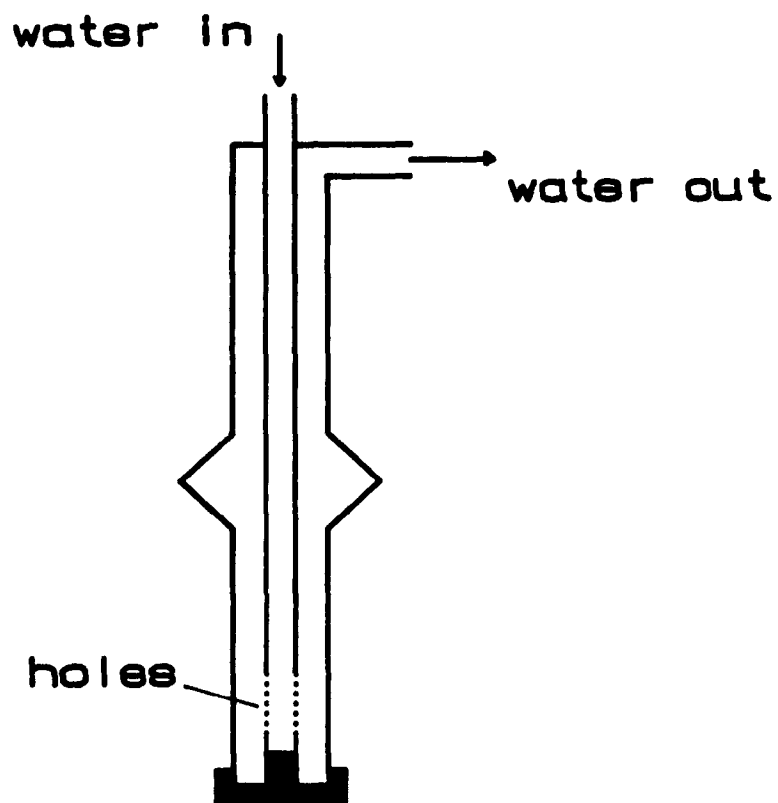


Figure 3.11 - Geometry of the central electrode used in the high speed filming

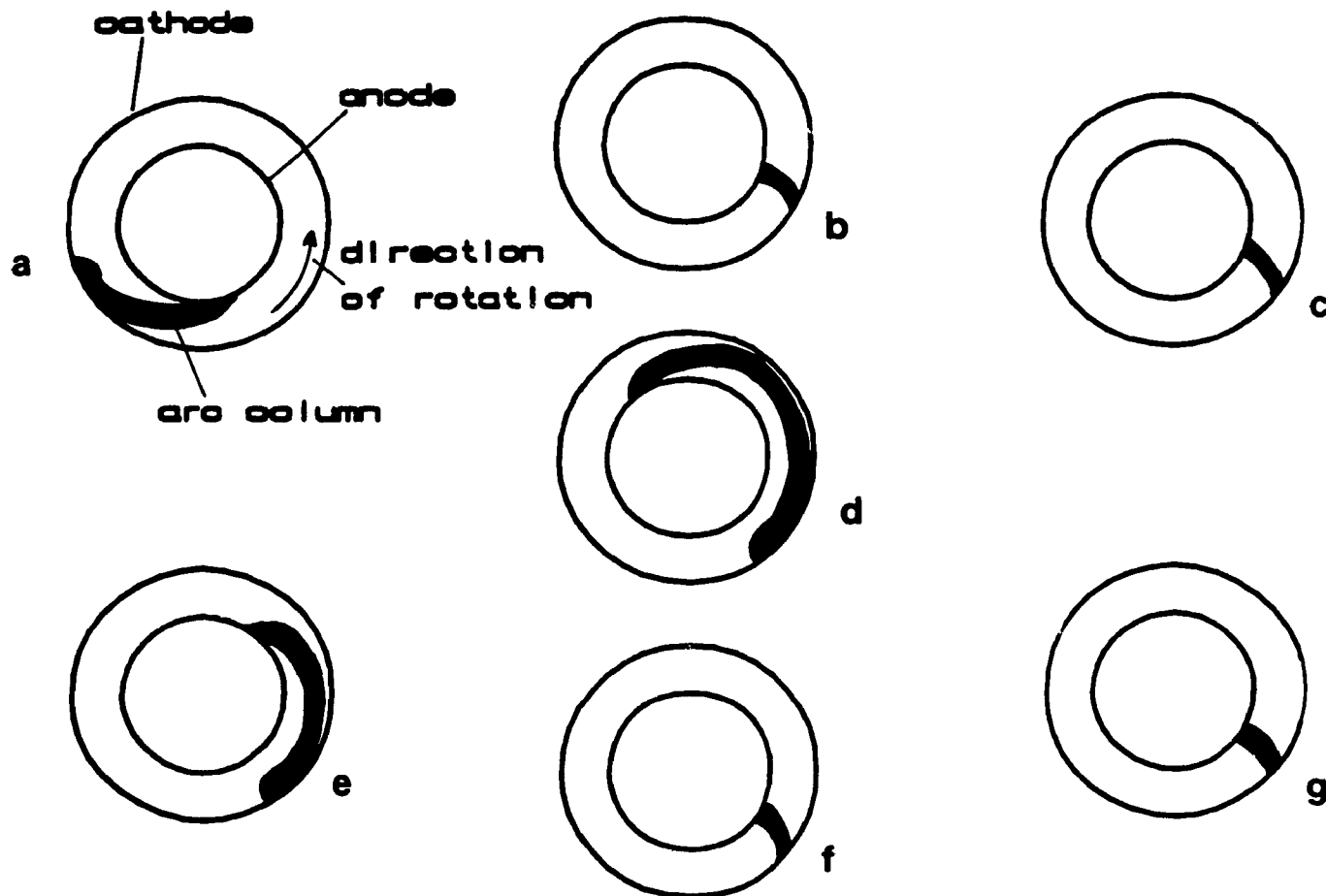


Figure 3.12 - Characteristic tracings of high speed filming

- |                   |                          |                          |                     |
|-------------------|--------------------------|--------------------------|---------------------|
| a) Argon          | b) Ar+0.3%CO             | c) Ar+0.3%N <sub>2</sub> | d) Helium (1 000 G) |
| e) Helium (100 G) | f) He+0.4%N <sub>2</sub> | g) Nitrogen              |                     |

TABLE 3.4

## Arc Operating Conditions for High Speed Movies

GAS	MAG. FIELD (G)	ARC CURRENT (A)	ARC VELOCITY (m/s)	ARC VOLTAGE (V)
Ar	1000	100	2-4	44
Ar+0.3%CO	10	140	4	20
Ar+0.3%N <sub>2</sub>	150	100	6	32
He	1000	110	20	105
He	100	110	20	60
He+0.4%N <sub>2</sub>	50	110	30	45
N <sub>2</sub>	200	100	30	55

## A) Qualitative Description

### a) Ar

The arc is long, extending for almost 30 degrees (360 degrees covers the whole picture); the arc cathode root lags behind the arc. The arc movement is "jerky", the arc staying in a fixed position for one or more frames. The attachment of the arc at the cathode produces a much brighter spot than at the anode. Just one cathode spot is visible, although there seem to be multiple anode attachments.

### b) Ar+0.3%CO

The arc is very short, occupying less than 5 degrees. The arc column is perpendicular to both electrodes; the arc cathode root does not lag behind the arc column. The arc movement is very "smooth", with minimal variations of rotational speed. The plasma seems to be slightly more constricted at the cathode than at the anode, but no bright cathode spot is noted.

### c) Ar+0.3%N<sub>2</sub>

The arc column is essentially perpendicular to both electrodes, occupying around 3 degrees. The arc movement is extremely jerky; the arc is sometimes stationary, staying in the same location for one or many frames. The arc splits into two or up to four parts for a short time (typically for 1 to 6 frames); although the overall arc movement is forward (Lorentz direction), the separate parts occasionally move in a retrograde direction.

### d) He (1 000 G)

The arc is extremely long, extending for about 150 degrees. The arc cathode root always lags behind the arc. The movement is jerky, although due to the high velocity it is not possible to see the arc stationary (the arc always moved between frames).

The arc attachment at the cathode is much brighter than at the anode.

e) He (100 G)

The arc is much shorter than at 1 000 G, extending for approximately 40 degrees, although the arc movement is still jerky. The cathode root still lags behind the arc column, but less than for 1 000 G.

f) He+0.4%N<sub>2</sub>

The arc is short, occupying less than 5 degrees. The arc movement is smoother than for pure He. Multiple cathode roots are sometimes detected, as is the splitting of the arc column.

g) N<sub>2</sub>

For this short arc, extending for about 5 degrees, multiple cathode roots can sometimes be seen. The arc column also seems to be split sometimes. The arc movement is similar than for He+0.4%N<sub>2</sub>.

B) Qualitative Analysis

a) Ar and Ar+0.3%CO

The easy electron emission of the surface when Ar contaminated with CO was used, generated a much shorter arc (less stretching), with the arc cathode root moving with the arc column and not lagging behind it. The movement of the arc is smooth (aerodynamic control), in contrast to the behavior of the pure gas, where the surface drag is the controlling mechanism for the arc movement. The latter generates a jerky movement where the arc stays at the same position for some time and then moves to a new spot. The bright spot at the cathode for the pure inert gas indicates a higher temperature region, which is probably a reflection of the higher current density

at this region (see Chapter V).

b) Ar+0.3%N<sub>2</sub>

The cathode root does not lag behind the arc column for two reasons: firstly, the electron emission is better due to the contamination of the inert gas and secondly, the magnetic field is very weak, and so does not stretch the arc. Although the nitrogen contamination caused a decrease in the surface drag when compared to pure Ar, it is not as effective as CO, as demonstrated by the jerky arc movement. When the arc splits, the two (or more) arc columns tend to move in opposite directions; the repulsive force could be due to the change in pressure caused by the compression of the gas by the ion flow (Emtage (29)). Since the external magnetic field is weak, one of the split arc columns may move in the opposite direction of the arc movement, i.e., retrograde motion.

c) He (1 000 G) and He (100 G)

The two arcs had the same overall velocity with different magnetic fields; this was shown in Figure 3.7b. This behavior was unique of helium and is discussed in Chapter VI. The arc was shorter for the smaller magnetic field because in this case, the Lorentz force was smaller, causing less stretching of the arc.

d) He+0.4%N<sub>2</sub>

The arc movement was smoother than for pure helium due to the decrease in the surface drag. In all cases when N<sub>2</sub> was used, either as the contaminant or as the main plasma gas, the arc column split and multiple cathode roots were observed. This is probably related to the cathode surface modifications caused by this gas, and is discussed in the next Chapter.

e) N<sub>2</sub>

The arc movement was similar to that for He contaminated with nitrogen, showing that for nitrogen, after the "minimum level of contamination" is achieved, the surface drag is independent of concentration.

C) Quantitative Analysis - Histograms

The film was analyzed frame by frame for each rotation of the arc. In doing so, it was possible to measure how much the arc attachment on the cathode moved from one frame to another. After one complete rotation, a histogram of the arc movement was created; this histogram is a plot of how many times (events) the arc attachment "jumped" a certain distance. The histograms are presented in pairs, for easy comparison. The results from the histograms are correlated with the erosion rates of the cathode in Chapter VI.

a) Ar and Ar+0.3%CO

Figure 3.13 compares the histograms for pure Ar and Ar contaminated with CO. The Ar plot is an average of 5 rotations, with an average arc velocity of 3.5 m/s and the Ar+0.3%CO plot is an average of 4 different rotations, with an arc velocity of 4 m/s. It can be seen from Figure 3.13 that the jumping distribution for Ar is much broader than for Ar+0.3%CO. The arc moved much more smoothly and uniformly with the contaminated Ar; these differences will be reflected in the instantaneous arc voltage (see next section) and on the erosion rate. It will be shown that the residence time of the arc in a certain area can be related to the erosion rate (Chapter VI).

It should be noted here that the distance travelled by the arc between frames does not necessarily give the residence time of the arc at a certain area, since the arc

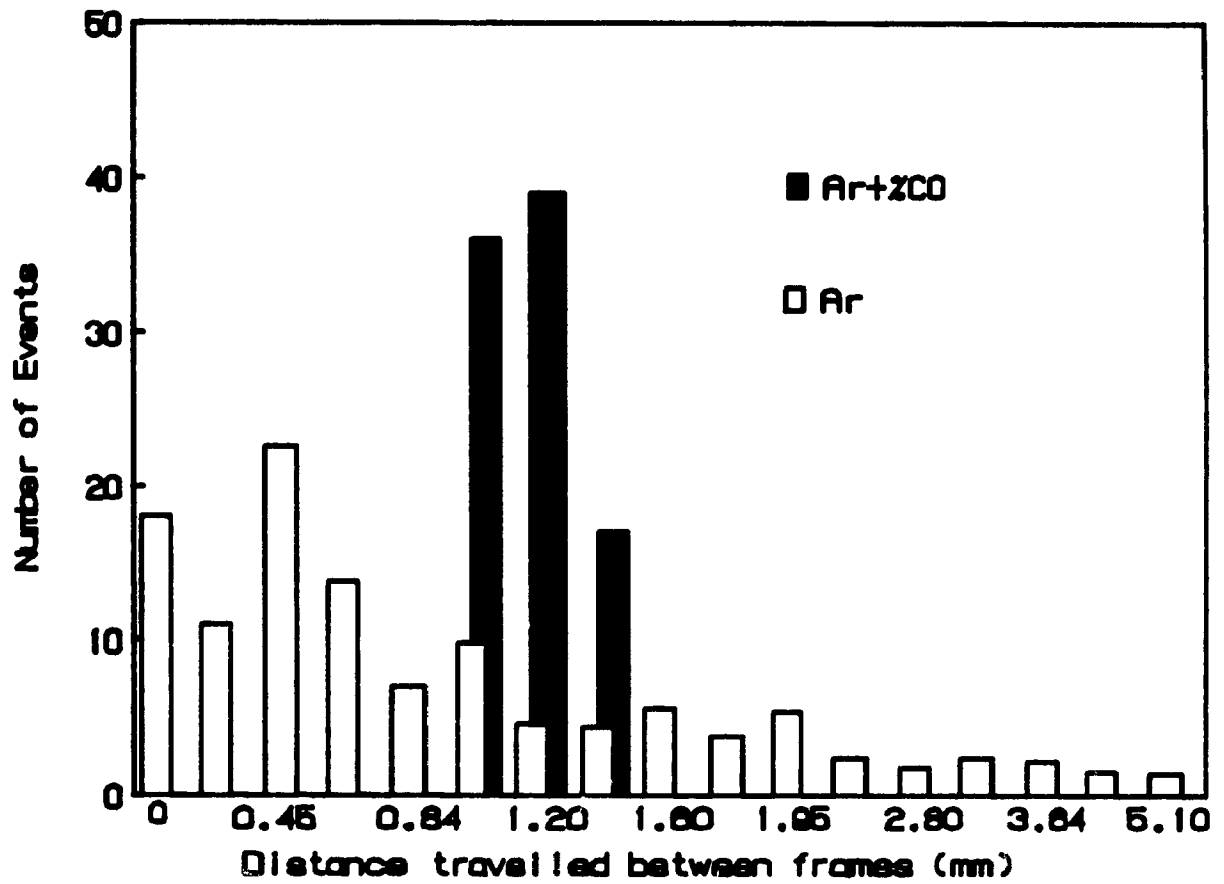


Figure 3.13 - Histograms from the high speed filming  
Results for argon and Ar+0.3%CO

could have moved to an intermediate position between frames; however for events of jump 0 (zero distance) this represents the minimum residence time of the arc in that particular position.

For the sake of comparison between the experiments, a "matching number" is defined. This number is a reflection of how many events two experiments had in common. Consider Ar and Ar+0.3%CO; around 100 jumps for Ar+0.3%CO and 120 jumps for Ar were measured per revolution. Of these 120 jumps for Ar, 20 jumps over all the distribution could be "matched" by corresponding Ar+0.3%CO jumps. For this case, the matching number is  $18 \pm 2$  % depending on whether the pure or contaminated Ar was used as a basis (20/120 or 20/100); this is a low matching number. As it will be seen in the next histograms, this number allowed easy comparisons between the results. A high matching number means similar arc behaviors.

b) Ar and Ar+0.3%N<sub>2</sub>

The histograms for Ar and Ar+0.3%N<sub>2</sub> are compared in Figure 3.14. For the contaminated Ar, the histogram is an average of 4 different rotations, with an arc velocity of 6 m/s. The two histograms show a very broad and similar distribution of "jumping distances". A reasonable interpretation is that although the surface drag was lowered by the contamination, the Lorentz force is small (low magnetic field) for the contaminated gas and these two effects balance each other. The matching number in this case is  $59 \pm 3$  % .

The number of events with "jumping distance" equal to zero is much larger for Ar+0.3%N<sub>2</sub> than for Ar. The temporal distribution of the zero jumping distances are shown in Figure 3.15 for the two gases and it may be noted that the arc in

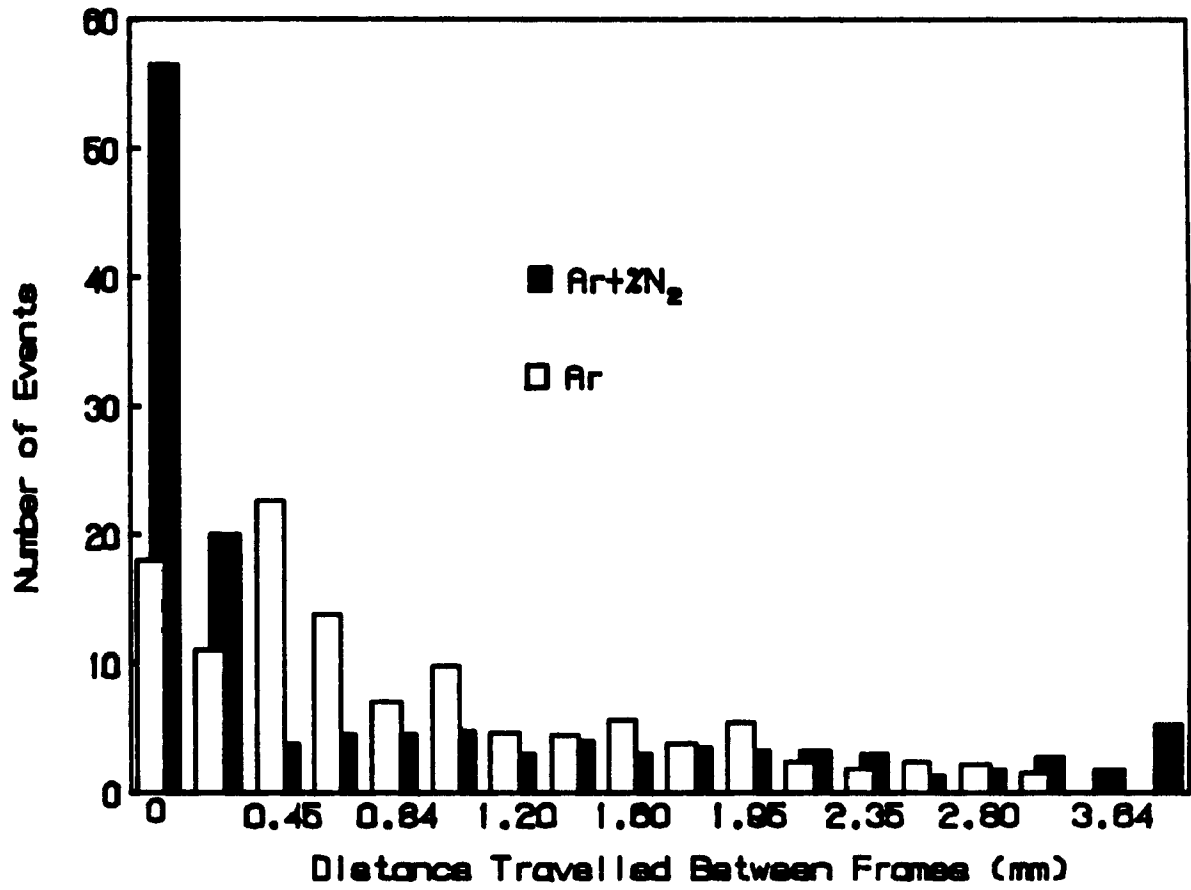


Figure 3.14 - Histograms from the high speed filming  
Results for argon and Ar+0.3%N<sub>2</sub>

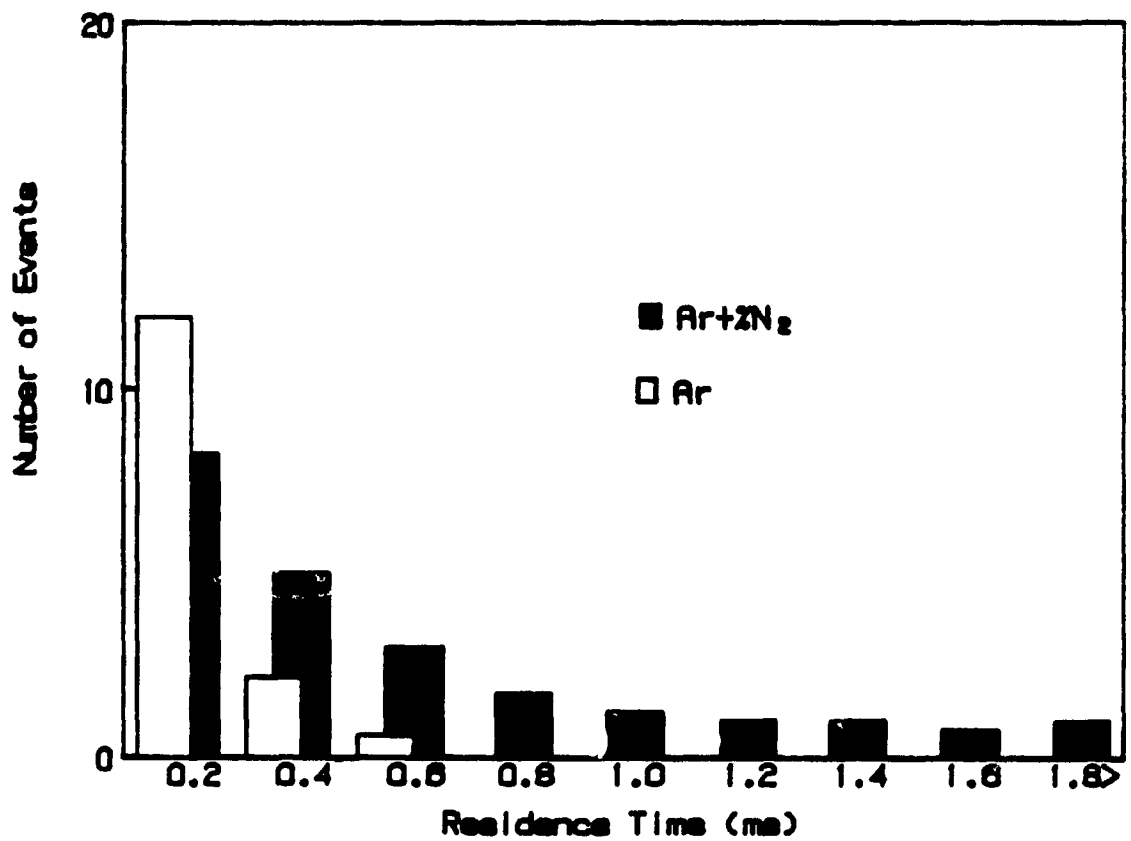


Figure 3.15 - Residence time of the arc attachment at the cathode  
Jumping distance zero - results for argon and Ar+0.3%N<sub>2</sub>

Ar+0.3%N<sub>2</sub> stays at a single spot for larger periods. This will have a direct impact on the erosion rates (Chapter VI).

It can be seen from Figures 3.13 and 3.14 that although the overall arc velocity in the three cases was similar, the arc movement was quite distinct for each experiment. Therefore any attempt to correlate arc velocity with erosion rates should also take into account the way the arc moves.

c) He (1 000 G) and He(100 G)

The histograms for these two cases are shown in Figure 3.16. The results are averages of 4 (1 000 G) and 3 (100 G) revolutions. The overall arc velocity was the same for both. It may be seen that with a lower magnetic field (lower Lorentz force), the jumping distance distribution is broader. The matching number for these two histograms is  $36 \pm 2 \%$ .

d) He+0.4%N<sub>2</sub> and N<sub>2</sub>

The histograms for these cases are presented in Figure 3.17. With similar arc velocities and magnetic field strength, the distribution of jumps is similar for both cases, with a matching number of  $64 \pm 3 \%$  (the highest number of all the experiments). This again confirms the idea that small amounts of N<sub>2</sub> in the gas affect the surface as much as with 100 % pure N<sub>2</sub>.

## 11) ARC CURRENT AND VOLTAGE FLUCTUATIONS

### A) Description

The arc current fluctuations can be an useful diagnostic tool for the arc movement. In order to measure these fluctuations a method was developed; it is described below.

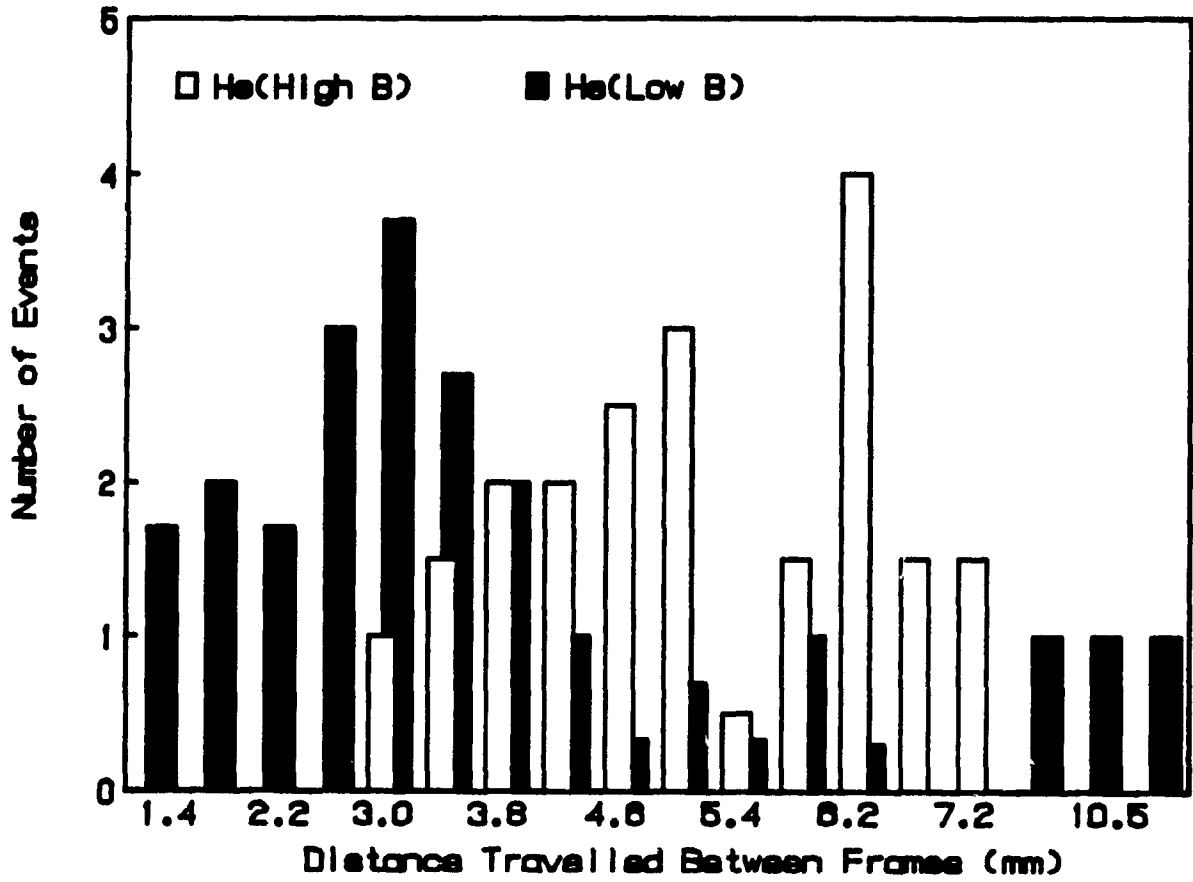


Figure 3.16 - Histograms from the high speed filming  
Results for helium at 1 000 G and 100 G

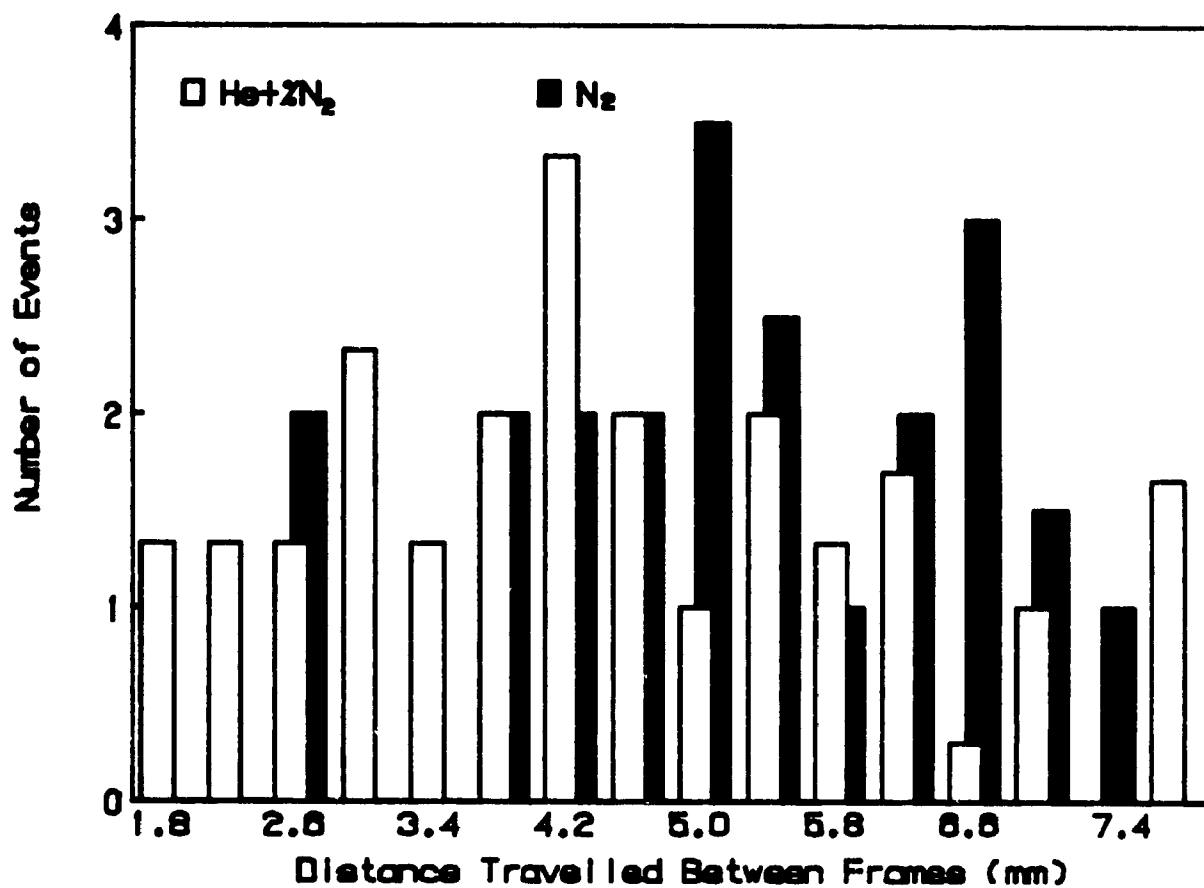


Figure 3.17 - Histograms from the high speed filming  
Results for He+0.4%N<sub>2</sub> and N<sub>2</sub>

A coaxial cable was used as a shunt after its impedance had been calibrated; the use of this type of a shunt is to minimize inductive effects. The shunt was connected in series with the cathode and the voltage drop across the shunt displayed on an oscilloscope. In this way it was possible to follow the short time duration arc current fluctuations. The power supply used for the arc has a power output control, i.e., it is possible to adjust the total power output but not the current or voltage individually. An increase in the arc length (stretching of the arc column) results in an increase in the arc voltage and this decreases the arc current for constant power output. Therefore for a certain power output, any arc current fluctuation was due to an arc voltage fluctuation; monitoring the arc current fluctuations is thus equivalent to monitoring the arc voltage fluctuations. The time constant of the measuring circuit was calculated and experimentally verified to be approximately 10 ns. The figures shown in the next pages are tracings of the photographs of the oscilloscope screen; the operating conditions were the same as the ones described in Table 3.3. In these figures, 1 mV is equivalent to an arc current fluctuation of approximately 10 A. (positive current fluctuation in down direction).

## B) Results

### a) Ar

Figure 3.18 shows the current fluctuations for Ar. It can be seen that the current continuously shows small amplitude variations and in addition there are approximately 25 large peaks in the arc current per revolution.

The large fluctuations (peaks) can be understood if one examines the way the arc moves. This is as follows: for pure argon, the arc movement is normally uniform, with a long arc column as shown in Figure 3.12. From time to time, the cathode arc

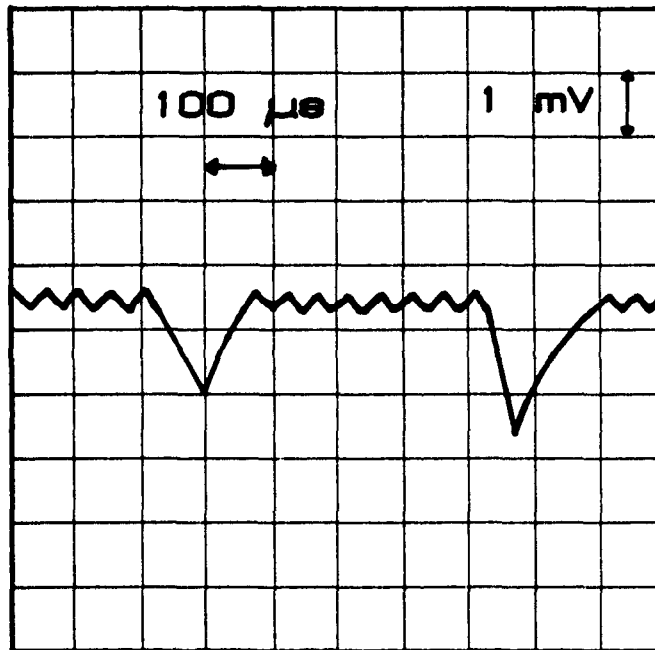


Figure 3.18 - Arc current fluctuations tracing for argon

attachment "jumps" to a position where the arc voltage is smaller; this represents a short arc column. The arc attachment at the cathode stays at that particular position but meanwhile the arc column is being forced to move due to the magnetic field.

This results in the stretching of the arc, increasing the overall voltage. When the voltage reaches around 44 V, the cathode arc attachment moves again, and the arc returns to its "normal" velocity and voltage. The peaks in arc current correspond to minima in arc voltage.

These peaks are correlated with the histograms developed in the last section. It can be seen from the histograms that there were around 20 jumps at value zero in average per revolution for Ar (Figure 3.13). These events indicate that the cathode arc attachment remained at a certain place for some time. The average number of arc current peaks for Ar running at 4 m/s was 25, similar to the number found with the high speed film. These peaks in current had a time duration between 100 and 200  $\mu$ s. The residence time of the arc in a event of jump zero is 1/5 000 s or 200  $\mu$ s for the high speed films, showing the similarities of the two methods.

The small arc current fluctuation seen continuously can be understood as "normal" arc motion, i.e., the arc moves to a new spot when the combined arc voltage and electron emission characteristics of the new spot are more favourable than those of the old spot. In this way, small arc current fluctuations should be expected, especially when the surface drag force is important.

b) Ar+0.3%CO and Ar+0.3%Cl<sub>2</sub>

The arc current shows no fluctuations for Ar contaminated with small amounts of either CO or Cl<sub>2</sub>, being constant at the value of 140 A as shown in Figure 3.19. This

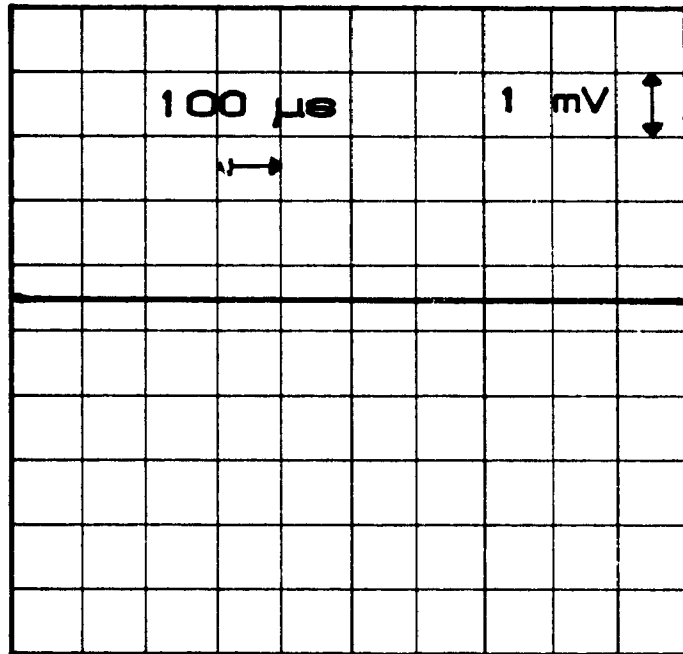


Figure 3.19 - Arc current fluctuations tracing for Ar+0.3%CO

is a reflection of the electron emission characteristics of the surface, i.e., the arc does not have to be stretched much to move to the next cathode spot, and therefore, no arc current fluctuation is generated. This situation was also seen in the high speed film and in the overall arc velocity (aerodynamic control). In reality the arc "jumps" continuously; but over very small distances, the resulting current fluctuations are very small.

c) Ar+0.3%N<sub>2</sub>

In the case of Ar contaminated with nitrogen, the arc current showed some fluctuations during the experiment, as shown in Figure 3.20. No large peaks characteristic of pure Ar were detected, but the fluctuations were larger than for CO (or Cl<sub>2</sub>) contamination.

This again is a reflection of the state of the surface or surface drag, i.e., the arc would be less stretched than for pure Ar but more than for CO contamination. These findings are consistent with the previously presented results for arc velocity, voltage and movement using different techniques.

d) Ar + > 4% CO (or Cl<sub>2</sub>)

It was shown in Figure 3.10 that the arc velocity decreased suddenly when more than 3-4 % CO was introduced in the Ar stream. It was suggested that a "thick" film was formed on the copper surface and that this increased the surface drag. The arc current fluctuations for Ar contaminated with more than 4 % CO is shown in Figure 3.21. Similar results were obtained substituting CO for Cl<sub>2</sub>.

The presence of peaks again suggests the idea of a more difficult arc movement (difficult electron emission or higher surface drag). The same kind of current fluctuations were found when pure CO was used and the same explanations can be

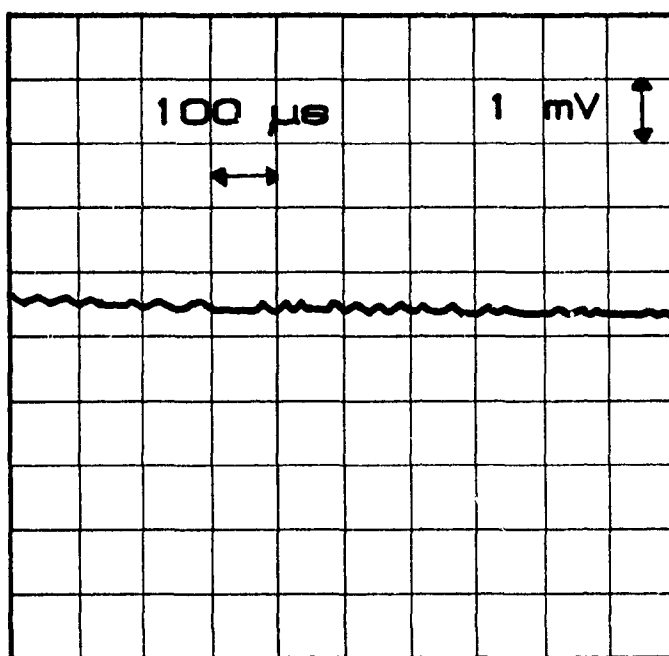


Figure 3.20 - Arc current fluctuations tracing for Ar+0.3%N<sub>2</sub>

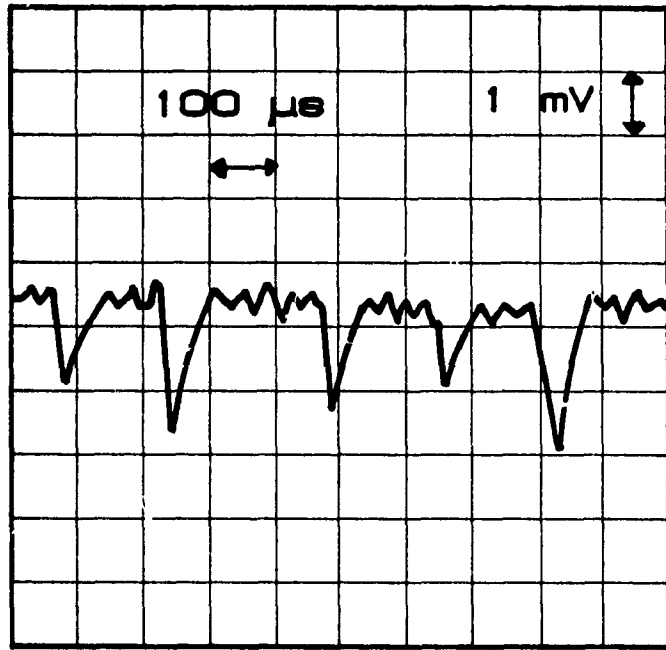


Figure 3.21 - Arc current fluctuations tracing for Ar+ > 4%CO

applied for that case. Again these findings are consistent with all the results presented previously.

e) N<sub>2</sub>

Figure 3.22a shows the arc current fluctuations when pure N<sub>2</sub> was used at B = 1 000 G. There are small peaks, similar to Ar+0.3%N<sub>2</sub>. This is another indication that : i) nitrogen reduces the surface drag, but the electron emission is not as good as for CO contamination (less than 1%) and ii) despite the fact that pure N<sub>2</sub> was used, the results are similar to those using less than 1 % of nitrogen in Ar. The latter suggests a saturation limit of nitrogen in copper.

The arc current fluctuations for pure N<sub>2</sub> for a magnetic field of 400 G are shown in Figure 3.22b. The peaks decreased in size and number, indicating that the arc was stretched less when moving from one site on the cathode to another at the lower value of magnetic field.

f) He

The arc current fluctuations for He at B = 1 000 G are shown in Figure 3.23a. It can be seen that there are many peaks in the arc current. The same analysis applied for pure Ar can be extended to helium to explain the presence of the peaks.

The residence time of the arc at a spot is between 30 and 50 μs. Since the time between two consecutive frames in the high speed film is 200 μs, it can be easily understood why no immobility (jump zero) was found for He.

Figures 3.23b and 3.23c display the arc current fluctuations for pure helium at B = 700 G and B = 400 G respectively. The number of peaks first decrease (700 G) and then disappear (B = 400 G). This indicates a "smoother" arc movement. The arc

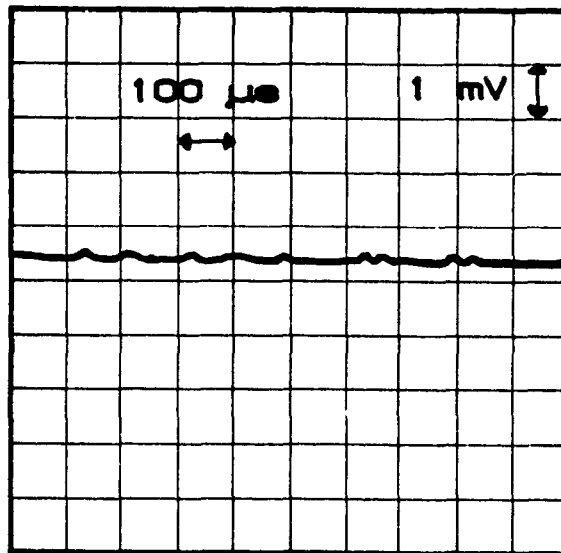
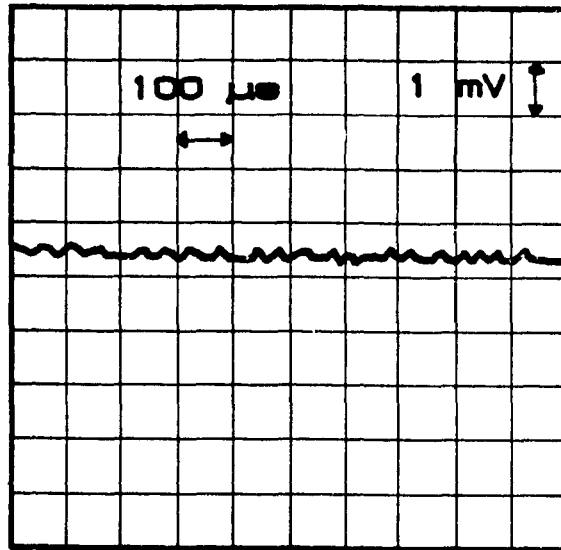


Figure 3.22 - Arc current fluctuations tracings for nitrogen

a) 1 000 G

b) 400 G

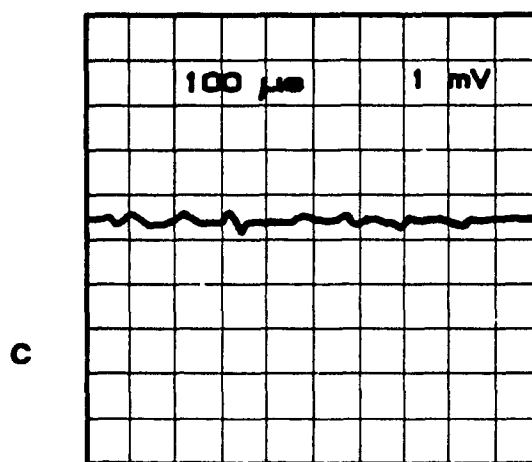
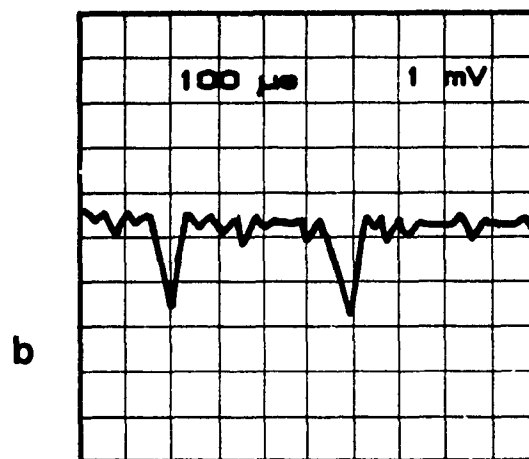
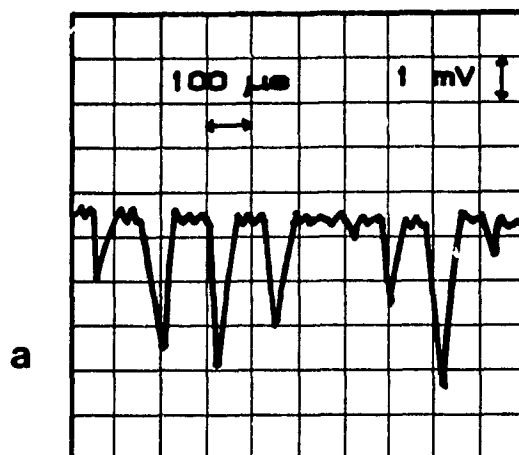


Figure 3.23 - Arc current fluctuations tracings for helium

a) 1 000 G

b) 700 G

c) 400 G

velocity for pure helium decreases with increasing magnetic field above 500 G as shown in Figure 3.7b. The arc movement is thus more difficult after 500 G, causing the peaks in the arc current. The singular arc movement for helium is discussed in Chapter VI.

g) He (contaminated with O<sub>2</sub>, N<sub>2</sub>, Cl<sub>2</sub>, CO)

In the case of O<sub>2</sub> and N<sub>2</sub> contamination in He, the arc current showed very small fluctuations and for CO or Cl<sub>2</sub>, no fluctuations were noted. The same explanations that were applied for Ar contaminated with these polyatomic gases can be used here.

## 12) CONCLUSIONS

In this Chapter, many of the fundamentals of the arc velocity and arc movement were discussed. It was seen that the previously proposed explanations for the arc movement are not valid and a new interpretation, based on our experimental results and theoretical analysis, was presented. The experimental results included arc velocity, arc voltage, high speed photography, arc current fluctuations. A summary of the most important findings of this part of the work is presented below.

a) The arc follows an aerodynamic type of equilibrium with the Lorentz force (for magnetically driven arcs) when the surface drag force is not important.

b) The relation between the arc velocity and the magnetic field strength is proposed to be  $Vel \propto B^{0.6}$ . This relation was verified for different plasma gases (Ar and He contaminated with CO and N<sub>2</sub> and for pure N<sub>2</sub>) and magnetic field strength ( $10 < B < 1700$  G).

- c) The relation between the arc velocity and arc current is proposed to be  $Vel \propto I^{0.56}$ . This relation was verified for air as the plasma gas and in the range of arc current  $100 < I < 850$  A.
- d) The existence of a new force affecting the arc movement, the surface drag force, was proposed. This force is related to the electron emission characteristics of the surface; more difficult it is for electrons to leave the cathode surface, higher is the surface drag force.
- e) The contamination of Ar and He with polyatomic gases decreased the surface drag, allowing the arc to follow the aerodynamic type of equilibrium. Without these contaminants or with an excess of them, the surface drag force is the major force opposing the arc movement.
- f) The magnitude of the surface drag is as follows: highest for pure Ar and He; intermediate for Ar and He contaminated with  $< 1\%$   $N_2$  and  $O_2$ , for Ar or He contaminated with  $> 4\%$  CO or  $Cl_2$  and for pure CO or air; smallest for Ar and He contaminated with  $< 1\%$  CO,  $CH_4$ ,  $Cl_2$ .
- g) The high scatter of the data for arc velocity vs magnetic field reported in the literature is probably due to the use of air as the plasma gas as well as the use of different operating conditions between experiments.
- h) High speed photographs and films showed the presence of long arcs for pure Ar and He and short arcs for these gases contaminated with polyatomic gases. The arc cathode attachment was seen to be lagging behind the arc column for the pure inert gases. From the films it was possible to estimate the maximum residence time for the arc in a same spot.

- i) Differences in arc movement between pure and contaminated Ar (or He) could be quantified using the histograms from the high speed films. The arc movement is more uniform and smooth for contaminated Ar and He than for pure inert gases.
- j) Arc current fluctuations were used as a diagnostic tool for the arc movement, confirming the findings of arc velocity and high speed film for different plasma gases. The residence time of the arc in a same spot was found to coincide with the values found with the high speed films. The arc current fluctuations followed the same trend as for the surface drag, i.e., higher the surface drag, higher the arc current fluctuations. The use of the arc fluctuations is thus proposed here to be used as a simple diagnostic tool for analysis of the behavior of the arc.
- k) Nitrogen was found to affect the arc movement independently of its concentration in the range 0.3 to 100 %. CO or Cl<sub>2</sub> below 4 % in volume in Ar or He enhanced the arc movement; above 4 % the arc movement became more difficult. These findings were confirmed by different diagnostic tools (arc velocity, arc movement, high speed film, arc current fluctuations).

REFERENCES

- 1) Szente, R.N.; "Cathode Erosion in Magnetically Rotated Arcs"; Master Thesis, Chemical Engineering Department, McGill Univ., Montreal, 50-51, 1986.
- 2) Reitz, J.R.; Milford, F.J.; "Foundations of Electromagnetic Theory"; Addison-Wesley Publishing Company, 2 ed., 148-150, 1967.
- 3) Roman, W.C.; Myers, T.W.; "Experimental Investigation of an Electric Arc in Transverse Aerodynamic and Magnetic Fields"; AIAA Journal, Vol. 5, n. 11, 2011-2017, 1967.
- 4) Fisher, E.; Uhlenbush, J.; Proc. 7<sup>th</sup> Int. Conf. on Phenomena in Ionized Gases Belgrade, Vol. 1, 725-728, 1965.
- 5) Malghan, V.R.; Benenson, D.M.; "Analysis of Cross-Flow Arcs in Transverse Magnetic Fields", IEEE Trans. Plasma Sci. Vol PS-1, n. 3, 38-46, 1973.
- 6) Daily, J.W.; Harleman, D.R.F.; "Fluid Dynamics", Addison-Wesley Publishing Company, 170-171, 1966.
- 7) Kopainsky, J.; Schade, E.; "Rotating High Current Arc", Journal of Applied Physics, Vol. 20 , 147-153, 1979.
- 8) Alferov, V.I.; Vitkovskaya, C.; Ustinov, Y.S.; Shcherbakov, G.; "Experimental Investigation of the Characteristics of an Electric Arc", Tephofizika Vysokikh Temperatur, Vol. 11, n.6, 1142-1146, 1973.
- 9) Guile, A.E.; Naylor, K.A.; "Further Correlation of Experimental Arcs in Transverse Magnetic Fields", Proc. IEE, Vol. 115, n.9, 1348-1354, 1968.
- 10) Secker, P.E.; Guile, A.E.; " Arc Movement in a Transverse Magnetic Field at Atmospheric Pressure", IEE Paper n. 3044S, 311-320, 1959.
- 11) Guile, A.E.; Adams, V.W.; Lord, W.T.; Naylor, K.A.; Proc. IEE, Vol. 116, 645-652, 1969.
- 12) Harry, J.E.; "The Measurement of the Erosion Rate at the Electrodes of an Arc Rotated by a Transverse Magnetic Field", Journal of Applied Physics, Vol. 40, n.1, 265-270, 1969.

- 13) Sharakhovskii, L.I.; "Experimental Study of an Electric Arc Moving in an Annular Ventilating Gap by the Action of Electromagnetic Forces", *Inzhenerno-Fizicheskii Zhurnal*, Vol. 19, n.6, 1046-1051, 1970.
- 14) Winsor, L.P.; Lee, T.H.; "Properties of a D-C Arc in a Magnetic Field", *AIEE Transaction*, Vol 75, 143-148, 1956.
- 15) Yas'ko, O.I.; "Correlation of the Characteristics of Electric Arcs Moving in Transverse Magnetic Fields", *Proc. IEE*, Vol. 116, n.3, 453-456, 1969.
- 16) Perry, R.H., Chilton, C.H.; *Chemical Engineering Handbook*, 5.ed., McGraw-Hill Book Company, 5.62, 1973.
- 17) Benenson, D.M.; Baker, J.; "Transverse Magnetic Field Effects on a Cross Flow Arc", *AIAA Journal*, Vol. 9 , n.8, 1441-1446, 1971.
- 18) Lowke, J.J.; "Simple Theory of Free Burning Arcs", *Journal Phys. D: Appl. Phys.*, Vol. 12, 1873-1886, 1979.
- 19) Johnson, J.R.; Choksi, N.M.; Euban, P.T.; "Entrance Heat Transfer from a Plasma Stream in a Circular Tube", *I& EC Process Design and Development*, Vol. 7, n.1, 34-41, 1978.
- 20) Shabol'tas, A.S.; Yas'ko, O.I.; " Velocity of an Electric Arc in an Annular Gap", *Inzhenerno-Fizicheskii Zhurnal*, Vol. 19, n.6, 1046-1051, 1970.
- 21) Bittencourt, J.; *Fundamentals of Plasma Physics*, Pergamon Press, 1986.
- 22) Rakhovskii, V.I.; " Experimental Study of the Dynamics of Cathode Spot Development", *IEEE Transac. on Plasma Science*, Vol. PS-4, n.2, 81-102, 1976.
- 23) Sherman, J.C.; Webster, R.; Jenkins, J.E.; Holmes, R.; "Cathode Spot Motion in High Current Vacuum Arcs on Copper Electrodes", *J. Phys. D: Appl. Phys.*, Vol. 8, 696-702, 1975.
- 24) Chen, I.C.; Xie, J.Z.; " Motion of Magnetically Driven Arcs on Oxidized Electrodes", *IEEE Transactions on Components Hybrids and Manufacturing Technology*, Vol. CHMT-5, 86-89, 1982.
- 25) Guile, A.E.; Lewis, T.J.; Secker, P.E.; "The Role of Surface Layers on Electron Emission and Cathode Root Motion of Cold Cathode Arcs", *International*

Conference on Gas Discharges, 473-479, 1970.

- 26) Guile, A.E.; "Model of emitting sites and erosion on nonrefractory arc cathodes with relatively thick oxide films", Proc. IEE, Vol. 121, n.12, 1594-1598, 1974.
- 27) Poeffel, K.; "Influence of the Copper Elec. Surface on Initial Arc Movement", IEEE Transac. on Plasma Science, Vol. PS-8, n.4, 443-448, 1980.
- 28) Chen, L.C.; Peng, Z.; "Influence of Electrode Surface State and Its Thermal Parameters on Motion of Magnetically Driven Arcs", IEEE, 57-60, 1986.
- 29) Emtage, P.R.; "Interaction of the cathode spot with low pressures of ambient gas", J. Appl. Phys., Vol 46, n.9, 3809-3816, 1975.

69

#### IV. SURFACE ANALYSIS

69

#### IV. SURFACE ANALYSIS

##### 1) INTRODUCTION

*Watson has been sitting on his favourite green velvet chair in Holmes' office for more than an hour; he seems disturbed. And he seems more disturbed when he looks at Holmes, who has been, surprisingly, dusting the office...*

*- Holmes, for God's sake, what are you doing cleaning the office? You just presented some of the most astonishing results on the behavior of the electric arc, which I must say I do not follow very well, and now you .. you just run up and down with that that ..stupid cloth, dusting off everythir.g.. Aren't you at least a little concerned about the conclusions you reached???*

*Holmes stops, looks at the face of the good Doctor and goes back to what he was doing before, cleaning the office... And Watson decides to go back to what he was doing, i.e., getting disturbed and frustrated...*

*After another hour, when Watson is almost asleep at the chair, Holmes suddenly jumps in the air and says:*

*- Watson, my dear fellow, what are you doing sitting there? We have a lot to do...*

*Watson, recovering from the sudden agitation in the office, could just say,*

*- What do we have to do, Holmes?*

*- Watson, where have you been in the past days? Didn't you see what we accomplished??*

*We solved the problem of the arc movement!!!*

*- But but but Holmes, I do not see ...*

*- Watson, stop mumbling man, and listen. Why do you think I was dusting off the house? Don't tell me you think I became concerned about the aspect of the office!*

*- I don't know, Holmes, you seemed so involved in cleaning that..*

*- That's exactly it, Watson! Don't you see? Everything matches! The dust, the arc movement, everything! The game is afoot!*

*Watson looks even more disturbed and Holmes decided to explain what was in his mind..*

*- Listen Watson, the contamination of the gas affects the arc movement, right?*

*- Right, Holmes.*

*- But it is not the gas! It is the surface of the cathode! That explains everything! Now be a good friend, and try to find one of your best magnifier lenses, no, better than that, let's go to your office and examine the cathodes under the microscope!*

*- But Holmes, what are you trying to see??*

*- The dust, Watson, the dust! What is happening with you? Come, come,..*

*And Holmes with some cathodes in one hand and pushing a confused Doctor with the other arm, rushes away from his office...*

Coming back to this work...

#### A) Chapter Guideline

In this Chapter the contamination of the cathode surface is discussed. It is first shown that the addition of polyatomic gases into inert gases or the use of certain polyatomic gases contaminates the cathode surface. The surfaces were analyzed using Auger and ESCA instruments in order to measure the level and composition of the contamination on the electrode surfaces. The ideas proposed in the last Chapter about electron emission, surface drag and surface contamination are analyzed here. Work function of the surfaces were measured using a Kelvin probe and the results indicate the importance of the surface contamination for electron emission. The cathode surfaces were also analyzed using a SEM to determine the state of melting of the surfaces as well as the thickness and composition of the layers formed on the surface. The most important findings of this work are summarized at the end of the Chapter.

#### B) Why Contamination?

It was shown in the last Chapter that contaminated inert gases had higher arc velocities than the pure inert gases. Contaminating with polyatomic gases or using the polyatomic gases alone affected in general the arc movement, the arc voltage and the cathode erosion rates.

Some researchers (Achttert et al (1), Farral et al (2), Athwal et al (3), Doan and Thorne (4), Niedermann et al (5), Porto et al (6)) have suggested that contaminations

on the cathode surface could be very important for the electron emission characteristics of the surface. These works were done in vacuum conditions, for field emission and vacuum arcs. In this Chapter the electrode surfaces will be examined for contamination using different techniques, in an attempt to explain some of the results presented in the last Chapter. The first consideration to be examined is the gas/surface contamination.

## 2) GAS CONTAMINATION - SURFACE CONTAMINATION

Contamination of the plasma gas can greatly affect the properties of the plasma especially if the contamination contains metal vapours (Chemiat and Andanson (7); Xi et al (8)). However in the present experiments, the plasma properties (voltage, heat losses) were the ones characteristic of the pure inert gas (Ar or He) as long as the contamination level of the polyatomic gases were less than 1 %. This was seen when the arc voltage for Ar contaminated with different polyatomic gases ( $\text{Cl}_2$ , CO,  $\text{CH}_4$ ) was compared; although the contaminant gases have different properties, the overall arc voltage and arc velocity were the same for Ar with these different contaminants.

However the contamination of the inert gases caused large variations in the arc velocities (increased), arc voltage (decreased) and in the arc movement (more uniform) when compared with the experiments using pure inert gases. As suggested before, this indicates a surface effect.

In the experiments with pure Ar and He, the arc voltage and velocity initially changed with time before reaching a steady state. Figures 4.1a and 4.1b show the arc voltage and arc velocity variations for Ar and He at the beginning of the experiments.

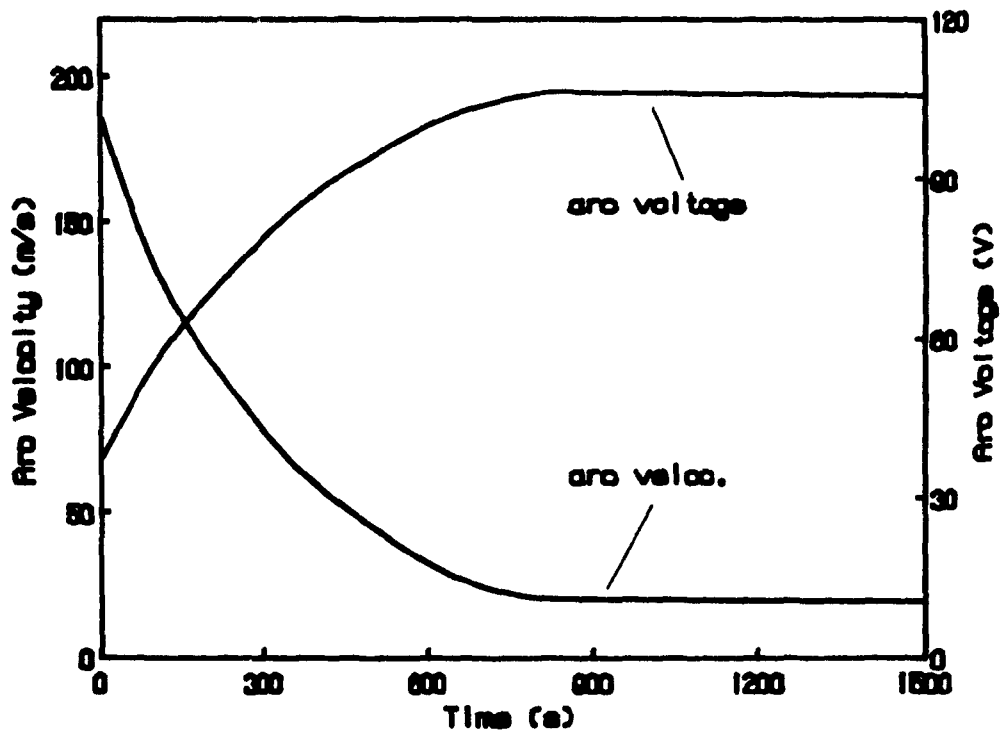
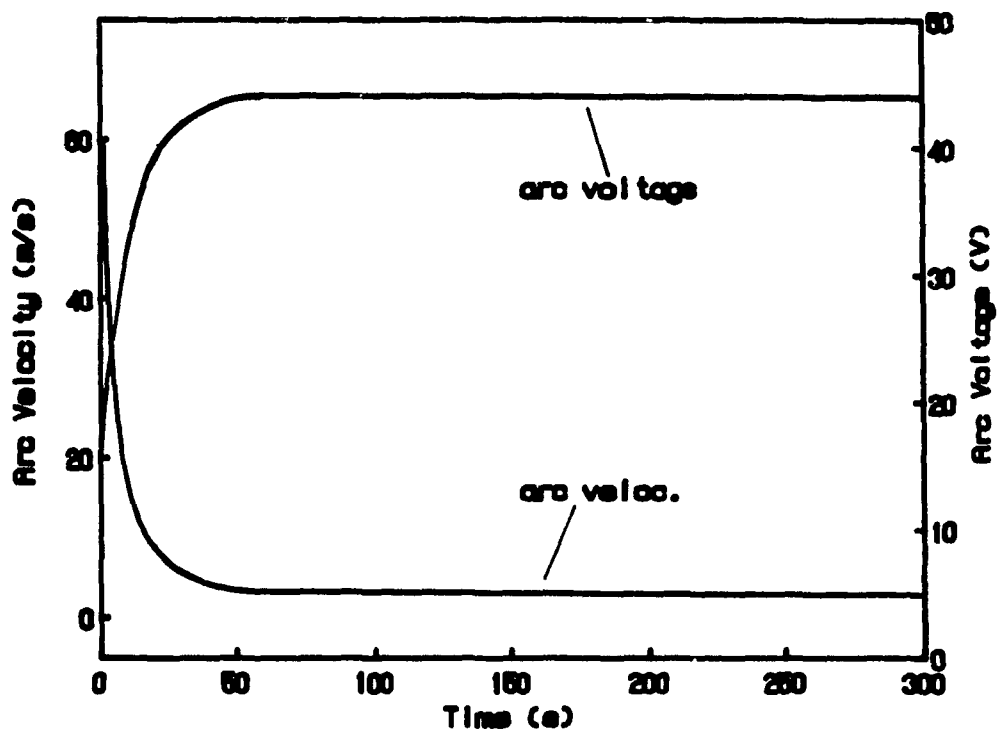


Figure 4.1 - Arc voltage and velocity variations with time (experiment started at 0 s)

a) Ar

b) He

It can be seen that, for Ar, the initial transient time was around 30 seconds; it was much higher in the case of He, i.e., around 15 minutes. These differences in time will be explained later in this Chapter, but for now it is important to understand that something was different at the beginning of the experiments. Since the gases were the same throughout the experiments, the conclusion is that the surface of the electrodes, although cleaned before each experiment with  $\text{HNO}_3$  and  $\text{CCl}_4$ , contained some sort of contamination, which disappeared during the experiment.

Another indication of this surface contamination was found in experiments in which the addition of the contaminant gas in the inert gases, for instance  $\text{N}_2$  in He, was stopped after the arc reached its steady state operation. In these cases, as it will be seen in the next sections, it took almost 15 minutes for the arc to operate again with the characteristics of pure He. A simplified calculation of the gas residence time inside the chamber is shown below.

Assuming the worst case, perfect mixing (in reality the flow pattern is close to a plug flow) inside the reactor, a mass balance would give:

$$m_{\text{He}}(t_2) = m_{\text{He}}(t_1) + \int Q C_{\text{in}} dt - \int Q C_{\text{out}} dt \quad 4.1$$

where  $m_{\text{He}}$  = mass (helium, for example) inside the chamber

$t$  = time

$Q$  = volumetric flow rate

$C$  = concentration

and the subscripts in and out are for inlet and outlet

Equation 4.1 can be written in a differential form as

$$d C_{out}/dt = Q (C_{in} - C_{out}) / V_l \quad 4.2$$

where  $V_l$  is the volume of the chamber

The solution of equation 4.2 is,

$$C_{out}(t) = C_{in} (1 - \exp (- Q t / V_l)) \quad 4.3$$

In our case,  $Q = 20$  l/min and  $V_l = 2.5$  l, which substituted in 4.3 gives :

$$C_{out} = 0.982 C_{in} \text{ after } 30 \text{ s}$$

$$C_{out} = 0.9998 C_{in} \text{ after } 1 \text{ min}$$

This means that after 1 minute of any gas inlet change, the gas leaving the chamber has 99.98% of the concentration of the gas entering the chamber. Therefore, it is not possible that the gas composition can be the only cause for the changes in the arc velocity and voltage, since these changes lasted for much longer times.

It has been mentioned that the amount of contamination (polyatomic gases) added to the inert gases was very small, normally less than 1 % in volume. The necessary flow rate of the contaminant gas for these experiments was determined by increasing its value from zero until both constant arc velocity and a minimum voltage were observed. Increases in the contaminant gas concentration beyond this level resulted in steady state voltages which increased with contaminant concentration. The values of the necessary contaminating gases concentrations are given in Table 4.1.

The contaminant concentration required for the minimum voltage was always slightly higher for helium than argon. Since the diffusivity of the contaminants in helium is

four times that of the contaminants in argon, the reasons for the differences in the effectiveness of contaminants must lie on the surface. This is probably related to the temperature of the surface, or current density, as discussed in the next Chapter.

**TABLE 4.1**  
Gas Contamination Concentration

Contaminant	Ar (ppm)	He (ppm)
N <sub>2</sub>	3000	4000
O <sub>2</sub>	400	500
CO	3000	4000
Cl <sub>2</sub>	3000	4000

### 3) AUGER AND ESCA

It was seen in the last section that the electrode surfaces were probably contaminated and this caused the variations observed in the arc velocity, voltage, movement, and erosion rates (Chapter VI). In order to determine the level and composition of the contaminants on the surface of the cathodes, an Auger electron spectroscope and an ESCA instrument (Electron Spectroscopy for Chemical Analysis) were used. A short description of the instruments is given below.

Excellent reviews have been published on Auger electron spectroscopy (Lea (9), Chang (10)). This method of analysis consists of bombarding the surface with an

electron beam in order to promote the emission of secondary electrons. These secondary electrons have very defined energy which depends only on the material being analyzed (for a certain beam power); in this way, elements and even compounds can be uniquely identified. The depth of analyses normally involves the first 5 monolayers, which is less than other surface analysis methods (SEM, UPS).

An argon ion gun is normally used with the Auger analyses. This gun emits argon ions which sputter the surface, removing layers and allowing the analysis of regions deep into the surface. This is called a Composition Depth Profile; examples will be given in the next section. Although it is possible to use AES to identify compounds, the method is more suitable for elemental analyses; the compounds are normally determined using an ESCA (Electron Spectroscopy for Chemical Analysis) instrument, which has the drawback of not being as sensitive for certain elements as AES.

ESCA uses an X ray tube as the source of radiation. The photon hits the surface of the sample, ionizing an electronic shell and an electron is ejected from the surface. This electron will be energy analyzed and an element (or compound) can be identified (Prutton (15)).

Tests were conducted to determine which electrode was important for the observed changes in the arc velocity and voltage, since in principle either electrode could be the cause of these changes. The tests consisted of running contaminated inert gases, stopping the arc, substituting one of the electrodes for a new one, and continuing the arc operation with pure inert gas. The results showed that only the cathode caused the changes, confirming the previous ideas of electron emission/surface drag, since the cathode is responsible for the emission of the electrons to maintain the arc.

#### 4) AES - ESCA RESULTS

The results obtained using an AES instrument are presented in the next pages. The graphs are plots of elemental concentration versus the depth into the surface, i.e., the plots represent the composition depth profiles. The samples for AES, ESCA and later SEM (Scanning Electron Microscope) analyses were cut at low speed from the cathodes using a non-lubricated saw; both heating of the cathodes and their contamination were avoided. Analyses were always carried out far from the cut surfaces.

##### A) Experiments With Pure Ar and He

When pure inert gases (Ar or He) were used as the plasma gases, no contamination could be added to the surfaces coming from the gases (see the composition of the gases, Chapter II). Therefore, any contamination found on the cathodes had its origin prior to the experiment or after the experiment (during the preparation of the sample for the Auger chamber). Figure 4.2 shows carbon contamination depth profiles for the following conditions:

- prior to the experiments, cleaning with  $\text{HNO}_3$  only
- prior to the experiments, cleaning with  $\text{HNO}_3$  and  $\text{CCl}_4$
- after 30 seconds operation with Ar
- after 5 minutes operation with He

The cathodes used in the arc experiments were cleaned with  $\text{HNO}_3$  and  $\text{CCl}_4$  before the experiments.

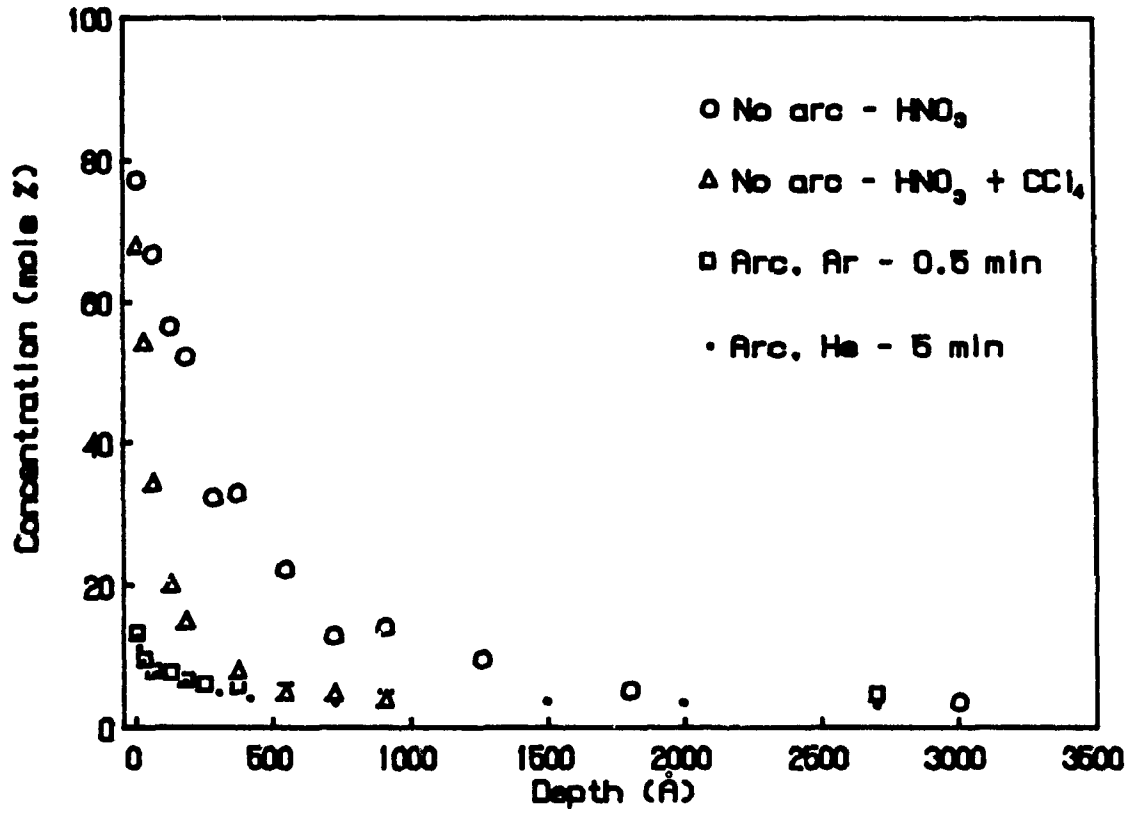


Figure 4.2 - Carbon concentration profiles - Auger analysis

The first curve shows severe contamination with carbon; this is for the cleaning with only  $\text{HNO}_3$ . The use of carbon tetrachloride reduces the level of contamination significantly, suggesting that the carbon may have come from the lubricant used in machining the cathodes.

It was previously shown (Figure 4.1) that the transient time for Ar was 30 seconds, after which the arc reached a steady state. For He, this transient time was around 15 minutes. It can be seen in Figure 4.2 that if the arc operates at relatively short times, the amount of carbon on the surface is reduced quite drastically. This shows that: a) the arc is very effective in removing contamination from the surface (see also Achtert et al (1)); b) the cathode is contaminated with carbon at the beginning of the experiments, even after the cleaning. The carbon causes a decrease in the surface drag (high arc velocity, low voltage) as suggested before (see also next sections); c) experiments which rely on short term (Hitchcock et al (11), (12)) or discontinuous experiments with multiple strikings (Poeffel (13)) may not be indicative of steady state conditions due to initial surface contamination.

The surface contamination of carbon (10-15 %) for both Ar (30 sec) and He (5 min) can be understood as being due to the reaction of atmospheric  $\text{CO}_2$  with the copper (Schreurs et al (14)) after the cathode is removed from the reactor. The residual values of 1-2% of carbon even deep within the surface are probably indicative of inefficient cleaning by the argon gun or a background level of carbon in the Auger system.

ESCA analysis of a pure copper standard (99.999 %) also showed carbon contamination of 12 % at the first layers, reducing to 1 % after 300 Å. Replacement of the standard helium gas used in the plasma experiments by helium 99.995 % pure (high grade purity) gave identical results.

The level of contamination of oxygen for both new and used cathodes (with Ar or He) was also determined using AES. The results are shown in Figure 4.3. The upper surface contamination was of the order of 10-15 % decreasing to about 1-2 % after 500 Å. The surface contamination is primarily due to the unavoidable surface oxidation of the sample during transport from the test chamber to the analysis system. The background level, probably due to the Auger system used, agrees well with results published by Porto et al (6).

Figure 4.4a and b shows the concentration profiles for chlorine for three different operating conditions, i.e., one new cathode cleaned with HNO<sub>3</sub> and CCl<sub>4</sub> and two cathodes after the cleaning operated for 1 min and 5 min in pure Ar. It can be seen from these figures that for the unused cathode there is Cl in the first 100 Å; after operating 1 min in Ar, the amount of Cl increased and extended to up 1 500 Å. The Cl essentially disappeared after 5 minutes operation.

This can be understood as Cl surface segregation; the bulk copper contains minute amounts of Cl, due to either contamination during the processing of the copper or during the machining of the cathodes. Heating up the surface with the plasma made the Cl migrate to the surface; this situation corresponds to the 1 min Ar run. If the experiment lasts long enough, the Cl contamination will be removed and a depletion of Cl will take place, as shown for 5 min Ar run. This Cl enrichment of the surface is similar to the surface migration of sulfur from the bulk to the surface of a heated copper sample (Harris (16), Hofmann and Erlewein (17), Lloyd et al (18)).

Figure 4.5 shows Cl concentration profile, for an experiment with pure He. This time the comparison is between two regions of the same cathode, i.e., at the center of the cathode where the arc runs most of the time and at a region closer to the edge of the cathode, where the arc seldom runs. It can be seen that the ideas proposed for

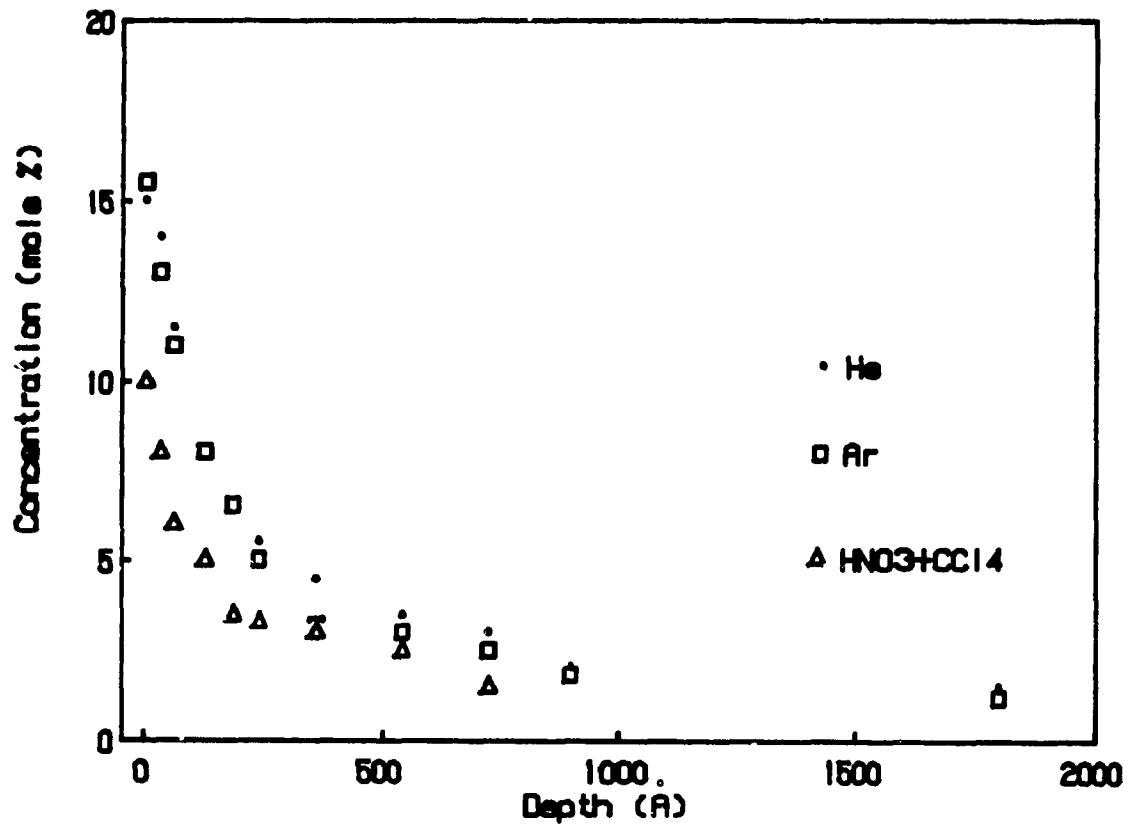


Figure 4.3 - Oxygen concentration profiles - Auger analysis

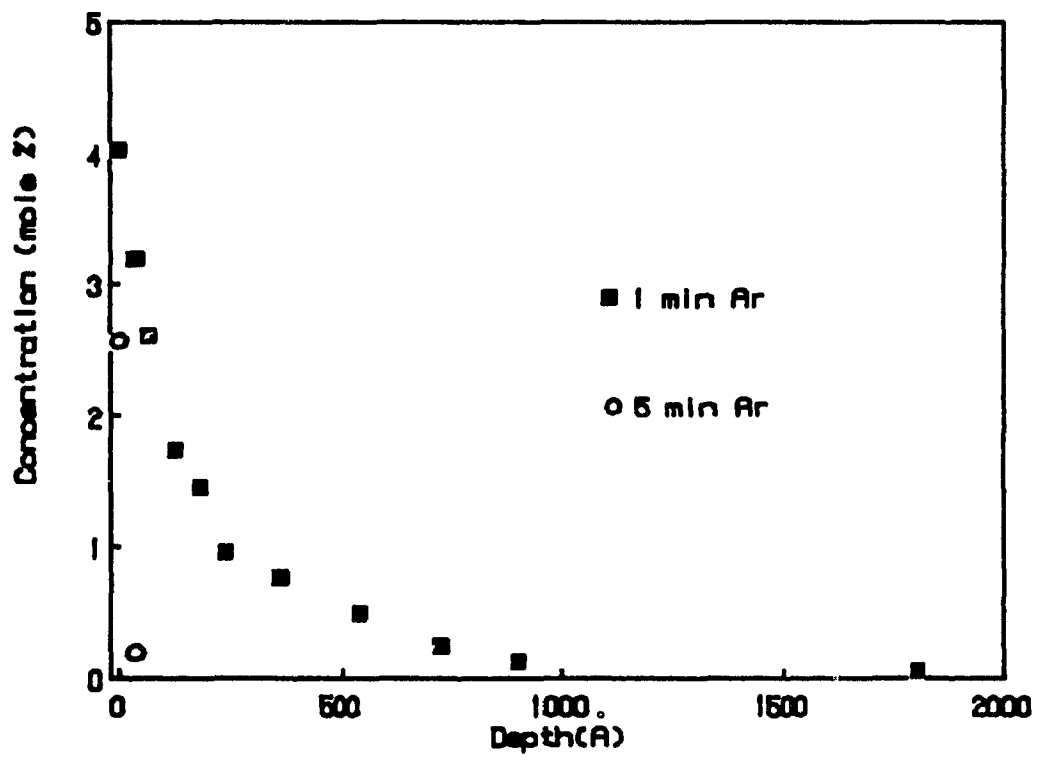
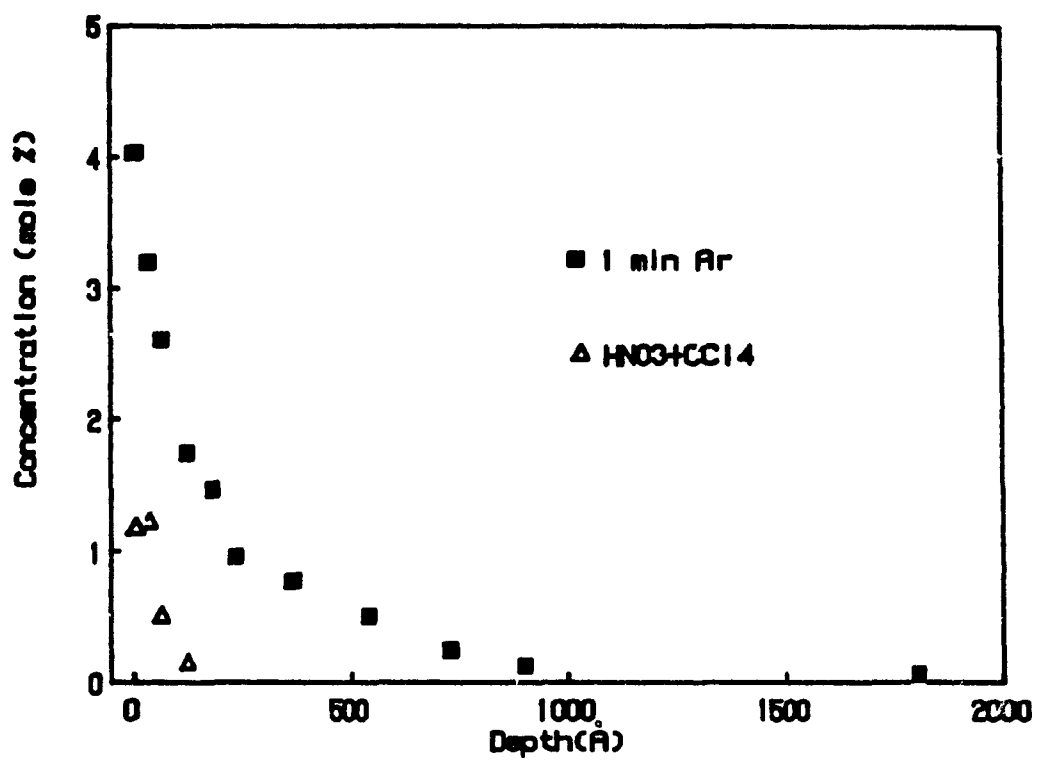


Figure 4.4 - Chlorine concentration profile

a) Clean cathode and 1 min Ar      b) 1 min Ar and 5 min Ar

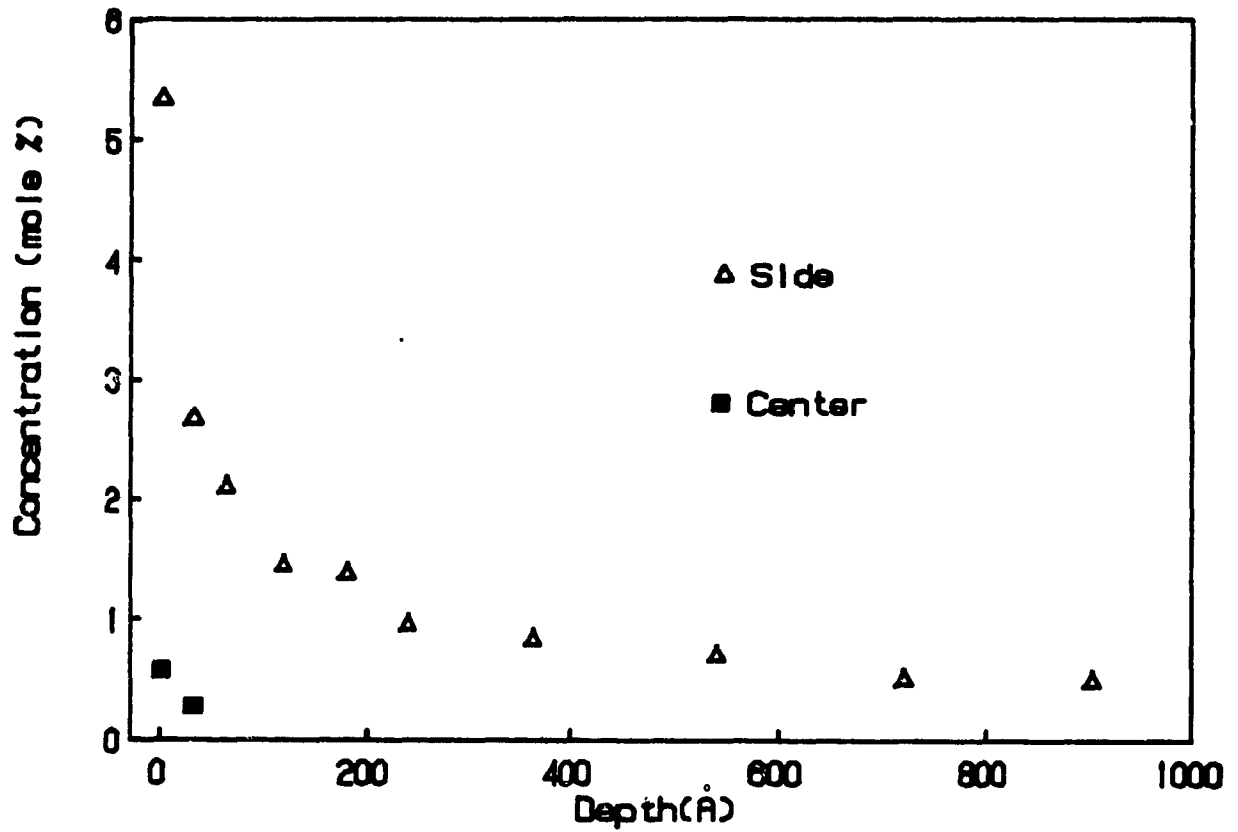


Figure 4.5 - Chlorine concentration profile for He  
Two regions on the same cathode

Ar are confirmed for He, i.e., in the region where the arc does not run and consequently does not remove material, the Cl is enriched at the surface (this region is heated up by radiation from the arc and by convection from the plasma). At the center, because of the removal of copper, there is a depletion of Cl. An enrichment of sulfur similar to the chlorine was also observed at the surface of the cathode, although in smaller quantities.

B) Experiments With Ar+0.3%N<sub>2</sub> and He+0.4%N<sub>2</sub>

The advantage of using N<sub>2</sub> as the polyatomic contaminant in the inert gases is that N<sub>2</sub> is not adsorbed and does not react with copper at room temperatures (Heskett et al (19)). Therefore any nitrogen found at the surface of the electrodes must come during the operation of the arc. This can confirm the idea of surface contamination caused by the gas contamination as suggested before. The results shown below are for Ar and He contaminated with 3 000 and 4 000 ppm of N<sub>2</sub> respectively; the experiments lasted for more than 30 min.

The concentrations of the other contaminants (C, O<sub>2</sub>, Cl<sub>2</sub>, S) were first analyzed before analyzing for nitrogen. The results were compared with pure Ar and He experiments.

Figure 4.6 shows the carbon concentration profiles for experiments with pure Ar and He and for both contaminated with nitrogen. It can be seen that the amount of carbon is approximately the same for all experiments; thus the addition of nitrogen produces no changes in the amount of carbon detected on the surface of the cathode. Similar observations were made for oxygen, chlorine and sulfur contamination.

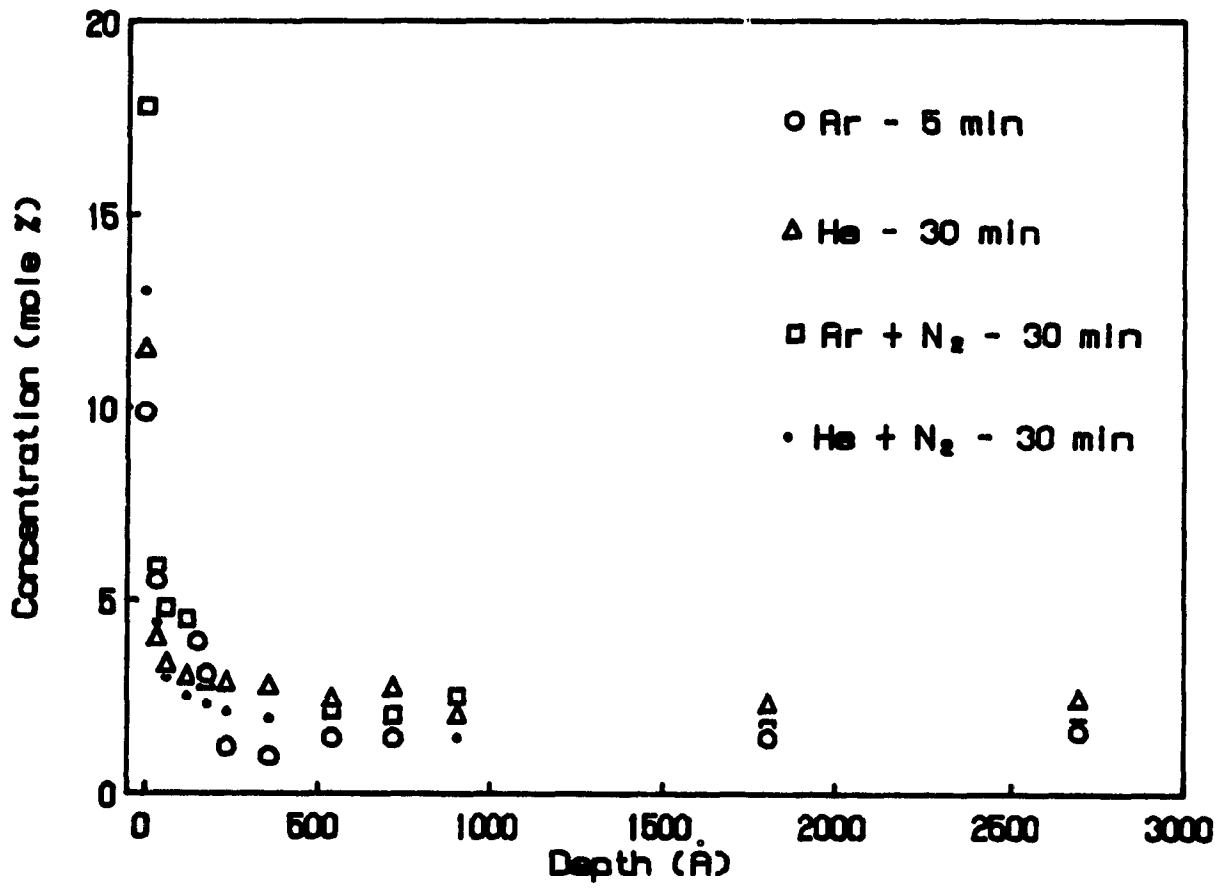


Figure 4.6 - Carbon concentration profile

Pure Ar and He; Ar+0.3%N<sub>2</sub>; He+0.4%N<sub>2</sub>

Figure 4.7 shows the nitrogen concentration profiles in the cathode after steady state operation in Ar and He contaminated with nitrogen. Analyses of fresh electrodes or electrodes with pure Ar and He arcs showed no detectable surface nitrogen. It can be seen that the operation of an arc using nitrogen containing gases contaminates the electrode surface with nitrogen. The single fact that nitrogen was found on the cathode surface corroborates the suggestions previously made that the surface contamination could lead to an easier arc movement (lower surface drag); it will be seen later in the Chapter that the contamination indeed affects the electron emission characteristics of the surface.

The maximum nitrogen concentration based on the measurements of all species is about 4 % and is approximately the same for both contaminated Ar and He plasma gases. These levels of contamination were also measured using an ESCA system. The actual level of nitrogen concentrations at the surface during the arc operation is expected to be higher since when analyzed, the electrode surfaces are unavoidably contaminated by carbon and oxygen picked up from the atmosphere. If the values of carbon and oxygen were subtracted, the nitrogen concentration at the surface during arc operation would be 6-7%.

Since nitrogen cannot diffuse into solid copper at appreciable rates, there are two possible explanations for the presence of nitrogen in the cathode: a) ionic bombardment or b) diffusion through liquid copper. Zomorrodian et al (20) studied the range distribution of ionic nitrogen in copper. From this work, and also from the work of Ziegler et al (21) and Roth (22) it is possible to estimate the energy required to implanting nitrogen ions in copper to a depth of 500 Å. This energy would be of the order of 50 keV, which is far too high for our experiments. The nitrogen ions in this work experience, at the most, a cathode fall acceleration which is around 10 eV. Therefore it is likely that the copper is melted to a depth of about 1 000 Å during

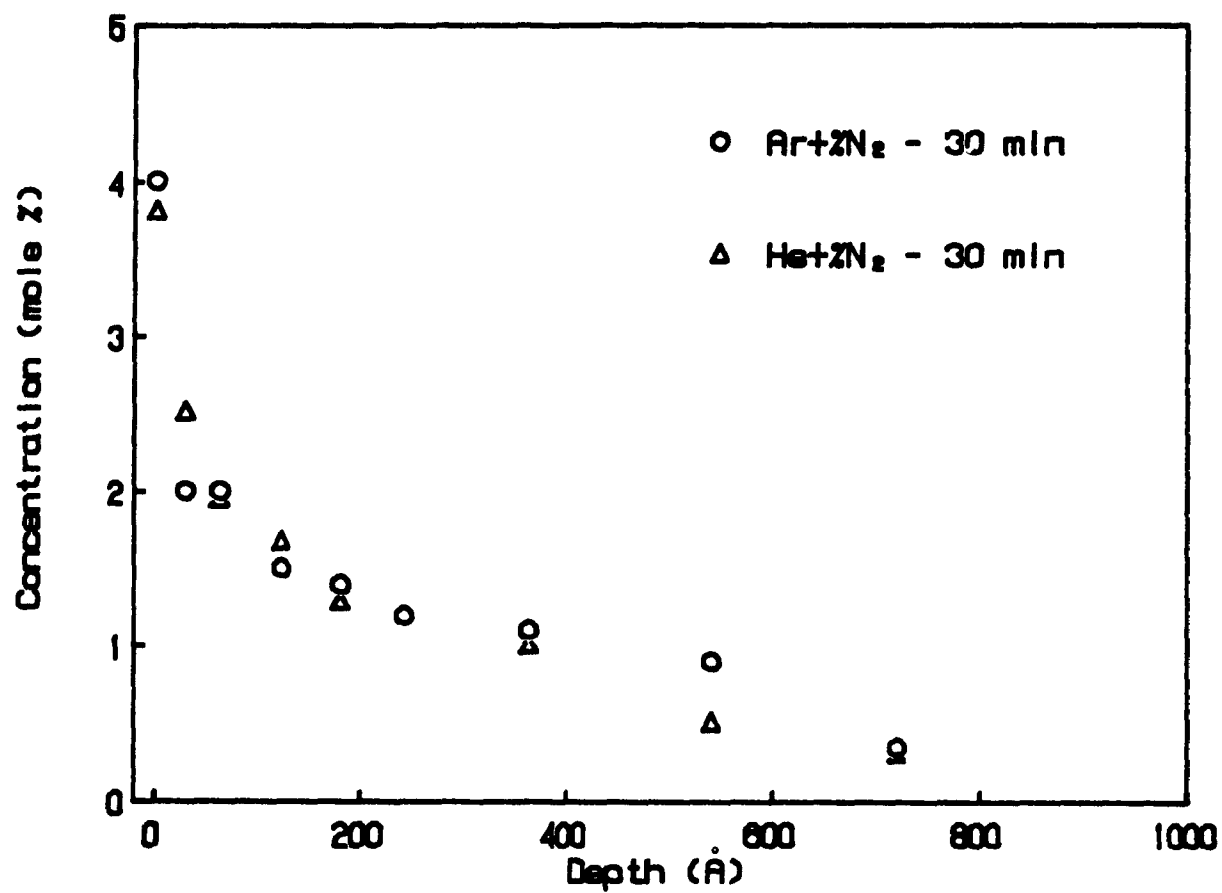


Figure 4.7 - Nitrogen concentration profile for Ar+0.3%N<sub>2</sub> and He+0.4%N<sub>2</sub>

the passage of the arc (for these experiments) and that positive nitrogen ions, attracted to the cathode (negative potential), diffuse into the liquid copper pool.

Once the nitrogen is incorporated into the copper cathode, it can react with the hot solid copper (after the passage of the arc, the surface solidifies very quickly - see Chapter VII). The simple fact that nitrogen was found at the surface is an indication of a nitrogen compound, although there is the possibility of a physical bond between nitrogen and copper (physisorption). ESCA analyses were performed to verify the existence of copper nitrogen compounds by checking for chemical shifts for nitrogen in the energy distribution curve. In order to do that, the nitrogen energy level for copper have to be compared to the nitrogen energy level for another metal, since ESCA cannot detect free nitrogen. The binding energy for BN is 397.9 eV (first orbital of nitrogen) and a binding energy of 398.2 eV was found for the nitrogen in the surface of the cathode. This small difference between these energy levels suggests the formation of a nitrogen compound at the surface. The compound is likely to be  $\text{Cu}_3\text{N}$ , as suggested by Porto et al (6) and Heskett et al (19).

It was previously suggested that increases in nitrogen in the gas beyond the levels used in these experiments (less than 1 %) resulted in increases of arc voltage which were attributed to changes in the arc column rather than at the electrode surface. An ESCA analysis of a cathode operated in pure nitrogen gave nitrogen concentrations very similar to those found for Ar and He slightly contaminated with  $\text{N}_2$ . This suggests that the electronic surface changes are essentially complete after even slight levels of contamination of an inert gas by nitrogen. Further macroscopic changes in arc characteristics are thus due to changes in the arc column.

Samples of cathodes were also analyzed after only 5 minutes of operation with  $\text{N}_2$  contaminated Ar and He; these again were identical to the 30 minutes exposure

times showing that after the arc characteristics have reached steady state, the surface composition remains constant.

The analysis of the surface for Ar+0.3%N<sub>2</sub> in a region towards the edge of the cathode showed lower concentration of N<sub>2</sub>, between 2-3 %. It is possible to conclude from this result that the arc, although it runs most of the time at the center of the cathode, also moves along the surface of the cathode.

The actual depth of nitrogen penetration into the cathode surface must be further evaluated. The measured depth of contamination could be higher than the true value during an experiment. This may be due to the pushing of contaminants into the metal by the sputtering process (Briggs & Seah (23)). A brief analysis indicates a possible depth error of the order of 15-20 %, which would give a maximum penetration depth of the order of 600 Å (instead of 750 Å as shown in Figure 4.7).

### C) Ar+0.3%N<sub>2</sub> and He+0.4%N<sub>2</sub> - Kinetics of Contaminant Removal

It was decided to examine the kinetics of nitrogen removal from cathodes which had been operated to steady state in nitrogen contaminated Ar and He. The experiments consisted of running in the contaminated gases for long times (> 30 min) and then stopping the addition of nitrogen, without stopping the arc. The changes in the arc characteristics and electrode surface were then examined as a function of time.

The zero minute curve of Figure 4.8 shows the steady state nitrogen concentration profile for experiments with He contaminated with nitrogen running for more than 30 minutes. The one and five minute curves indicate that the arc was running in pure helium for 1 and 5 minutes after the addition of nitrogen was stopped.

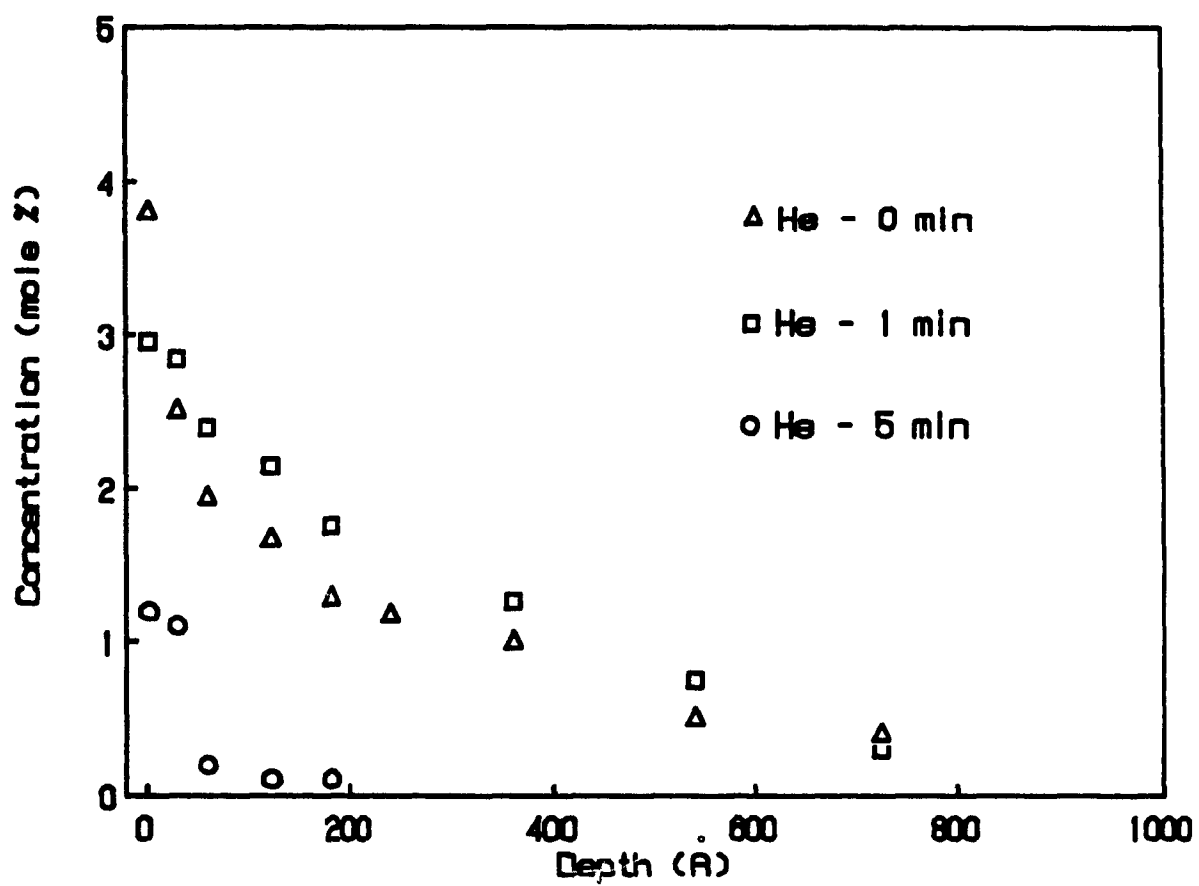


Figure 4.8 - Nitrogen concentration profile

Kinetics of nitrogen removal by a helium arc

After one minute no great change is noticed in the nitrogen profile. During this time the arc velocity dropped from 180 to 140 m/s and the arc voltage increased from 52 to 65 V. After 5 min the level of contamination is much smaller, the arc velocity decreased to 90 m/s and the voltage increased to 85 V. The increased voltage and reduced velocity are an indication of increased surface drag on the arc and subsequent stretching of the arc as discussed in Chapter III. After 15 min the arc showed the operating characteristics of pure He and the surface did not contain any nitrogen.

Figure 4.9 shows the change of arc velocity and nitrogen concentration at the surface with time. It can be seen that there is a direct correlation between them. Since the gas residence time in the chamber was calculated to be of the order of 30 seconds, the long time to return to the arc characteristics of pure He can only be explained through the surface contamination; this is the last evidence needed to confirm the surface contamination/drag/arc velocity/arc voltage relationship proposed in Chapter III.

Figure 4.10 gives the nitrogen removal kinetics in argon; it is shown that the removal of nitrogen is much faster for argon than for helium. After one minute the arc velocity decreased from 30 to 9 m/s while the voltage increased from 38 to 43 V; the surface concentration of nitrogen fell by a factor of two. After 3 minutes of operation the arc showed all the operating characteristics of pure argon and the surface showed only traces of  $N_2$ . The differences for Ar and He removal kinetics can be understood when their erosion rates are compared.

The erosion rate for  $Ar+0.3\%N_2$  is  $3 \mu g/C$  (see Chapter VI) and that for  $He+0.4\%N_2$  is  $0.6 \mu g/C$ . Multiplying these values of erosion by the arc current and the time that it took for the arc to remove the nitrogen contamination, it is possible to obtain:

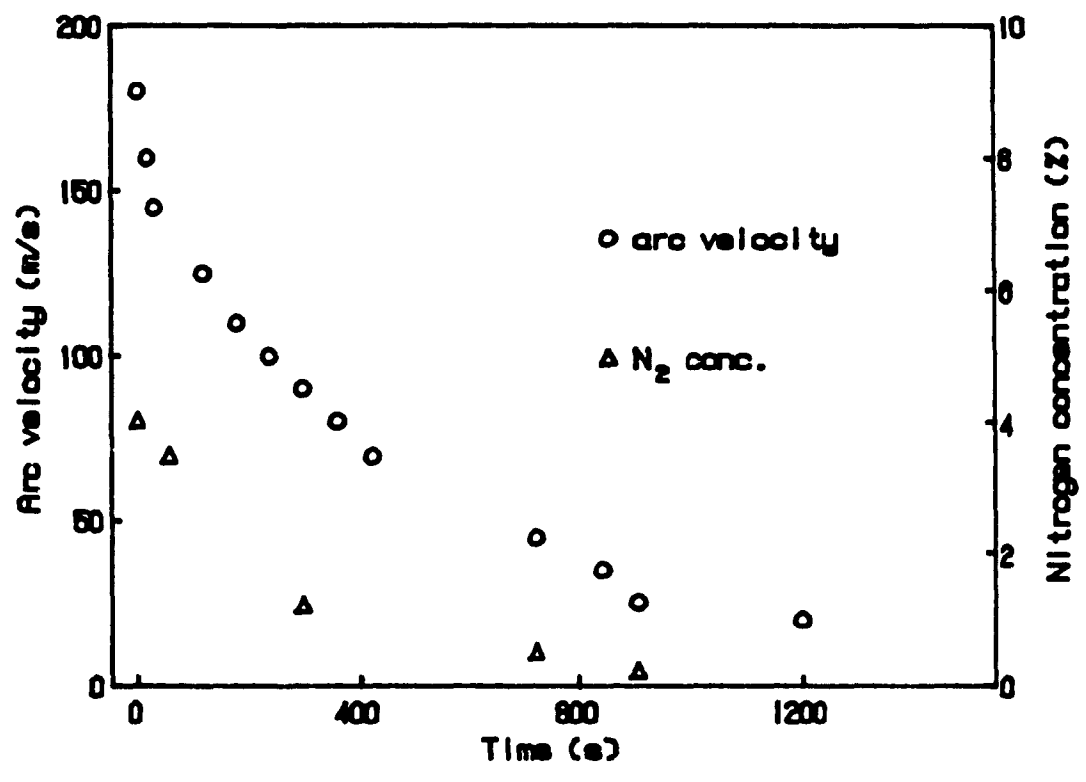


Figure 4.9 - Arc velocity and nitrogen concentration changes with time  
After stopping nitrogen addition in helium

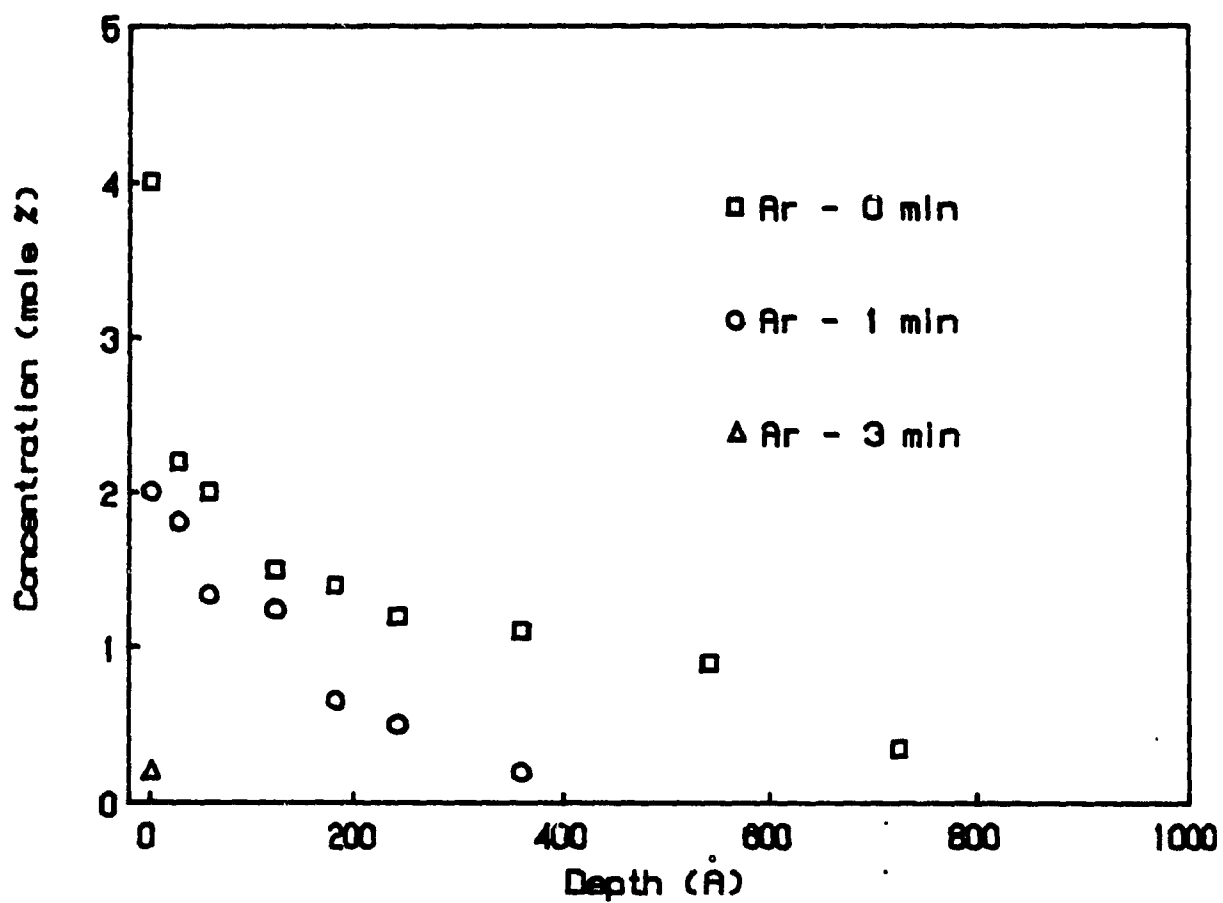


Figure 4.10 - Nitrogen concentration profile

Kinetics of nitrogen removal by an argon arc

For Ar, material removed = 0.054 g

For He, material removed = 0.059 g

This calculation is just an approximation, since the erosion rates change with the time of operation, being lowest for the contaminated surfaces and highest for the clean surfaces. Nevertheless this calculation indicates that the rate of nitrogen removal is related to the overall erosion rate of the arcs. This again confirms the idea of surface contamination, i.e., once the contaminated layer is removed, the arc operates as in the pure inert gas. This also explains the initial changes in arc velocity/voltage when operating with pure inert gases, since the native layer of contaminants must first be removed. It also explains why pure Ar reached a steady state faster than pure He.

Another interesting observation about the "artificial" carbon contamination of the surface using CO (or CH<sub>4</sub>) added to the inert gas is that it produced similar arc characteristics as at the beginning of the experiments with pure Ar and He when "native" carbon contamination is present. This indicates that the important thing here is the carbon and not its source; it also has implications on the electron emission mechanism as it is discussed in Chapter VI.

The transient times after contamination for both inert gases are presented in Table 4.2 below. The same inverse relationship between removal time and erosion rates can be seen in this Table. Because the arc removes approximately 60 Å/s of the cathode (in the case of pure He, erosion rate = 1 μg/C), it should in 5 minutes have cleaned all the surface of nitrogen. The fact that nitrogen remains after 5 minutes can be explained by a migration into the surface due to wear (Roth (22)).

**TABLE 4.2**  
**Transient Times for Removal of Contamination**

Contamination	Time for Removal (after stopping addition) (seconds)	Erosion Rate (for contam. gas) ( $\mu\text{g}/\text{C}$ )
N <sub>2</sub>	180	3.0
Ar	900	0.4
Cl <sub>2</sub>	900	0.5
N <sub>2</sub>	900	0.6
He	900	0.6
Cl <sub>2</sub>	900	0.6

### 5) WORK FUNCTION

The contamination of the cathode surface was shown to produce changes in the arc velocity/voltage. Another method to determine changes in the electronic state of the surface due to contamination is by examining the work function of the surface. In simple words the work function is the energy required by an electron from the highest occupied energy level in the metal (Fermi level) to escape from the surface.

A simple analysis will show the effect of contamination on the work function. The work function of a polycrystalline surface may be defined as (Knapp (24)):

$$\varphi = \xi - \lambda/e$$

where  $\phi$  = work function

$\xi$  = mean electrostatic potential across the metal surface

$\lambda$  = the bulk chemical potential of the electrons

Equation 4.3 has been derived by Lang and Kohn (25);  $\xi$  depends on the surface condition, i.e., it depends on the presence of atoms or molecules adsorbed on the surface (Knapp (24), Riviere (26)). Thus any contamination of the surface results in changes in the work function caused by changes in the mean electrostatic potential. The contamination of a surface has been studied by analyzing changes in the work function by different researchers (see for example Abon et al (27), Jacobi et al (28), Taylor et al (29)).

The most common methods to determine the work function are field emission, diode and capacitor methods. In this work, the use of the capacitor method was chosen for its simplicity and versatility. The method consists of a vibrating plate brought into close proximity of the sample in order to create a capacitor between the plate and the surface of the sample. The plate vibrates at a fixed frequency, varying the capacitance in the system, and generates an ac current if electrically connected to an external circuit. This potential in the external circuit is a standard for the work function. The plate is known as the Kelvin probe for work function measurements (Besoché and Berger (30), Binder et al (31)).

The samples were prepared following the same procedure as for the Auger and ESCA analysis. The results obtained are presented in Table 4.3 below.

TABLE 4.3  
Work Function Measurements

Gas	$\Delta\phi$ (eV)
Ar	0.00
He	0.00
Ar+0.3%N <sub>2</sub>	- 0.18
Ar+0.3%CO	- 0.70
Ar+10%Cl <sub>2</sub>	+ 1.00

The value,  $\Delta\phi$ , in Table 4.3 is the difference between the work function of the sample and a clean copper standard. The surfaces were sputtered prior to the measurements to a depth of 30-50 Å to remove the oxide (carbon) layer that normally is formed during the sample preparation (see last section).

It can be seen that neither Ar nor He gave any variation of the work function of clean copper as expected, since the inert gases should not form any compound with copper and any physisorbed molecule would be removed at ambient temperature in the high vacuum conditions of the analysis chamber ( $10^{-9}$  atm).

The surface contaminated with nitrogen did show a decrease in the work function; the value found of - 0.18 eV corresponds well with studies conducted by Burkstrand et al (32) for variations of the work function of copper with implanted ionic nitrogen.

They also found that increasing the partial pressure of nitrogen in the chamber in order to increase the amount of nitrogen adsorbed in the copper did not change further the work function. This finding is similar to what was observed in this work, where further increase in the amount of nitrogen in Ar or He did not change the characteristics of the surface.

The addition of CO in Ar formed a carbon layer on the top of the cathode surface. The change in the work function was larger, - 0.7 eV. This large change in the work function corroborates the results presented before, where CO caused larger changes in the arc velocity/voltage than did nitrogen. A decrease in the work function indicates that the electrons can leave the surface more easily (less energy necessary for removing the electron from the surface), decreasing the surface drag as mentioned before. Abon et al (27) showed results for changes in the work function of platinum (111 face) for carbon deposits; in their case, the  $\Delta\phi$  was around - 0.6 eV, a value close to what was found here.

A "thick" layer due to chlorine contamination ( $\text{Ar} + > 10\% \text{Cl}_2$ ) produced an increase in the work function of approximately 1 eV. Chlorine is known to form thick films on copper (van Veen et al (33)) and likely to increase the work function due to the formation of negative dipoles with copper (Riviere (26)). As mentioned before, the arc movement was affected by the thickness of the film, being more erratic and with lower arc velocities for thick films. The work function results corroborate those findings

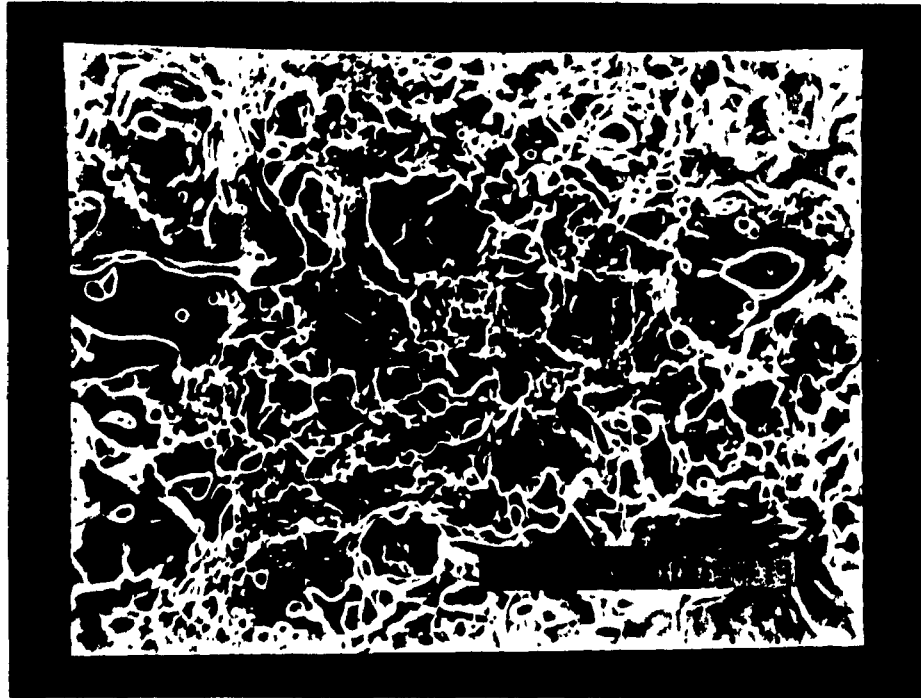
## 6) SEM

Scanning electron microscopes (SEM) have been employed in cathode phenomena studies by many researchers (Daalder (34), Juttner (35), Fu (36)), specially for current density measurements (see next Chapter), although almost all of these works were restricted to vacuum arcs or single arc passages. The SEM was employed here to study the variation of the surface topography (and even composition) when different plasma gases were used.

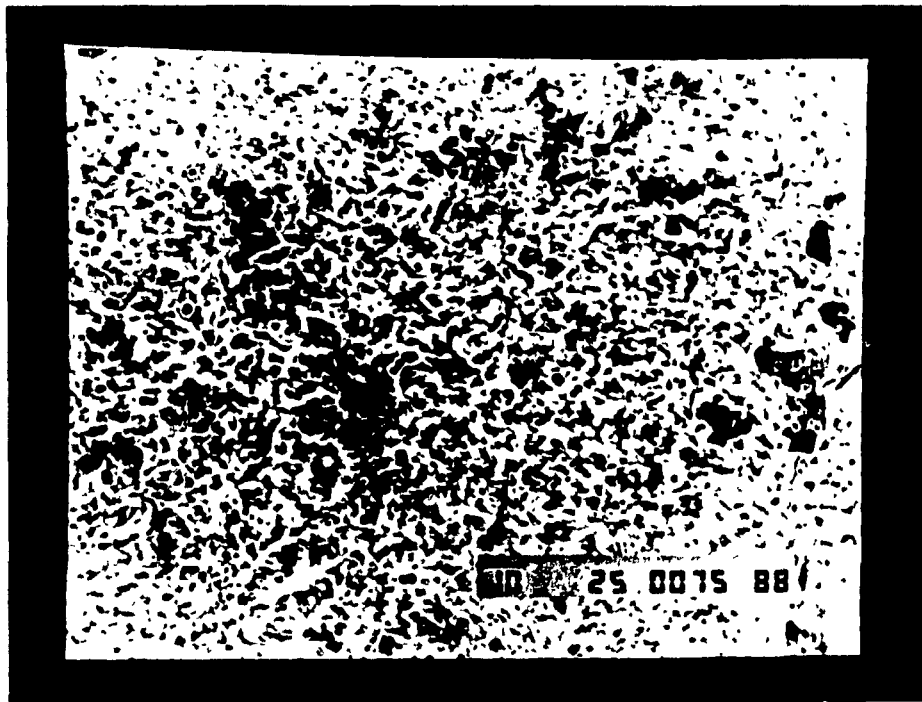
### A) Helium

Figure 4.11a shows the center of the cathode for an experiment using pure He; the experiment lasted for 30 minutes. No information about cathode spot size can be retrieved from this picture because of the multiple passages of the arc (the arc moves at 200 rotations per second for He). Melted copper is found in the picture, comparable to what Kimblin (37) found for vacuum arcs. This could indicate similar mechanisms for vacuum and atmospheric arcs as is discussed in Chapter VI.

Moving from the center of the cathode towards the edge, the heavily melted copper region changes to areas where the surface seems to have suffered less melting, as shown in Figure 4.11b. This fact can be understood as an indication that the arc strikes more often at the center of the cathode than at the edges; this is expected because of the proximity of the anode to the center of the cathode. Figure 4.12a shows a part of the cathode very close to the edge. There is no sign that the arc has moved on this region; the surface is as before the experiment as illustrated in Figure 4.12b. The marks on the surface were caused during the machining of the cathodes.

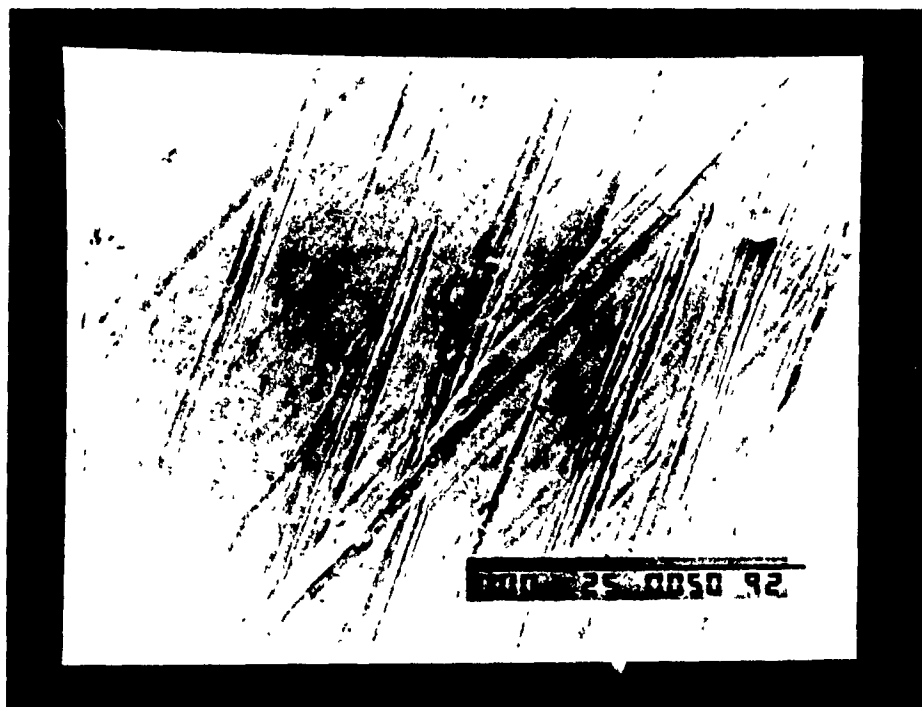


a



b

Figure 4.11 - SEM photograph of a cathode after an experiment using helium  
a) center      b) intermediate region between center and edge



a



b

Figure 4.12 - SEM photograph of a cathode

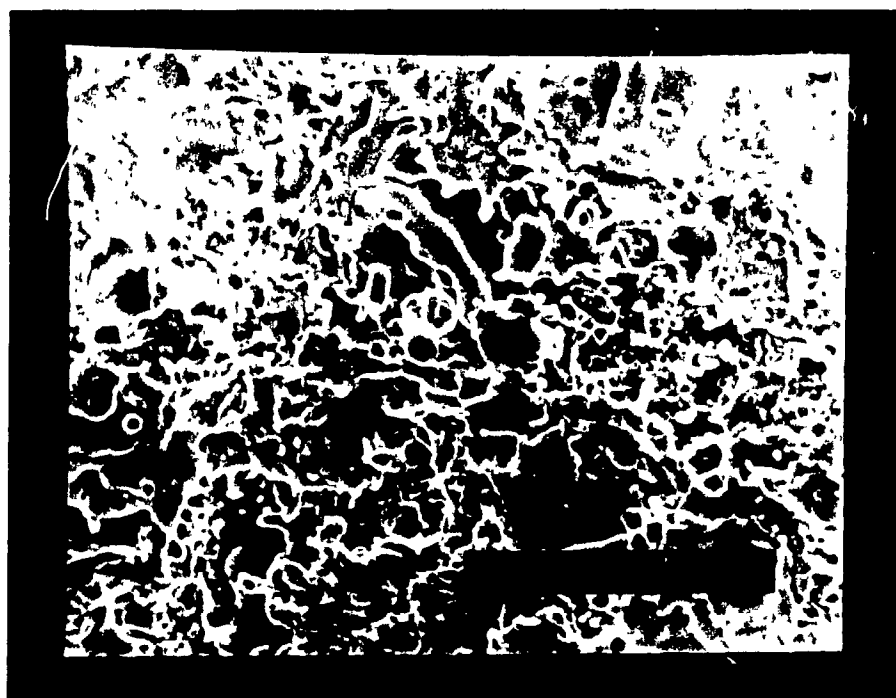
a) after an experiment with helium - edge of the cathode; b) prior to the experiment

B) Ar+0.3%N<sub>2</sub>

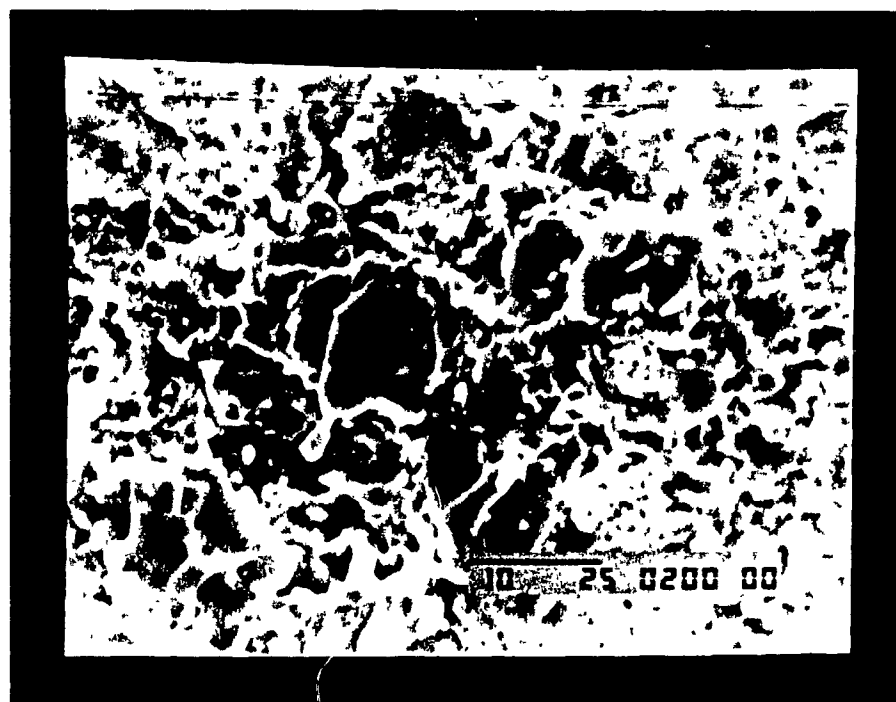
The center of the cathode for experiments with Ar+0.3%N<sub>2</sub> also showed heavy melting as seen in Figure 4.13a. Even the area towards the edge of the cathode (Figure 4.13b), shows heavy melting, indicating that the arc also ran in this region; this was not the case with helium. This corroborates the AES results which indicated the presence of nitrogen even in regions not at the center of the cathodes.

C) Ar+0.3%CO

Figure 4.14a shows the center of the cathode for experiments with argon contaminated with 3 000 ppm of CO. Irregularly spaced "islands" are present on the surface. The copper surface does not seem to have been heavily melted, as shown in Figure 4.14b. The islands were further analyzed in Figure 4.15a. Using the back scattering facility of the SEM, the islands were identified as being made of carbon, while the surrounding surface was just copper. The difference in the brightness of the photograph indicates different elements and the same light colour was found for pure He cathodes; this can be seen in Figure 4.15b. It is likely that the islands are just clusters of carbon particles, caused by an excess of CO injection (more than the arc can remove). It was mentioned before that the arc moves faster and more uniformly for Ar contaminated with small amounts of CO and the fact that the copper is less melted supports this. The carbon islands are not responsible for the easy arc movement, since the arc moves the same way when the formation of the islands is avoided (careful addition of CO in argon to have always the minimum amount). The islands are also very "thick" (> 10 μm thick) which would cause difficulties in the arc movement (see next section).



a

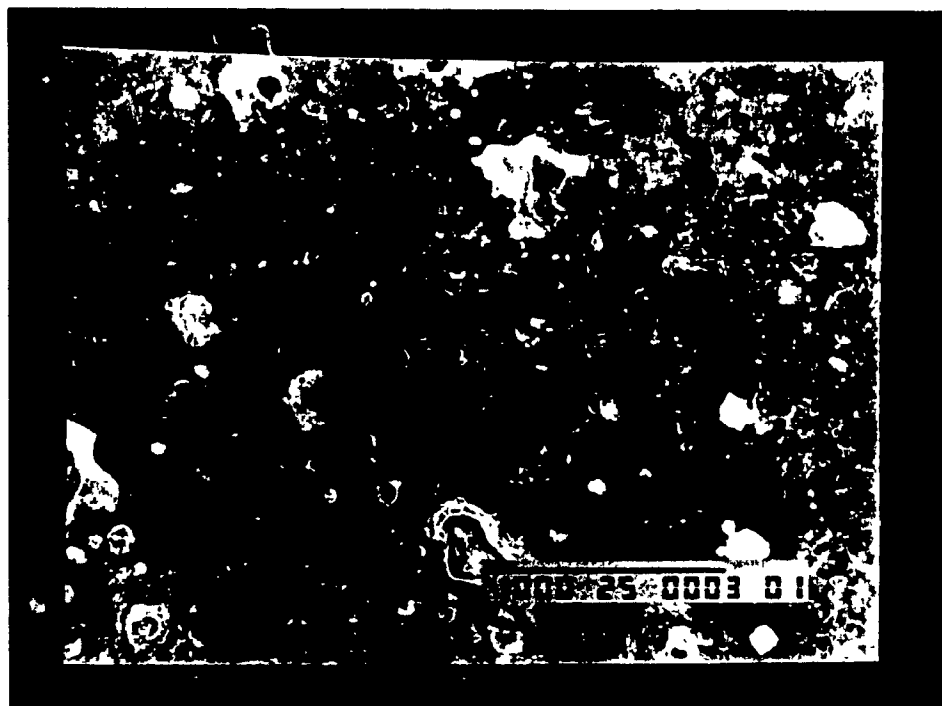


b

Figure 4.13 - SEM photograph of a cathode after an experiment using Ar+0.3%N<sub>2</sub>

a) center

b) edge



a



b

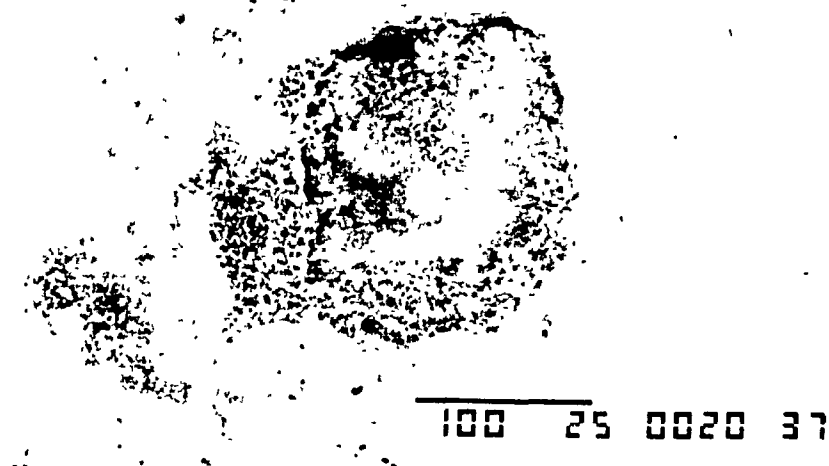
Figure 4.14 - SEM photograph of a cathode after an experiment using Ar+0.3%CO

a) center

b) center - higher magnification



a



b

Figure 4.15 - SEM photograph of a cathode after an experiment using Ar+0.3%CO  
a) carbon island      b) back scattering photograph of similar region

#### D) Ar+10%CO

Figure 4.16a shows the center of the cathode in an experiment with argon contaminated with more than 10 % CO. The carbon islands seen before can not be found in this experiment; the surface looks very uniform. A closer examination of the center of the cathode reveals a thick film (approximate thickness 10  $\mu\text{m}$ ) formed at the surface. The cracks in the film can be seen in Figure 4.16b. The film is formed by small particles with an approximate diameter of 0.4  $\mu\text{m}$ . These particles were identified as carbon particles as discussed below.

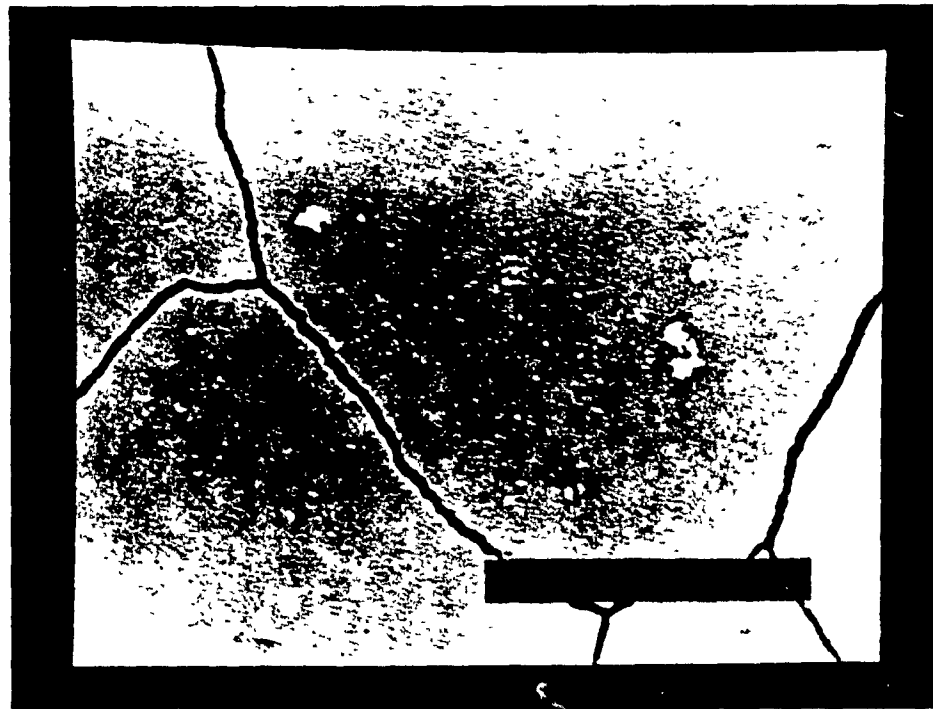
Moving from the center towards the edge of the cathode, the film becomes discontinuous, as shown in Figure 4.17a. Back scatter analysis shows that the film is made of carbon, dark region in Figure 4.17b, with a copper base appearing lighter in the figure. The presence of the thick film for concentrations of CO above 1% in Ar has been suggested before (Chapter III); since the arc stays at the center of the cathode most of the time, the CO would decompose and carbon particles deposit around this region, forming the film. Less particles would reach the edge of the cathode, making the film discontinuous there. The thick film affected the arc movement as explained before has a direct effect on the cathode current density and erosion rate (next Chapters).

#### 7) CONCLUSIONS

In this Chapter it was shown that the contamination of the cathode surface can indeed explain the results obtained in the last Chapter when polyatomic gases or inert gases contaminated with polyatomic gases were used as the plasma gases. A summary of the principal results and conclusions obtained in this work is presented below.



a

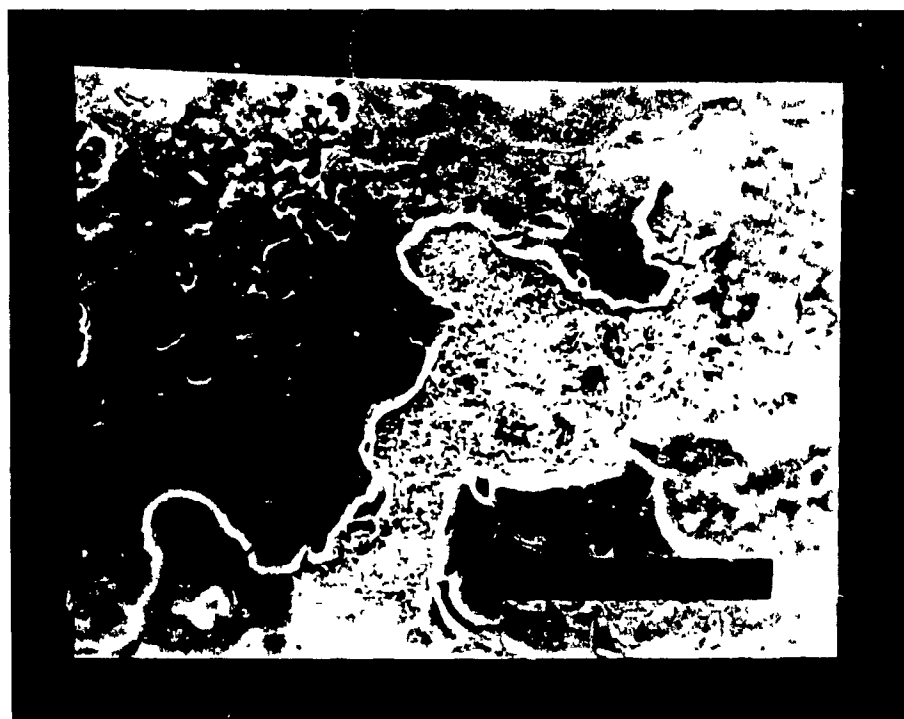


b

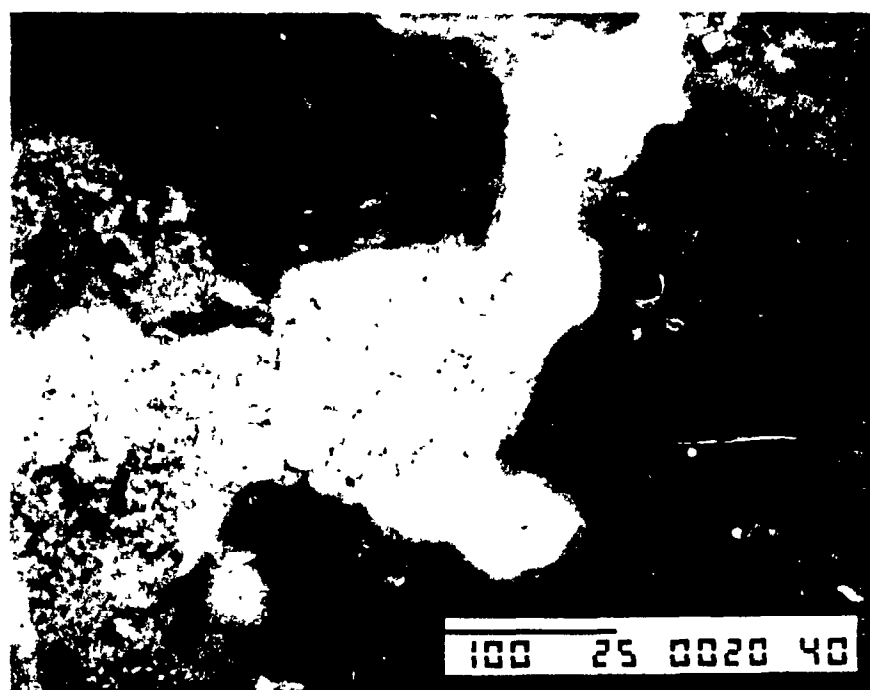
Figure 4.16 - SEM photograph of a cathode after an experiment using Ar+10%CO

a) center

b) center - higher magnification



a



b

Figure 4.17 - SEM photograph of a cathode after an experiment using Ar+10%CO

a) edge    b) back scattering photograph of similar region

- a) It was shown using Auger and ESCA spectroscopy that contamination of the inert gases (Ar and He) with polyatomic gases contaminates the surface of the cathode.
- b) The changes in the arc velocity and arc voltage caused by contamination of the inert gases are due to cathode surface contamination rather than changes in the plasma gas.
- c) Cleaning the cathode surface with  $\text{HNO}_3$  and  $\text{CCl}_4$  did not remove the carbon contamination prior to the experiments but the use of the arc is quite effective for the removal of any contaminating layer. The changes in the arc characteristics for Ar and He at the beginning of the experiment are due to this carbon contamination. This suggests that the results for arc velocity and erosion rate for short term experiments previously reported in the literature were probably obtained during conditions that are not reproducible and therefore resulting in the scatter in the data.
- d) Chlorine was found in the outer regions of the cathode which were less eroded than the center; chlorine was also found in short term experiments. Both facts point to a segregation of chlorine from the bulk towards the surface due to temperature gradients.
- e) Nitrogen was found at the surface of the cathode when it was used as the contaminant for the inert gases or as the pure plasma gas. The presence of nitrogen to depths between 500 and 1 000 Å suggests that the cathode surface was melted to this depth.
- f) The oxygen found at the surface of the cathode is independent of the plasma gas used and is probably due to the exposure of the sample after the experiment to atmospheric air.

g) Arcs running in helium remove the contamination layer more slowly than arcs in argon; since removal is by volatilization, this is an indication that the surface for argon arcs is hotter than for helium.

h) Surface analysis at the cathode indicated that copper contaminated with nitrogen has a lower work function than pure copper; carbon contaminated copper has an even lower work function for low levels of contamination; thick films of chlorine formed on the cathode surface increase the work function. These results corroborate the ideas of arc movement/surface drag/ electron emission discussed in the last Chapter.

i) SEM photographs showed melted regions at the center of the cathode for He and Ar+0.3%N<sub>2</sub>. For the latter the region close to the edge of the cathode also showed signs of melting; the melting indicates that the arc moved along these regions. Argon contaminated with 3 000 ppm of carbon monoxide showed less copper melting; carbon islands were found on the surface. The islands are likely to be caused by an excess addition of carbon monoxide to argon. Argon contaminated with 10 % carbon monoxide showed a thick carbon film (10 μm) at the center of the cathode; the film becomes discontinuous towards the edge of the cathode where the arc spent less time.

REFERENCES

- 1) Achtert, J; Altrichter, B.; Juttner, B.; Pech, P.; Pursch, H.; Reiner, H.D.; Rohrbeck, W.; Siemroth, P.; Wolf, H.; "Influence of Surface Cont. on Cathode Proc. of Vac. Discharges", Plasma Phys. Vol 17, 419-431, 1977.
- 2) Farrall, G.A.; Owers, M.; Hudda, F.G.; "A SEM study of electron emission and topography of surfaces subjected to arcing at high current in vacuum", IEEE PES Winter Meeting, N.Y., Paper C 75 102-9, 1975.
- 3) Athwall, C.S.; Bayliss, K.H.; Calder, R.; Latham, R.V.; "Field Induced Electron Emission from Artificially Produced Carbon Sites on Broad Area Copper and Niobium Electrodes", IEEE Trans. Plasma Science, Vol PS-13, n.5, 226-229, 1985.
- 4) Doan, G.E.; Thorne, A.M.; "Arc in Inert Gases", Phys. Rev. 48, 49-52, 1934.
- 5) Niedermann, P.; Sankarraman, N.; Noer, R.J.; Fisher, O.; "Field Emission from Broad Area Niobium Cathodes: Effects of High Temperature Treatment", J. Appl. Phys., vol. 59, n.3, 892-901, 1986.
- 6) Porto, D.R.; Kimblin, C.W.; Tume, D.T.; "Experimental observations of cathode spot surface phenomena in the transition from a vacuum metal vapor arc to a nitrogen arc", J. Appl. Phys., vol. 53, n.7, 4740-4749, 1982.
- 7) Chemicat, B.; Andanson, P.; "Electrical Conductivity of a Arc Column Contaminated with Copper Vapor", J. Phys. D: Appl. Phys., vol. 18, n.11, 2183, 1985.
- 8) Xi, C.; Chyou, Y.P.; Lee, Y.C.; Pfender, E.; "Heat Transfer to a Particle Under Plasma Conditions with Vapor Contamination from the Particle", Plasma Chemistry and Plasma Processing, vol 5, n.2, 119, 1985.
- 9) Lea, C.; "Composition-depth profiling using Auger electron spectroscopy", Metal Science, vol. 17, 357-367, 1983.
- 10) Chang, C.C.; "Auger Electron Spectroscopy", Surface Science, vol.25, 53-79, 1971.
- 11) Hitchcock, A.H.; Guile, A.E.; "Effect copper oxide thickness on number and size of arc cathode emitting sites", IEE Proc., vol.124, 148-152, 1977.
- 12) Hitchcock, A.H.; Guile, A.E.; "Erosion of cop. cath. by moving arcs at currents of 45-800 A", Proc. IEE, vol. 122, n.7, 763-764, 1975.

- 13) Poeffel, K.; "Influence on the Copper Electrode Surface on Initial Arc Movement", IEEE Trans. Plasma Science, Vol. PS-8, n.4, 443-448, 1980.
- 14) Schreurs, J.; Johnson, J.L.; McNab, I.R.; "High Current Brushes part VI: Evaluation of Slip Ring Films", IEEE Transactions on Components, Hybrids and Manufacturing Technology, vol. CHMT-3, n.1, 83-88, 1980.
- 15) Prutton, M.; Surface Physics, Oxford University Press, 2 ed., 1985.
- 16) Harris, L.A.; "Observations of Surface Segregation by Auger Electron Emission", J. Appl. Phys., vol. 39, n.3, 1428-1431, 1968.
- 17) Hofmann, S.; Erlewein, J.; "Determination of the diffusion coefficient atoms in metals via surface segregation", Scripta Metallurgica, vol. 10, 857-860, 1976.
- 18) Lloyd, J.N.; Vook, R.W.; Pope, L.E.; "UHV-AES Investigations of Sulfur Surface Segregation in Precious Metal", IEEE Trans. Comp. Hybrids Manuf Tech. Vol CHMT-9, n.1, 1986.
- 19) Heskett, D.; Baddorf, A.; Plummer, E.W.; "Nitrogen induced reconstruction of Cu(110): Formation of a surface nitride", Surface Science, vol. 195, 94-102, 1988.
- 20) Zomorrodian, A.; Tougaard, S.; Ignatiev, A.; "Range distribution of low energy nitrogen ions in metals", Physical Review B., vol. 30, n.6, 3124-3130, 1984.
- 21) Ziegler, J.F.; Biersack, J.P.; Littmark, U.; "The stopping and range of ions in solids", Volume 1 - The stopping and ranges of ions in matter, Ed. J.F. Ziegler, Pergamon Press, 1985.
- 22) Roth, J.R.; "Theory of Plasma Ion Implantation for Hardening Metals", 14 IEEE International Conference Plasma Science, Paper 6Y6, 1987.
- 23) Briggs, D.; Seah, M.P.; Practical surface analysis by Auger and ESCA, John Wiley and Sons, N.Y., 36, 1983.
- 24) Knapp, A.G.; "Surface Potentials and their Measurement by the Diode Method", Surface Science, vol. 34, 289-316, 1973.
- 25) Lang, N.D.; Kohn, W.; "Theory of Metal Surfaces: Work Function", Physical Review B., vol. 3, n.4, 1215-1223, 1971.
- 26) Riviere, J.C.; Solid State Surface Science, Ed. Mino Green, Marcel Dekker, N.Y. 1969.

- 27) Abon, M.; Billy, J.; Bertolini, J.C.; Tardy, B.; "Work function changes associated with hydrocarbon fragments on the Pt(111) face", *Surface Science*, vol. 167, L187-193, 1986.
- 28) Jacobi, K.; Zunicker, G.; Gutmann, A.; "Work Function, Electron Affinity and Band Bending of Zinc Oxide", *Surface Science*, vol. 141, 109-125, 1984.
- 29) Taylor, J.L.; Weinberg, W.H.; "Method of continuously measuring work function changes", *J. Vac. Sci. Tech.*, vol.15, n.6, 1811-1814, 1976.
- 30) Besoche, K.; Berger, S.; "Piezoelectric driven Kelvin probe for contact potential difference studies", *Rev. Sci. Instrum.*, vol. 47, n.7, 840-842, 1976.
- 31) Bindner, P.E.; Selkirk, E.B.; Norton, P.R.; United States Patent, Patent Number 4649336, 1987.
- 32) Burkstrand, J.M.; Kleiman, G.G.; Tibbetts, G.G.; Tracy, J.C.; "Study of the N-Cu(100) System", *J. Vac. Sci. Tech.*, vol. 13, 291-295, 1975.
- 33) van Veen, G.N.A.; Baller, T.; Dielerman, J.; de Vries, A.E.; "Nanosecond ultraviolet laser induced etching of Si and Cu exposed to chlorine", *J. Vac. Sci. Tech.*, vol. A5, n.4., 1606-1607, 1987.
- 34) Daalder, J.E.; "Cathode Spots and Vacuum Arcs", *Physica*, vol. 104C, 91-106, 1981.
- 35) Juttner, B.; "Erosion Craters and Arc Cathode Spot in Vacuum", *Plasmaphysik*, vol.1, 25-48, 1979.
- 36) Fu, Y.H.; "Correlation Between Time Resolved Vacuum and Arc Voltage and Cathode Erosion Structure", *IX Int. Conf. on Gas Disch. Applications*, 59-62, 1988.
- 37) Kimblin, C.W.; "A review of arcing phenomena in vacuum and in the transition to atmospheric pressure arcs", *IEEE Trans. Plasma Science*, vol. PS-10, 322-330, 1982.

V. CURRENT DENSITY

## V. CURRENT DENSITY

### 1) INTRODUCTION

- Well, I have to admit Holmes, I am getting excited about this "arc". It seems that you were right again; the game was afoot... The arc mystery is finally solved. Holmes, are you listening to me?

- Yes, Watson, I am listening, but I am afraid I have to disagree with you... I don't know what, but I have the feeling that we are forgetting something... It can't be that simple, Watson, it just can't. There is something that we are missing, but I can't think of what...

- Holmes, it seems you cannot relax, even if I prove to you that Moriarty is in jail... Not that he is, but Holmes, let's just have a cup of tea to celebrate this big achievement, and forget about everything else!

And as Watson talks, he starts cleaning the table and making faces towards Holmes to remind him to make the tea... Fifteen minutes later, they are enjoying the tea and Watson keeps talking, and talking and talking...

- Holmes, I don't know what you put in this tea, but it certainly tastes different.. Did you try those old herbs that we got from India some time ago?

- No, Watson, I just added some mint leaves and a bit of synup ... I hope it does not taste too bad...

- Of course not, Holmes, I kind of like it. It just have a different, how can I say, consistency. It is like if its density is different and..

- That's it Watson!! You found the answer!!!

Holmes almost dropping his cup on the floor rushes to his desk and start writing...

- Holmes, what happened? What did I find?

- The missing factor, Watson, you just found the missing factor. We measured a lot of things of the arc, but we forgot one of the most important parameters, my dear friend. We forgot the arc density!!!

- The what Holmes?

- The arc density!! Think Watson, think. If the arcs have different sizes, the heat over a certain area will be different. We must find the arc density!

- But how can we measure such a thing as the arc density Holmes?

- That's exactly the problem...How?? I think I have the answer for that. We are going to need some wire to make a coil. Then we need....

Coming back to the thesis...

### A) Chapter Guideline

In this Chapter the current density of the arc attachment is discussed. The current density is a very important parameter in erosion studies. Three techniques are normally employed for the measurement of the current density; it is shown that these methods could not be applied in this work and therefore a new technique was developed. After describing the new method, current density results are given for different plasma gases and operating conditions. It is shown that the current density can be very different depending on the operating conditions and plasma gases.

### B) Why Current Density?

There are two significant classes of heat sources on the cathode surface: an external one, caused by particle impact on the surface and an internal one, called Joule heating, due to the passage of the electric current in the volume of the cathode (it is discussed in Chapter VII that the heating of the cathode by radiation and convection has too low a flux to be important in erosion). Both sources are related to the area of attachment of the arc on the surface of the cathode. The size and shape of the arc attachment on the electrodes is thus very important in electrode erosion studies. The arc attachment dimension is also an important parameter to understand the mechanism of electron emission of the cathode, as discussed in the next Chapter.

Three types of techniques are commonly used to determine the arc attachment and the current density; they are based on A) optical measurements of the arc root during an experiment or on B) the examination of erosion tracks after an experiment or on C) the voltage induced in a probe in a split electrode. The most important features of each technique are examined in the next section.

## 2) DESCRIPTION OF THE PREVIOUS METHODS

### A) Optical Technique

This method employs high speed photography to determine the dimensions of the bright plasma near the cathode (or anode). This bright region is identified as being the arc attachment. The main problems with this technique are: a) identification of the plasma cloud in front of the cathode with the arc attachment b) temporal and spatial resolution of the instruments due to the small size and lifetime of the cathode spot. Rakhovskii (1,2) reported values for the current density in the range of  $10^4 - 10^5$  A/cm<sup>2</sup> for copper cathodes in vacuum; similar results were found by Smith et al (3).

### B) Erosion Tracks

This technique is based on the marks left on the surface of the cathode after the passage of the arc. The dimensions of the craters are supposed to be the dimensions of the arc attachment. The researchers normally used a scanning electron microscope for the analysis. The main problems with this method are: a) identification of the craters (tracks) with the cathode spot (it has been suggested that the craters can be formed as a consequence of the action of the cathode plasma on the cathode surface or other effects (Haptzche et al (4) and Gabovich et al (5)); b) determination of how many spots are active at the same time, to estimate the current flowing per spot; c) the one-shot nature of the method, needing a near new surface which is impractical in any industrial plasma application; d) the conditions of the surface are not necessarily the same in each experiment (thickness of contaminating layers) which make it hard to compare results.

The technique has been employed by many researchers (Sanger et al (6), Juttner (7), Djakov et al (8), Guile (9), Daalder (10)) and the current density obtained is in the range  $10^7 - 10^8$  A/cm<sup>2</sup>.

The problem with the methods presented above is that they are indirect methods, i.e., both are based on measurements of physical parameters that have to be then correlated to the current density of the arc attachment. Also both methods are almost impossible to use in industrial plasma torches.

### C) Voltage Induced in a Probe

The novel technique developed to measure the size of the arc attachment at the electrodes is based on a method previously used by Drouet et al (11) for current distribution on the electrode surface for intermittent experiments. Their method is described below.

A cylindrical cavity is made below the electrode surface as shown schematically in Figure 5.1. A narrow slit runs from the cavity to the electrode surface. The arc is driven by an external magnetic field; as the arc passes across the slit, the arc current on the left of the slit decreases while that on the right increases. The changes in the current generate a variation in the magnetic field within the cavity. A small coil located inside the cavity picks up this variation, the whole system acting like a transformer.

The voltage signal from the coil can be displayed on an oscilloscope, where the signal is directly discretized or stored for later discretization. The signal can be transformed into a linear current distribution in the direction of the arc movement using equation 5.1 and 5.2 (the detailed derivation of these equations can be found in Beaudet (12)).

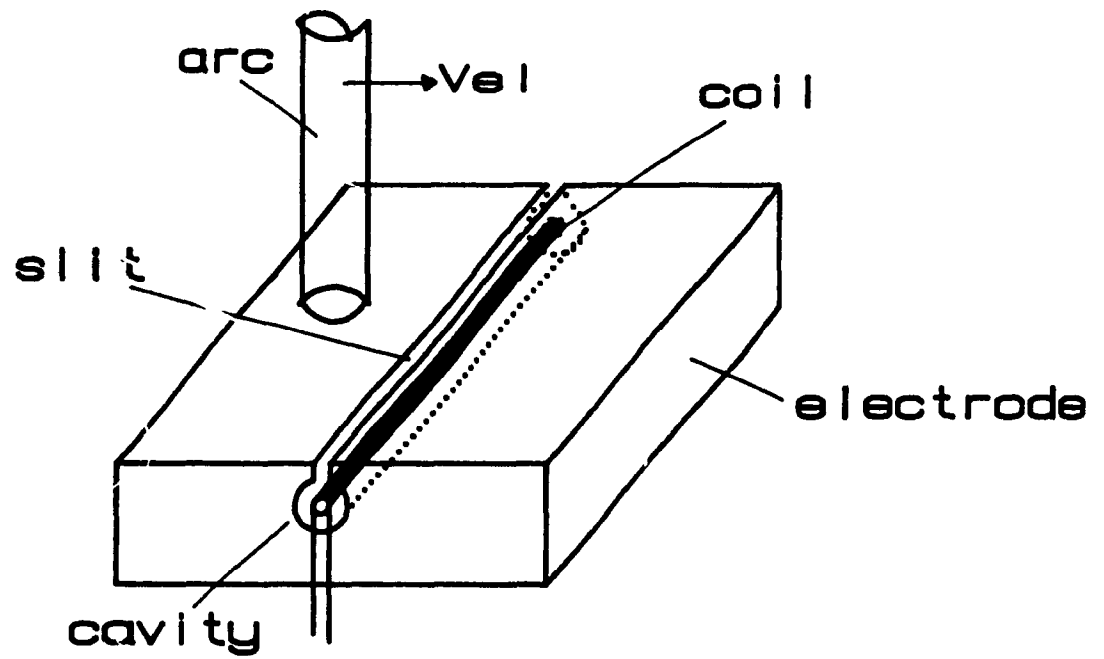


Figure 5.1 - Schematic representation of the slit current density probe

$$dI/dt = J_x v_x \quad 5.1$$

$$dI/dt = V(t)/M \quad 5.2$$

where  $I$  = arc current

$t$  = time

$J_x$  = linear current distribution of the arc attachment in the direction  $x$  of the arc movement

$J_x = \int J_{xy} dy$  (the limits of  $\int$  are  $y_1$  and  $y_2$ , arc size in the  $y$  direction)

$J_{xy}$  = current density of the arc attachment

$v_x$  = arc velocity ( $x$  direction)

$V(t)$  = signal (voltage) from the coil

$M$  = mutual inductance (cavity-coil)

Equation 5.3 can be obtained from 5.1 and 5.2;

$$J_x = V(t) / (v_x M) \quad 5.3$$

It can be seen from equation 5.2 that the technique requires the system to be calibrated to obtain  $M$ . The determination of  $M$  can be done by injecting a high frequency current from a pulse generator across the slit; the current is forced to circulate around the cavity and the signal obtained from the coil can be used to determine the variation of the impedance cavity-coil ( $Z$ ) with frequency. If the transfer impedance  $Z$  is linearly dependent of the frequency, the impedance is inductive and therefore:

$$Z = w M \quad 5.4$$

where  $Z$  = transfer impedance (cavity-coil)

$w$  = frequency

$M$  = mutual inductance (cavity-coil)

In order to determine the linear current distribution using the above technique the cathode (cylindrical geometry) was cut in half after a cavity of 1 mm diameter had been made 0.1 mm below the cathode surface (cathode wall thickness is 2.5 mm). A space of 0.01 mm was machined from the surface to the cavity of each side of the cathode in order to have a slit of 0.02 mm when the two parts were reunited. A copper ring was made to hold the two halves together and to guarantee the electrical contact between the parts. The cathode is shown schematically in Figure 5.2a. A 400 turn coil was made of very fine insulated copper wire and the impedance of the system for different frequencies was measured; this is shown in Figure 5.3a.

It can be seen from this figure that the impedance did not vary linearly with frequency (slope of the line is 0.87), indicating that the transfer impedance was not purely inductive, i.e., the two halves did not have good electrical contact. In order to correct this, part of the ring above the slit and part of the external cathode wall at the same location was removed and solder was poured in this "hole". This is illustrated in Figure 5.2b.

The impedance obtained in this arrangement is shown in Figure 5.3b and now is linearly dependent on the frequency (slope of the line is 0.99); the phase angle of the injected current and the signal from the coil is 90 degrees for the whole range of frequencies, as it should be for pure inductive impedance. The mutual impedance obtained from the calibration is  $5.2 \times 10^{-9}$  Henry.

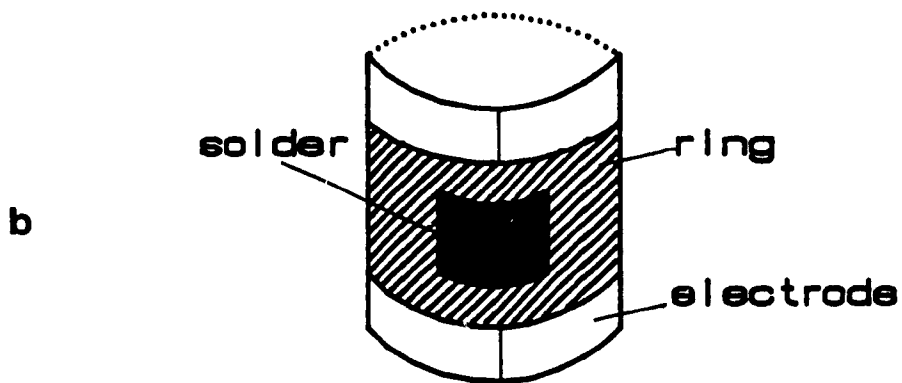
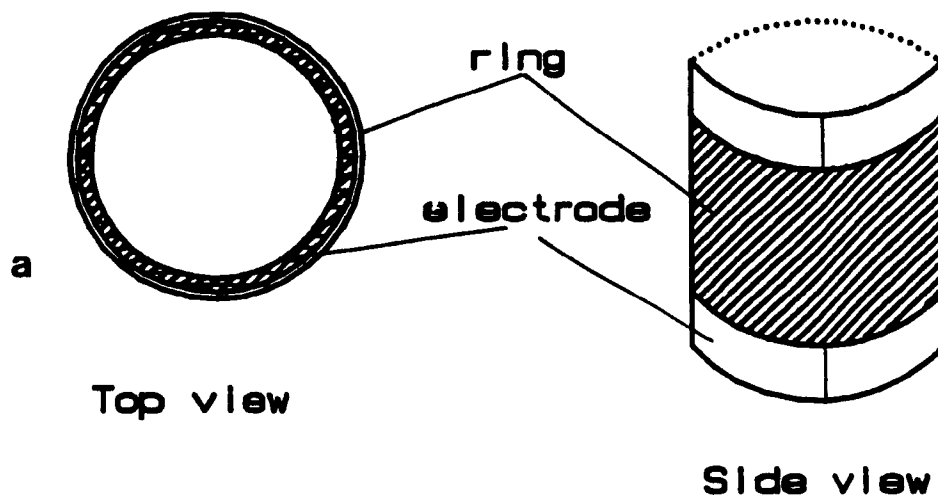


Figure 5.2 - Schematic representation of the cylindrical cathode

a) with copper ring

b) with copper ring and solder

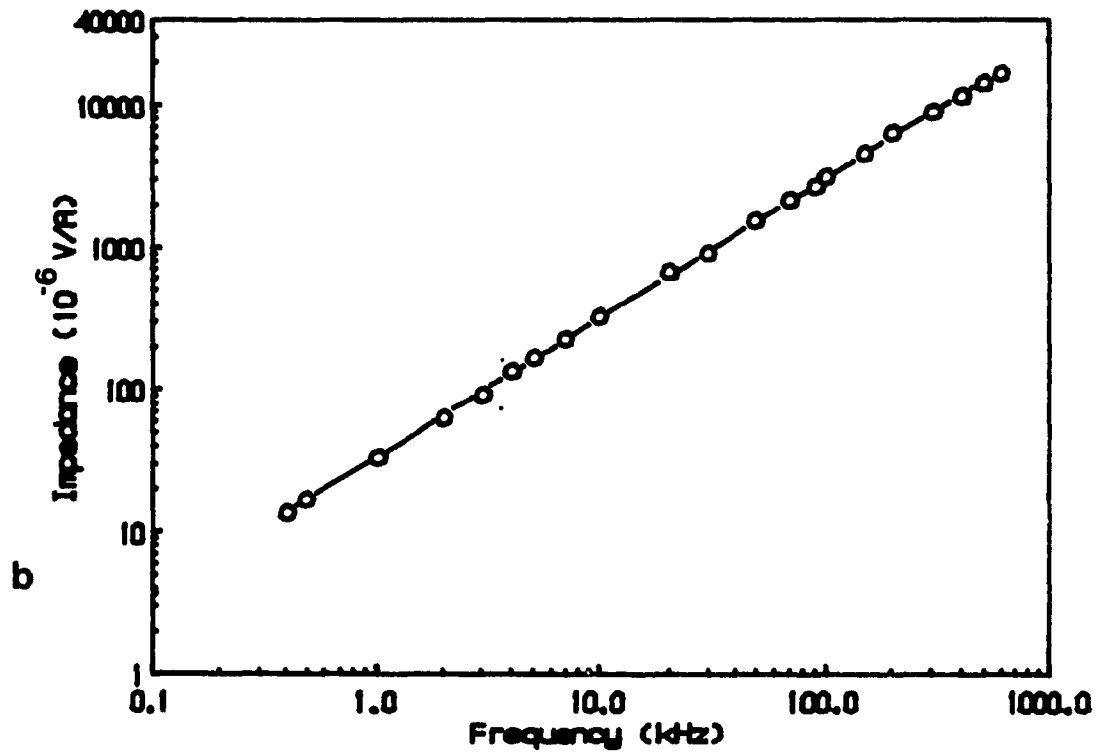
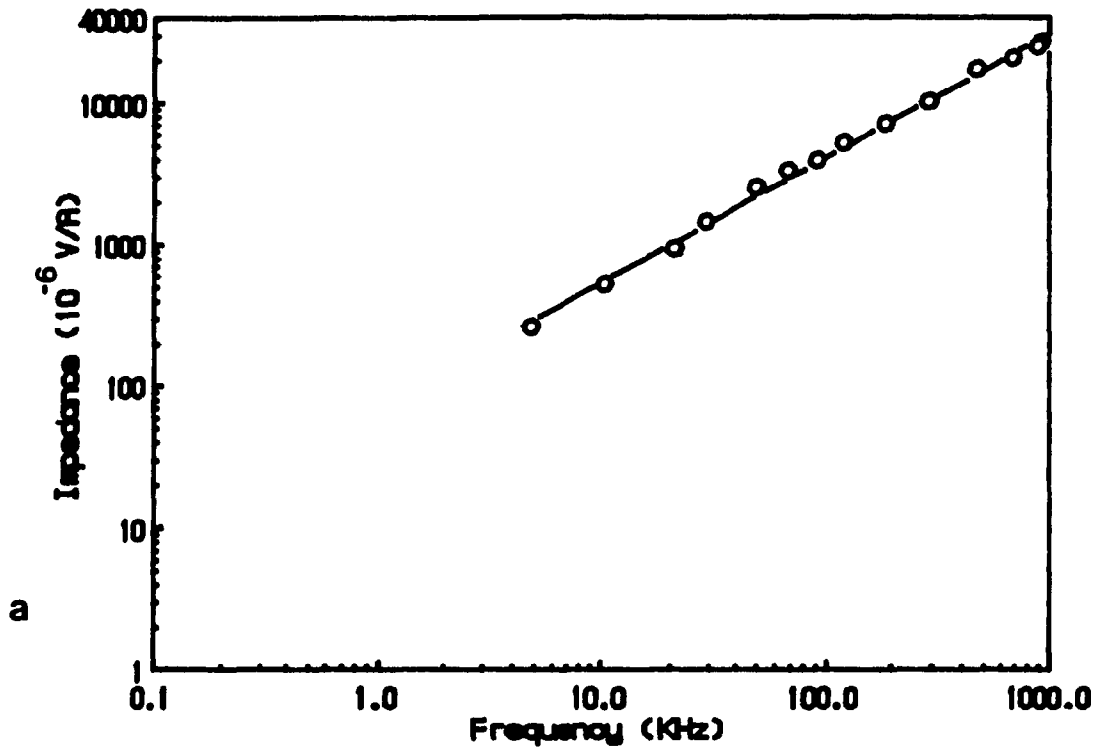


Figure 5.3 - Impedance of cavity-coil system vs frequency

a) with copper ring

b) with copper ring and solder

Experiments were conducted with different plasma gases and operating conditions. It was noted that even with the fastest arcs and lowest erosion rates (high magnetic field and contaminated surfaces) the slit was partially destroyed after 1 s of operation. Copper bridges were formed, connecting the two sides of the slit and invalidating the calibration obtained for the system. A different method had to be developed. The technique described in the next pages provides a direct measurement of the arc attachment at the electrode surface for industrial plasma torches.

### 3) NOVEL TECHNIQUE

#### A) Description

The major innovation of the new technique is the complete removal of the slit to avoid the melting problem and the formation of the copper bridges. The system now is formed just by the cavity and the insulated coil inside it. As a result the probe can now be used for long periods of time.

The presence of the arc in the vicinity of the cavity still induces a voltage in the coil. The problem of this technique is that the direct calibration of the system is no longer possible. This problem was solved using Fourier analysis and is described below.

#### B) Fourier Analysis

A generic system can be characterized by its frequency response, which is also referred to as the transfer function of the system. The transfer function can be determined by acquiring  $x(t)$  and the corresponding  $y(t)$  of the system, where  $x(t)$  represents the input and  $y(t)$  the output signal. The signals  $x(t)$  and  $y(t)$  can then be

transformed into the frequency domain using Fourier transformation. "Dividing"  $Y(w)$  by  $X(w)$  (frequency domain representation for  $y(t)$  and  $x(t)$  respectively) one obtains  $H(w)$  which is the transfer function of the system (Ramirez (13)).

The system without the slit can be calibrated by considering an "imaginary" system as follows: the input  $x(t)$  of this system is the coil signal obtained using the system with the slit for a certain set of operating conditions; the output  $y(t)$  is the signal obtained with the system without a slit for the same operating conditions. The transfer function of this "imaginary" system  $H(w)$  is generated using Fourier transformations. This transfer function can then be used with any signal obtained from the no slit system to synthesize the signal which would have been produced using the slit system, i.e.,

$$X_1(w) = Y_1(w) H(w) \quad 5.5$$

and transforming back into time,

$$x_1(t) = \text{Fourier}^{-1} X_1(w) \quad 5.6$$

where  $H(w)$  = transfer function

$Y_1$  = Fourier transformation of  $y_1$

$y_1$  = signal obtained from the no slit system for any condition

$x_1$  = signal calibrated with the transfer function

$X_1$  = Fourier transformation of  $x_1$

$\text{Fourier}^{-1}$  = anti-transformation of Fourier

The signal  $x_1$  is the signal from the no slit system after calibration (it would had been obtained with the slit system if this latter was able to stand longer experiments).

C) Calibration of the No Slit System

A cylindrical cavity was made with the same dimensions and located at the same depth into the cathode as for the slit system. The same coil was used for both systems.

The signal obtained from the slit system is shown in Figure 5.4a. The signal was obtained using pure helium as the plasma gas; the operating conditions are summarized in Table 5.1 below.

**TABLE 5.1**  
Operating Conditions for Signal from the System With Slit

Plasma Gas	Arc Velocity (m/s)	Arc Current (A)	Time (s)	B (G)
He	160	110	0.5	1000

The time in the Table refers to when the signal was obtained, i.e., the signal was obtained approximately 0.5 s after the experiment had started.

The reasons for the high arc velocity in pure helium are related to the contamination of the cathode prior to the experiment as explained in the last Chapters. The major contaminant is carbon as mentioned before.

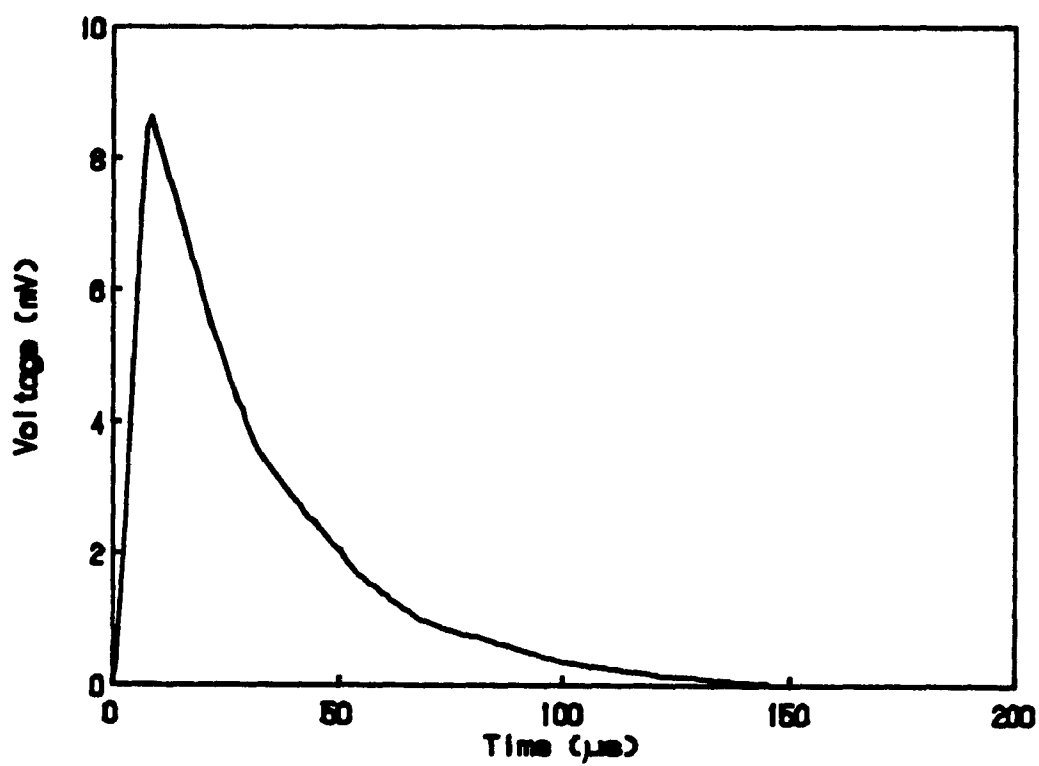
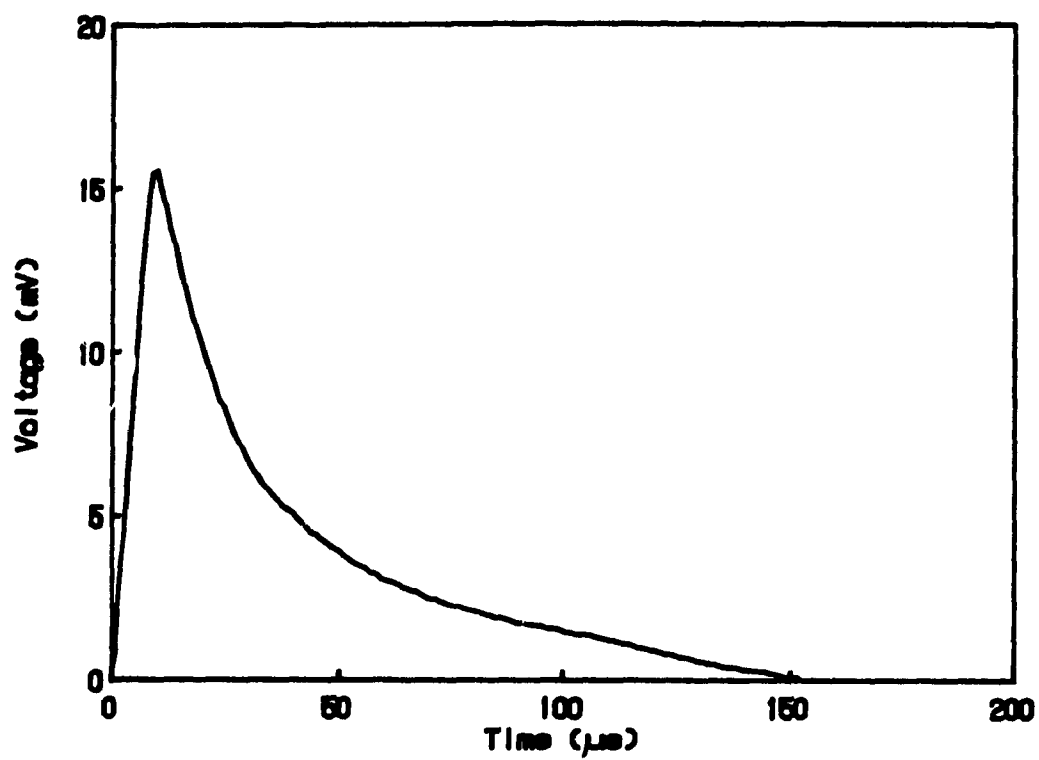


Figure 5.4 - Signal obtained using He and He+0.4%CO at 160 m/s

a) slit system

b) no slit system

Pure helium was also used as the plasma gas for the no slit system at the same operating conditions as for the slit system. Signals were obtained during the first 5 seconds of the experiments. The arc velocity was approximately 150 m/s. The slightly different arc velocity when compared with the slit system signal is probably due to different contamination level of carbon (and also oxygen) which cannot be exactly controlled. Since the signal obtained with those different arc velocities could be slightly different, it was decided to use helium contaminated with 4 000 ppm of CO and adjust the magnetic field in order to obtain exactly 160 m/s (the surface conditions have been shown in Chapter III and IV to be similar for He+0.4%CO and pure He with carbon contamination prior to the experiment). The signal using contaminated He at 160 m/s is indeed very similar to the one obtained with pure He at 150 m/s for the no slit system and it is shown in Figure 5.4b.

The transfer function was obtained using the signals shown in Figure 5.4a as the input and in Figure 5.4b as the output. This was done using the Fast Fourier Transform algorithm (FFT). A signal obtained using pure CO at 95 m/s and 100 A is shown as an example in Figure 5.5. This signal is the one obtained directly from the no slit system. Also shown in Figure 5.5 is the same signal after being calibrated with the transfer function.

The validity of the calibrated signal can be checked by integrating the signal (voltage vs time). The integral divided by M (established before) should be equal to the total arc current (measured independently using a shunt in series with the cathode) as shown in equation 5.2. The error after integration and comparing with the known arc current is less than 2 %, indicating that the method is valid and can in fact be used to estimate the linear current distribution at the arc foot in the direction of the arc motion.

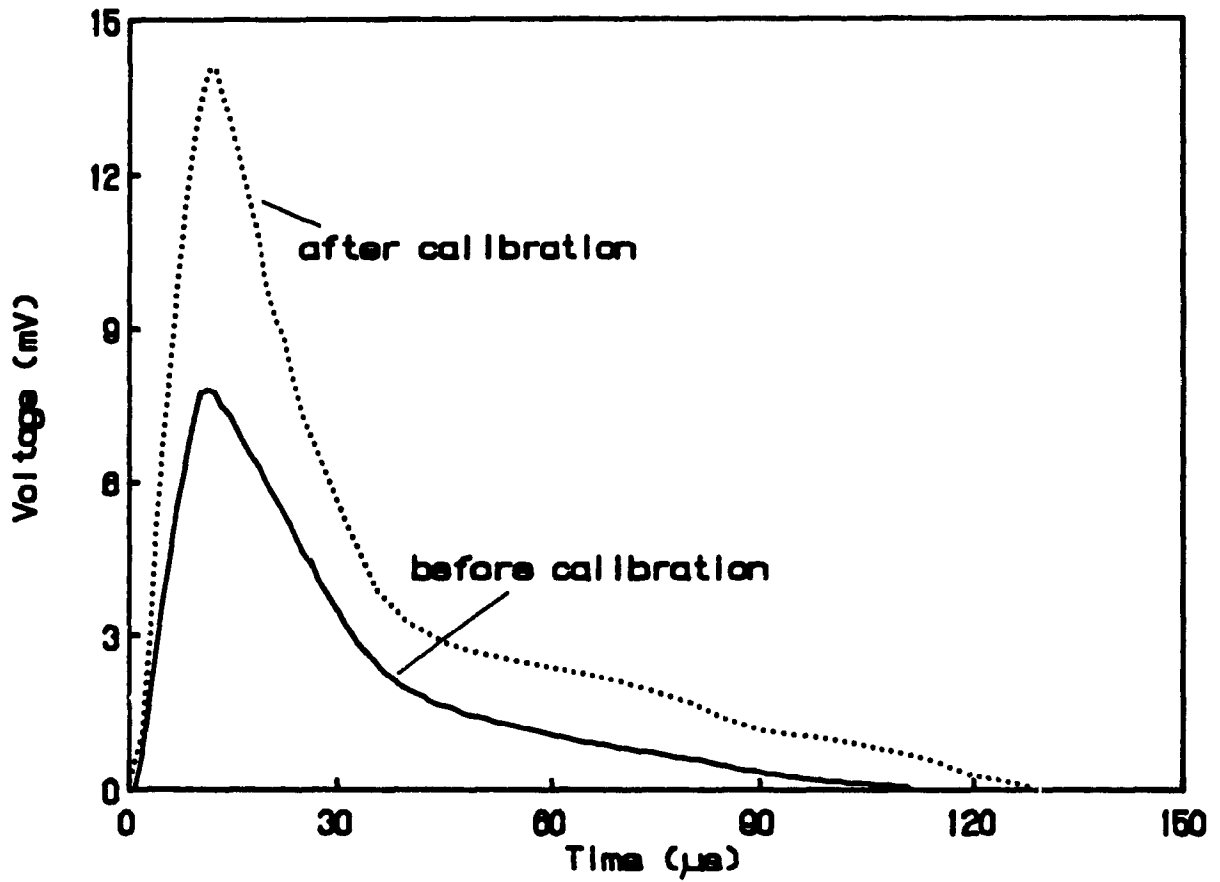


Figure 5.5 - Signal obtained from the no slit system using CO at 95 m/s  
Before and after calibration with the transfer function

The linear current distribution at the arc foot on the electrode surface in the direction of the arc movement can be obtained from the calibrated signal and using equation 5.3. This was done for different operating conditions and plasma gases; the results are shown in the next section. It should be noted here that although the technique is suitable for measurements of the arc foot it has insufficient resolution for measurements on cathode (or anode) microspots. For the latter a different method has been employed for short experiments (Drouet et al (16)).

#### 4) RESULTS

The linear current distribution was obtained for different operating conditions and plasma gases. All the results were obtained with the same cathode and coil and are shown after being calibrated and transformed using equation 5.3.

##### A) Pure Ar and Ar+0.3%CO

The linear current distributions for Ar and Ar contaminated with 3 000 ppm of CO are displayed in Figure 5.6. The operating conditions were as follows:

**TABLE 5.2**  
Operating Conditions for Figure 5.6

Gas	Current (A)	Velocity (m/s)	B (G)	Voltage (V)	Erosion Rate ( $\mu\text{g}/\text{C}$ ) (steady state)
Ar	95	8	1000	40	13.5
Ar+0.3%CO	140	9	100	21	0.5

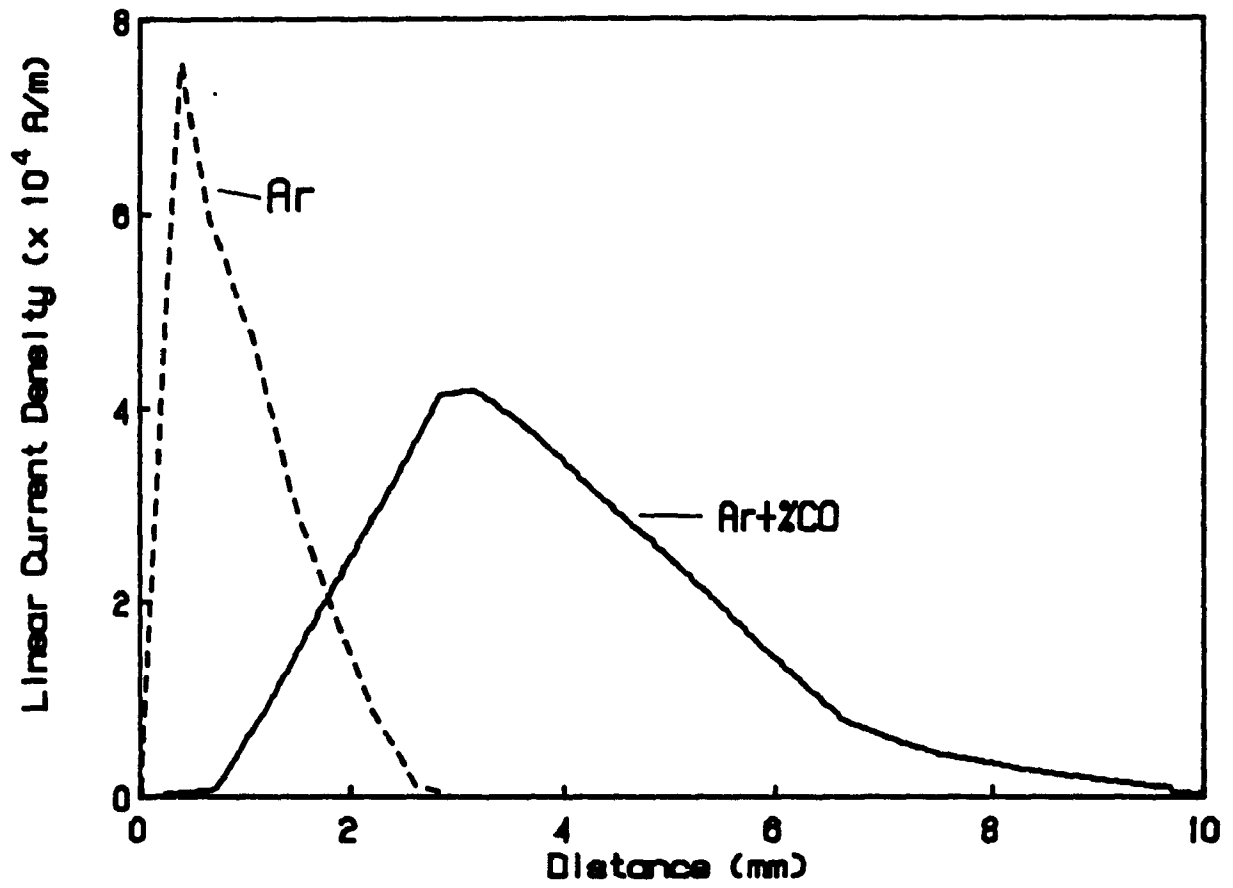


Figure 5.6 - Linear current distribution

Ar and Ar+0.3%CO at similar arc velocities

The current distribution for pure Ar was obtained approximately 20 seconds after the beginning of the experiment. It represents a transient condition since steady state operation with pure argon is achieved only after about 30 seconds, when the entire contaminant layer found on the cathode prior to the experiment has been removed as it has been discussed in Chapter IV. The value for Ar+0.3%CO was obtained at steady state.

It can be seen that the arc attachment is more constricted for Ar, even with the higher magnetic field (see next section). The magnetic field was reduced for Ar+0.3%CO to obtain similar arc velocities for the sake of comparison. The more constricted attachment results in higher surface temperature and higher erosion rates.

It is also interesting to observe the lack of symmetry of the current distribution; the current is more concentrated in the "front" of the arc attachment. This has been observed by other researchers (Beaudet (12), Anders et al (15)); the asymmetry increases for higher magnetic fields (arc velocities).

The change in the current distribution from clean to contaminated surfaces is probably a reflection of the work function and electron emissivity of the surface; when the surface is contaminated with carbon, the work function decreases, increasing the electron emissivity of the surface (Chapter IV). This will allow a larger area of the surface to emit electrons simultaneously, increasing the size of the arc attachment.

The current density can be estimated assuming a cylindrical distribution (to calculate the current density it would be necessary to know also the current distribution in the direction transverse to the arc motion); the maximum current density for the operating conditions shown in Table 5.2 is  $1 \times 10^4$  A/cm<sup>2</sup> for Ar and around  $2 \times 10^3$  A/cm<sup>2</sup> for Ar+0.3%CO. These values are comparable to the results obtained by

Beaudet (12) at the anode using the slit system for intermittent experiments. The results are also similar to the ones found using the optical method (Rakovskii (2)) and by Kucherov et al (14)). It should be noted here that there are evidences (Kucherov et al (14)) that the current density increases with arc current.

#### B) Ar+0.3%CO and He+0.4%CO

The magnetic field was varied between 1 000 G and 10 G for Ar and He contaminated with 3 000 and 4 000 ppm of CO respectively. The linear current distribution for different arc velocities (different magnetic fields) are shown in Figure 5.7a-d for Ar+0.3%CO and in Figure 5.8a-c for He+0.4%CO. The arc current was 140 A for the experiments with Ar+0.3%CO and 110 A for He+0.4%CO. The peak in the linear current distribution varied from  $2.5 \times 10^4$  A/m at 75 m/s to  $5.1 \times 10^4$  A/m at 4 m/s for Ar+0.3%CO. At the same time, the maximum dimension of the arc attachment changed from 17 to less than 10 mm. The changes for He+0.4%CO were: peak linear current, 1.1 to  $3.7 \times 10^4$  A/m and maximum dimension, 32 to 9 mm, for 230 and 44 m/s respectively.

It is hard to separate the effect of the magnetic field on the arc attachment distribution from that of the arc velocity, since the two are closely coupled. One possible way of examining this question is given below.

The "minimum equivalent arc diameter" is given in Table 5.3 for Ar+0.3%CO and He+0.4%CO for different operating conditions. The minimum equivalent diameter is found assuming cylindrical symmetry of the attachment and assuming the value of the peak current density for over the entire area of the attachment.

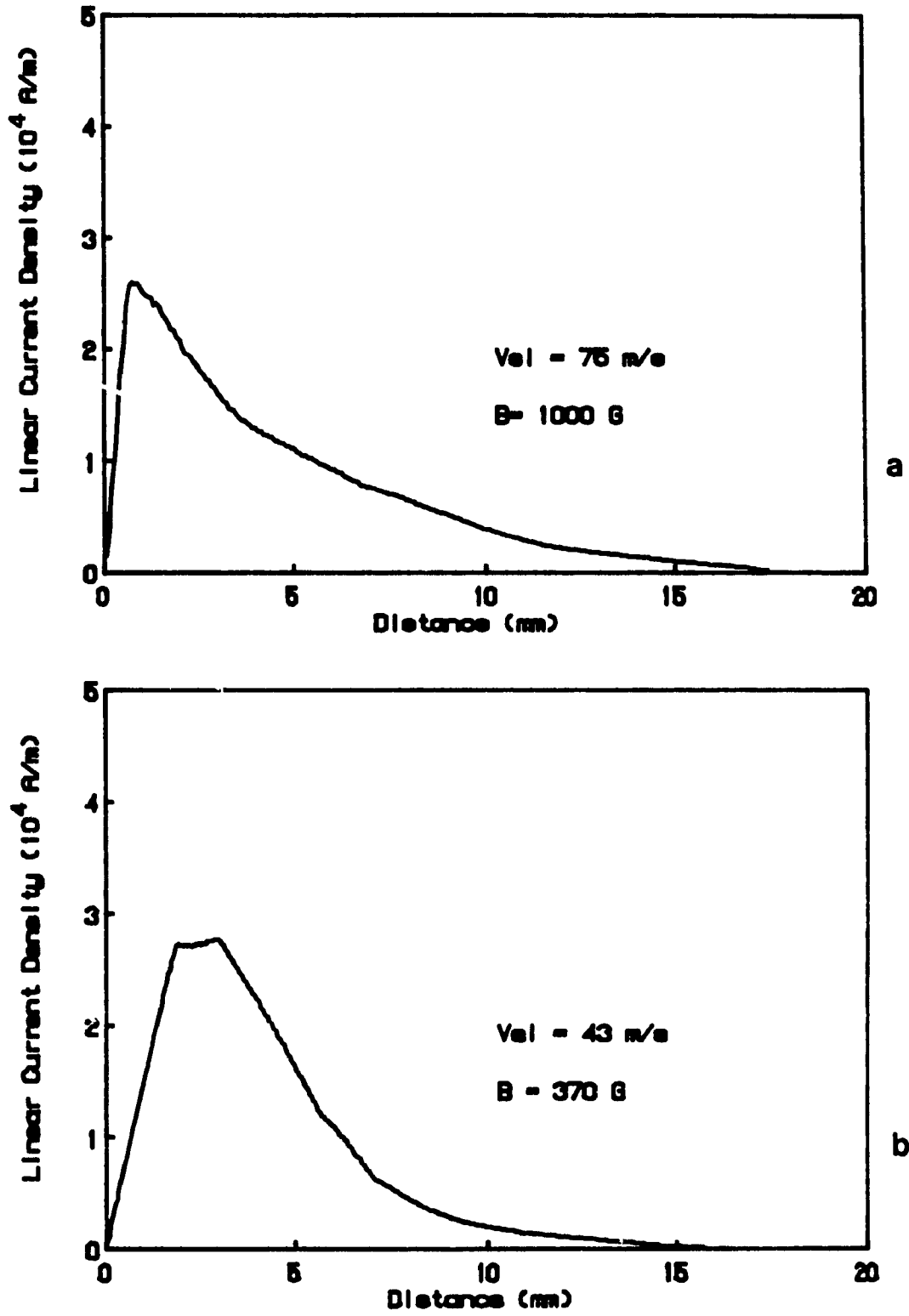


Figure 5.7 - Linear current density for Ar+0.3%CO

a) 75 m/s; 1 000 G    b) 43 m/s; 370 G

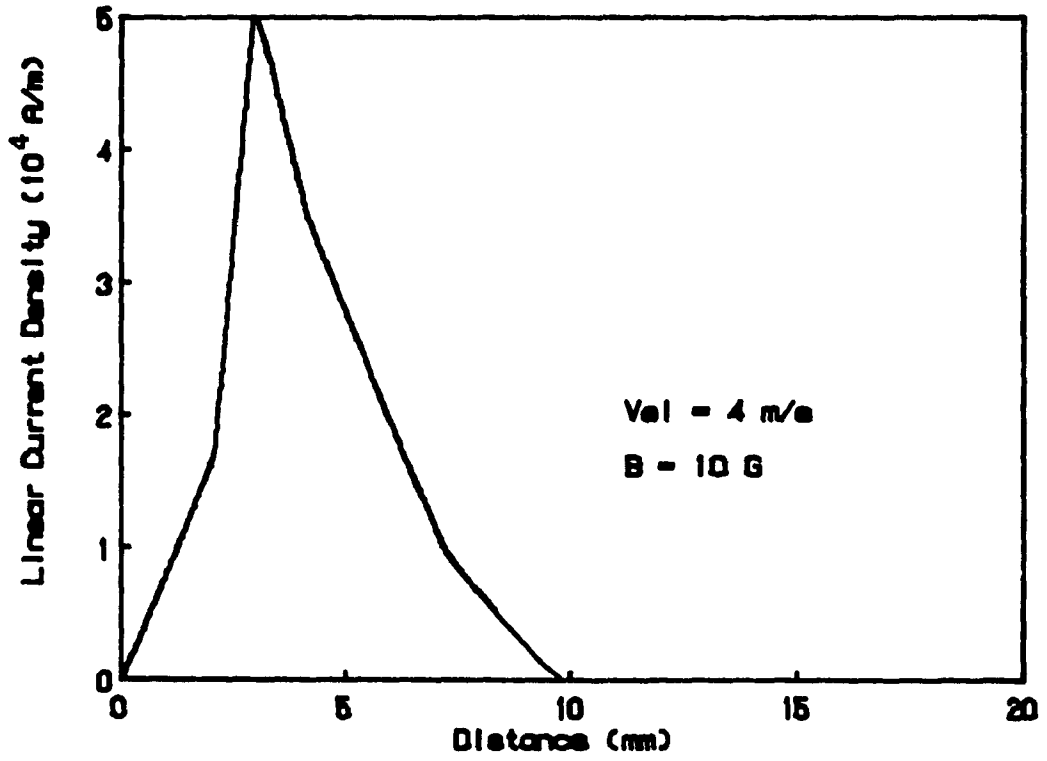
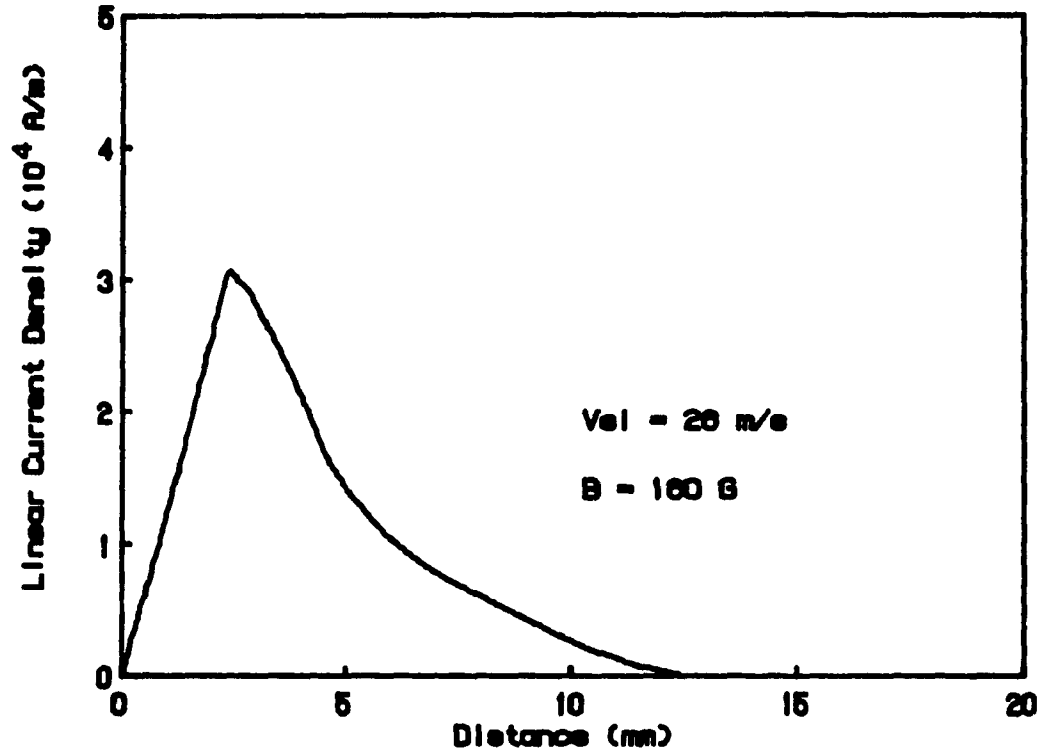


Figure 5.7 - Linear current distribution for Ar+0.3%CO

c) 26 m/s; 160 G    d) 4 m/s; 10 G

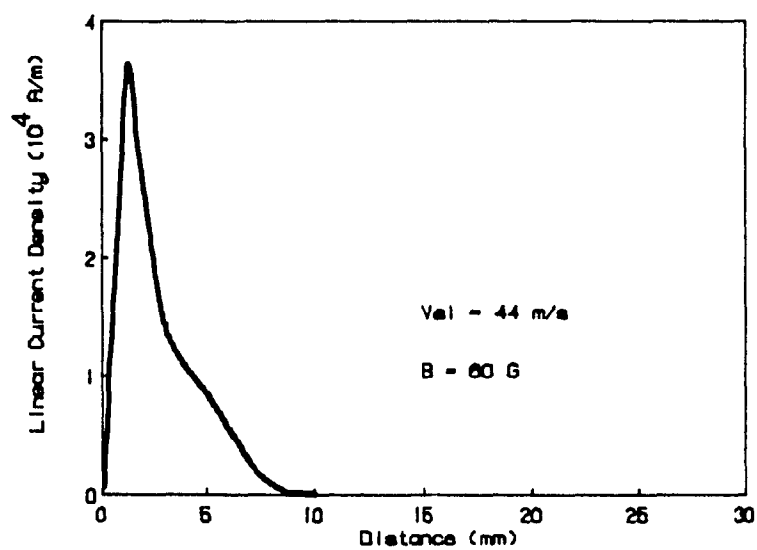
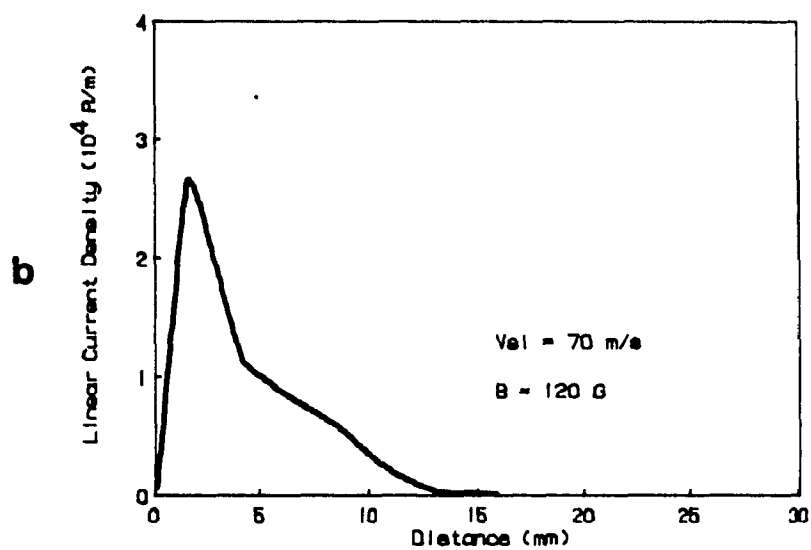
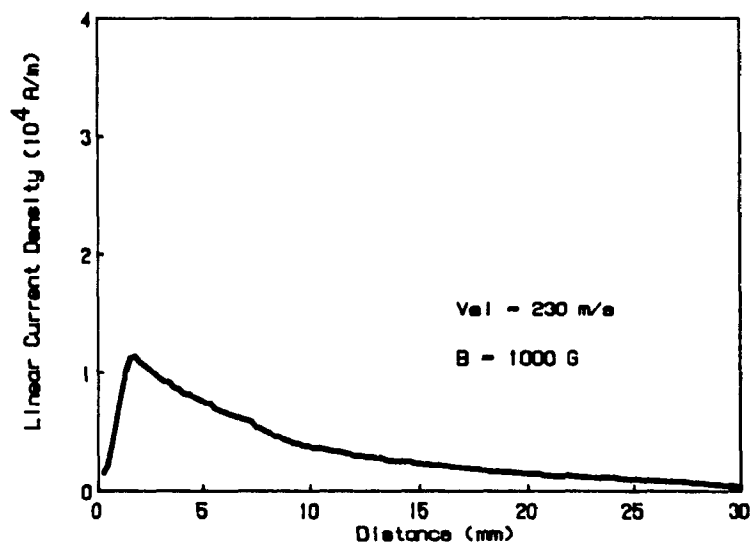


Figure 5.8 - Linear current distribution for He+0.4%CO

a) 230 m/s; 1 000 G    b) 70 m/s; 120 G    c) 44 m/s; 60 G

$$D_{eq} = (4 I / (J \pi))^{1/2} \quad 5.7$$

where  $D_{eq}$  = minimum equivalent diameter  
 $I$  = arc current  
 $J$  = current density (peak current distribution)

The minimum equivalent diameter is different for Ar+0.3%CO and He+0.4%CO for similar arc velocities (44-43 and 75-70 m/s). It is almost the same for similar magnetic fields (160-120 and 30-60 G), although the same conclusion does not apply for high values of magnetic fields (1 000 G). Therefore it seems that the magnetic field (Lorentz force) is the important parameter to be examined for arc attachment, at least for magnetic fields below 200 G. This is further discussed in the next section.

**TABLE 5.3**  
 Minimum Equivalent Diameter for Ar+0.3%CO and He+0.4%CO

Gas	Magnetic Field (G)	Arc Velocity (m/s)	Min. Equiv. Diam. (mm)
Ar+0.3%CO	1000	75	2.7
Ar+0.3%CO	370	43	2.6
Ar+0.3%CO	160	26	2.4
Ar+0.3%CO	30	9	2.1
He+0.4%CO	1000	230	3.4
He+0.4%CO	120	70	2.3
He+0.4%CO	60	44	2.0

### C) Pure Helium

It was seen in Chapter III that arcs in pure helium had an unique behavior. The arc velocity seems to follow the aerodynamic drag model for values of magnetic field up to 500 G (arc velocity 95 m/s). If the magnetic field is increased beyond this value, the arc velocity decreases, reaching 20 m/s for 1 000 G.

The linear current distribution for pure He is shown in Figure 5.9 for magnetic fields at 1 000 G and 120 G, at similar arc velocities (23 and 30 m/s) and at the same arc current (110 A). Although the arc velocity is slightly higher for 120 G than for 1 000 G, the former has the highest peak in the linear current distribution, as well the most constricted attachment. This corroborates the idea that the magnetic field is a more important parameter than the arc velocity for the current distribution. These differences in current distribution can explain some of the findings of the erosion rates for pure He; this subject is explored in the next Chapter.

### D) Pure CO

It has been shown that the arc velocity decreases if the concentration of CO in Ar or He goes above 4% in volume. It will be seen in the next Chapter that the erosion rate increases at the same time. It was seen that these changes are associated with the formation of a "thick" carbon layer on the cathode surface.

The linear current distribution for pure CO is shown in Figure 5.10. The arc current was 95 A and the magnetic field 1 000 G for this experiment. It can be seen that the current distribution is more constricted for CO than for Ar or He contaminated with 3 000 ppm of CO, for He contaminated with 4 000 ppm of N<sub>2</sub> or for pure nitrogen at the same operating conditions. The peak in the linear current is also the second

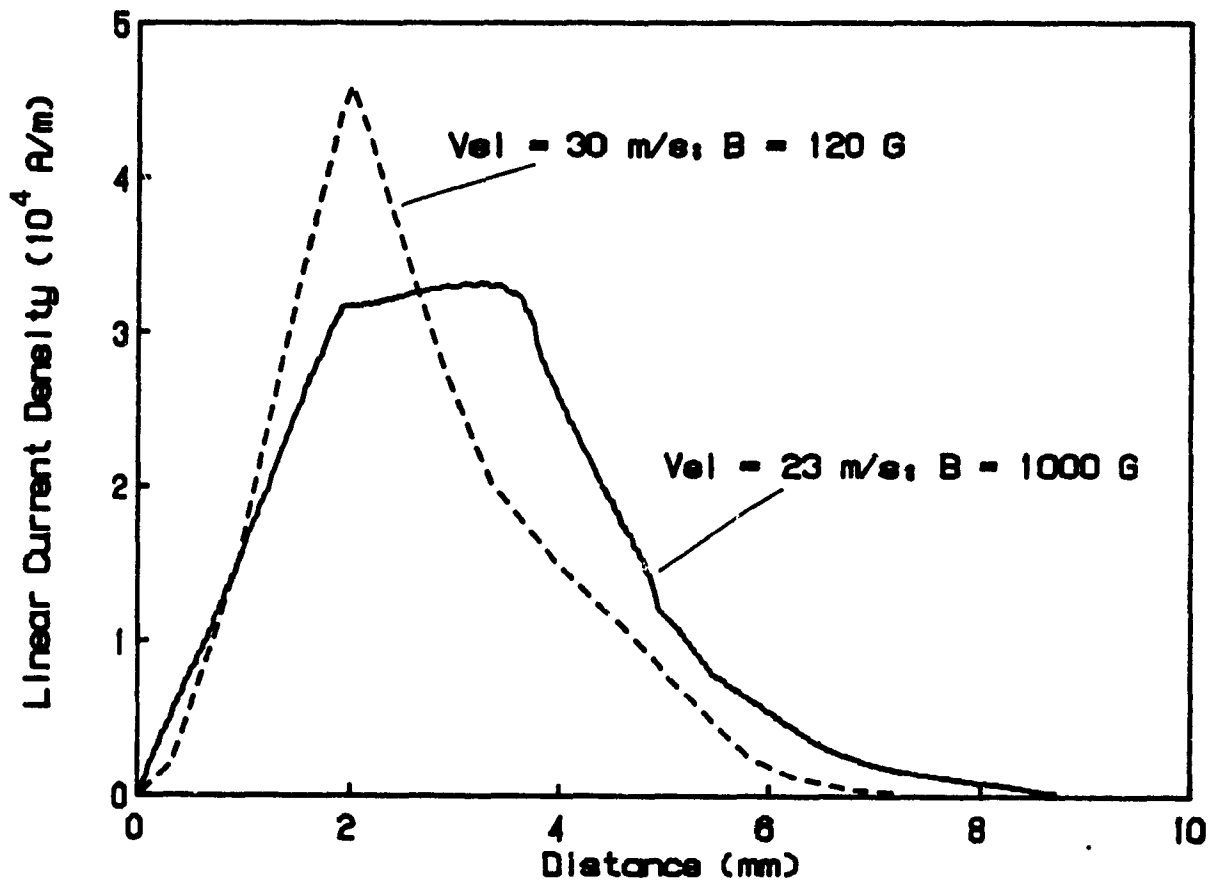


Figure 5.9 - Linear current distribution for pure He  
1 000 G and 120 G at similar arc velocities

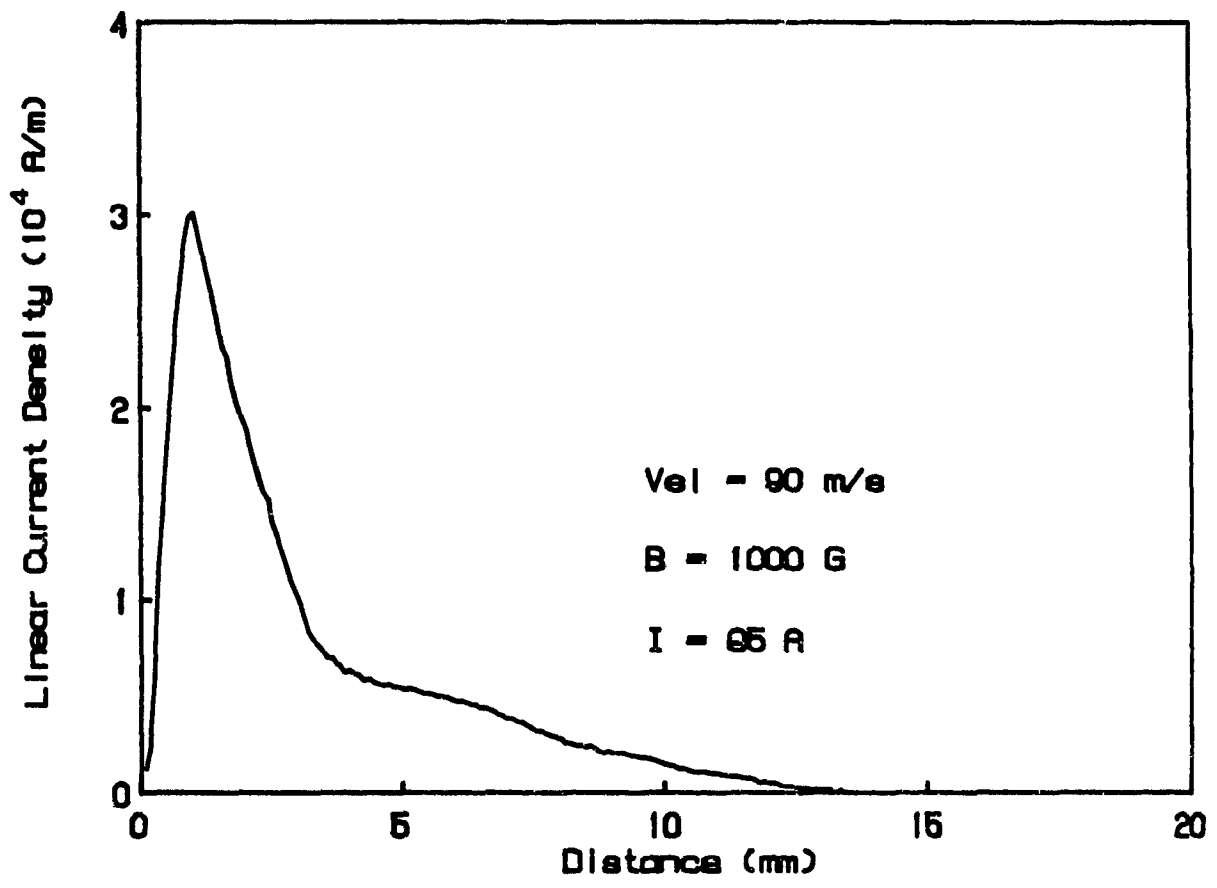


Figure 5.10 - Linear current distribution for pure CO at 1 000 G and 90 m/s

highest (Ar is the highest) for those operating conditions. The high value for current density suggests a high value for the erosion rate, as observed.

E) N<sub>2</sub> and He+0.4%N<sub>2</sub>

The effect of reducing the magnetic field (and therefore the arc velocity) on the linear current distribution for pure N<sub>2</sub> is shown in Figure 5.11a and 5.11b. The same trend is followed, i.e., the arc attachment constricts as the magnetic field is reduced. This can also be seen in Figure 5.12a-c for He contaminated with 4 000 ppm of N<sub>2</sub> at different magnetic fields and the same arc current (110 A).

The injection of N<sub>2</sub> was stopped and the arc slowly removed the N<sub>2</sub> contamination on the cathode surface as explained in Chapter IV. The linear distribution 2 minutes after stopping the nitrogen injection in helium is shown in Figure 5.13. The current distribution for He+0.4%N<sub>2</sub> at the same magnetic field strength (800 G) is also shown in Figure 5.13 for the sake of comparison. It can be seen from these figures that the arc attachment started to constrict after the addition of nitrogen in helium was stopped; the current distribution was eventually the same as for pure helium 15 minutes after the nitrogen addition was stopped.

F) Anode

The linear distribution for the arc attachment on the anode was obtained by inverting the polarity of the electrodes. These experiments could not last long because of the erosion at the cathode, now the center electrode. The result shown in Figure 5.14 was obtained using pure Ar 10 seconds after the beginning of the experiment. The magnetic field was 1 000 G and the arc was still moving quickly because of the

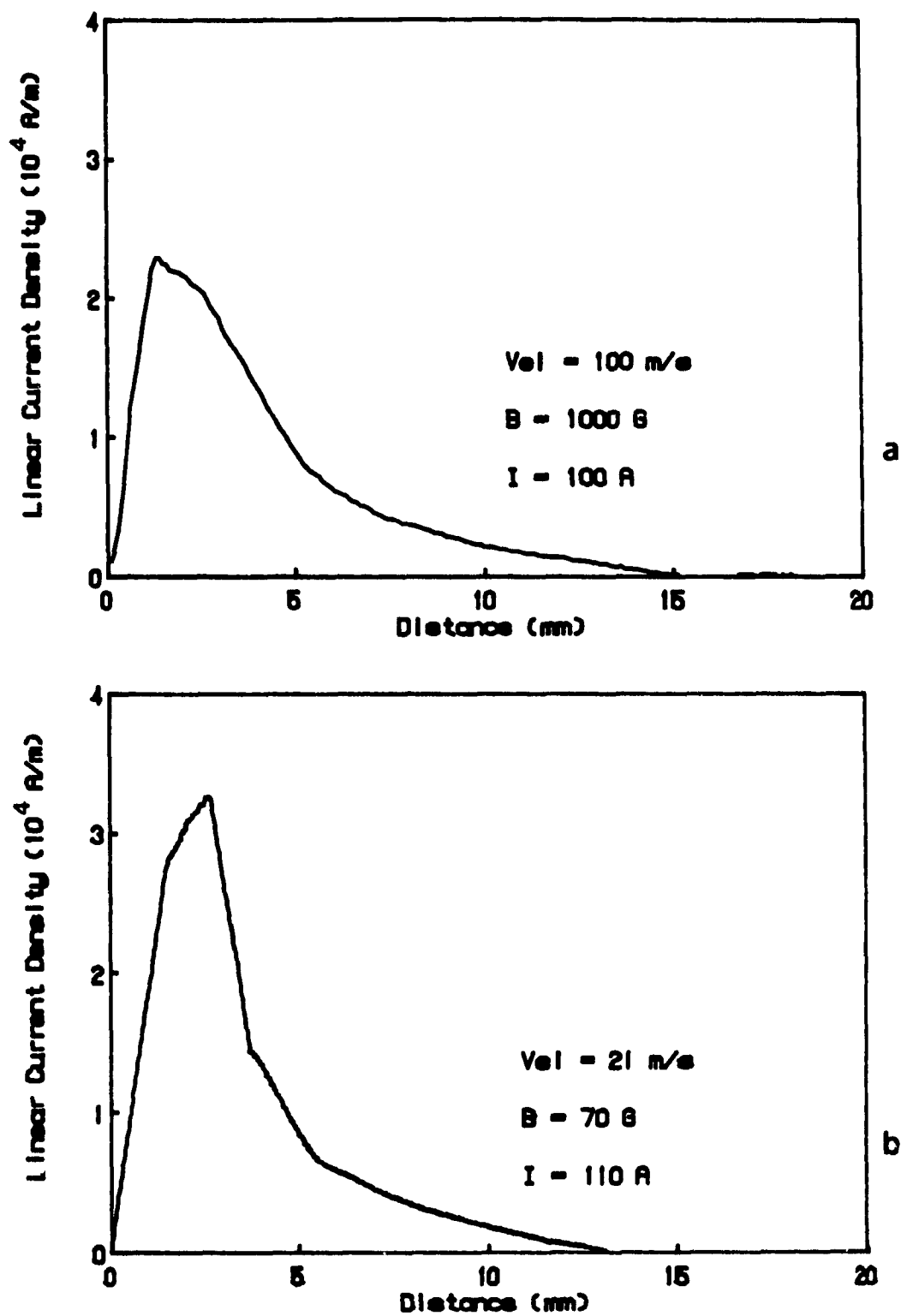
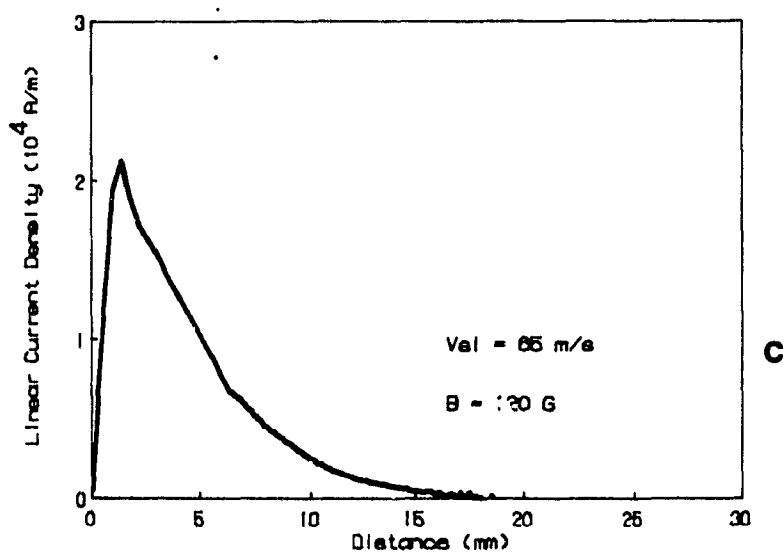
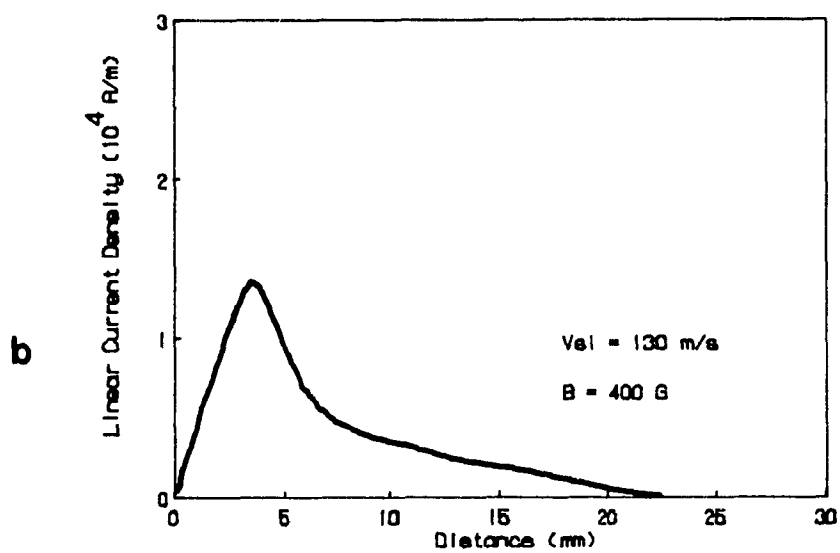
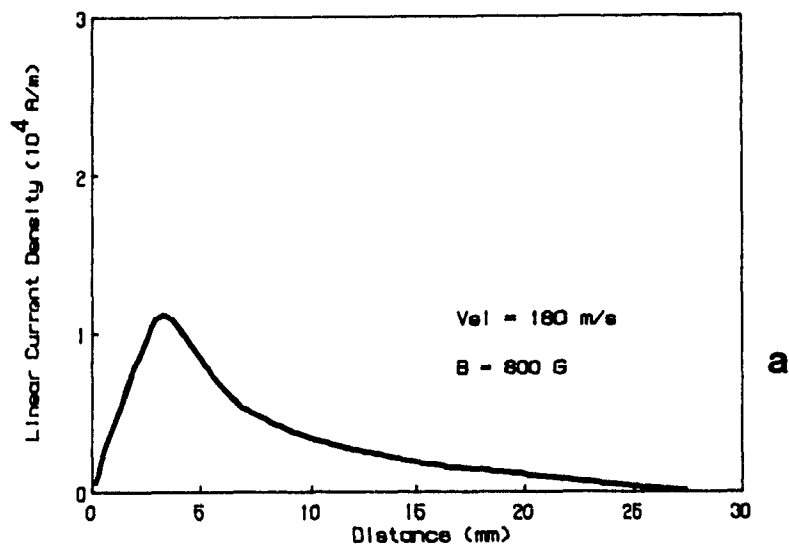


Figure 5.11 - Linear current distribution for pure nitrogen

a) 100 m/s; 1 000 G

b) 21 m/s; 100 G

Figure 5.12 - Linear current distribution for He+0.4%N<sub>2</sub>

a) 180 m/s; 800 G    b) 130 m/s; 480 G    c) 65 m/s; 120 G

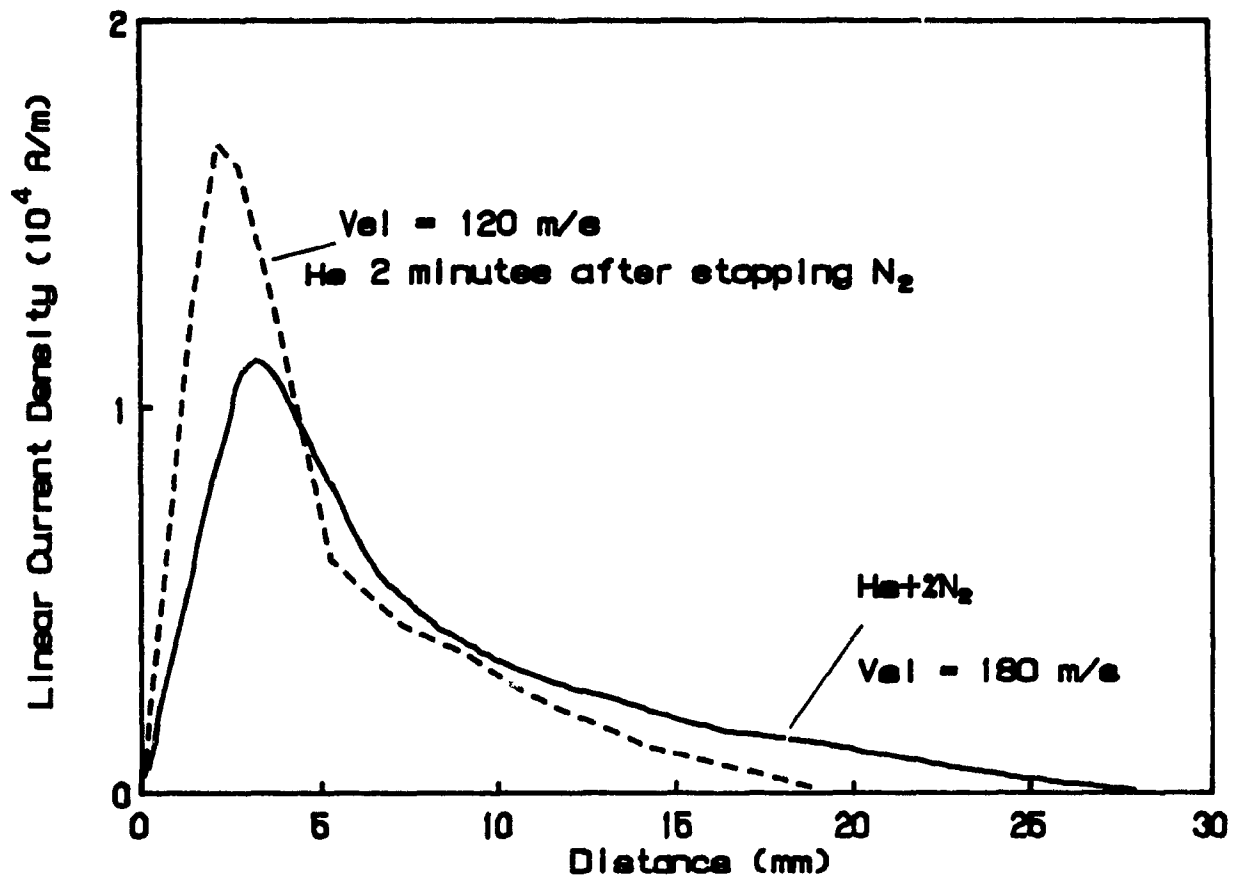


Figure 5.13 - Linear current distribution for He+0.4%N<sub>2</sub> and He (2 minutes after stopping the addition of nitrogen) at similar magnetic fields

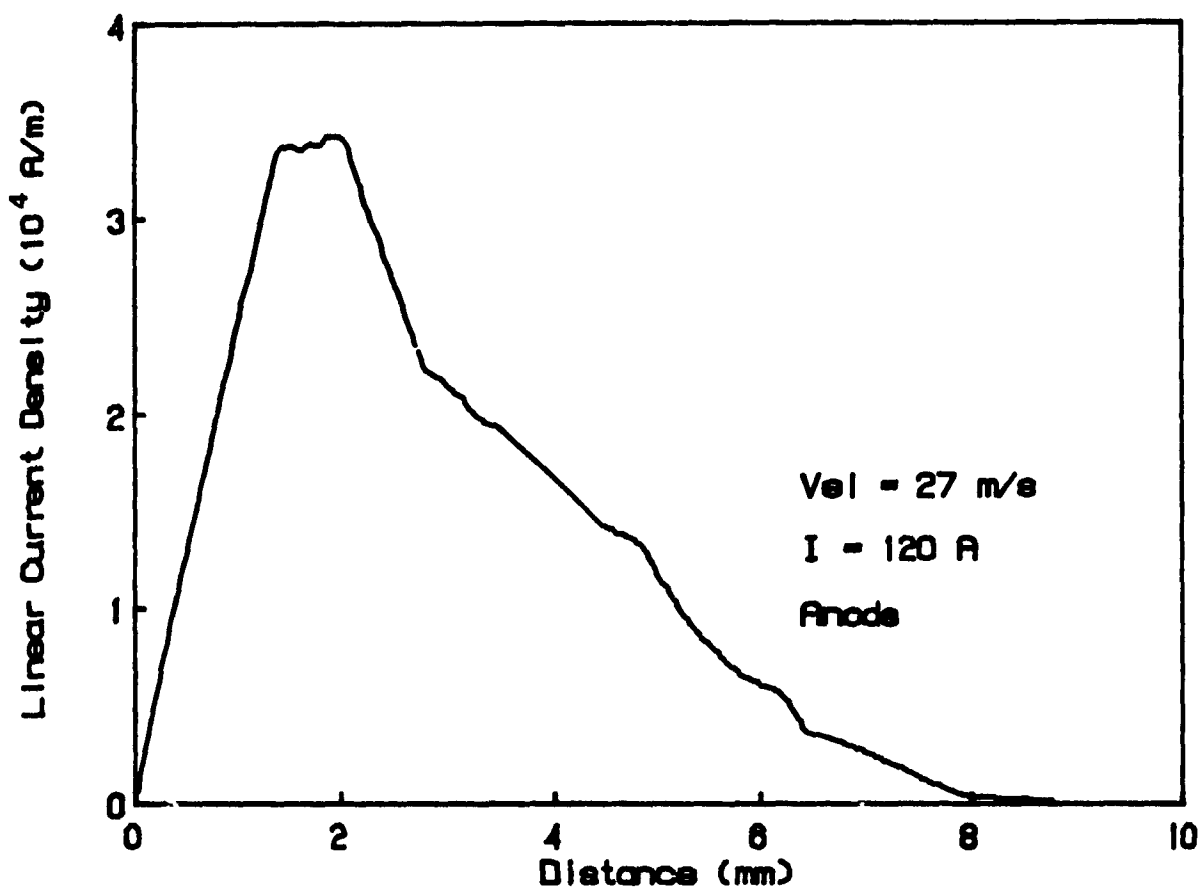


Figure 5.14 - Linear current distribution for anode - argon at 1 000 G and 27 m/s

electrode contamination at the beginning of an experiment as discussed before. The anode attachment is less constricted than that for the cathode (Figure 5.6); this will result in lower erosion rates for the anode as discussed in the next Chapter.

#### G) Summary

The linear current distributions obtained for different plasma gases and operating conditions are summarized in Table 5.4. The equivalent diameter was calculated according to the procedure described before.

#### H) Cathode Spot - Signal Splitting

It was mentioned before that the technique was suitable for measurements on the arc foot attachment but not for the cathode (anode) microspots. However it was observed that for some operating conditions the signal was made of individual contributions. This is illustrated in Figure 5.15 for Ar+0.3%CO at 4 m/s ( $B = 10$  G). This division of the signal was seen only for Ar and He contaminated with CO and to a smaller extent for He contaminated with N<sub>2</sub> and pure nitrogen and always at low magnetic fields (but not necessarily low velocities, since the splitting was observed for He+0.4%CO at 30 m/s). It seems that there are around 50 individual contributions to the arc for Ar+0.3%CO.

A possible interpretation of the splitting of the signal is that it represents the individual spots which make up the arc attachment. These spots are more dispersed for low magnetic fields and contaminated surfaces and once the arc passes over the cavity, each one of the spots will originate a signal. The formation of these spots is further discussed in the next Chapter.

TABLE 5.4

Summary of Results Obtained With the No Slit System

Gas	B (G)	I (A)	Vel (m/s)	Peak ( $\times 10^4$ A/m)	Max. Dim. (mm)	Deq (mm)
Ar	1000	90	8	7.5	2.5	1.2
Ar+0.3%CO	1000	140	75	2.5	17.0	2.7
Ar+0.3%CO	370	140	43	2.7	15.5	2.6
Ar+0.3%CO	160	140	26	3.1	12.5	2.4
Ar+0.3%CO	30	140	9	4.2	10.0	2.1
Ar+0.3%CO	10	140	4	5.1	9.5	1.9
He	1000	110	23	3.3	8.5	2.1
He+0.4%CO	1000	110	230	1.2	32.0	3.4
He+0.4%CO	120	110	70	2.6	13.0	2.3
He+0.4%CO	60	110	44	3.6	8.5	2.0
He	120	110	30	4.7	6.5	1.7
CO	1000	95	90	3.0	12.0	2.0
N <sub>2</sub>	1000	100	100	2.2	14.5	2.4
N <sub>2</sub>	100	110	21	3.2	12.0	2.1
He+0.4%N <sub>2</sub>	800	110	180	1.1	27.0	3.6
He+0.4%N <sub>2</sub>	120	110	65	2.2	17.0	2.6
Anode	1000	120	27	3.3	8.0	2.2

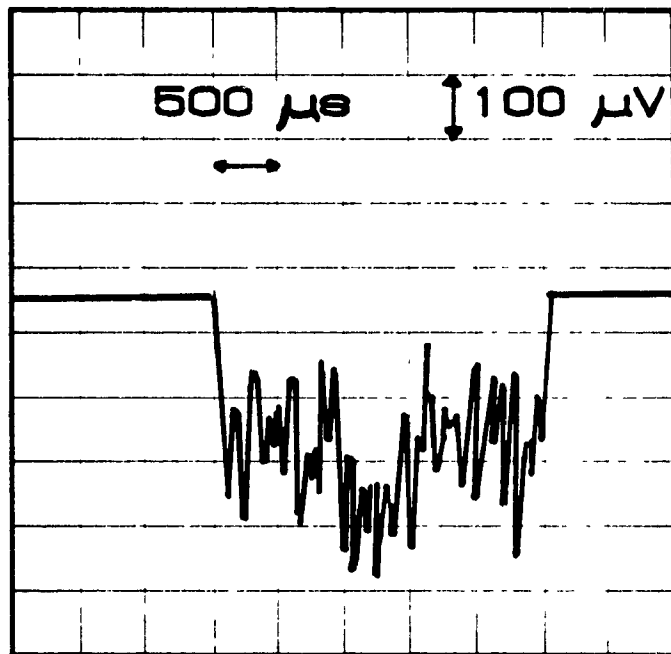


Figure 5.15 - Signal for Ar+0.3%CO at 4 m/s and 10 G - splitting of the signal

## 5) CONCLUSIONS

In this Chapter a novel technique to measure the linear current distribution of the arc attachment at the anode or cathode of a moving arc was described. A summary of the most relevant conclusions and results obtained in this work is given below.

a) The technique is capable of measurements for experiments of long duration and different operating conditions and plasma gases, which are prerequisites for the application of the technique in industrial plasma torches. The results are reproducible and have an estimated error of less than 5 % (the integral of the linear current distribution curves are compared with the arc current values obtained using a shunt).

b) The peak of the linear current distribution compares well with results previously published by other researchers. Assuming cylindrical symmetry the current density is estimated to be in the range  $10^3 - 10^4$  A/cm<sup>2</sup> at the cathode depending on the gas mixture and arc velocity.

c) Pure argon has the highest peak value of linear current distribution, and the most constricted arc foot attachment. Pure helium has an equivalent diameter almost twice as large as for pure argon.

d) Lower peak current distribution values were found for Ar and He contaminated with CO or N<sub>2</sub> than for the pure inert gases. The arc attachment constricts as the magnetic field is decreased (arc velocity decreases also) for Ar+0.3%CO, He+0.4%CO, N<sub>2</sub> and He+0.4%N<sub>2</sub>. The results suggest that the magnetic field strength is more important for the current distribution than the arc velocity.

- e) The linear current distributions for pure He at similar arc velocities but with different magnetic fields also suggests the importance of the magnetic field strength. The arc attachment showed a constriction for lower magnetic fields.
- f) Pure carbon monoxide seems to have a more constricted attachment than for the other plasma gases (except for argon) at the same operating conditions.
- g) The arc attachment decreased in size when the addition of nitrogen in helium was stopped. This was expected since pure He has a more constricted attachment and supports some of the ideas of surface contamination presented before.
- h) It was possible to measure the arc attachment on the anode surface for pure argon; the attachment is larger than for the cathode for similar operating conditions.
- i) The splitting of the signal for Ar and He contaminated with 3 000 and 4 000 ppm of CO, He+0.4%N<sub>2</sub> and pure nitrogen for low magnetic fields suggests that the arc attachment is made of many individual current emitting sites.

## REFERENCES

- 1) Rakhovskii, V.I.; "State of the art of physical model of vacuum arc cathode spots", IEEE Trans. Plasma Science, vol. PS-15, n.5, 481-487, 1987.
- 2) Rakhovskii, V.I.; "Current Density per Cathode Spot in Vacuum Arcs", IEEE Transactions on Plasma Science, vol. PS-12, n.3, 199-203, 1984.
- 3) Smith, G.P.; Dollinger, R.; Malone, D.P.; Gilmour, A.S.; "Relative cathode spot and cell areas and currents in a copper cathode vacuum arc", J. Appl. Phys. 51, 3657-3662, 1980.
- 4) Haptzache, E.; Beitr. Plasmaphys., n.12, 245-255, 1972.
- 5) Gabovich, M.D.; Poritskii, V.Y.; "Sixth All Union Conference on the Physics of a Low Temperature Plasma", Volume 1, 198-200, 1983.
- 6) Sanger, C.C.; Secker, P.E.; "Arc Cathode Current Density Measurements", J. Phys. D: Appl. Phys. , vol. 4, 1941-1945, 1971.
- 7) Juttner, B.; "Characterization of the cathode spot", IEEE Trans. Plasma Science, vol. PS-15, n.5, 474-480, 1987.
- 8) Djakov, B.E.; Holmes, R.; "Cathode spot structure and dynamics in low current vacuum arcs", J. Phys. D: Appl. Phys., vol. 7, 569-580, 1974.
- 9) Guile, A.E.; "Joule heating in emitting sites on nonrefractory arc cathodes", IEE Proc., vol. 127, Pt. A, n.7, 452-457, 1980.
- 10) Daaider, J.E.; "Cathode erosion on metal vapour arcs in vacuum", Thesis, Tech. Univ. Eindhoven, Netherlands, 1978.
- 11) Drouet, M.G.; Beaudet, R.; Jutras, R.; "Measurement of the distributions of the current in a moving arc at the electrode surface", AIAA/ASME Thermophysics and Heat Transfer Conference, Boston, Paper n. 74-713, 1974.
- 12) Beaudet, R.; "Etude d'un arc électrique soufflé par champ magnétique", Ph.D. Thesis, INRS-Energie, 1973.
- 13) Ramirez, R.W.; The FFT - Fundamentals and Concepts, Prentice Hall International, 1985.

- 14) Kucherov, Y.R.; Pustoganov, A.V.; Zavidei, V.I.; "CO<sub>2</sub> welding with a zirconium cathode", *Automatic Welding*, 56-57, 1983.
- 15) Anders, S.; Juttner, B.; Pursch, H.; Siemroth, P.; "Investigations of the current density in the cathode spot of a vacuum arc", *Contrib. Plasma Phys.*, vol. 25, n.5, 467-473, 1985.
- 16) Drouet, M.G.; Gruber, S.; "Dynamic measurements and a simplified model of cathode emission in a moving arc", *IEEE Trans. PAS-95*, 105-109, 1976.

## VI. EROSION ANALYSIS

## VI. EROSION ANALYSIS

### 1) INTRODUCTION

*It was raining hard. For the past week, Watson hadn't heard from Holmes and decided to check if everything was right with his old friend... He walked quickly, trying to not get completely soaked...*

*A block from Holmes' house Watson started to hear music from a violin; he guessed it had to be coming from the second floor of that house that he knew so well. After all, it had been almost 15 years now since he started to be completely amazed at that house, that second floor, that office, but mainly at the inhabitant of the office, his good friend Holmes...*

*Watson stopped at the door of the house und knocked... and knocked.... After almost five minutes, tired of waiting and starting to get desperate with all that rain, he started shouting:*

*- Holmes!! Open the door!!! Holmes??!!! Open the Dooooooooorr!!*

*Suddenly Holmes came to the window:*

*- Who is there?*

*- It's me Holmes, Watson. Please open the door!*

*- Watson, what are you doing standing up there? Come inside at once, man! You can catch a cold staying in the rain!!*

*And closing the window, Holmes in a fraction of a second is opening the door and welcoming Watson...*

*- Well well well, Watson, just the man I needed..*

*- Holmes, why did you take so long to open the door?? I have been here knocking at the door for almost 10 minutes!!*

*- Oh, I'm sorry Watson. I was thinking about something . and I guess I didn't hear you..But come, come, I have exciting news to tell you...*

*And saying this, Holmes runs upstairs, followed by an intrigued and chilled Watson...*

*Watson almost dropped his coat on the floor as he entered in Holmes' office. He almost couldn't believe in his eyes. His voice was still trembling when he finally managed to speak:*

*- Holmes, what happened? Who did this??*

*Holmes took somctime to understand what his friend was saying..*

*- Oh, this? Holmes pointing to the room... - Don't worry, Watson, it's all right. I did it.*

*- But Holmes, what is all this about? What happened here?*

*Watson still couldn't believe in the mess of the room... Papers spread all over the place,*

*cathodes, hundreds of them mixed with pieces of cookies, bread laying on the floor; all books removed from the shelves and piled up on the chairs, table, with hundreds of papers and that gigantic black machine in the middle of the room...*

*- Watson, clean a chair and sit down. Don't pay attention to the office. As you can see I have been working here for the past few days... Put listen, dear friend, because I have good news... I think I found the answers!!*

*- That is incredible Holmes! Congratulations!! I knew you could do it!! But Holmes, the answers for what??*

*Watson finally finds a chair not completely full and sits on the edge...*

*- Watson, Watson, my good friend, what answers?? The answers for the electrode erosion of course!!! It was in front of our nose all this time! So elementary, my dear Watson. Sometimes I wonder if I am losing my skills... But that doesn't matter now... Watson, are you ready for this?*

*- Of course, Holmes! Please tell me now before you forget it!*

*- Don't worry, Watson, that wouldn't happen... Besides I wrote my conclusions somewhere...*

*Holmes walks through the books and papers until he gets close to the table and picks up some notes...*

*- Ah, here they are!! My conclusions! Well, the whole idea is very simple... I started suspecting the effect of the arc velocity and then.....*

Well, it is time to come back to this story...

#### A) Chapter Guideline

The erosion of the electrodes is discussed in this Chapter. This chapter contains all the cathode erosion results obtained in this work using different plasma gases and operating conditions. A simple conceptual model for the cathode erosion is proposed, based on results from this work and that previously reported by other researchers. The erosion results are analyzed according to the model and good agreement is found between the model and the experimental results. The erosion of the anode as well as the singular behavior of the arc movement in pure helium are discussed at the end of the Chapter.

## B) Cathode Erosion Results in the Literature

Erosion phenomena for copper cathodes operating at atmospheric pressure still remain a puzzle, with many contradictory results reported in the literature. Some of the factors suggested as important for erosion rates are : arc velocity, water cooling rate for the cathode, magnetic field strength, thickness of the contaminant films on the cathode surface, duration of the experiment, plasma gases used, purity of the copper, etc. Some of these factors seem rather questionable and it can be safely said that no theory or model can explain all the results reported.

The majority of the cathode erosion results presented in the literature were obtained for low pressure conditions, i.e., "vacuum" arcs. It has been suggested (Kimblin (1), Guile(2)) that the fundamentals of atmospheric arcs and vacuum arcs are the same; therefore some of the results from this work are compared with vacuum arc results whenever data are not available for atmospheric arcs.

## 2) RESULTS

The units for erosion rate,  $\mu\text{g}/\text{C}$  and how the erosion results were obtained were described in Chapter II. It was mentioned in Chapter III that the results from this work using air as the plasma gas for magnetically moving arcs were similar to results published previously by other researchers. These cathode erosion rates for air are shown in Table 6.1 for similar operating conditions and cathode geometry; they indicate that no systematic error was made in this work. These are practically the only results that can be compared directly with the literature.

**TABLE 6.1**  
Copper Cathode Erosion Results Using Air at Atmospheric Conditions

Author	Erosion Rate ( $\mu\text{g/C}$ )	Arc Current (A)	Arc Velocity (m/s)
This work	1.5	100	60
Harry (3)	1.6	200	86
Guile (4)	1.4	100	60

The results obtained for the erosion rates of the electrodes for different plasma gases and operating conditions are shown in Table 6.2 . The errors associated with the results are less than: 10% for erosion rates, 5% for arc velocities, 0.1% for magnetic fields, 5% for arc voltage, 2% for arc current, 10% for power input for the cathode and anode. The results were obtained for steady state operation (arc voltage, velocity) and comprise experiments lasting a minimum of 5 minutes for pure argon up to 4 hours in other gases. The symbols used in Table 6.2 are defined after the Table.

**TABLE 6.2**  
Erosion Results and Operating Conditions for this Work

Gas	E ( $\mu\text{g}/\text{C}$ )	Vel (m/s)	Vol (V)	B (G)	I (A)	Pc (%)	Pa (%)	GFR (l/m)
Ar	13.5	2	44	1000	100	83	15	20
Ar	8.0	4	44	1000	100	83	15	10
Ar	7.0	5	45	1000	100	83	15	7
Ar	6.5	6.2	45	1000	100	83	15	5
Ar	6.1	6.8	46	1000	100	83	15	3
Ar	4.7	10.5	48	1000	100	83	15	0.2
Ar	25.0	2	34	260	100	80	15	20
Ar	50.0	2	33	200	100	78	15	20
He	1.0	20	110	1000	110	82	16	20
He	3.5	20	54	60	110	73	26	20
He	6.1	10	48	26	110	57	42	20
He	0.6	95	58	500	110	57	30	20
CO	4.2	100	80	1000	100	60	30	20
Ar+0.3%CO	0.4	75	22	1000	140	48	40	20
Ar+0.3%CO	0.7	40	21	300	140	50	43	20
Ar+0.3%CO	0.5	10	17	50	140	55	44	20
Ar+0.3%CO	0.4	5	17	12	140	55	44	20
Ar+4%CO	1.5	32	46	1000	100	68	30	20
Ar+10%CO	1.6	34	61	1000	100	68	30	20
Ar+20%CO	1.7	44	65	1000	100	70	29	20

TABLE 6.2  
(continuation)

Gas	E ( $\mu\text{g}/\text{C}$ )	Vel (m/s)	Vol (V)	B (G)	I (A)	Pc (%)	Pa (%)	GFR (l/m)
Ar+50%CO	2.7	65	75	1000	100	67	30	20
He+0.4%CO	0.5	230	47	1000	110	64	36	20
He+0.4%CO	1.4	155	44	470	110	55	45	20
He+0.4%CO	1.88	100	40	260	110	57	43	20
He+0.4%CO	1.8	70	38	130	110	58	42	20
He+0.4%CO	1.5	43	35	58	110	57	42	20
He+0.4%CO	1.3	24	34	26	110	59	40	20
N <sub>2</sub>	1.7	100	85	1000	100	65	28	20
N <sub>2</sub>	1.4	115	81	1000	100	65	32	10
N <sub>2</sub>	1.1	120	78	1000	100	70	30	0.2
N <sub>2</sub>	1.0	125	101	1440	100	60	27	20
N <sub>2</sub>	1.0	135	102	1575	100	60	28	20
N <sub>2</sub>	9.0	15	49	50	100	51	46	20
N <sub>2</sub>	7.1	30	51	130	100	50	45	20
N <sub>2</sub>	7.6	50	55	270	100	51	45	20
N <sub>2</sub>	4.5	62	60	395	100	50	45	20
N <sub>2</sub>	3.4	70	68	525	100	55	43	20
N <sub>2</sub>	3.0	80	72	660	100	55	43	20
N <sub>2</sub>	2.6	92	77	790	100	59	39	20
N <sub>2</sub>	6.1	38	48	130	100	53	44	10
N <sub>2</sub>	4.0	47	47	130	100	54	44	0.2
Ar+0.3%N <sub>2</sub>	3.0	34	38	1000	100	69	31	20

TABLE 6.2  
(continuation)

Gas	E ( $\mu\text{g/C}$ )	Vel (m/s)	Vol (V)	B (G)	I (A)	Pc (%)	Pa (%)	GFR (l/m)
Ar+0.3%N <sub>2</sub>	27.3	6	30	53	100	70	30	20
He+0.3%N <sub>2</sub>	0.6	130	52	1000	110	64	36	20
He+0.3%N <sub>2</sub>	1.2	100	40	260	110	53	47	20
He+0.3%N <sub>2</sub>	0.6	50	35	87	110	53	47	20
He+0.3%N <sub>2</sub>	0.5	20	33	24	110	53	47	20
Ar+0.04%O <sub>2</sub>	2.0	35	34	1000	100	88	12	20
Ar+0.3%H <sub>2</sub> S	1.5	63	22	1000	100	-	-	20
Ar+25%He	9.4	3.5	49	1000	100	74	26	20
Ar+50%He	6.6	6	58	1000	100	75	25	20
Ar+75%He	2.4	18	71	1000	100	73	26	20
Ar+0.3%Cl <sub>2</sub>	0.4	70	22	1000	100	50	40	20
Ar+0.3%CH <sub>4</sub>	0.5	70	22	1000	100	49	40	20
Ar	13.5	2.8	45	1000	200	83	15	20
Ar	13.6	3.0	46	1000	250	85	15	20

E = erosion rate

Vel = arc velocity

Vol = arc voltage

I = arc current

B = magnetic field strength

Pc = power input to the cathode in percentage

Pa = power input to the anode in percentage

GFR = gas flow rate

### 3) CONCEPTUAL CATHODE EROSION MODEL

A simple conceptual model was developed to explain and analyze the results for cathode erosion rate. The justifications for the model are presented after its description.

#### A) Model

The erosion of copper cathodes is a physical phenomenon, depending on the temperature of the cathode surface within the arc attachment region. The arc attachment is made of individual contributions, the cathode spots. The cathode spots can be grouped closer together or at greater spacing according to the external magnetic field strength and surface conditions. The erosion rate reaches a minimum value when the spots are further apart. The erosion rate is also affected by the residence time of the arc attachment over the same region of the cathode surface.

#### B) Applicability and Physical Evidences for the Model

##### a) Erosion of copper cathodes

This work was focused on copper cathodes. Although some of the results can be applied to other materials (brass, for example), this has to be done with care, since differences exist for refractory materials (tungsten, carbon). More details are given at the end of the chapter.

b) Erosion is a physical phenomenon; it depends on surface temperature

When the reaction of the plasma gas with the cathode surface is not severe, the removal of material from the cathode is due to volatilization of copper. Ejection of particles is also possible due to the "explosion" of the surface on localized areas due to extreme temperatures. The highest temperature of the surface is found where the arc attaches and it lasts until the arc attachment moves to another region. A description of the heat sources of the arc attachment as well as the temperature field of the cathode surface are discussed in the next Chapter.

c) Arc attachment is made of cathode spots

The electric arc constricts in the vicinity of the cathode forming the arc attachment. This has been observed for different cathode materials (mercury (Kesaev (5)), tungsten and carbon (Herring and Nichols (6)), copper and brass (Harris (7))) and operating conditions.

The arc attachment at the cathode is made of individual cells or cathode spots. This has been suggested for vacuum arcs (Kesaev (5), Harris (7), Miterrauer (8), Kislink (9), Emtage (10)) as well as for atmospheric arcs (Drouet and Gruber (11)). These researchers calculated that each cell would be able to carry currents between 0.5 and 3 A, have a dimension between 0.1 and 1  $\mu\text{m}$  and a lifetime between 0.1 and 1  $\mu\text{s}$ . The existence of these cells has been disputed by Daalder (12) and Djakov and Holmes (13).

In this work splitting of the cathode attachment was observed for low magnetic fields and contaminated surfaces. The results obtained from the current density probe indicate the existence of approximately 50 spots which means an average current of

2-3 A per spot for a 140 A arc. The maximum dimension of each spot is around 20  $\mu\text{m}$ , with a minimum equivalent diameter of approximately 4  $\mu\text{m}$  (estimated using the procedure presented in last Chapter).

d) Grouping of cathode spots

i) Magnetic field

It has been reported that an external magnetic field aligns the cathode spots in the direction of the magnetic field lines, decreasing the spread of the spots (Emtage (14), Fang(15), Juttner (16), Drouet (17)).

Splitting of the cathode arc attachment was observed in this work using the current density probe for low magnetic fields. No splitting could be seen when high magnetic fields were used (the range for low and high magnetic fields are discussed later in this Chapter). This can be understood as an alignment of the spots in the direction parallel to the magnetic lines for high magnetic fields as shown in Figure 6.1 (see "Effect of magnetic field on spot distribution" later in the Chapter). In this case, since the probe is also parallel to the magnetic field, the signal generated from the probe should indicate one single spot for the attachment as observed. When the magnetic field is reduced, the spots are spread over the arc attachment and when the latter passes over the probe, the presence of individual spots could be detected.

ii) Surface contamination

The contamination of the cathode surface seems to affect the behavior of the arc attachment. It has been observed for vacuum arcs with copper cathodes contaminated with oxides that the erosion tracks left after the passage of the arc, i.e., the craters, were very small in diameter and spread over a larger area when compared to the craters produced by the arc on clean copper surfaces (Hantzsche (18), Rakhovsky

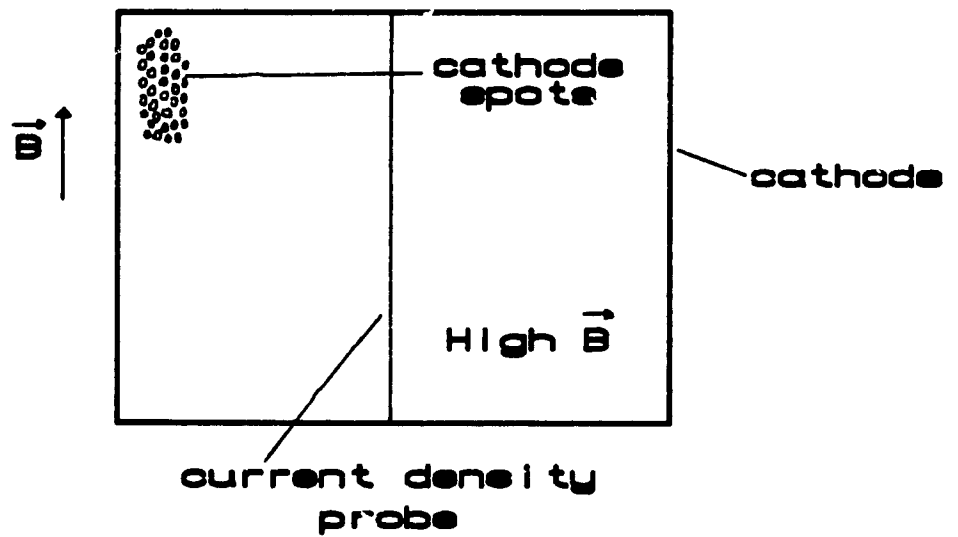
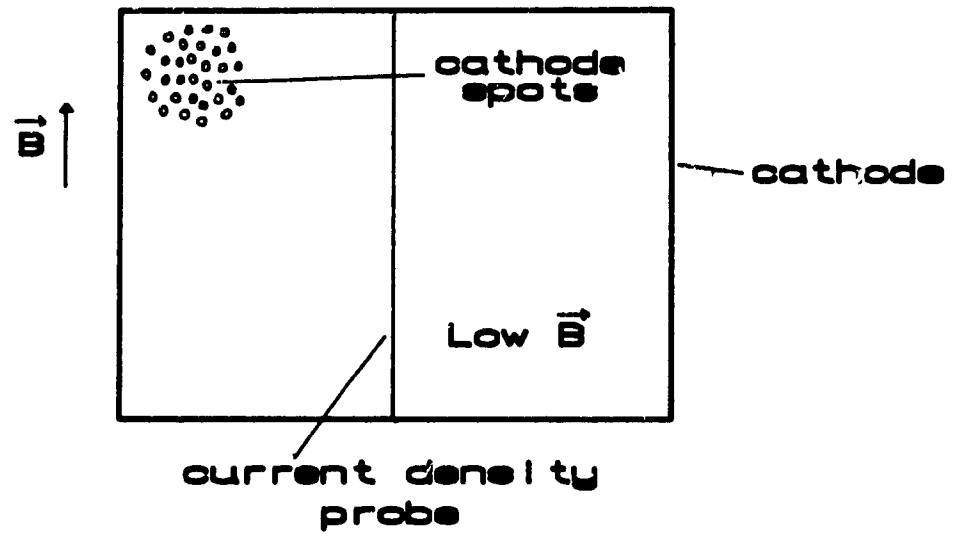


Figure 6.1 - Alignment of cathode spots in the direction of the magnetic field

(19), Achtert (20)). The same observations were reported by Porto et al (21) for copper cathodes when  $N_2$  was added in increasing amounts for low pressure arcs. In this work the spreading of the cathode spots (or splitting of the arc attachment) was seen for Ar and He contaminated with 3 000 ppm of CO and to a lesser degree for He contaminated with 3 000 ppm of  $N_2$ . It was shown in Chapter IV that the contamination of the inert gases with polyatomic gases resulted in contamination of the cathode surface.

e) Minimum erosion rate for isolated spots

Hitchcock and Guile (22) reported a minimum erosion rate for copper cathodes of the order of  $0.3 \mu\text{g/C}$  using air at atmospheric pressure.

A minimum erosion rate of around  $0.4 \mu\text{g/C}$  was found in this work for Ar and He contaminated with CO at high magnetic fields as well as for Ar+0.3%CO and He+0.4% $N_2$  at low magnetic fields. Slightly lower values, around  $0.3 \mu\text{g/C}$ , were found for very short time experiments (10 s experiments). Therefore it seems that for the whole range of operating conditions ( $0 < B < 1\ 500\ \text{G}$ ,  $80 < I < 150\ \text{A}$ , different plasma gases) there was a minimum value for the erosion rate of the cathode which compares well with the value found by Hitchcock and Guile. In all these cases the minimum value was found for contaminated surfaces, where the spots are further apart.

f) Residence time of the arc attachment

It has been suggested that decreasing the residence time of the arc attachment over the same region of the cathode reduces the erosion rate for vacuum (Daalder (23)) and atmospheric arcs (Harry 24)).

The reduction of the arc velocity resulted in higher erosion rates in our experiments (with the exception of low magnetic field for Ar+0.3%CO, He+0.4%CO and He+0.4%N<sub>2</sub> -see analysis of the results). The erosion rate for arcs running at the same overall velocity but with different residence time distributions were as follows: higher erosion rates were found for arcs having the higher number of "short distance jumps", i.e., higher residence time of the arc attachment.

### C) Understanding the Model

Erosion is caused by localized heat that cannot be dissipated either by conduction through the cathode or radiation and convection from the cathode surface. In order to keep the balance of energy, material volatilizes from the cathode surface resulting in the erosion of the electrode. The localized heat is due to the constricted zone of the electric arc on the cathode surface, the arc attachment (and this further divided in cathode spots). The arc attachment was discussed in the last chapters; what follows is a discussion of the microstructure of the arc attachment, the cathode spots.

The temperature of the surface under the cathode spots is the highest on the surface and the temperature decreases rapidly around the spot. If the spots are spread over a "large" region of the surface the temperature field of one spot does not interfere significantly with that of other spots and therefore the material between spots does not volatilize. When the spots are grouped close together, the region between them is also very hot and material leaves from the region around the spots as well as under them.

Therefore for the same power input, the cathode erosion rate will be higher if the cathode spots are in close proximity. This implies that if the spots can be created far apart and on regions which are cold (because there has not been a spot there

recently) the erosion rate will reach a minimum, due to the volatilization of material just under the cathode spots. The spots have a short lifetime and can, in principle, be formed anywhere on the cathode surface. However the spots are formed preferentially where the electrons can leave the surface easily. The electron emission is a function of the temperature of the surface, the electric field above the surface and the work function of the surface. Higher temperature, higher electrical field and lower work function facilitate the electron emission.

Places with localized high electric fields would be microprotrusions; some researchers have suggested the existence of these regions (Hantzsche et al (25), Juttner (16)). However Noer et al (26) refutes this suggestion and Cox (27) using a SEM with a resolution of  $0.06 \mu\text{m}$  was not able to detect protrusions. It seems that the necessity of the microprotrusions for the electron emission is at least questionable.

Assuming a homogeneous electric field above the surface, the cathode spots will be formed where the temperature is higher and/or the work function is lower. It was shown in Chapter IV that contamination on the copper surface can decrease the work function of the surface. The micro-movement of the arc or the formation of the spots can be understood as follows:

- the spot stays at a certain position until conditions for the formation of a new one exist. It has been suggested (Leycuras (28)) that the plasma cloud formed above the cathode spot can reduce the effective work function of the region. Therefore a new spot will be formed preferentially on regions below the plasma cloud if the other conditions of the region are the same. This means that in the case of magnetically driven arcs at atmospheric pressure the new spots will be formed in the direction of the arc movement, since the plasma and electric arc are under the influence of the Lorentz force and therefore will be pulled in the direction of the arc movement. The

surface may be clean or contaminated. In the first case, the spots will be formed close to each other because this is the region where the temperature is high enough for electron emission (work function is "high"). In the case of contaminated surfaces, the work function is reduced and the formation of spots can occur in places further from the old spots. In fact in the immediate vicinity of existing spots will be hot and part of the contamination layer will have been volatilized, forcing the new spots to be further away. The difference in behavior of the spots determines the different erosion rates, because in the case of clean surfaces the material between spots will also volatilize increasing the erosion rate.

The influence of the external magnetic field on erosion is examined next. It has two opposing effects; a higher magnetic field increases the arc velocity reducing its residence time, but at the same time serves to reduce the distance between the spots by aligning them in the direction of the magnetic field which enhances the erosion. These effects are further examined below.

σ) Effect of magnetic field on arc residence time

This has been discussed in Chapter III, and only the most relevant aspects are summarized here. The Lorentz force due to the external magnetic field moves the arc column. If for some reason the arc attachment stays longer in one region of the cathode surface the arc will be stretched until the attachment moves to a new location due to more favourable conditions. This happens for every gas and cathode surface condition; the difference is that for contaminated surfaces where the work function is low, the arc attachment moves to a new location with smaller "effort", while for clean surfaces the arc attachment movement is more difficult. The longer the residence time of the attachment, the higher the erosion rate.

φ) Effect of magnetic field on spot distribution

The second effect of the magnetic field is to align the cathode spots in the direction of the magnetic lines. Low magnetic fields allow the formation of new cathode spots in any direction and therefore the spread of the spots is larger, reducing the erosion rates at the same arc velocity.

An apparent paradox of the effect of the magnetic field on the arc attachment dimension must be explained here. In Chapter V it was shown that a decrease in magnetic field strength resulted in a more constricted attachment which at first seems to contradict the above discussion. The explanation is that the current distribution probe measures the attachment dimension in the direction of motion of the arc, i.e., perpendicular to the magnetic field, while the alignment of the spots is parallel to the magnetic field. The constriction observed in Chapter V as the magnetic field was decreased was thus simply because the arc and plasma cloud and then the arc attachment were stretched less in the direction of arc motion. At lower magnetic fields ( $< 250$  G) the stretching becomes of minor importance and then further reductions of field strength would result in a spread of the arc in all directions.

A final point to be addressed concerns the mobility of the cathode spots. If indeed electron emission is easiest at the highest surface temperatures the cathode spot should stay at that location indefinitely. However, this is not the case and possible explanations for this fact are described below.

i) Although the temperature is high at the cathode spot, material has been volatilized from that location, "cleaning" the surface of contamination, i.e., increasing the work function. A nearby spot, at lower temperature but lower work function or higher electric field might be more favourable for electron emission (also if the plasma cloud

is above this region, it decreases the effective work function). Once the new spot starts to emit electrons, the temperature rises at this new location and more electrons are emitted from this new spot, eventually extinguishing the old spot.

ii) The electrical conductivity of copper decreases with increasing temperatures (Kittel (39)) increasing the resistance for electron flow to existing cathode spots.

iii) For magnetically driven arcs, it is very hard for the attachment to stay at a certain position. The arc column is being stretched and either the arc attachment moves or the arc is extinguished.

In summary, if the cathode spots can be formed in extremely short times, over a large region, the erosion reaches its minimum value. Although in principle the spots can be created so fast that no erosion is detected, in reality the spots exist for a short time but enough to volatilize some material from the cathode. Any condition that makes the spots to remain longer time at the same region (high work function, low arc velocity) increases the erosion rates.

#### 4) QUALITATIVE ANALYSIS OF EROSION RATES

The results shown in Table 6.2 were analyzed using the concepts developed for the model in the last section. Based on this model, the cathode erosion rate, which depends on the heat flux to the electrode, can be understood as a function of:

$$E = f(\sigma, D_s, S_{pl}) \quad 6.1$$

where  $E$  = erosion rate

$\sigma$  = residence time of the arc attachment

$D_a$  = arc attachment diameter

$S_{pl}$  = distance between spots (splitting)

The effect of these parameters on the erosion results is qualitatively discussed for the different plasma gases and operating conditions; some quantitative analysis is done in the next chapter.

#### A) Residence Time (Arc Velocity) and Arc Attachment Splitting

##### a) Nitrogen

It is possible to change the arc velocity by changing the magnetic field strength or the gas flow rate (reducing the gas flow results in higher gas temperature in the arc path giving lower density and lower aerodynamic drag). Figure 6.2 shows the variation of erosion rate with arc velocity for pure nitrogen arcs. The change in the arc velocity was due to the magnetic field. The erosion rate seems to be inversely proportional to the arc velocity,

$$E \propto 1/V_{el}$$

6.2

The same data are now plotted in a log-log scale in Figure 6.3. The erosion rates for two new gas flow rates (10 and 0.2 l/min) at two discrete magnetic field strengths of 1 000 and 130 G have also been plotted in Figure 6.3. The results seem to indicate a change in the slope of erosion rate vs arc velocity.

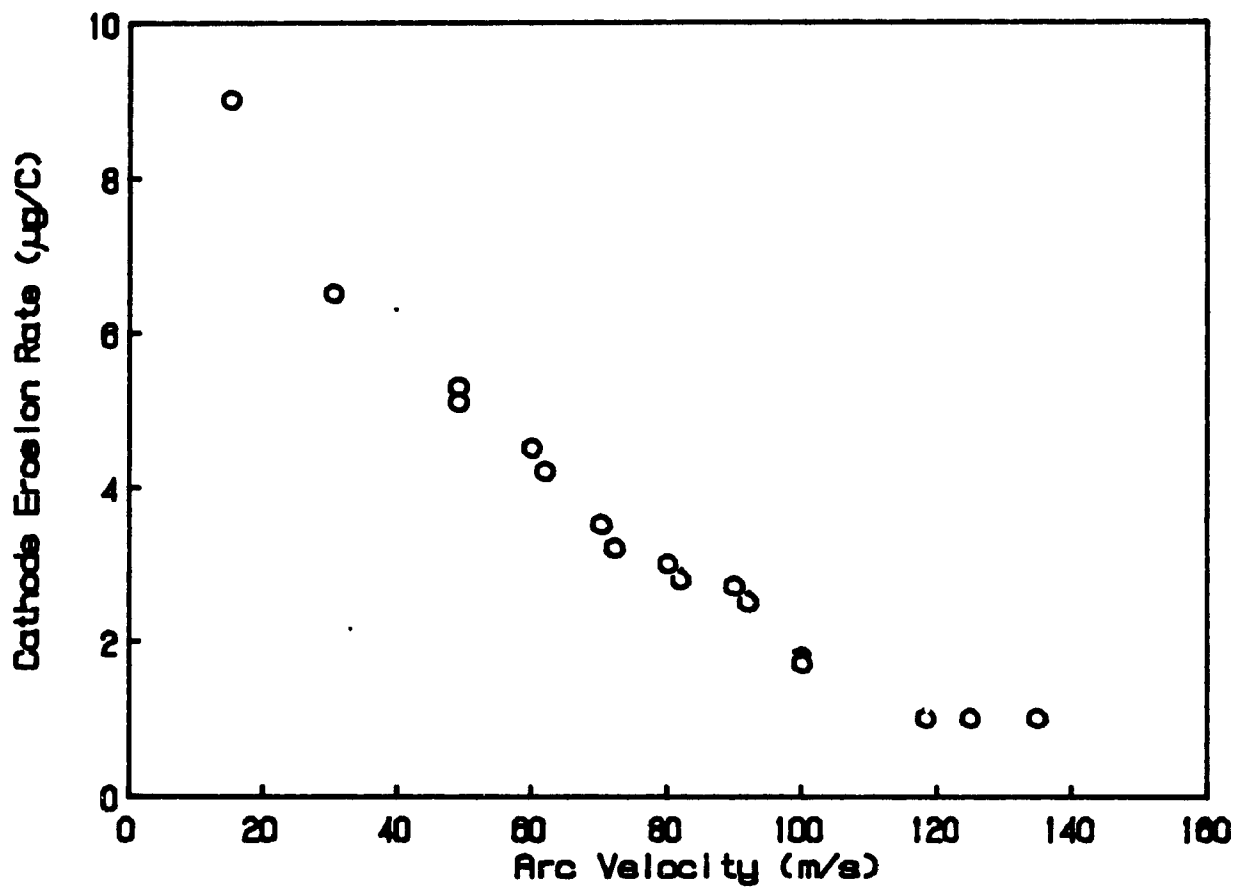


Figure 6.2 - Cathode erosion rate vs arc velocity for pure nitrogen arcs

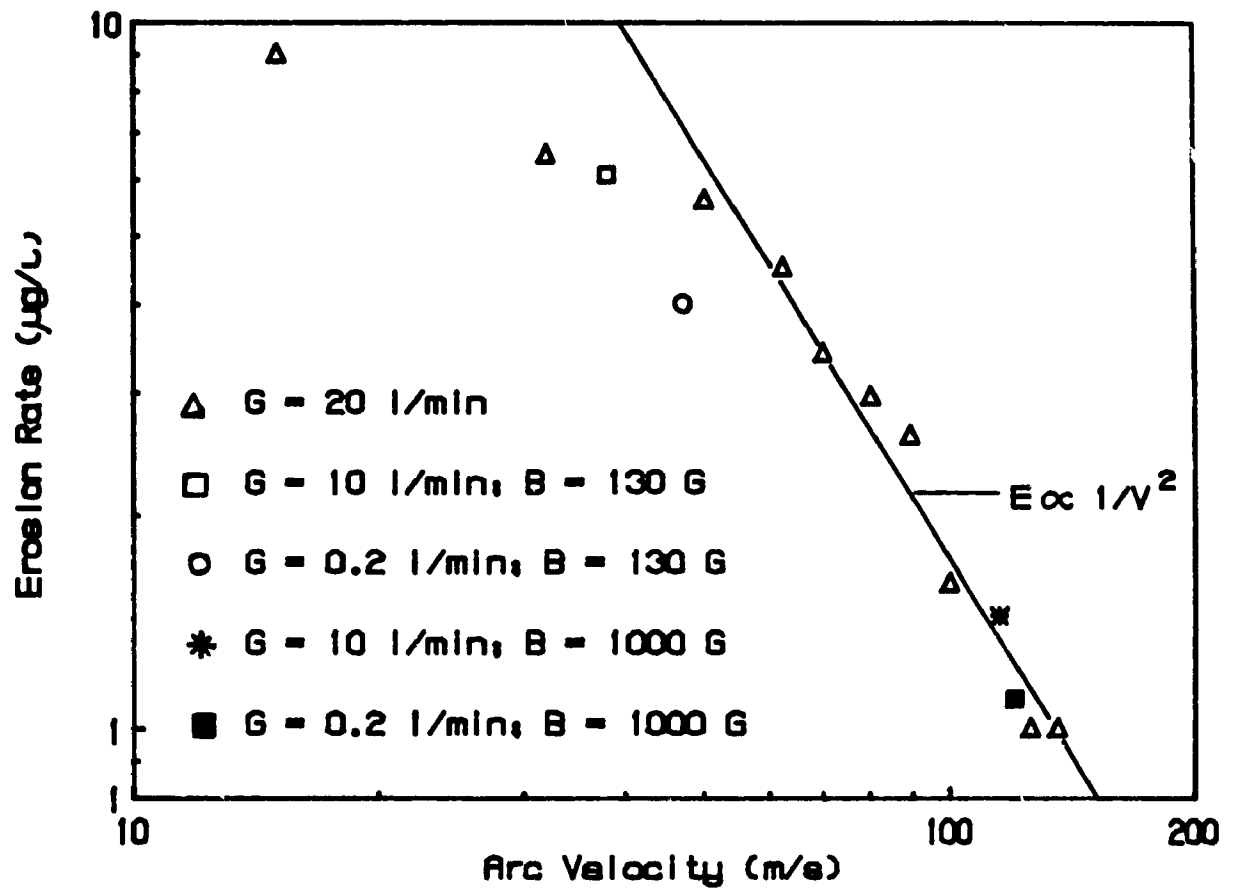


Figure 6.3 - Log plot of cathode erosion rate vs arc velocity for N<sub>2</sub> arcs

For arc velocities between 125 and 50 m/s (for 20 l/min gas flow rate) the erosion rate is given by:

$$E \propto 1/Ve^2$$

6.3

The erosion rate seems to be a weaker function of arc velocity below 50 m/s. At a nitrogen flow rate of 20 l/min, an arc velocity of 50 m/s is achieved with a magnetic field of the order of 250 G. The decrease in the gas flow rate resulted in higher arc velocity and lower erosion rates. The following interpretation of the results is proposed:

- For magnetic fields higher than 250 G, the cathode spots are aligned and closely spaced due to the magnetic field. The erosion rate increases very quickly with arc velocity for lower arc velocities. However decreasing the magnetic field to values lower than 250 G allowed the spots to separate from each other, causing a weaker dependence of erosion rate on arc velocity. The division of the arc attachment was observed with the current density probe for nitrogen for magnetic fields lower than 200 G (Chapter V).

The lower gas flow rate results are consistent with these ideas. At a field of 250 G (gas flow rate of 20 l/min) the arc velocity was 50 m/s and the erosion rate 5.6  $\mu\text{g}/\text{C}$  while for a field of 130 G (gas flow rate of 0.2 l/min) the arc velocity was 47 m/s and the erosion rate was 4.0  $\mu\text{g}/\text{C}$ . Thus even for a lower velocity, the erosion rate was 29 % lower at the lower magnetic field. To verify that it was the magnetic field and not the gas flow rate, which was producing the changes in erosion rate, the gas flow rate was reduced from 20 to 0.2 l/min at a magnetic field of 1 000 G. It is evident from Figure 6.3 that these high magnetic field results are in good agreement with the results using higher gas flow rates.

The inverse proportionality of the erosion rate with arc velocity in the velocity range 15-130 m/s thus seems to be due to a combination of the effects of lower residence time and arc splitting.

b) He+0.4%CO, He+0.4%N<sub>2</sub>, and Ar+0.3%CO

The magnetic field was varied in order to obtain different arc velocities for Ar and He contaminated with 3 000 and 4 000 ppm of CO respectively and He contaminated with 3 000 ppm of nitrogen; an increase in magnetic field strength always gave an increase in arc velocity (see Chapter III). The erosion rates obtained for the different plasma gases and arc velocities are plotted in Figure 6.4. For the three mixtures of gases the erosion rate first increased and then decreased as the arc velocity was continuously decreased. The transition from an increase to a decrease in the erosion rate for decreasing arc velocities occurred at a magnetic field strength of around 250 G, for all three gas combinations. This can be seen in Figure 6.5, where the erosion rates obtained for different magnetic fields for these three gases are plotted.

The same reasoning given above for pure N<sub>2</sub> arcs can be used here to explain this apparently anomalous behavior. As shown in Chapter V, the arc attachment splits for low magnetic fields and so the negative effect of increased residence time at low velocities is counteracted by the positive effect of a more widely spaced cathode spots.

Therefore it seems that for N<sub>2</sub>, He+0.4%CO, He+0.4%N<sub>2</sub>, Ar+0.3%CO and possibly for other polyatomic gases (Cl<sub>2</sub>, CH<sub>4</sub>, etc) the erosion rate increases when the magnetic field is decreased from 1 000 G (or more) to around 250 G; thereafter the erosion rate increases more slowly with reduced velocities (N<sub>2</sub>) or even decrease (He+0.4%CO, He+0.4%N<sub>2</sub>, Ar+0.3%CO).

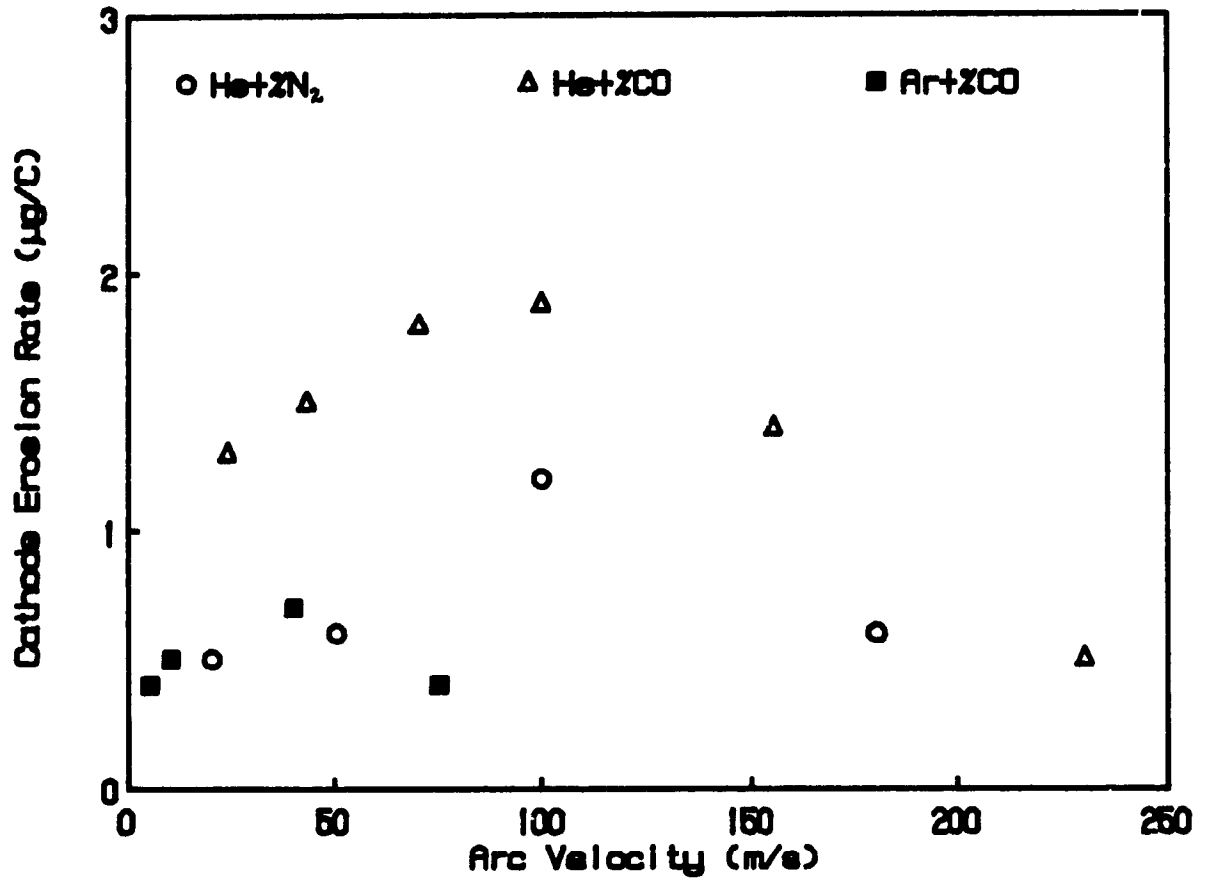


Figure 6.4 - Cathode erosion rate vs arc velocity

He+0.4%CO, He+0.4%N<sub>2</sub>, Ar+0.3%CO

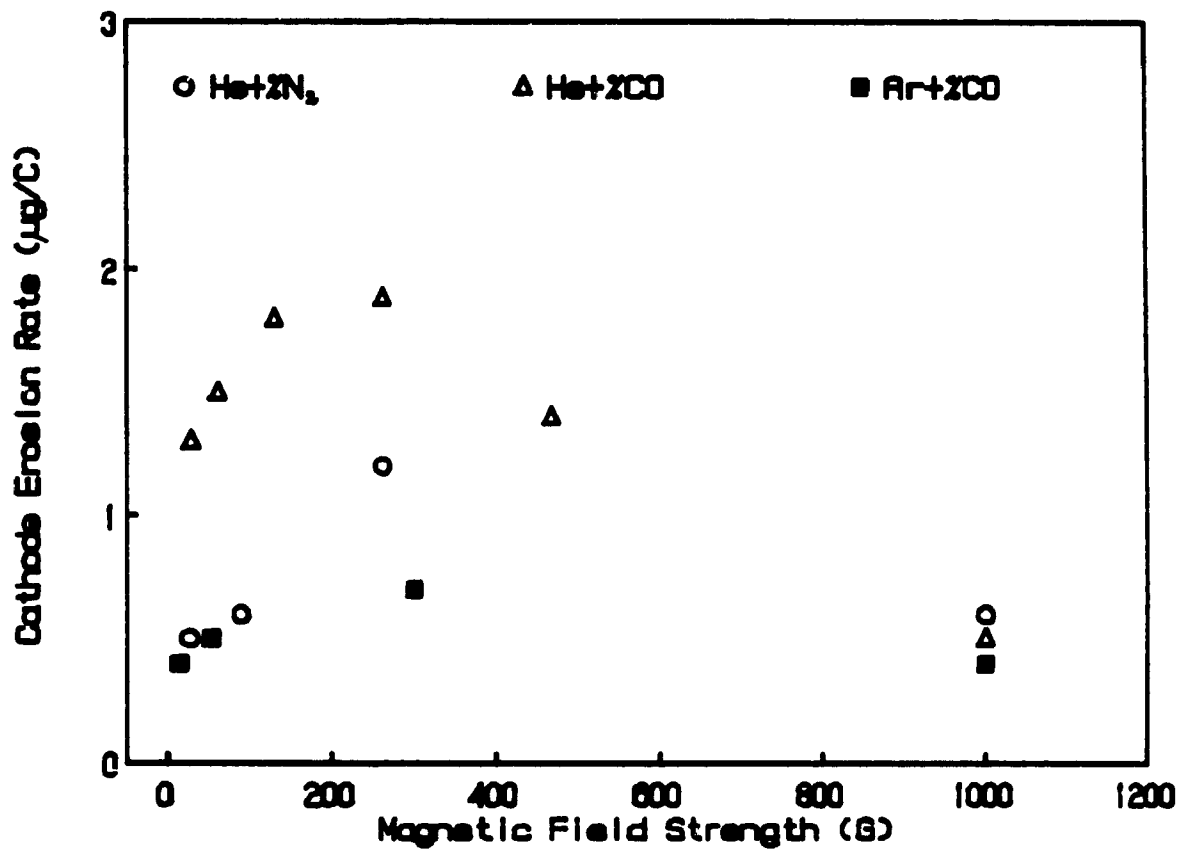


Figure 6.5 - Cathode erosion rate vs magnetic field  
He+0.4%CO, He+0.4%N<sub>2</sub>, Ar+0.3%CO

c) Ar

In pure argon the arc velocity did not change as the magnetic field strength was increased from 200 to 1 000 G although the erosion rate changed from 50  $\mu\text{g}/\text{C}$  to 13.5  $\mu\text{g}/\text{C}$  respectively (see C) Residence Time); below 200 G the arc was unstable. The arc velocity could be increased by reducing the gas flow rate which again reduced the gas density and aerodynamic drag on the arc. The arc velocity increased from 2 to 10.5 m/s as the gas flow rate was decreased from 20 to 0.2 l/min. This relatively high sensitivity of velocity to gas flow rate was observed because the axial velocity of the gas within the electrode was relatively large (1 m/s at 20 l/min) compared to the arc velocity around the circumference of the cathode (2 m/s).

The erosion rates in pure argon obtained at different gas flow rates are plotted in Figure 6.6. The data can be correlated by:

$$E \propto 1/V_{\text{el}}^{0.6}$$

6.4

showing that the erosion rates in argon are a weaker function of arc velocity than those of nitrogen. The differences in the arc velocity ranges for the two gases makes any further comparison difficult. For argon the relative velocity changes greatly (by a factor of five but the absolute change in velocity is small while for nitrogen the relative change is small (factor of 1.2) but the absolute change is great (20 m/s). The theoretical variation of electrode surface temperature distribution with arc velocity is modelled in the next chapter.

B) Current Density

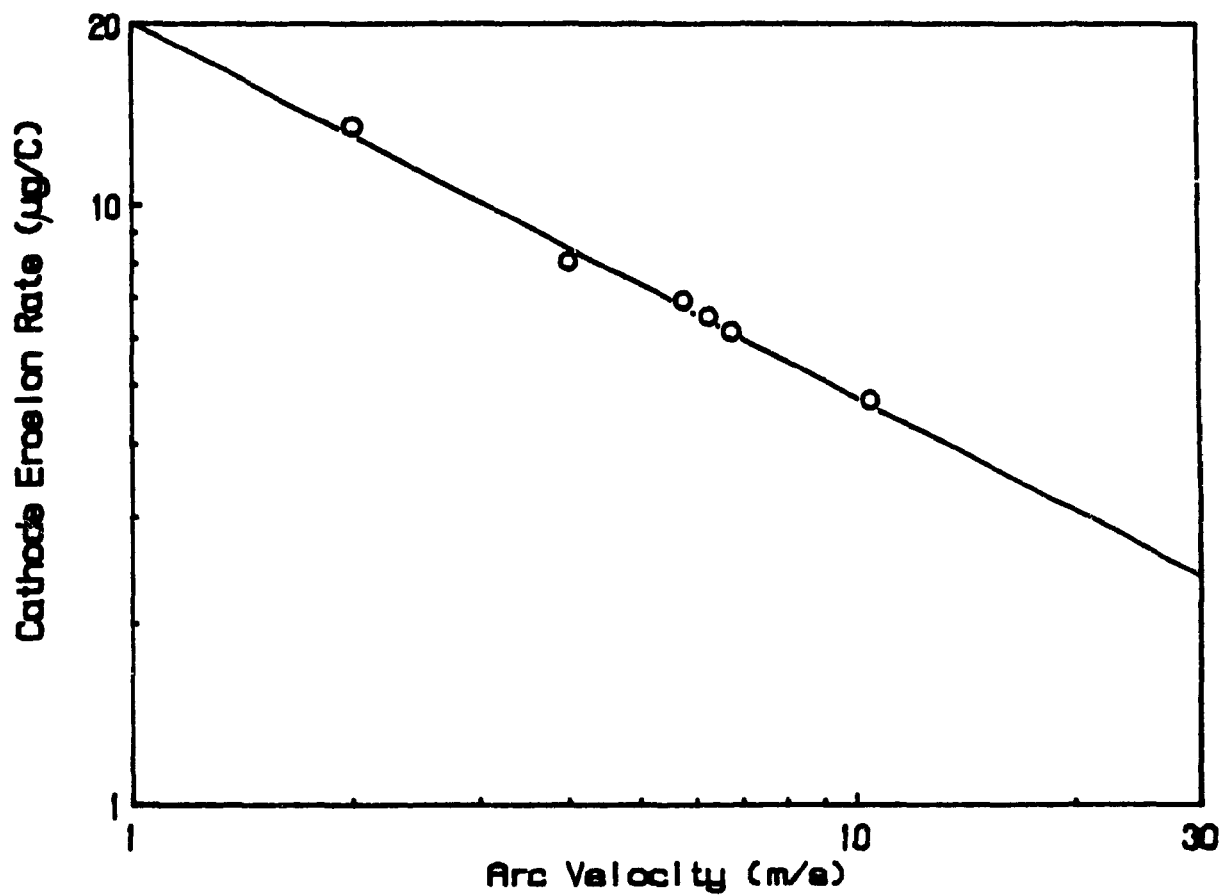


Figure 6.6 - Cathode erosion rate vs arc velocity for Ar at different gas flow rates  
(20 l/min = 2m/s; 0.2 l/min = 10.5 m/s)

a) Ar and He

Pure argon and pure helium at the same magnetic field (1 000 G) had different erosion rates (13.5  $\mu\text{g}/\text{C}$  and 1  $\mu\text{g}/\text{C}$  for Ar and He respectively) but they also had different arc velocities (2 m/s and 20 m/s for Ar and He respectively). Therefore no direct comparison is possible. However, assuming that the results from reducing the gas flow rate for Ar can be extrapolated to 20 m/s, from Figure 6.6 it can be seen that the erosion rate would be around 3  $\mu\text{g}/\text{C}$  for pure Ar at 20 m/s. Both Ar and He produce the same kind of clean surface and therefore similar surface drag forces and residence time distributions (for similar arc velocities).

The higher erosion rate of argon compared to helium might thus be an indication of higher current density for argon; this is indeed what was observed in Chapter V. If the minimum equivalent arc diameters measured in Chapter V ( $D_{\text{eq}} = 1.2$  mm for Ar and 2.1 mm for He) are correlated with the above erosion rates we have:

$$E_{\text{Ar}} / E_{\text{He}} = (D_{\text{eqAr}} / D_{\text{eqHe}})^n \quad 6.5$$

which gives approximately  $n = -2$  or that the erosion rate is inversely proportional to the square of the arc diameter or proportional to the mean current density, i.e.;

$$E \propto J \quad 6.6$$

b) He+0.4%CO and He+0.4%N<sub>2</sub>

The current density is also the main reason for the different erosion rates observed between He contaminated with 4 000 ppm of CO and He contaminated with 4 000 ppm of N<sub>2</sub> for low magnetic fields (Figure 6.3). The values for minimum equivalent diameter presented in Chapter V were interpolated for 100 m/s; the erosion rates

obtained for these two mixtures of gases at 100 m/s are given below. Correlating the erosion rates with the minimum equivalent diameter at 100 m/s we obtain:

$$\frac{E_{\text{He}+\% \text{CO}}}{E_{\text{He}+\% \text{N}_2}} = \left( \frac{Deq_{\text{He}+\% \text{N}_2}}{Deq_{\text{He}+\% \text{CO}}} \right)^n$$

$$1.88 / 1.2 = \left( 3 / 2.55 \right)^n$$

which gives  $n = -2.6$ . This number is reasonably close to the value obtained for pure Ar and He ( $n = -2$ ); differences in the residence time distribution, for example, could alter the values of the erosion rate enough to cause differences in the value of  $n$ .

### c) Ar+He

Helium was added in increasing amounts to argon. The magnetic field was always at 1 000 G and the arc current 100 A for all experiments (except the arc current for pure helium, kept at 110 A). The results for these experiments are given in Table 6.2; the erosion rates and arc velocities are summarized in Table 6.3 below. It can be seen that the arc velocity increases from 2 m/s (pure Ar) to 18 m/s (25 % Ar) for the same operating conditions (gas flow rate, arc current and magnetic field). The increase in the arc velocity is caused by the change in the gas density (lower for helium) and arc characteristics (higher power for helium resulting eventually in higher gas temperature in the arc path). The erosion rates for argon-helium mixtures are similar to the values obtained for pure argon at the same arc velocities (for pure argon the different values of arc velocities were obtained using different gas flow rates) up to around 50 % helium in argon. At higher concentrations of helium and for similar arc velocities, the erosion rate values are intermediate between the values obtained for pure helium and for pure argon.

These results can be understood when the current densities are examined. Helium arcs have lower current densities at the cathode surface than argon arcs. Therefore as the concentration of helium in argon is increased beyond 50 %, the current density is smaller than for pure argon; for similar arc velocities, the mixture has lower erosion rates than pure argon. For high concentrations of helium, the current density keeps decreasing but eventually is always larger than for pure helium, since argon is still present. Therefore for similar arc velocities, the erosion rate for the mixture is higher than for pure helium, but lower than for pure argon as observed.

**TABLE 6.3**  
Erosion Rates and Arc Velocities for Argon and Helium Mixtures

Gas	Arc Velocity (m/s)	Erosion Rate ( $\mu\text{g/C}$ )
Ar	2.0	13.5
Ar	4.0	8.0
Ar	6.2	6.6
Ar	10.5	4.7
Ar	20.0	3.0*
Ar+25%He	3.5	9.8
Ar+50%He	5.5	7.0
Ar+75%He	18.0	2.4
He	20.0	1.0

\* extrapolated from Figure 6.4

### C) Residence Time

#### a) Argon

The erosion rate for pure argon increased with decreasing magnetic field although the overall arc velocity was the same, as shown in Table 6.2. The reasons for this high increase in the erosion rate ( $13.5 \mu\text{g}/\text{C}$  to  $50 \mu\text{g}/\text{C}$  for 1 000 G and 200 G respectively) are related to the residence time of the attachment over the same region and secondarily to the increase in the current density for lower values of magnetic field strength (for the range of magnetic field strength used in these experiments, the arc attachment probably did not change significantly; also the surface is clean with pure Ar). The lower magnetic field resulted in a broader distribution of jumps for pure helium and Ar+0.3%N<sub>2</sub> (Chapter III) with a higher number of jumps zero (zero distance). The longer the arc attachment stays at a certain position, the higher the surface temperature around that region and the higher the erosion rate.

#### b) Ar and Ar+0.3%N<sub>2</sub>

The erosion rate for Ar+0.3%N<sub>2</sub> was higher than for pure Ar ( $27.3 \mu\text{g}/\text{C}$  and  $13.5 \mu\text{g}/\text{C}$  for Ar+0.3%N<sub>2</sub> and Ar respectively) even though the argon arc had a lower arc velocity (2 m/s for Ar and 6 m/s for Ar+0.3%N<sub>2</sub>). The current density was not measured for Ar+0.3%N<sub>2</sub>, but it was probably lower than for pure argon (for Ar+0.3%CO the current density was lower than for pure argon and the current densities for contaminated He were lower than pure He). Therefore the explanation for the higher erosion rate for Ar+0.3%N<sub>2</sub> must be the residence time distribution. Indeed the residence time distributions for Ar+0.3%N<sub>2</sub> showed far more occurrence of a stationary arc than did those of Ar (Chapter III). This is probably due to the

lower magnetic field used for Ar+0.3%N<sub>2</sub> (53 G) than for pure Ar (1 000 G) in order to have similar arc velocities.

#### D) Residence Time and Current Density

##### a) Helium

The erosion rate for pure helium at the same arc velocity (20 m/s) but different magnetic field strength (1 000 G and 100 G) is higher for the lower magnetic field (3.0 μg/C and 1.0 μg/C for 100 G and 1 000 G respectively). It was seen in Chapter V that the minimum equivalent arc diameter is smaller for the lower magnetic field (1.7 mm and 2.1 mm for 100 G and 1 000 G respectively). In this case the splitting of the arc attachment was not observed, since the surface was clean. Although equation 6.6 was obtained for just two cases (Ar - He and He+0.4%CO - He+0.4%N<sub>2</sub>) it might be used for a first analysis of the effect of the arc attachment current density (equivalent minimum diameter) on the erosion rate:

$$E_{100} / E_{1000} \propto (2.1/1.7)^2 = 1.5$$

The current density alone cannot explain the differences in the erosion rates. However the residence time distribution was also different for the two magnetic fields; the distribution is broader for the low magnetic field, with a larger number of short jumps than for high magnetic field (Chapter III). This would result in a higher erosion rate for 100 G. Therefore both factors, current density and residence time distribution have to be considered for the erosion rates of pure helium at different magnetic fields.

b) Ar+0.3%CO and CO

The erosion rates for argon contaminated with 3 000 ppm of CO and pure CO are quite different (0.4  $\mu\text{g}/\text{C}$  for Ar+%CO and 4.2  $\mu\text{g}/\text{C}$  for CO) for similar arc velocity (75 m/s for Ar+0.3%CO and 100 m/s for CO) at 1 000 G. It was shown in Chapter III that if more than 2-3% of CO is added to argon, the arc velocity decreases, and the arc movement becomes jerky, increasing the residence time of the arc attachment. The current density for both gases at the operating conditions described above are also different; the minimum equivalent diameter for Ar+0.3%CO is 2.7 mm and for CO is 2.0 mm. Applying the same rational as before, equation 6.6 would give :

$$E_{\text{Ar}+\% \text{CO}} / E_{\text{rCO}} \propto (2.0/2.7)^2 = 0.5$$

Therefore the differences in the current density and in the residence time have to be taken into account when the erosion rate of these two gases is compared. The effect of the different arc velocities (75 to 100 m/s) on the erosion rates was not considered in the above discussion; since the arc velocity for pure CO is higher than for Ar+0.3%CO, the erosion rate for the former should be even higher at similar arc velocities, validating more the effect of the current density and residence time distribution on erosion rate.

E) Residence Time, Current Density and Arc Attachment Splitting

Pure argon and argon contaminated with 3 000 ppm of CO for the same arc velocity (4 m/s) had different erosion rates (8.0  $\mu\text{g}/\text{C}$  and 0.4  $\mu\text{g}/\text{C}$  for Ar and Ar+0.3%CO respectively). The magnetic field strengths were different for these experiments, 1 000 G for Ar and 10 G for Ar+0.3%CO. Three factors have to be considered here for the comparison of the erosion rates: residence time, current density and arc

attachment splitting. Argon has a broad residence time distribution (Chapter III), with some stationary arc periods, while Ar+0.3%CO has a very narrow residence time distribution and no stationary arcs. The current density is higher for Ar than for Ar+0.3%CO (Chapter V); the minimum equivalent diameter are 1.2 mm for Ar and 1.9 mm for Ar+%CO at the steady state operating conditions specified above. And finally it was shown in the last chapter that at low magnetic field Ar+0.3%CO gives widely spread spots; this is not the case for Ar at the magnetic field strength used in these experiments. All three factors point to a higher erosion rate for pure Ar than for Ar+0.3%CO as observed but it is not possible at this stage to separate their contributions.

## 5) OTHER ASPECTS OF CATHODE EROSION

### A) Power Input to the Cathode

The power input to the cathode was measured calorimetrically. Table 6.2 shows that no direct relationship exists between this power input and erosion rate. This is because the main contribution to the power input is due to radiation from the arc and its flux is too dilute to cause erosion. The greatest part of the arc radiant energy goes to the cathode simply because of the geometry used here (when the polarity of the electrodes was inverted, the percentage of the total power going to the electrodes changed from 75 - 25 % for the cathode and anode respectively to 40 - 60 % for the cathode and anode respectively).

### B) Cathode Spots - Similarities With Vacuum Arcs

It has been suggested by different authors (Rakhovsky (25); Beilis et al (29)) that there are two types of cathode spots for vacuum arcs: type I, explosive spots,

transient quick-moving with high current density; type II, quasi-stationary, slow moving with low current density. The same authors suggested that type I occurs for contaminated surfaces and the type II on clean surfaces. These models were developed to explain the different erosion rates and crater sizes between oxide contaminated and clean surfaces; contaminated surfaces gave lower erosion rates and small crater sizes than clean surfaces. Theoretical aspects of the electron emission were considered to support each type of cathode spot. Hantzsche (30,31) and Mitterauer and Till (32) studied the cathode spot based on numerical calculations and concluded that only an essentially nonstationary explosive nature of the cathode spot existed.

No attempt was made, in this research, to establish a theory for the formation of the cathode spots. However some similarities can be found among the results from this work and the ones reported for vacuum arcs. It has been mentioned before that the phenomena related to vacuum arcs are essentially similar to atmospheric arcs. The different erosion rates (higher for vacuum arcs) could be explained due to a redeposition of volatilized material on the cathode surface for increasing pressures (Meunier and Drouet (33)). The decrease in the crater size for increasing nitrogen pressure (from  $10^{-6}$  to 100 Torr) has been suggested to be due to nitrogen contamination of the copper (Porto et al (21)).

It has been shown throughout the thesis that for low magnetic fields, contaminated surfaces produced a large separation of the cathode spots, while for clean surfaces the spots remain aggregated even for low magnetic fields. It therefore seems possible that the two types of cathode spots presented above are just a reflection of the higher work function for clean surfaces; if the surface is contaminated, the spots would be formed far apart, decreasing the erosion rate and the crater size. For clean surfaces the spots will stay close together, since the temperature of the region must

be high enough to compensate for the high work function in respect of electron emission. The explosive nature of the cathode spot suggested by other authors (Type I) implies a minimum erosion rate; material volatilizes just from regions below the spots. The minimum erosion rate in this work was found for contaminated surfaces and widely spaced spots.

### C) Electron Emission

The electron emission for copper cathodes is believed to be controlled by the Thermo-Field mechanism (TF emission). This mechanism of electron emission uses the concepts developed originally by Fowler-Nordheim (34) with the concepts for thermionic emission expressed by the Richardson equation with the modified Schottky effect (Herring and Nichols (6)). The general equation describing the TF emission was first described by Murphy and Good (35); many modifications to this original work have been suggested, one of the most recent by Hantzsche (36). The correct formulation of the TF mechanism is still questionable, but the general relationship is

$$j_e = f(T, E, \varphi) \quad 6.7$$

where  $j_e$  = electron emission current density

$T$  = surface temperature

$E$  = electric field above the surface

$\varphi$  = work function of the surface

Higher temperature and electric field but lower work function results in higher current density. Unfortunately lack of agreement on both the functional form and the numerical parameters of equation 6.7 allow the prediction of current densities from  $10^6$  to  $10^{14}$  A/m<sup>2</sup>. The knowledge of the correct form of the electron emission

mechanism and of the values of the parameters are necessary for any theoretical study of cathode erosion, since the lifetime of the cathode spot, the spot mobility, the energy input per spot, the size of the cathode spot, are all related to the electron emission characteristics of the cathode.

#### D) Anode Erosion Rate

The erosion rate for the anode was measured using helium as the plasma gas. The polarity of the electrodes was inverted in order to have the anode as the test electrode. The time duration of the experiment was only 4 minutes because the now smaller cathode, showed severe erosion. No weight loss was detected in the anode, indicating that the erosion rate for the anode was at the most  $0.1 \times 10^{-6}$  g/C (the precision of the scale used was better than 0.001 g). The low erosion rate for the anode was also seen indirectly during the cathode erosion experiments because the central electrode (anode for these cathode erosion experiments) could be used for at least 50 hours for different plasma gases. The lower erosion for the anode is probably due to the lower current density when compared with the cathode, as shown in the last Chapter. The anode also does not present anode spots for currents lower than 1 000 A (Cobine (37)) and therefore the heat is dissipated over the entire arc attachment.

#### E) Arc Movement in Pure Helium

The arc velocity for pure He showed the peculiar and unique variation with magnetic field given in Chapter III. The arc seems to follow a type of aerodynamic equilibrium, with an increase of the arc velocity with magnetic field according to equation 3.11a up to approximately 500 G, when the velocity is 95 m/s. The arc velocity then decreases for further increases in the magnetic field, reaching 20 m/s for 1 000 G.

Another interesting characteristic is that if the arc is running at 95 m/s for 500 G and the magnetic field strength is increased to 1 000 G, the arc velocity stays at 95-100 m/s for some time and then starts to decrease reaching 20 m/s after 2-3 minutes.

The magnetic field strength can not be directly responsible for the decrease in the arc velocity because it takes some time for the arc velocity to decrease from 95 to 20 m/s after the magnetic field is at 1 000 G. One possible reason for this odd behavior of helium that can also explain why the same behavior was not seen for argon deals with the arc column length. In Table 6.4 the variation of arc velocity and arc voltage with magnetic field is given.

It can be seen that the arc voltage increased much more between 520 and 780 G than between any other two values. This transition is where the arc velocity suddenly decreased for higher magnetic fields. The arc becomes very long above 520 G; this was seen using high speed photography and in the arc voltage. Pure helium had by far the longest arc column of all plasma gases. Therefore it is possible that the surface in front of the arc attachment is hotter for this long arc than for short arcs, since during more time this region was exposed directly to the radiation from the arc. Although, in principle, hotter surfaces emit electrons better, and therefore would make the arc movement easier, they may also result in the volatilization of minute impurities or melting of surface irregularities which would make the electron emission easier. A decrease in the arc velocity by 50 % was reported for aluminum cathodes when these were heated from 300 K to 770 K (Nurnberg et al (38)). Thus the lower arc velocity for helium for higher magnetic fields may be a reflection of the high surface temperature caused by the longer arc column. Since the arc column for argon is much shorter than for helium, no changes in the surface temperature associated with the length of the arc is noticed for pure argon when the magnetic field is varied. The same rational can be used for the other plasma gases (instead of argon).

TABLE 6.4

Arc Velocity and Voltage for Different  
Magnetic Field Strengths in He

Magnetic Field (G)	Arc Velocity (m/s)	Arc Voltage (V)
1000	20	110
900	28	108
780	40	105
520	95	60
440	90	54
390	85	53
260	70	48
180	60	44
130	52	40
104	45	39
78	38	38
52	28	36
26	15	35
12	10	34

## 6) CONCLUSIONS

In this chapter a conceptual model of cathode erosion was developed and the erosion rate data were analyzed using the model as a guideline. The principal findings and ideas discussed are summarized below.

a) In the conceptual model, the arc attachment is made of individual contributions, the cathode spots. These can be grouped together if the magnetic field is high and the surface is clean. Longer residence time of the attachment on a local surface, more closely spaced cathode spots and higher current densities all result in higher erosion rate.

b) It is proposed that there is a minimum erosion rate for copper cathodes caused by the erosion of material immediately below the cathode spots. The minimum erosion rate is in the range 0.1-0.3  $\mu\text{g/C}$ .

c) Experimental evidence was given for the model from this and other works. These included: the existence of cathode spots, the alignment of spots with magnetic field, the effect of surface contamination on arc movement and erosion results, the effect of higher residence time of the arc attachment on erosion rates.

d) Cathode erosion rate were presented for: Pure Ar, He, N<sub>2</sub>, CO, air, and mixtures of Ar and He with N<sub>2</sub>, O<sub>2</sub>, Cl<sub>2</sub>, CO, CH<sub>4</sub>, H<sub>2</sub>S; the magnetic field was varied between 10 and 1 500 G, the gas flow rate between 0.2 and 20 l/m, and the arc current between 100 and 140 A. The anode erosion rate was always much less than the cathode, even when the polarity of the electrodes was inverted.

- e) The erosion rate seems to be directly related to current density of the arc attachment at the cathode. This was verified comparing experiments between pure Ar and He and He contaminated with CO and N<sub>2</sub>. The erosion is also inversely proportional to the arc velocity for N<sub>2</sub> arcs, but is less sensitive to changes in the arc velocity for low velocities in argon. The splitting of the arc attachment considerably reduces the erosion rates for similar arc velocities (N<sub>2</sub>) and is responsible for a decrease in the erosion rate for low arc velocities in Ar+0.3%CO, He+0.4%CO and He+0.4%N<sub>2</sub>.
- f) The residence time of the arc attachment was particularly important for pure argon experiments with similar arc velocities but different magnetic fields. Important differences between arc velocity (Vel) and arc attachment residence time for erosion rates were shown. Higher residence times increased the erosion rate. This was also seen comparing Ar+0.3%N<sub>2</sub> and Ar at similar arc velocities.
- g) Argon contaminated with 3 000 ppm of CO had a much lower erosion rate than pure CO for similar arc velocities and magnetic field. The reasons given for this are higher residence time and current density for CO arcs.
- h) The reduction in the erosion rate when 3 000 ppm of CO were added to argon for similar arc velocities are attributed to a combination of a decreased residence time of the arc attachment, a decreased current density and a spreading of the cathode spots.
- i) In the apparatus used, the total power input to the cathode is higher than for the anode but does not have a direct relation with the erosion rates. The heat is mainly caused by radiation from the arc. When the polarity of the electrodes was inverted, the percentage of the heat going to the anode was higher than for the cathode.

j) The peculiar arc movement behavior of helium appears to be a result of higher surface temperatures in the region in front of the arc attachment caused by an unusually long arc column.

REFERENCES

- 1) Kimblin, C.W.; "A review of arcing phenomena in vacuum and in the transition to atmospheric pressure arcs", IEEE Trans. Plas. Sci. , Vol PS-10, n.4, 322-330, 1982.
- 2) Guile, A.E.; Hitchcock, A.H.; "The erosion of copper cathodes from vacuum to atmospheric arcs", J. Appl. Phys., Vol 49, n.7, 4275-4276, 1978.
- 3) Harry, J.E.; "The measurement of the erosion rate at the electrodes of an arc rotated by a transverse magnetic field", J. Appl. Phys., Vol 40, n.1, 265-270, 1969.
- 4) Guile, A.E.; Hitchcock, A.H.; "Effect of water cooling on erosion of the copper cathode of a rotating arc", Proc. IEE, Vol 122, n.5, 579-580, 1975.
- 5) Kesaev, I.G.; Sov. Phys. - Tech. Phys., Vol 8, 447, 1963.
- 6) Herring, C.; Nichols, M.H.; "Thermionic Emission", Reviews of Modern Physics, Vol 21, n.2. 185-270, 1949.
- 7) Harris, L.P.; "Arc Cathode Phenomena", Vacuum Arcs - Theory and Application J.M. Lafferty, editor. John Willey & Sons, 1980.
- 8) Mitterauer, J.; "Cathode erosion in highly transient cold cathode arc spots", Proc. 12<sup>th</sup> Int. Conf. Phen. Ioniz. Gas., 248, 1975.
- 9) Kislink, P.P.; Bell Lab. Rec. 34, 218, 1956.
- 10) Emtage, P.R.; "Interac. of the cathode spot with low pressures of ambient gas", J. Appl. Phys., vol 46, n.9, 3809-3814, 1975.
- 11) Drouet, M.G.; Gruber, S.; "Dynamic measurements of cathodic emission in a moving arc", IEEE Trans. Pow. App. Sys., Vol PAS-95, n.1, 105-112, 1976.
- 12) Daalder, J.E.; IEEE Trans. Pow. App. Sys., Vol PAS-93, 1747, 1974.
- 13) Djakov, B.E.; Holmes, R.; J. Phys. D: Appl. Phys., Vol 4, 504, 1971.
- 14) Emtage, P.R.; Gorman, J.G.; Heberlain, J.V.R.; Holmes, F.A.; Kimblin, C.W.; Slade, P.G.; Voxhall, R.E.; "The interaction of vacuum arcs with transverse magnetic field", Proc 13<sup>th</sup> Int. Conf. Ion. Gases, 673-674, 1977.

- 15) Fang, D.Y.; "On the lateral spread of moving cathode spot of vacuum arcs in a transverse magnetic field", XVI Int. Conf. Phen. Ion. Gases, 276-277, 1983.
- 16) Juttner, B.; "Formation time and heating mechanism of arc cathode craters in vacuum", J. Phys. D: Appl. Phys., Vol 14, 1265-1275, 1981.
- 17) Drouet, M.G.; "The physics of the retrograde motion of the electric arc", IEEE Trans. Plas. Sci., Vol PS-13, n.5, 235-241, 1985.
- 18) Hantzsche, E.; "Theory of cathode spot phenomena", Physica, Vol 104C, 3-16, 1981.
- 19) Rakhovsky, V.I.; IEEE Trans. Plas. Sci., Vol PS-4, 81, 1974.
- 20) Achter, J.; Altrichter, B.; Juttner, B.; Pech, P.; Pursch, H.; Reiner, H.D.; Rohrbeck, W.; Siemoth, P.; Wolff, H.; "Influence of surface contaminations on cathode processes of vacuum discharges", Plasma Phys., Vol 17, 419-431, 1977.
- 21) Porto, D.R.; Kimblin, C.W.; Tuma, D.T.; "Experimental observations of cathode spot surface phenomena in the transition from a vacuum metal-vapor arc to a nitrogen arc", J. Appl. Phys., Vol 53, n.7, 4740-4749, 1982.
- 22) Hitchcock, A.H.; Guile, A.E.; "The erosion of copper cathodes by moving arcs at currents of 45 to 800 A", Proc. Inst. Elec. Eng., Vol 122, 763-764, 1975.
- 23) Daalder, J.E.; "Erosion and the origin of charged and neutral species in vacuum arcs", J. Phys. D: Appl. Phys., Vol 8, 1647-1659, 1975.
- 24) Harry, J.E.; "The measurement of the erosion rate at the electrodes of an arc rotated by a transverse magnetic field", J. Appl. Phys., Vol 40, n.1, 265-270, 1969.
- 25) Hantzsche, E.; Juttner, B.; Puchkarov, V.F.; Rohrbeck, W.; Wolff, H.; "Erosion of metal cathodes by arcs and breakdown in vacuum", J. Phys. D: Appl. Phys., Vol 9, 1771-1781, 1976.
- 26) Noer, R.J.; Niedermann, Ph.; Sankarraman N.; Fisher, O.; "Electron field emission from intentionally introduced particles on extended niobium surfaces", J. Appl. Phys., Vol 59, n.11, 3851-3860, 1986.
- 27) Cox, B.M.; J. Phys. D: Appl. Phys., Vol 8, 2065-2073, 1975.

- 28) Leycuras, A.; "Observation of high temperature electron injection in dense argon and mercury: application to cathode spot", *J. Appl. D: Appl. Phys.*, Vol 11, 2249-2256, 1978.
- 29) Beilis, I.I.; Kanzel, V.V.; Rakhovsky, V.I.; Proc. 6<sup>th</sup> All Union Conf. Electrical Contacts (Moscow), 1973.
- 30) Hantzsche, E.; "Thermal runaway prevention in arc spots", *IEEE Trans. Plas. Sci.*, Vol. PS-11, 115-121, 1983.
- 31) Hantzsche, E.; "Remarks on explosive emission in arc spots", Proc 12<sup>th</sup> Int. Conf. Phenomena on Ionized Gases, Vol 1, 237, 1975.
- 32) Mitterauer, J; Till, P.; "Computer simulation of the dynamics of plasma surface interactions in vacuum arc cathode spots", *IEEE Trans. Plas. Sci.*, Vol PS-15, n.5, 488-501, 1987.
- 33) Meunier, J.L.; Drouet, M.G.; "Experimental study of the effect of gas pressure on arc cathode erosion and redeposition in He, Ar, and Sf6 from vacuum to atmospheric pressure", *IEEE Trans. Pla. Sci.*, Vol PS-15, n.5, 515-519, 1987.
- 34) Fowler, R.H.; Nordheim, L.W.; Proc. Roy. Soc. Lond. Ser A 119, 173, 1928.
- 35) Murphy, E.L.; Good, R.H.; "Thermionic emission, field emission and the transition region", *Physical Review*, Vol 102, n.6, 1464-1472, 1956.
- 36) Hantzsche, E.; "The thermofield emission of electrons in arc discharges", *Beitr. Plasma Phys.*, Vol 22, 325-346, 1982.
- 37) Nurnberg, A.W.; Fang, D.Y.; Bauder, V.; Behrisch, R.; Brossa, F.; "Temperature dependence of the erosion of Al and TiC by vacuum arcs in a magnetic field", *J. Nuclear Materials*, Vol 103&104, 305-308, 1981.
- 38) Cobine, J.D.; "Vacuum Arc Anode Phenomena", *Vacuum Arcs - Theory and Applications*, J.M. Lafferty, editor, John Willey & Sons, 1980.
- 39) Kittel, C.; *Introduction to Solid State Physics*, John Wiley & Sons, 5 ed. 1976.

**VII. HEAT TRANSFER ANALYSIS**

## VII. HEAT TRANSFER ANALYSIS

### 1) INTRODUCTION

*Watson has been waiting in front of the bakery for 15 minutes. He is trying to avoid thinking about the pastries on the window... He starts to wonder where Holmes was. The message that he received seemed so urgent... Holmes was in a hurry to do something important and he needed help, and Watson was pleased that Holmes had asked him to help... "Be there at 9 pm" was written in the note... And this is the place, 42 Elm St., in front of Ashcrof's bakery. And now it is already half past nine, but where is Holmes?? Watson suddenly sees a man carrying a big, black box. Although the man was almost 100 meters away, Watson knew that the man was Holmes...*

*- Holmes, is that you? Watson shouts as he walks in his direction.*

*- Sshhhhh, Watson, don't shout! Come here and help me! Holmes stops and puts the heavy box on the floor...*

*- For God's sake, Holmes, this is the box that was in your office, a week ago!*

*- Very good, Watson, very good...*

*- But Holmes, what are you doing with it in the middle of the night, in the middle of the city??*

*- We are taking it to a mathematician, Watson!*

*- We?*

*- Oh, yes, I forgot. I was wondering, Watson, if you could help me carrying the box...*

*- Of course I'll help you, Holmes, but why didn't you call for a cab?*

*- Well, this a long story, Watson, but Norbert was afraid someone would know about the box, and try to steal it...*

*- But Holmes, what is in the box anyway? And who is Norbert?*

*- Not in the box, but what is the box! I will tell you on the way... Now, please, lift this side and I will take care of the other side...*

*And saying this, Holmes lifts one side and few seconds later, a curious Watson is helping him to carry the box. After five minutes walking with the box in the most complete silence, Watson whispers:*

*- Holmes, aren't you going to tell me what is all this about??*

*- Oh, I'm sorry Watson... I was thinking about something else and... But anyway... this heavy box we are carrying is going to solve the erosion problem!!*

*- But how, Holmes?*

*- The box, my dear friend, is the most incredible machine ever created by mankind... It is a computer!!*

*- A what Holmes?*

- *A computer. An abbreviation for a machine which can solve arithmetic operations extremely fast!!*

- *But how is it going to help us in the cathode problem? Why are we taking it to this Norbert?*

- *Well, Norbert is the mathematician who had the concept of the machine; someone that I know built it and we are taking it to Norbert, since he is the only man who can operate it... About the cathode problem, well I had few ideas in the past days and I think we can simulate the theory with equations, and the computer will solve these equations... But don't worry, Watson, it sounds more difficult than in reality it is... Oh, well, here we are. Let's put the box on the floor and see if he is in...*

*Watson with great relief puts the box on the floor and see Holmes going towards a house 20 meters away. A minute later, Holmes comes back and Watson notices a great excitement on his friend's eyes...*

- *Let's take the box inside the house, Watson, Albert is waiting...*

*Two minutes later, Watson sees himself in the middle of an office even more messy than Holmes'... And in the middle of the room, an young fellow stands smiling...*

- *Dr. Watson, it is a pleasure to meet you. My name is Norbert Wiener...*

And returning to this thesis...

#### A) Chapter Guideline

This Chapter contains the heat transfer analysis for the electrode erosion studies. Firstly a brief description of the heat sources is given; then an ideal heat transfer study for electrode erosion is described. Two different approaches were used to solve a simplified version of the ideal heat transfer model: the first examines the macroscopic view of the arc attachment while the second examines the microscopic view, i.e., the cathode spots. The two methods are described in some detail and results from the simulations are given. The most important conclusions are summarized at the end of the Chapter. It should be emphasized here that no extensive parametric study was conducted in this part of the work; this Chapter is rather an examination, using heat transfer analysis of some of the ideas of erosion phenomena suggested in the past Chapters.

## B) Heat Source and Losses

It was previously suggested that the erosion of the cathode is due to the volatilization of the electrode surface caused by high temperature. The electric arc is the source of energy that produces the high temperature in the region close to the surface. The arc generates heat directly or indirectly in four different ways: radiation, convection (from the plasma), Joule heating and ion bombardment. The radiation and convection terms affect a large area; although they can account for a large amount of energy deposited on the cathode they are too diffuse to cause erosion of the electrode and can in general be neglected for erosion studies (Pock (1), Hantzsche (2), Miterrauer and Till (3)). The Joule heating and ion bombardment are therefore the main heat sources for the erosion of the electrodes; they are related to the cathode spot and a short description of each one follows.

### a) Joule heating

The flow of electrons in a metal generates heat. This is known as Joule or resistive heating and can be expressed by:

$$Q_j = j_e^2 \eta \quad 7.1$$

where  $Q_j$  = Joule heating

$j_e$  = electron current density

$\eta$  = electrical resistivity of the metal

Joule heating can become an important source of heat if the current is constricted in a small volume as it is the case for cathode spot, since the local current density is very high in this case. It has been suggested (Daalder (4)) that the Joule heating

is the main heat source for electrode erosion. It is emphasized here that the value of the current density at the cathode spot is not, in general, easy to estimate (see Current Density Chapter) and that the electrical resistivity of the material changes with temperature and with the state of the material (solid or liquid). Therefore the computation of the Joule heating term can be very difficult and the values obtained questionable.

b) Ion bombardment

Positive ions are accelerated towards the cathode and eventually they transfer their kinetic energy to the cathode when they hit its surface; this produces heat and represents the ion bombardment heat source.

A "sheath" is formed above the surface of the cathode due to the presence of positive ions, creating a high voltage drop region known as the space charge zone; this voltage drop, the cathode fall, is responsible for the acceleration of the ions towards the cathode. The space charge region is characterized by the Mackeown (5) and Langmuir (3) equations, for the electric field at the surface and the thickness of the space charge region respectively. The energy transferred by the ions into the cathode can be estimated by:

$$Q_i = j_+ (U_c + E_i - \varphi) \quad 7.2$$

where  $Q_i$  = ion bombardment heating

$j_+$  = positive ion current density

$U_c$  = cathode fall voltage

$E_i$  = ionization potential

$\varphi$  = work function

The ion bombardment term is a surface heat source (in comparison the Joule heating term is a volume heat source). Juttner (6) and Hantzsche (2) estimated that this term is the dominant heat source for the erosion of the electrodes. The calculation of the ion bombardment heat term contains uncertainties in the cathode fall value as well as in the accommodation coefficient of the ions on the surface and in the ionic current density. As with the Joule heating term, predictions of the value of the ion impact heating are questionable.

c) Heat losses

The cathode loses heat by radiation (surface of the electrode), convection (gas), conduction (through the metal) and evaporation of electrode material. The most important term here by far is the cooling by conduction through the metal (Daalder (4)). The erosion of the electrode is indeed caused by the inability to dissipate the localized heating caused by a short and intense heat source (the cathode spot).

## 2. IDEAL HEAT TRANSFER STUDY

A conceptual model for the erosion of the cathode was presented in Chapter VI. The model comprises the arc attachment, the cathode spot, the current density, the residence time of the arc attachment and cathode spot splitting. To simulate this erosion model the heat transfer at the cathode should be modeled as outlined below:

- 1) Heat transfer (including phase changes) should be modeled in a three dimensional cylindrical geometry to simulate a plasma with cylindrical electrodes.
- 2) The heat source is the arc attachment made up of individual cathode spots.

- 3) Stochastic creation of cathode spots of known size and lifetime should be simulated.
- 4) The spatial distribution of cathode spots according to the effects of magnetic field and contamination should be simulated.
- 5) The effect of the macroscopic arc attachment size, velocity and residence time on the cathode should be simulated.
- 6) The characteristics of the heat sources (Joule heating and ion bombardment) should be known.

This ideal study would be extremely difficult to carry out since there is great uncertainty in all of the following:

- 1) Quantity and distribution of heat generated by Joule heating and ion bombardment.
- 2) Dimensions of both the arc attachment (macroscopic) and the cathode spots (microscopic).
- 3) Number and distribution of cathode spots in time and space.
- 4) Cathode spot lifetime.
- 5) Process of spot creation.
- 6) Pressure above the cathode spot (for evaporation computations).

In addition to the above uncertainties, there are some intrinsic mathematical difficulties due to the extremely short time scale of cathode spots and to the moving boundary conditions (Stefan problem) because of the melting and volatilization of material. Therefore many simplifications had to be made in the modelling of the heat transfer involved in the erosion process. Two approaches were used and are described in the next pages. The first one (macroscopic model) simulates the cylindrical geometry and the moving heat source (arc moving at a certain velocity);

the second approach (microscopic model) simulates the cathode spot(s) fixed on the cathode with finite lifetime(s).

### 3. THREE DIMENSIONAL CYLINDRICAL GEOMETRY

The approach chosen here consists of simulating the concentric cylindrical geometry of the electrodes used in the experimental part of this work and a moving heat source (arc attachment moving on the cathode surface). The heat transfer problem was reduced to solving the heat conduction equation in cylindrical coordinates. The geometry used for the simulation is shown in Figure 7.1. The objective of this study was to predict the temperature profile in the cathode for different arc velocities, arc attachment diameters, power input to the cathode and cathode wall thicknesses. Therefore a moving heat source on the surface of the cylindrical cathode could be simulated. The model was developed by Mostaghimi and Munz (7); the following simplifying assumptions were made:

- a) All heat input to the cathode was grouped into a surface source.
- b) No melting or volatilization occurs at the cathode.
- c) The heat losses were due to transient conduction through the metal and convection to the gas above the cathode.
- d) The heat input is assumed to be uniformly distributed over the arc attachment, i.e., no individual cathode spots were considered.
- e) The arc attachment moves over the cathode circumference at a constant velocity.
- f) Thermal properties are assumed constant over the whole range of temperature.

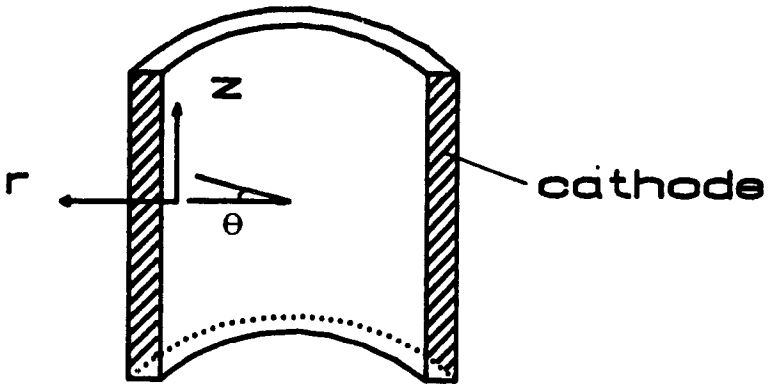


Figure 7.1 - Geometry for the 3 D simulations

The resulting heat conduction equation for the cathode could then be expressed in fixed cylindrical coordinates. This coordinate system was then transformed into one that travels tangentially with the arc. The resulting equation to be solved is time independent, since the temperature field stays constant for an observer travelling with the arc. The derivation of this equation, following the original model, is described in the Appendix A. The mathematical model is described by the following equation:

$$\frac{1}{r} \frac{\partial}{\partial r} (r \frac{\partial \Phi}{\partial r}) + \frac{1}{r^2} \frac{\partial^2 \Phi}{\partial \theta^2} + \frac{\partial^2 \Phi}{\partial z^2} + a \frac{\partial \Phi}{\partial \theta} = 0 \quad 7.3$$

The change in coordinate system is as follows:

$$r = r'/R_i, \quad \theta = \theta' - w_r t', \quad z = z'/R_i$$

where ' indicates the fixed cylindrical coordinates

$r$  = radial coordinate

$\Phi$  = nondimensional temperature,  $\Phi = (T - T_0) k / (q R_i)$

$T$  = cathode temperature

$T_0$  = surrounding gas temperature

$k$  = thermal conductivity

$q$  = heat flux input ( $W/m^2$ )

$R_i$  = cathode internal radius

$\theta$  = theta coordinate

$z$  = z coordinate

$a$  =  $Vel R_i k / (\rho C_p)$

$Vel$  = arc velocity

$\rho$  = density

$C_p$  = thermal capacity

$b$  =  $h R_i / k$

$h$  = heat transfer coefficient on the inside cathode surface

$\omega_r$  = radial frequency,  $\text{Vel} / R_i$

with the following boundary conditions:

$$\begin{array}{ll} \partial\Phi/\partial r = 1 & r=1, \theta=0, z=0 \\ \partial\Phi/\partial r = b\Phi & r=1, \theta \neq 0, z \\ \partial\Phi/\partial z = 0 & z = \pm L/R_i \text{ (L is the cathode length in z direction)} \\ \Phi = \Phi_0 & r = R_0/R_i \\ \Phi \Big|_{\theta} = \Phi \Big|_{\theta+2\pi} & r, z \\ \partial\Phi/\partial\theta \Big|_{\theta} = \partial\Phi/\partial\theta \Big|_{\theta+2\pi} & r, z \end{array}$$

To solve this equation a control volume approach was chosen and the finite difference equations were solved iteratively by the use of a Tri-Diagonal Matrix Algorithm. A FORTRAN program was originally written by Mostaghimi and Munz (7) and small modifications to this program were made in the present study (adapting the program to the main frame system and changes in the grid system used). The simulations were made on the McGill University main frame system. There is no analytical solution for this problem in this geometry; solutions for selective problems of moving heat sources can be found in Carslaw and Jaeger (8).

#### 4) PARAMETERS FOR THE 3D APPROACH

The input parameters for the simulations using the three dimension cylindrical geometry approach were: arc velocity, input power to the cathode, arc attachment diameter, cathode wall thickness. Also the copper thermal conductivity, inside gas temperature (for convective cooling), outer cathode wall temperature, heat transfer coefficient (for the gas) and cathode dimensions must be specified. The values for

these physical parameters were as follows for all the simulations:

Thermal conductivity	- 385 W/mK (assumed constant)
Thermal diffusivity	- 0.0001 m <sup>2</sup> /s
Gas temperature	- 293 K
Outside cathode wall	- 293 K
Heat transfer coefficient	- 38.5 W/m <sup>2</sup> K
Cathode internal radius	- 1.65 cm
Cathode length in z direction	- 1 cm

A non-uniform grid density was used; the grid spacing is very dense in the vicinity of the arc attachment and decreases with increasing distance from the arc attachment. A short description of the grid system used is given in the Appendix B. The grid density was tested and modified extensively until the results were grid independent.

## 5) RESULTS FOR THE 3D APPROACH

### A) Comparison with the Literature

The results from this simulation were first compared with a study conducted by Baliga et al (9). They considered the problem of heat transfer to the anode in a semi infinite disk of a given thickness. A constant heat flux over the disk simulates the arc; cylindrical coordinates were used in their study. Their results can be compared with the ones obtained in this simulation when the arc velocity is zero. Copper was used for both studies. Table 7.1 compares the heat flux required to produce melting in each of the simulations.

TABLE 7.1

Comparison Between Results from this Simulation and the Literature

Reference	Thermal conductivity (W/mK)	Input heat flux required for melting ( $\times 10^8$ W/m <sup>2</sup> )	Radius of arc attach. (mm)	Wall thickness (mm)
Baliga	417.3 - 64.4 $\psi$	1.75	3.3	2.5
This work	385	1.80	3.3	2.5

$$\psi = T/1000$$

It can be seen that for similar geometries the results compare well, considering that small differences in the required heat flux can be due to the different thermal conductivity values used in the two works (constant in this work and temperature dependent in the other work). No temperature profile is given in Baliga et al's work to compare with the one obtained in this study. It can be concluded from this analysis that no systematic error was made in this study. The results still depend on assumptions which must be further discussed.

### B) Heat Flux Input

Appropriate values for the heat flux to the cathode due to Joule heating and ion bombardment had to be estimated for the simulations. It was decided to use two values of power input as extreme cases, 100 and 1 000 W. These values were based on the calculations of Prock (1), who computed theoretical values for net power input to the cathodes. For molybdenum cathodes the total power input was approximately

700 W for 100 A arcs (without considering radiation). Daalder (4,10) also obtained experimental results indicating that up to 30 % of the total arc power is lost by conduction in the cathode. In the present study much of the energy flowing to the cathode comes from radiation (see the values of power to the cathode in Table 6.2). This radiation energy causes no erosion because it is dissipated over a large area of the cathode. Therefore for the simulation studies the amount of power that causes erosion (localized heat) is necessarily smaller than the total power going to the cathode. For short arcs (for example, Ar+0.3%CO at low magnetic fields) the radiation effect was minimized; there 30 % of the total power going to the arc would represent approximately 800 W (see Table 6.2). Therefore the range 100 to 1 000 W covers the probable amount of energy going to the cathode due to the Joule heating and ion bombardment.

### C) Arc Velocity - Results and Discussion

Cathode temperature profiles were obtained for different arc velocities, while keeping all other parameters constant at: 1 000 W for the input power, 1 mm for the arc attachment diameter (this value is based on the results obtained with the current density probe, Chapter V) and 2.5 mm for the thickness of the cathode wall (this is the value for the cathodes used in the experimental work).

The maximum temperature reached (center of the attachment at the surface of the cathode) for the different arc velocities is shown in Figure 7.2. Two dimensional plots of the temperature profile are given for two arc velocities, 0 and 2 m/s, in Figure 7.3a and 7.3b respectively. The contour curves shown in the two dimensional plots were not very smooth due to the graphics routine used.

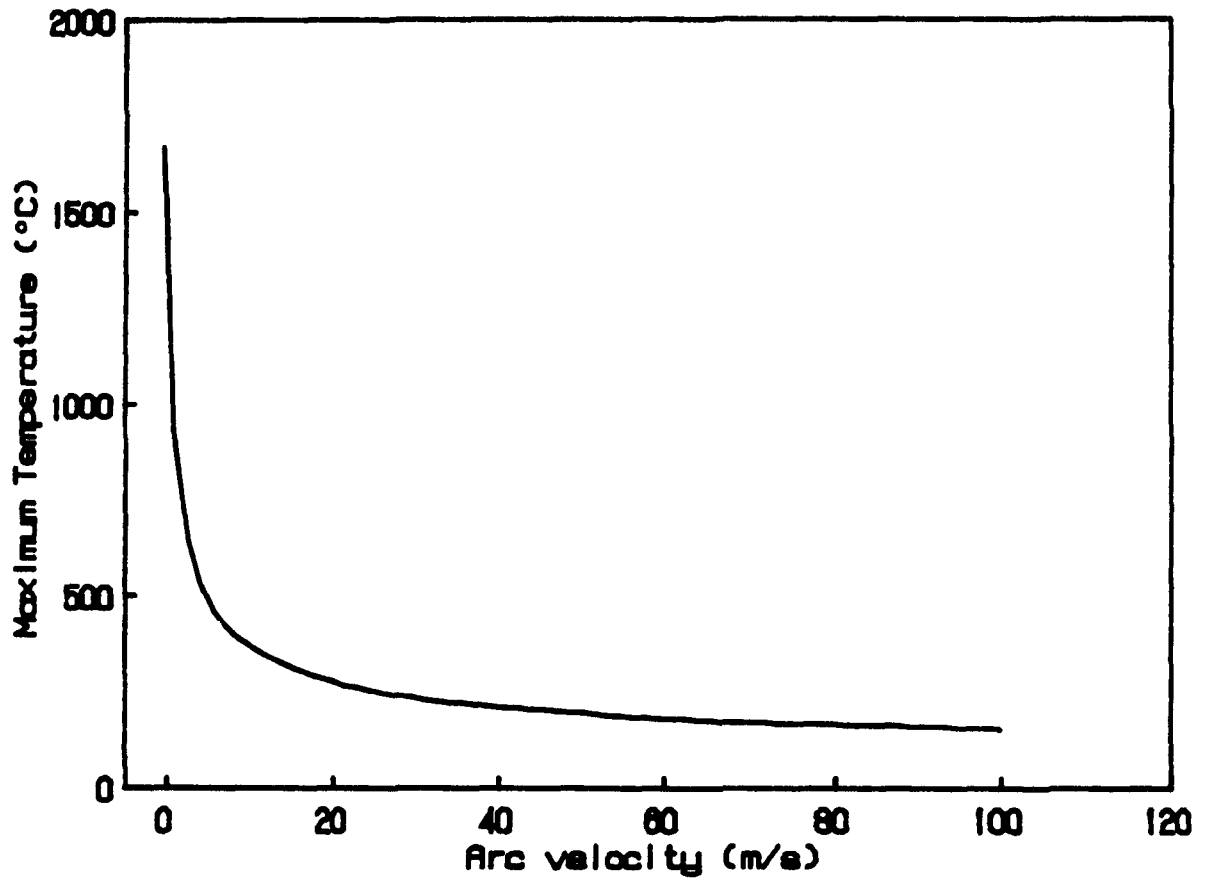


Figure 7.2 - Maximum temperature of the cathode (center of the arc attachment)  
Power = 1 000 W; Arc attach. diameter = 1 mm; Wall thickness = 2.5 mm

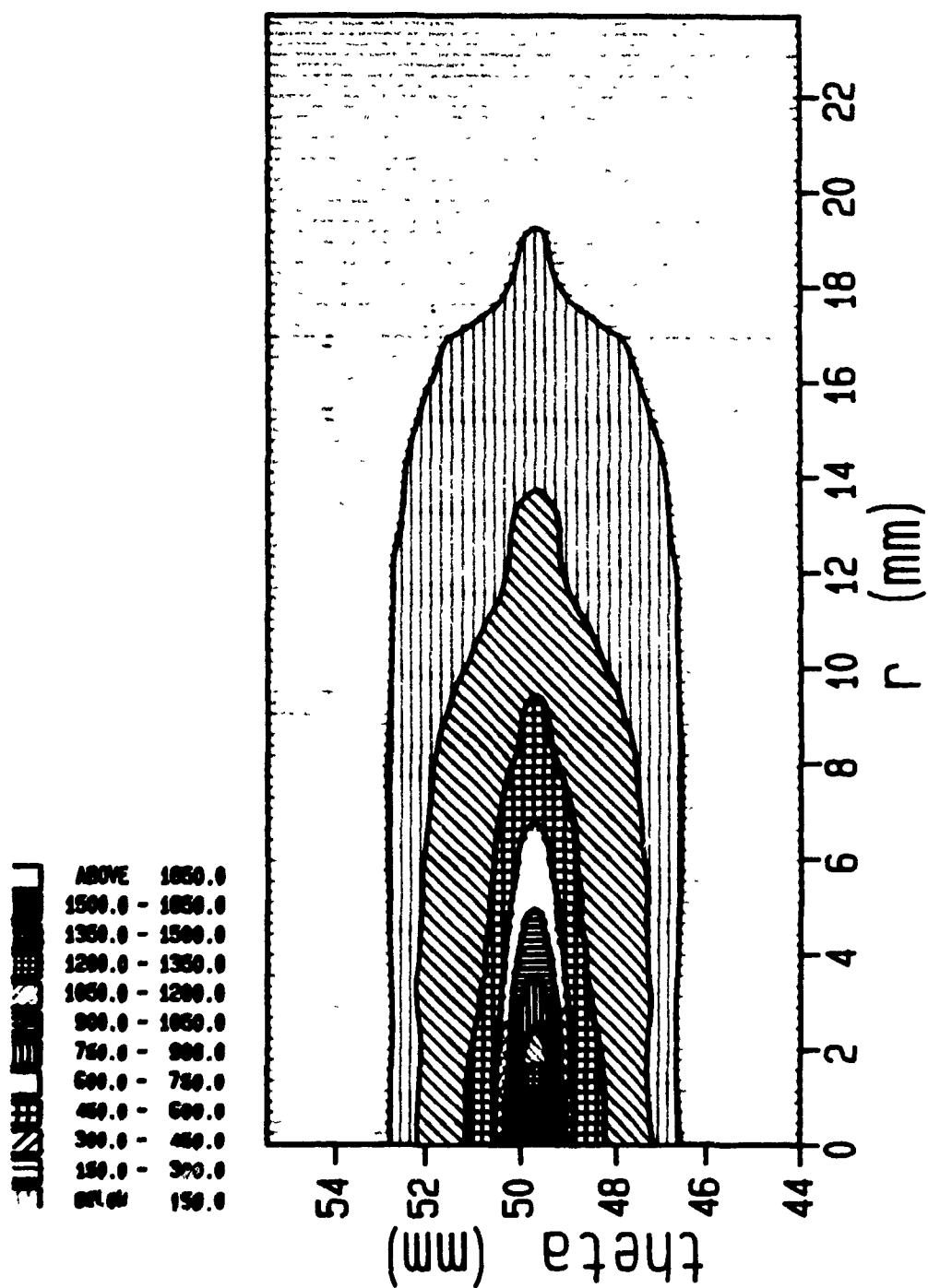


Figure 7.3 - Two dimensional cathode temperature

Power = 1 000 W; Arc attach. diameter = 1 mm

a) Arc velocity = 0 m/s

In this figure the theta coordinate (angular coordinate) is plotted as distance from the arc attachment center in mm

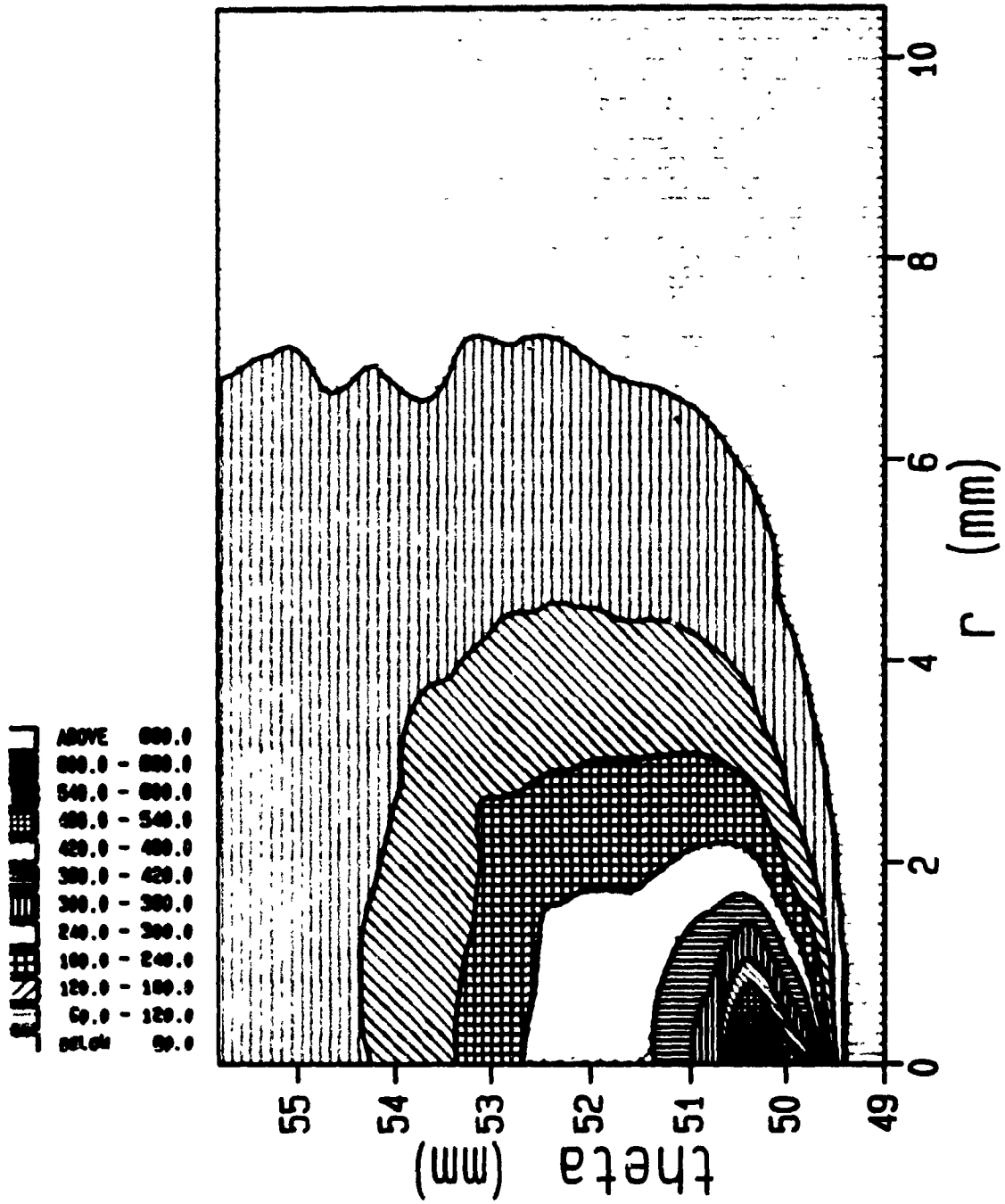


Figure 7.3 - Two dimensional cathode temperature

b) Arc velocity = 2 m/s

It can be seen from Figure 7.2 that the maximum temperature of the surface shows an exponential decrease with arc velocity. The cathode erosion rate is a function of the cathode temperature, since the erosion is caused by the volatilization of material. The temperature results suggest that the cathode erosion rate should initially be a strong function of the arc velocity but that at high velocities it should change little with arc velocity. This was observed experimentally in this work (see for example Figure 6.1, erosion rate vs arc velocity for pure nitrogen arcs; Szente et al (12)).

However it can also be seen from Figure 7.2 that the temperature was not high enough to have material volatilized, i.e., no erosion of the cathode would have occurred even for stationary arcs (0 m/s).

The low temperatures found in these simulations indicate that the parameters used did not represent the erosion phenomena. The power deposited at the cathode due to Joule heating and ion bombardment is likely to be less than the 1 000 W used in these simulations; therefore the incorrect parameter is probably the diameter of the arc attachment, i.e., the power density. It was expected that 1 mm represents an upper limit for the arc attachment; but as also explained in Chapter VI, the arc attachment is probably made of individual contributions, the cathode spots. It is possible that the overall arc attachment diameter is of the order of 1 mm, with much smaller multiple cathode spots. The power density would then be much higher for the cathode spots and local temperatures could exceed the boiling point for copper. This is further discussed in the next section.

Figure 7.3 shows that the temperature decreases dramatically from the surface to inside the cathode. The high temperature is located in the first 10  $\mu\text{m}$  from the surface. An indirectly confirmation of this high temperature at the first layers of the cathode was suggested in Chapter IV, when the nitrogen contamination profiles were discussed.

Another point to be noted here is the asymmetry of the temperature field in the  $\theta$  direction. The temperature profile is symmetrical for stationary arcs, but become asymmetrical for arc velocities up to 10 m/s with higher temperatures at regions upstream of the cathode for an observer travelling with the arc. Beyond 10 m/s the temperature field becomes increasingly symmetrical for higher arc velocities. This can be seen in Figure 7.3a and b for 0 and 2 m/s arc velocity respectively. The asymmetry of the temperature field is found for moving heat sources over a slab (Carslaw and Jaeger (8) page 270). For high arc velocities the temperature field becomes almost symmetrical again because for increasing values of  $a$  (see equation 7.3), the term  $a \frac{\partial \phi}{\partial \theta}$  becomes dominant and therefore:

$$\nabla^2 \phi + a \frac{\partial \phi}{\partial \theta} = 0 \quad 7.4$$

if  $a \frac{\partial \phi}{\partial \theta} \gg \nabla^2 \phi$

$$\therefore a \frac{\partial \phi}{\partial \theta} = 0 \quad 7.5$$

$\frac{\partial \phi}{\partial \theta} = 0$ , i.e.,  $\phi$  becomes symmetrical in  $\theta$

The same conclusions regarding the effect of arc velocity on the cathode temperature field may be reached as the power input is decreased from 1 000 W to 100 W. The difference is that for the lower power input, lower temperatures are obtained. The maximum temperatures are approximately 10 times smaller for 100 W than for 1 000 W. As an illustration, the maximum temperature obtained for two different arc

velocities (2 and 10 m/s) and three different power input (1 000, 500 and 100 W) are shown in Figure 7.4.

#### D) Arc Attachment Diameter - Results and Discussion

Temperature profiles were obtained for different arc attachment diameters keeping the other parameters constant. The maximum temperatures obtained using 1 000 W as the power input, 2 m/s as the arc velocity, 2.5 mm cathode wall thickness and arc attachment diameter varying from 0.01 to 2 mm are shown in Figure 7.5. The two dimension plot of one condition (0.1 mm arc attachment diameter) is shown as an illustration in Figure 7.6.

It can be seen in Figure 7.5 that the maximum surface temperature reaches extremely high values. These temperature values have no physical meaning, they are shown here just to illustrate the changes of temperature with arc diameter (the high temperatures can be found if ionic particles are considered, i.e, it has been observed experimentally that ions can be ejected from the surface of the cathode at velocities of the order of  $10^4$  m/s, which represents temperatures of the order of  $10^5$  K). The model predicts these high temperatures because no melting or volatilization of material is considered. The results indicate that a small error in evaluating the arc attachment diameter could result in a large variation in the cathode temperature. They also indicate that the power density and not the power is the key parameter for erosion studies.

#### E) Wall Thickness - Results and Discussion

Temperature profiles were also obtained for different cathode wall thickness maintaining the other parameters constant. The input power was kept at 1 000 W,

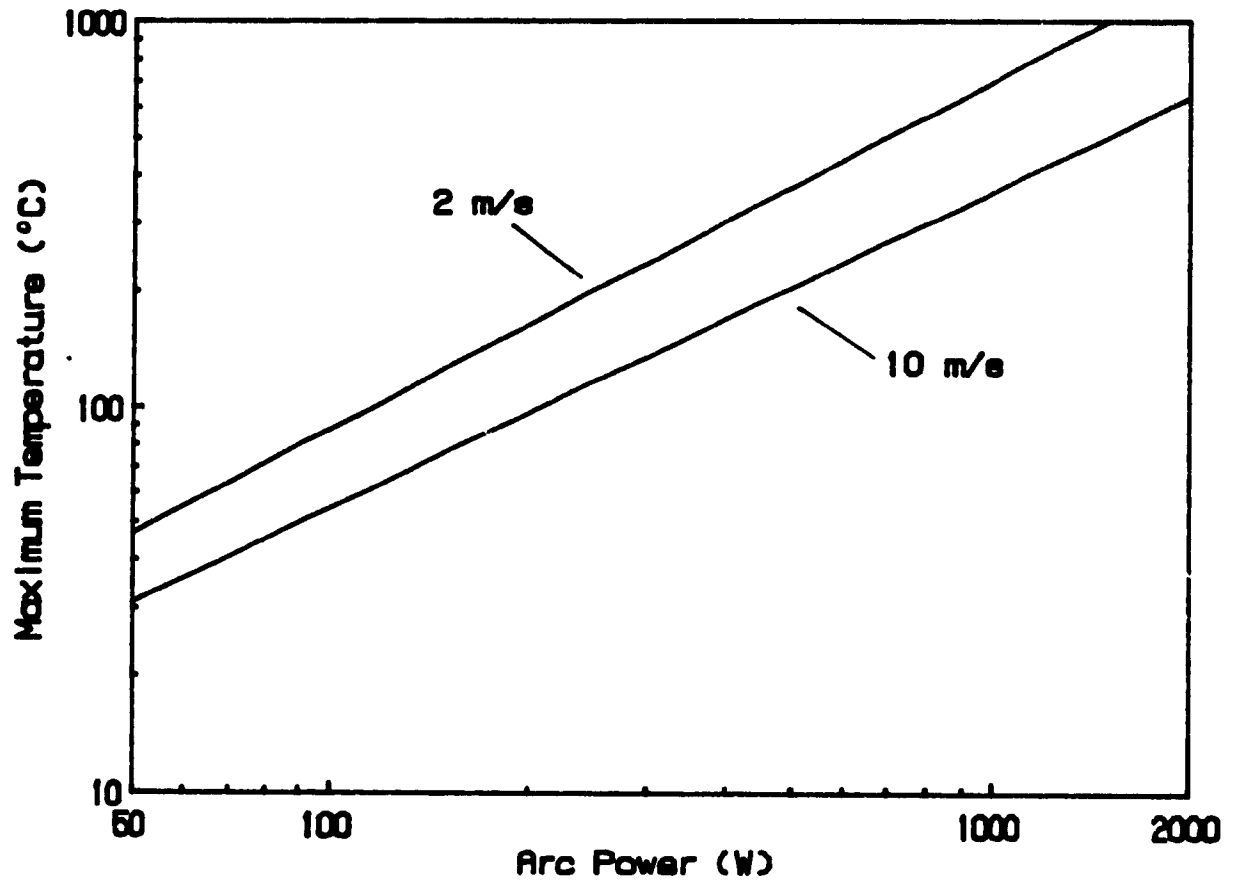


Figure 7.4 - Maximum cathode temperature for different input powers  
Arc attach. diameter = 1 mm; Wall thickness = 2.5 mm

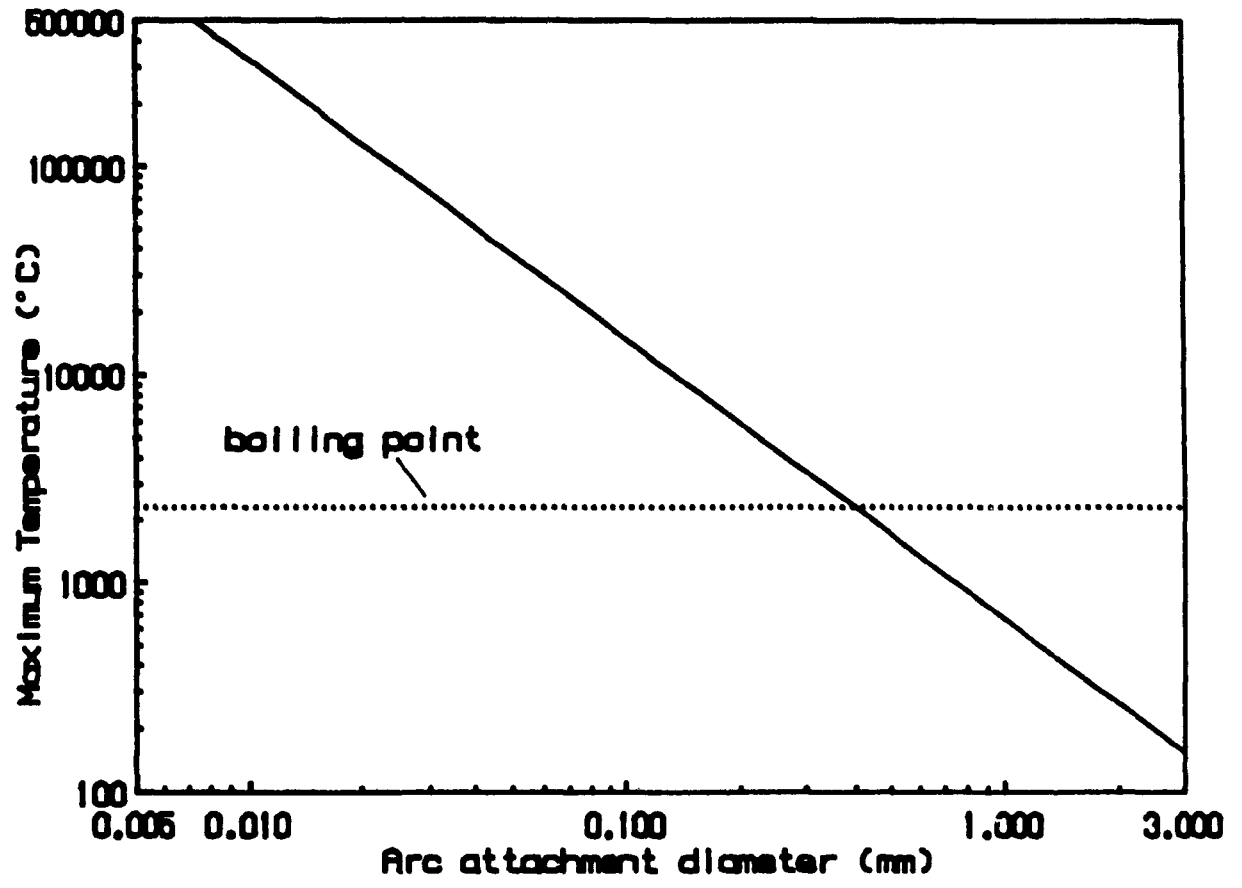


Figure 7.5 - Maximum cathode temperature for different arc attachment diameters  
Power = 1 000 W; Vel = 2 m/s; Wall thickness = 2.5 mm

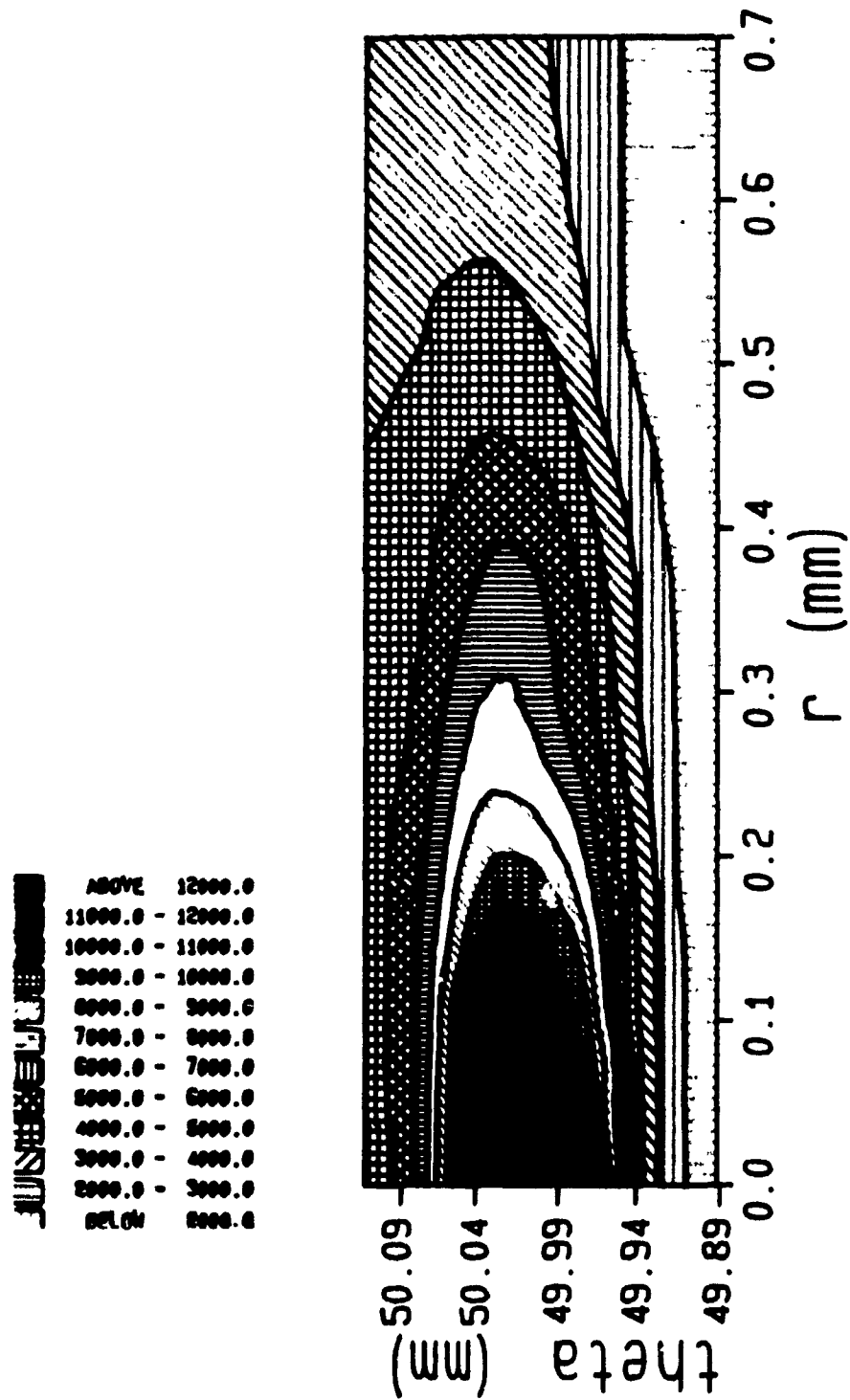


Figure 7.6 - Two dimensional cathode temperature

Power = 1 000 W; Vel = 2m/s; Arc attach. diameter = 0.1 mm

In this figure the theta coordinate is plotted as distance

from the arc attachment center in mm

the arc attachment diameter was 1 mm and the arc velocity was 2 m/s. The maximum temperature for the range 1.5 mm to 10 mm wall thickness is shown in Figure 7.7.

It can be seen from Figure 7.7 that the temperature field is insensitive to wall thickness. This indicates that no benefit is obtained if the cathode wall thickness is reduced (in an attempt for better cooling); this is because basically all the temperature gradient happens in a very thin layer at the top of the cathode (less than 100  $\mu\text{m}$ ). Wall thicknesses smaller than 1 mm would give short lifetime even at low erosion rates and would not possess the necessary structural strength.

#### F) Erosion Rate - Results and Discussion

Once the temperature profile is obtained it is possible to estimate the volume of the cathode that can in principle be removed. This is done by considering the region which has temperatures above 2 300 °C (boiling point of copper at atmospheric conditions). This region represents an upper limit for the erosion since no melting or volatilization was considered in the simulations; if the latent heat for both melting and volatilization was taken into account the temperatures would be lower. The region above 2 300 °C was estimated in the following way:

- it was assumed that the temperature field was symmetrical for  $\theta$  and  $z$ , i.e., the region that had temperatures above 2 300 °C was calculated just in one direction,  $z$ .
- the boiling region was further supposed to have a triangular shape, as shown schematically in Figure 7.8. This is because the heat source is a flat disk and not a point (in this last case the temperature field would approximate a semi circle). The triangular shape was verified examining the temperature profiles.

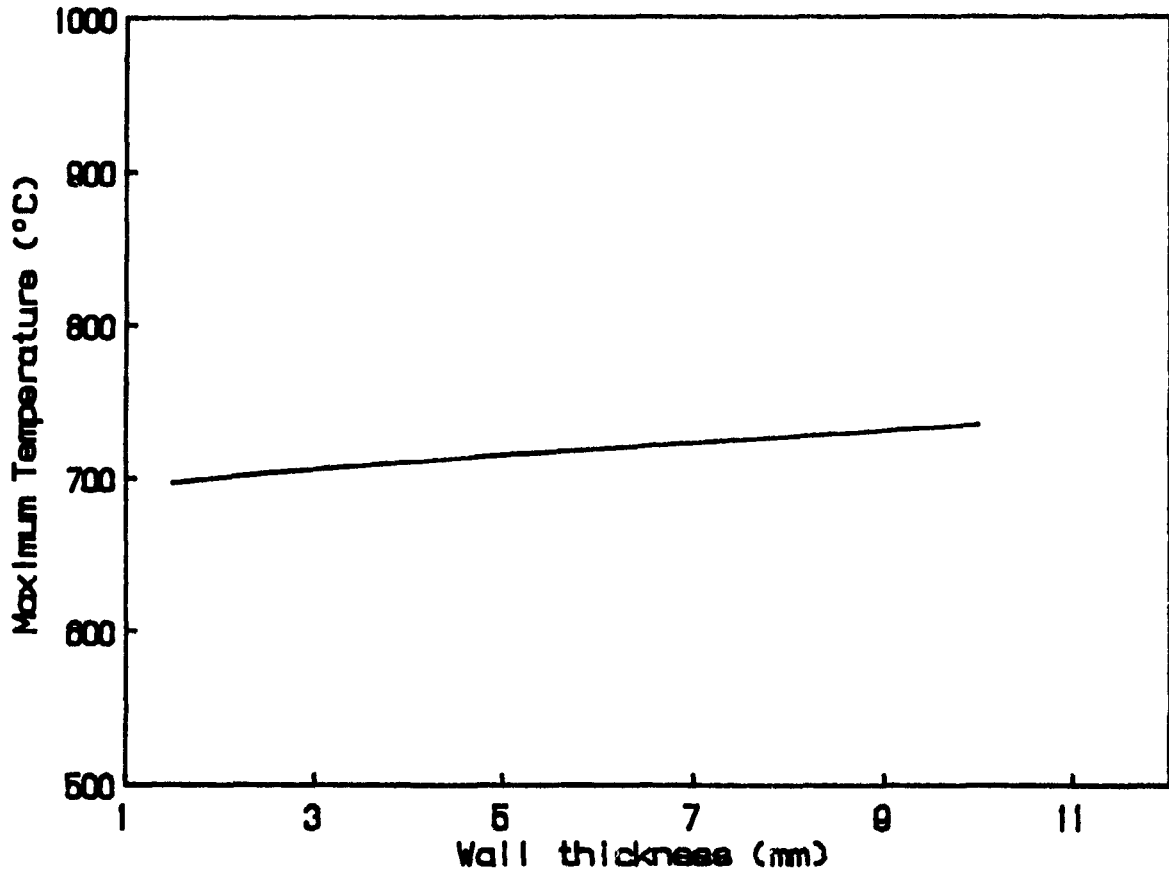


Figure 7.7 - Maximum temperature of the cathode for different wall thicknesses  
Power = 1 000 W; Vel = 2 m/s; Arc attach. diameter = 1 mm

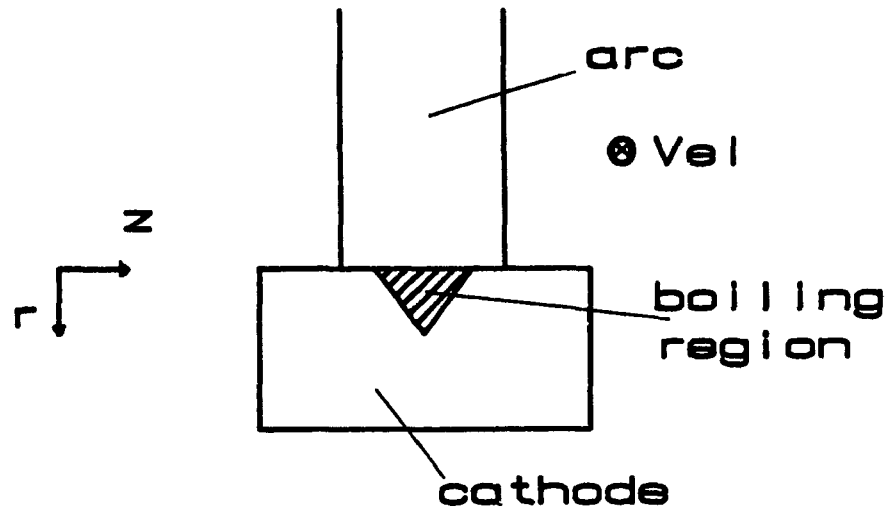


Figure 7.8 - Schematic representation of the cathode boiling region

- the area defined by this triangle was then multiplied by the arc velocity in order to determine the erosion rate (in other words, this represents the volume that would be volatilized during a unit time).

The erosion rate results for different arc attachment diameters are shown in Table 7.2 for three different power inputs, 100, 500 and 1 000 W at two different arc velocities, 2 and 10 m/s. The cathode wall thickness was 2.5 mm for all. The arc diameter values in Table 7.2 for each power input represent the maximum arc diameter for which the temperature field showed values above 2 300 °C.

As expected the erosion rate increases for smaller arc diameters and decreases with higher arc velocities. The actual values are at least two orders of magnitude higher than the experimental results found in this work. Possible explanations for this discrepancy are:

- no melting or volatilization latent heats were considered. The error involved in this simplification can be evaluated considering the values for the latent and sensible heat for copper (Perry (11)). They are:

sensible heat -	$5.44 + 0.001462 T$	cal/deg mol
heat of fusion -	3110	cal/mol
heat of volatilization -	72810	cal/mol

The latent heat for volatilization is larger than the sensible heat (considering the temperature variation from solid at room temperature to boiling point). A substantial overestimation of the volume volatilized occurs; the error can be as high as five times.

**TABLE 7.2**  
**Erosion Rates for the 3D Simulations**

Power (W)	Arc Diameter (mm)	Arc Velocity (m/s)	Erosion Rate ( $\times 10^2 \mu\text{g/C}$ )
1000	0.2	2	0.8
1000	0.2	10	0.5
1000	0.1	2	1.5
1000	0.1	10	0.8
1000	0.05	2	2.4
1000	0.05	10	1.4
1000	0.02	2	4.0
1000	0.02	10	3.8
1000	0.01	2	4.8
1000	0.01	10	4.5
500	0.1	2	0.7
500	0.1	10	0.6
500	0.05	2	1.1
500	0.05	10	0.8
500	0.02	2	2.4
500	0.02	10	2.3
500	0.01	10	2.8
100	0.01	2	0.8
100	0.01	10	0.4

- The approximation of the true temperature profile by the triangular one used is expected to give errors of not more than 100%.
- Because a variable density grid had to be used for mathematical stability and limitations on computational time, the interpolation of grid points far from the surface to locate the 2 300 °C isotherm introduces considerable error.

### G) Overall Discussion of the 3D Simulation Results - Summary

The results from the simulation of the macroscopic heat transfer problem considering the three dimensional cylindrical geometry with a moving heat source helped to understand some of the findings of the experimental work and ideas developed in the past Chapters. The effect of the arc velocity on the erosion rate discussed in Chapter VI was simulated here and the results compare qualitatively very well. The simulation results also emphasize the importance of determining the arc attachment diameter correctly, since for the same power input, the surface temperature and temperature distribution are a strong function of arc attachment diameter. The results also indicate that since the large temperature gradient happens at the very top of the surface of the cathode, no benefit is obtained if the wall thickness of the cathode is reduced from 10 to 1 mm. The model could not predict correctly the erosion rates when compared with the experimental results for reasons already exposed. The results from these simulations indicate that it is not possible to have a large amount of heat (1 000 W) going into a small arc attachment diameter ( $< 100 \mu\text{m}$ ).

## 6) TWO DIMENSIONAL GEOMETRY - FIXED HEAT SOURCE

The second approach used to simulate the erosion phenomena was to consider a two dimensional cylindrical geometry with a fixed heat source. This approach was chosen in order to study the cathode temperature profile by considering a cathode spot with a finite lifetime. The possibility of multiple cathode spots and the grouping of the spots was also possible in this study. The heat transfer problem was reduced to solving the heat conduction equation in two dimensions in cylindrical coordinates with a heat source. The heat source simulates the cathode spot. The following simplifying assumptions were made:

- a) No melting or volatilization were considered. This again could result in temperatures above the boiling point of copper.
- b) Two dimensional cylindrical coordinates (r,z) were used; the coordinates are shown schematically in Figure 7.9.
- c) A volumetric generation term, with a radius r and depth z was used to simulate the Joule heating (volumetric) and ionic bombardment. The heat source had a finite lifetime, after which the power input was zero.
- d) The only mechanism for heat losses is conduction through the cathode.

The following two dimensional cylindrical heat transfer equation had to be solved with the appropriate boundary conditions:

$$a(k r \partial T/\partial r)/\partial r + a(k r \partial T/\partial z)/\partial z + q r = \rho C_p r \partial T/\partial t \quad 7.6$$

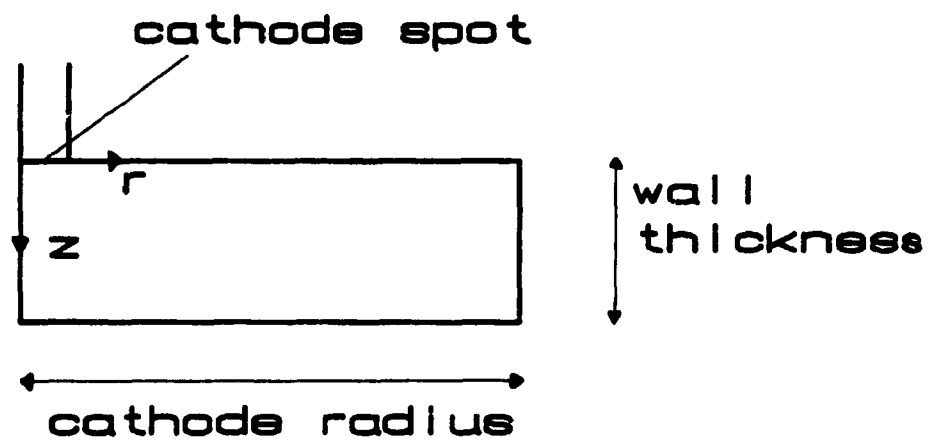


Figure 7.9 - Geometry for the 2 D simulations

Boundary conditions:

$$\begin{array}{ll} \partial T / \partial r = 0 & r = 0 \\ \partial T / \partial r = 0 & r = R \\ T = 300 \text{ K} & z = 0 \\ \partial T / \partial z = 0 & z = L_w, r > r_i \end{array}$$

where  $k$  = thermal conductivity

$\rho$  = density

$r$  = radial coordinate

$z$  =  $z$  coordinate

$T$  = temperature

$t$  = time

$q$  = heat generation term

$q = q_0$  for  $t < t_i, r < r_i, z < (L - z_i)$

$C_p$  = heat capacity

$L_w$  = cathode wall thickness

$r_i$  = cathode spot radius (heat source radius)

$z_i$  = cathode spot depth (heat source depth)

$t_i$  = cathode spot lifetime

$q_0$  = power input ( $\text{W}/\text{m}^3$ )

The two dimensional partial differential equation was solved using a commercial package available on the McGill University main frame computer. The program is called PROTRAN and uses finite element method (Galerkien method) to solve partial differential equations. The partial differential equation must be reformated to use the program. The reformated equation used in this simulation is given in the Appendix C. The grid mesh used was very dense in the vicinity of the cathode spot

and decreased as it moved away from the spot. The grid system used is described in the Appendix D.

## 7) PARAMETERS FOR THE 2D APPROACH

The input parameters for the 2D simulations were: power input, cathode spot dimensions (radius and depth), cathode spot lifetime, and the dimensions of the cathode. The following physical constant values were used for all simulations:

- copper thermal conductivity - 385 W/mK
- copper heat capacity - 385 J/kgK
- copper density - 8933 kg/m<sup>3</sup>

The program was tested with simple cases (superficial heat source with semi infinite cartesian coordinates at steady state) and the results compared extremely well with analytical solutions.

## 8) RESULTS FOR THE 2 D MODEL

### A) Comparison With The 3 D Approach And Cathode Spot Lifetime

The evolution of the cathode maximum temperature (top of the cathode surface at the center of the cathode spot) with cathode spot lifetime is shown in Figure 7.10. The total power input was 1 000 W, the cathode spot diameter 1 mm and the dimensions of the cathode were radius 5 cm and thickness 2.5 mm. The heat input was considered to be generated in the top 1 000 Å of the cathode; dividing the

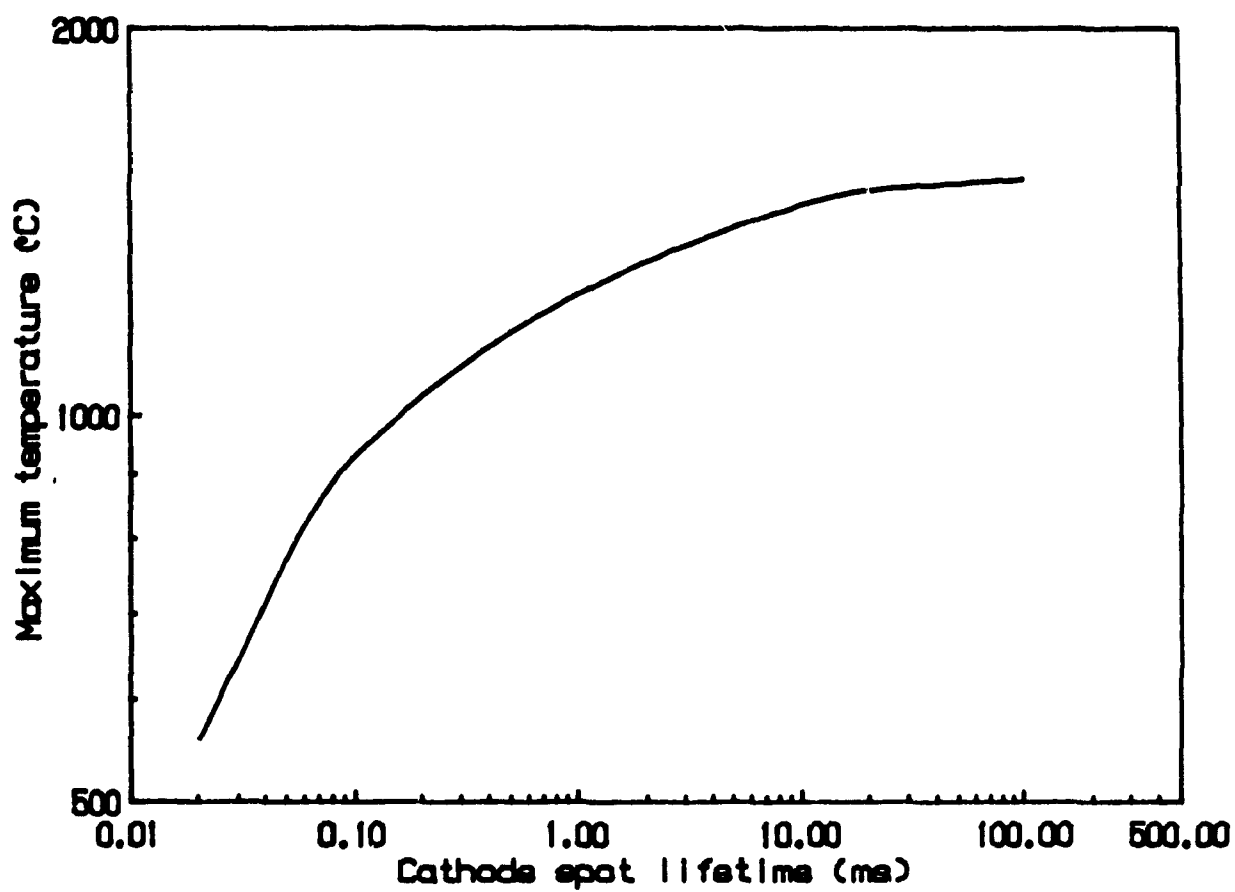


Figure 7.10 - Maximum cathode temperatures for different cathode spot lifetimes  
Power = 1 000 W; spot diameter = 1 mm; cathode radius = 5 cm

total input power of the generation term by the product of the cathode spot area and the depth, gives the power input density (volumetric heat source) needed for the simulations.

It can be seen that the increase in the temperature is extremely fast; less than 0.1 ms after the heat pulse started, the temperature already was 60 % of its "steady state" value at 100 ms (in reality the steady state value was determined by eliminating the time dependent term from equation 7.6 and solving the remaining partial differential equation). The results obtained with this simulation compare very well at the same conditions with the results obtained with the 3D simulation discussed in the last sections (maximum temperature for 3D simulation was 1 660 °C at 0 m/s arc velocity (steady state); maximum temperature for the 2D simulation was 1 550 °C (steady state)).

The power input for the remaining 2D simulations was fixed at 20 W. This value was determined as a maximum value for the input power of a single cathode spot, considering that 1 000 W was the maximum input power for the arc attachment and that 50 cathode spots could exist simultaneously (based on results from the current density probe). This value should only be considered as a rough estimation of the power input per single cathode spot and not as an accurate value. The objective of these 2D simulations was similar to the 3D simulations, i.e., to examine the influence of some parameters on the temperature field and erosion rates and not to determine absolute and final values of the temperature of the cathode and its erosion rate.

The final maximum cathode temperature is reached much faster with low power (20 W) than with high power (1 000 W). After approximately 0.001 ms the temperature at the center of the cathode spot at the cathode top surface was already at 90 % of its value at steady state.

### B) Cathode Spot Diameter - Results and Discussion

Two different cathode spot diameters were used in these simulations, 10  $\mu\text{m}$  and 1  $\mu\text{m}$ . These values were chosen based on the results from the current density probe (Chapter V) and previously published results by other researchers. The maximum cathode temperature for a 1 ms cathode spot lifetime and the two cathode spot diameters are shown in Table 7.3. A two dimensional plot of the temperature field for the 1  $\mu\text{m}$  diameter is shown in Figure 7.11.

It can be seen from these results that the power density has a most important influence on the temperature of the cathode as discussed in the 3D simulations.

**TABLE 7.3**  
Cathode Maximum Temperature for Different Cathode Spot Diameter

Power (W)	Cathode Spot Diameter ( $\mu\text{m}$ )	Cathode radius (cm)	Max. Temperature ( $^{\circ}\text{C}$ )
20	1	5	3500
20	10	5	490

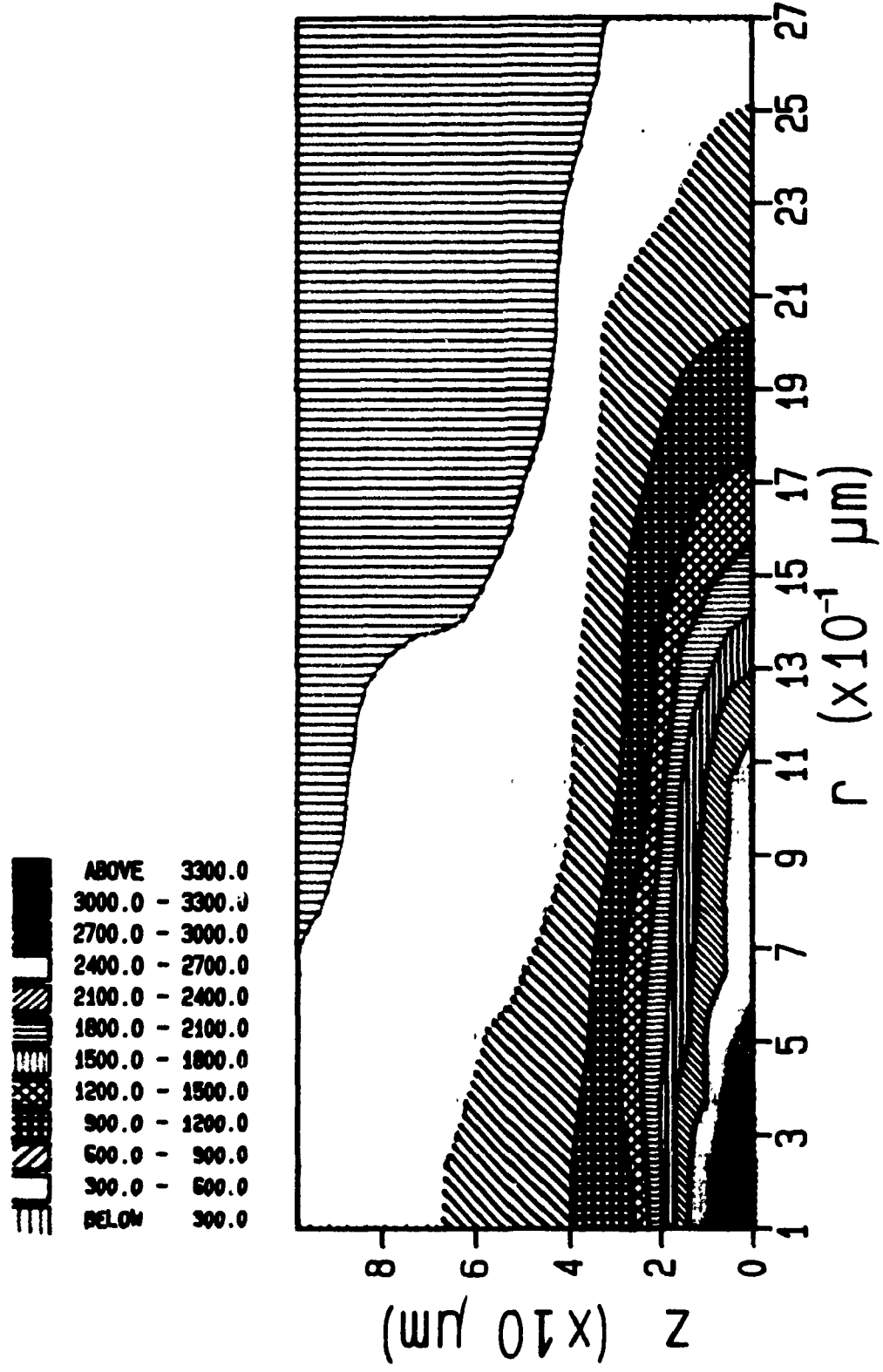


Figure 7.11 - Cathode temperature profile for the 1 μm cathode spot diameter

Power = 20 W; cathode radius = 5 cm; spot lifetime = 1 ms

### C) Multiple Spots - Results and Discussion

In order to simulate the influence of one spot temperature field on the next spot (grouping of the cathode spots as suggested in Chapters V and VI), the cathode radius was reduced. The insulating boundary of the cathode simulates the second cathode spot temperature field; a smaller cathode radius simulates cathode spots closer from each other.

Three cathode radii were used: 5 cm (representing the isolated or single cathode spot; this was the radius used in the other simulations), 10 D, and 1.5 D. The 10 D, and 1.5 D, cathode radius simulates a cathode spot separated at a distance of 10 D, and 1.5 D, from another spot (D, is the cathode spot diameter) respectively.

Two values for cathode spot diameter D, were used, 10  $\mu\text{m}$  and 1  $\mu\text{m}$ . The cathode radii used in these simulations are shown in Table 7.4. The maximum cathode temperature results for the three cathode radii, two different cathode spot diameters and different cathode spot lifetime are shown in Figure 7.12.

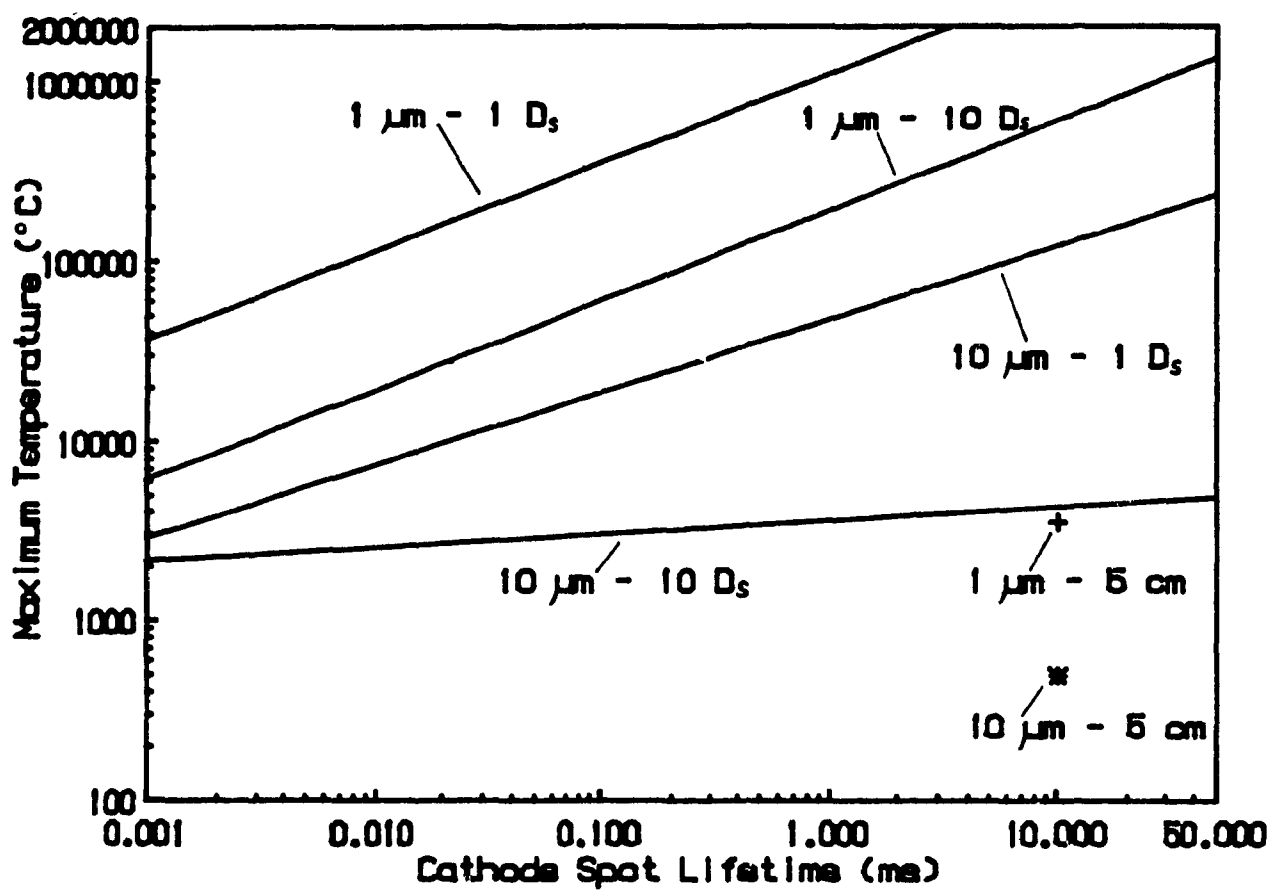


Figure 7.12 - Maximum temperature of the cathode for different cathode radii, cathode spot diameters and cathode spot lifetimes

**TABLE 7.4**  
**Cathode Radii Used to Simulate Multiple Cathode Spots**

Cathode Spot Diameter D, ( $\mu\text{m}$ )	Distance Between Spots (simulated)	Cathode Radius ( $\mu\text{m}$ )
10	isolated	50 000
1	isolated	50 000
10	10 D,	100
1	10 D,	10
10	1.5 D,	15
1	1.5 D,	1.5

The dramatic effect of the grouping of cathode spots can be seen from these results. The influence of the grouping of the cathode spots due to magnetic field and surface contamination on erosion rates was suggested in Chapter VI; those ideas are confirmed in these simulations. Therefore not only is the power density very important, but so is the geometric distribution of the spots in the arc attachment. These results also suggest that the formation of new cathode spots are much easier in the vicinities of the cathode spot (< than 100 D, away) than far apart, due to the high temperatures of these regions.

#### D) Cathode Erosion - Results and Discussion

The qualitative analysis of the temperature field for erosion estimation is divided in two parts; first, for cathode spots with a diameter of 10  $\mu\text{m}$  and then for cathode spots of 1  $\mu\text{m}$  diameter.

a) Cathode spot diameter - 10  $\mu\text{m}$

The temperature profiles indicate that there is no erosion of the cathode (temperatures below the boiling point of copper) for a cathode spot 10  $\mu\text{m}$  diameter for cathode radius greater than 100  $\mu\text{m}$  and any duration of cathode spot lifetime. For a cathode radius of 100  $\mu\text{m}$ , volatilization of material can occur for cathode spot lifetimes greater than 0.1 ms. Up to 1 ms, the first 10  $\mu\text{m}$  of material reaches the copper boiling point in the vicinities of the cathode spot, as shown in Figure 7.13. If the cathode radius is reduced to 15  $\mu\text{m}$ , erosion occurs for the first 10  $\mu\text{m}$  after cathode spot lifetimes greater than 0.001 ms. As the cathode spot lifetime is increased, the vaporization isotherm penetrates deeper.

b) Cathode spot diameter - 1  $\mu\text{m}$

When the cathode spot diameter is 1  $\mu\text{m}$ , the erosion of the cathode starts even for a large cathode radius (5 cm). For 5 cm cathodes, the erosion reaches 1 000 Å if the cathode spot lifetime is greater than 0.001 ms as can be seen in Figure 7.14. For a cathode radius of 10  $\mu\text{m}$ , temperatures higher than the copper boiling point are found up to 10 000 Å into the cathode, for cathode spot lifetimes greater than 0.001 ms. As the cathode spot lifetime is increased, the vaporization isotherm penetrates deeper still. If the cathode radius is reduced to 1.5  $\mu\text{m}$ , the electrode reaches the boiling point temperature immediately (the minimum cathode spot lifetime that could be simulated was 0.00001 ms, below which the calculations start to not converge) to depths greater than 1  $\mu\text{m}$ .

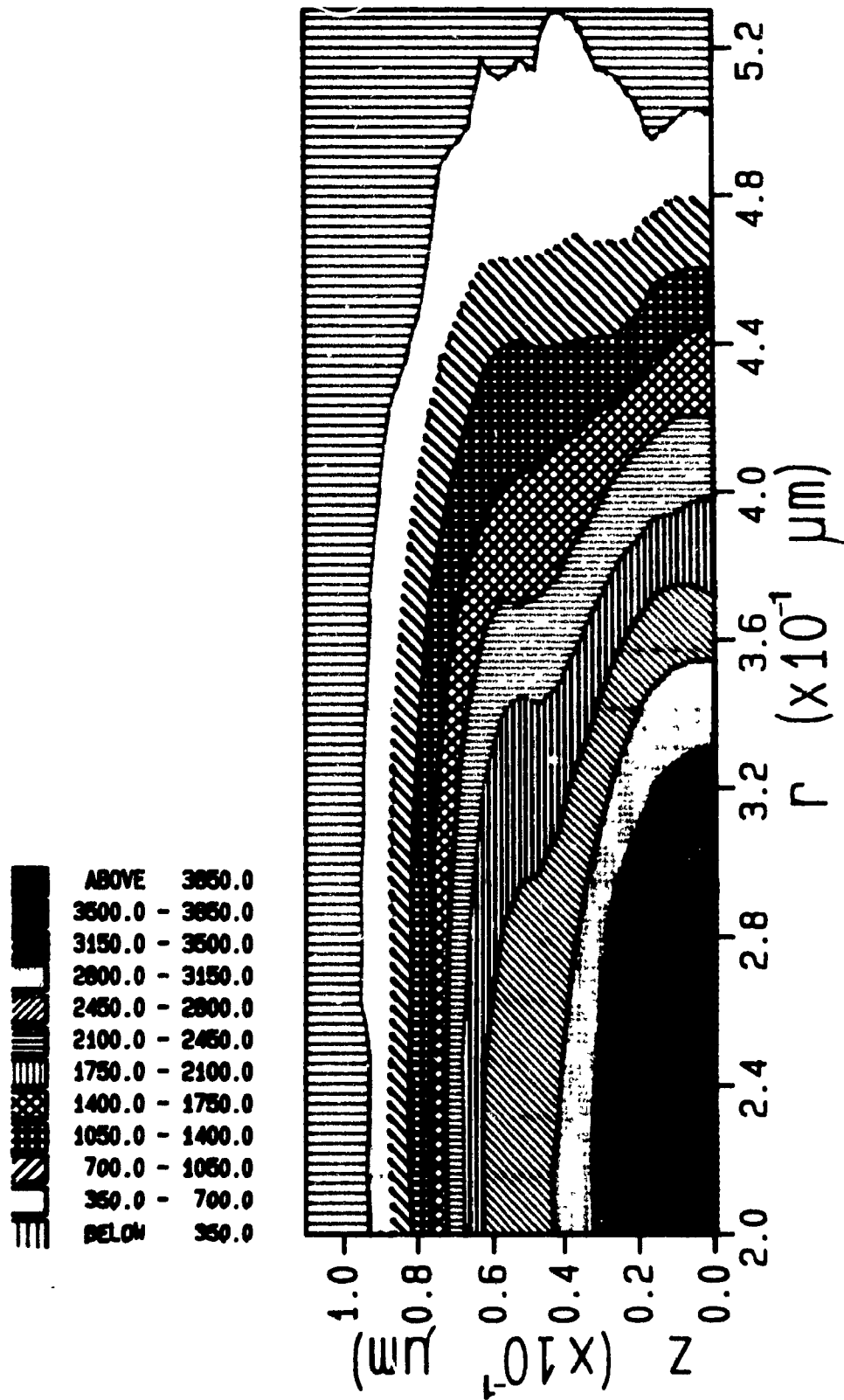


Figure 7.13 - Cathode temperature profile

Cathode radius =  $100 \mu\text{m}$ ; spot diameter =  $10 \mu\text{m}$ ; spot lifetime = 1 ms

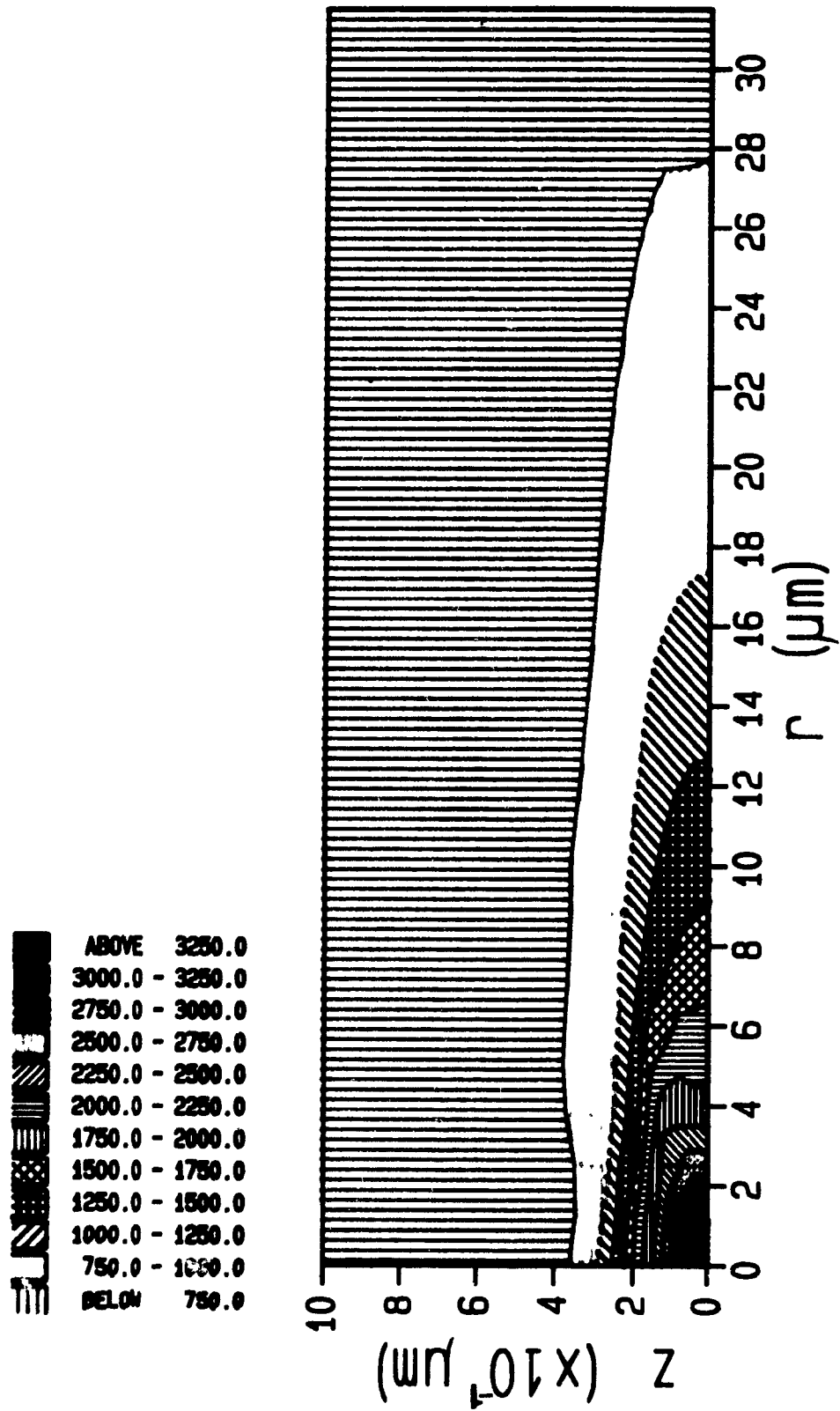


Figure 7.14 - Cathode temperature profile

Cathode radius = 5 cm; cathode spot diameter = 1 μm; spot lifetime = 0.001 ms

### E) Overall Discussion of the 2 D Simulation Results - Summary

The temperature profiles obtained with the 2 D approach compare well with the results obtained with the 3 D approach at similar conditions. One of the most important conclusions from these 2 D simulations was the effect of proximity of cathode spots; when the spots are close to each other (simulated with the reduction of the cathode radius) the temperature of the cathode increases dramatically in the vicinity of the cathode spot. This has been suggested in the Chapter VI. The effect of cathode spot diameter and cathode spot lifetime was also examined. It should be pointed here that as with the 3 D approach, the 2 D simulations were done to study the effect of certain parameters and no attempt was made to determine the correct values of power input, cathode spot lifetime or to generate the experimental erosion rates. However the results indicate that even with extremely short cathode spot lifetimes it is possible to have cathode erosion, as long as the spots are grouped together. The results from the simulations indicate also that little or no erosion should occur if the cathode spot is large at a power input of 20 W per cathode spot for spots that are widely spaced. These results corroborate the idea suggested in the last Chapter of a minimum erosion rate caused by the individual cathode spots; the erosion rate in this case should be small.

### 9) CONCLUSIONS

In this Chapter two different approaches for the simulation of the erosion phenomena were examined. These studies aimed to determine the importance of different parameters on the erosion of the cathode. Temperature profiles were obtained for different operating conditions; the most important findings are summarized below.

### A) 3 D Approach- Macroscopic Model

a) Temperature profiles for the cathode were obtained using a three dimensional cylindrical coordinates and a moving heat source simulating the cathode arrangement and the arc attachment on the cathode respectively. The temperature of the cathode surface decreases with increasing arc velocities, this being more important for arc velocities between 0 and 20 m/s. The higher temperature zone is restricted to the very top of the surface ( $< 10 \mu\text{m}$ ), confirming the results and suggestions presented along the thesis.

b) The arc attachment diameter has an important effect on the temperature profiles; the significant increase in the temperature field with decreasing arc diameter indicates that the power density is a more important parameter than the power itself.

c) There is little influence of the cathode wall thickness on the cathode temperature profiles in the range 1 - 10 mm thick.

d) However the erosion rates obtained from the simulations did not compare well with the experimental values reported in other Chapters. Reasons for these differences were discussed. It was concluded that the arc attachment can not be much smaller than  $100 \mu\text{m}$  if 1 000 W is deposited at the arc attachment region. Also if the arc attachment is larger than 1 mm, no erosion would occur even for 1 000 W.

### B) 2 D Approach- Microscopic Model

a) Temperature profiles for the cathode were obtained using 2 D cylindrical geometry (assuming angular symmetry) and a fixed heat source (simulating the cathode spot). The results from these simulations compare very well with the temperatures obtained

using the 3 D model at similar operating conditions.

b) The maximum temperature of the cathode increases extremely quickly with cathode spot lifetime for 1 000 W. For low powers (simulating the cathode spot), 20 W, the maximum temperature is reached in a very short time of the cathode spot lifetime (less than 0.001 ms). The results also showed a restricted zone in the vicinity of the cathode spot at the topmost surface where the high temperatures can be found.

c) The diameter of the arc attachment was varied between 10 and 1  $\mu\text{m}$ ; the results confirmed the importance of the power density for erosion studies (more constricted arc attachments result in much higher temperatures).

d) The grouping of the cathode spots was simulated using different cathode radii (the walls were insulated for radius greater than the cathode radius). The results from these simulations show a dramatic effect of cathode spot grouping on the temperature field and cathode erosion rates; it is possible to have no erosion for isolated spots and a large erosion for cathode spots 100  $\mu\text{m}$  further apart for otherwise same operating conditions. This confirms the results and ideas formulated in the past Chapters on the importance of cathode spot grouping for erosion phenomena. The results also indicate that the individual cathode spots, carrying small power (20 W), can indeed cause erosion; the erosion rates in these situations are small, confirming the idea of an unavoidable minimum erosion rate presented in the previous Chapter.

**REFERENCES**

- 1) Prock, J.; "Time Dependent Description of Cathode Crater Formation in Vacuum Arcs", IEEE Trans. Plasma Science, Vol PS-14, n.4, 482-496, 1986.
- 2) Hantzsche, E.; "On the heat sources of the arc cathode spot", Plasmaphysick, Vol 2, 59-79, 1979.
- 3) Miterrauer, J; Till, P.; "Computer simul. dynamics of plasma surface interact. in vacuum arc cathode spots", IEEE Trans. Plasma Science, Vol PS-15, n.5, 488-500, 1987.
- 4) Daalder, J. E.; "A cathode spot model and its energy balance for metal vapour arcs", J. Phys. D: Appl. Phys. , Vol. 11, 1667-1683, 1978.
- 5) Mackeown, S.; "The cathode drop in an electric arc", Physical Review, Vol 34, 611-613, 1929.
- 6) Juttner, B.; "Formation time and heating mechanism of arc cathode crater in vacuum", J. Phys. D: Appl. Phys., Vol. 14, 1265-1275, 1981.
- 7) Mostaghimi, J.; Munz, R.J.; "Modelling of heat transfer in cylindrical cathodes for plasma torches", 9<sup>th</sup> Int. Symp. Plas. Chem., Italy, Sept 1989.
- 8) Carslaw, H.S.; Jaeger, J.C.; Conduction of Heat in Solids, Oxford University Press, 2 edition, 266-270, 1959.
- 9) Baliga, B.R.; Liu, C.H.; Pfender, E.; "Critical steady state heat flux causing melting/evaporation of the anode in high intensity arc", AIAA -ASME Thermophysics and Heat Transfer Conf. , May 1978.
- 10) Daalder, J.E.; J. Phys. D: Appl. Phys., Vol 10, 2225, 1977.
- 11) Perry, R.H.; Chilton, C.H.; Chemical Engineers' Handbook - McGraw-Hill Book Company, 5 ed., 1973.
- 12) Szente, R.N.; Munz, R.J.; Drouet, M.G.; Plasma Chemistry and Plasma Processing, 1987.

## VIII. CONCLUSIONS

## VIII. CONCLUSIONS

### 1. CONCLUSIONS

What follows is a summary of the almost 50 conclusions presented at the end of each Chapter of the thesis. After this summary, recommendations for future work and contributions to knowledge are presented.

a) Steady state, reliable erosion measurements were made for copper cathodes under a wide variety of operating conditions for Ar, He, N<sub>2</sub>, CO, Cl<sub>2</sub>, H<sub>2</sub>S, CH<sub>4</sub>, O<sub>2</sub>, and mixtures of these gases. For selected experiments the arc current was varied between 100 and 250 A. The magnetic field strength used to move the arc was varied between 10 and 1 700 G. The gas flow rate was varied between 0.2 and 20 l/min although most experiments used the highest flow rate. The operating pressure was fixed at 1.1 atm.

b) Studies of the arc movement for a magnetically rotated arc showed the Lorentz force, which pulls the arc forward, is opposed by aerodynamic drag and a newly proposed force called the surface drag force. When the latter was small, the arc velocity could be predicted using a newly proposed relationship between arc velocity, magnetic field and arc current for different plasma gases. The relationship,  $V \propto B^{0.6} I^{0.36}$ , which is based on the both theoretical considerations and experimental results from this thesis and the literature is valid for at least the ranges  $10 < B < 1\ 700$  G and  $100 < I < 850$  A.

c) The surface drag force is related to the electron emission characteristics of the cathode surface and increases as electron emission becomes more difficult. It could

be reduced by adding less than one per cent (by volume) of polyatomic gases (e.g. CO, Cl<sub>2</sub>, N<sub>2</sub>, CH<sub>4</sub>, O<sub>2</sub>) into the inert gases Ar or He. The creation of a contaminant layer on the cathode surface facilitates the emission of electrons. If the layer becomes thick (> 10 microns), as is the case for the addition of more than 2-3 % of CO, the surface drag once more increases and becomes the major force opposing the arc motion. The thickness of carbon layers formed by CO addition were measured using a scanning electron microscope.

d) The relationship between cathode surface contamination and arc movement was confirmed by examining the arc motion (by high speed filming and current fluctuation measurements) and the surface depth concentration profiles by using Auger and ESCA spectroscopy. Work function measurements with a Kelvin probe proved that electron emission was easier for slightly contaminated surfaces than for clean surfaces or those covered by a thick contaminant layer.

e) The equivalence of results obtained from the high speed filming technique and the measurement of arc current fluctuations was confirmed by examining histograms of arc jump distance and residence time at a point. This shows that the latter technique, which is much easier and cheaper than filming, can be used for arc movement studies.

f) It was found that chemical cleaning (nitric acid and carbon tetrachloride) is insufficient to remove the carbon/oxygen layers which form naturally on the electrodes; this makes the validity of erosion experiments made under transient conditions questionable. The arc is quite effective in cleaning the cathode and it was shown that the time required to reach steady operation in inert gases is directly related to the time required to remove the contaminant layer. This was shown by Auger and ESCA analyses and confirmed by using nitrogen as a tracer. The presence

of nitrogen to a depth of up to 1 000 Å suggests that the cathode surface was melted to this depth.

g) A new technique was developed and used to measure linear current distributions of arcs on the electrode surface; the technique is suitable for applications in industrial torches.

h) The current distribution on the cathode surface is primarily a function of the plasma gas, arc current and magnetic field. A more constricted attachment was found under higher erosion rate operating conditions. Under certain conditions, the current distribution probe was able to resolve the presence of individual contributions to the arc which may be due to individual cathode spots.

i) A simple conceptual model was developed for cathode erosion. The erosion rate is a function of the arc attachment residence time on the cathode surface, the current density, and the distance between cathode spots. Higher residence times, higher current densities, and more closely spaced spots all lead to higher erosion rates. It appears that a minimum erosion rate of approximately  $0.1 \mu\text{g/C}$  caused by the unavoidable evaporation of material below the cathode spots should be achievable. The grouping of cathode spots is due to higher local work function of the cathode and is strongly influenced by the presence of contaminants and the effect of the magnetic field used to move the arc.

j) Cathode erosion is fundamentally a physical problem (in the absence of direct chemical attack) and can, in principle, be simulated by an appropriate heat transfer model. Two models were used in this work; the macroscopic model simulated the movement of the arc over the cathode surface while the microscopic model simulated the time-varying behavior of the individual cathode spots and their spacings. Both

models gave temperature distributions within the cathode and were used to estimate erosion rates.

k) Some experimental results could be explained using the simple heat transfer models. In particular, the following were observed: reduction of the cathode temperature (and thus erosion rate) for low arc residence times; the restriction of the high temperature zone to within about 1 micron of the cathode surface; reduction of erosion rate for larger attachments (lower current densities); dramatic increase in erosion rate for closely spaced spots.

## 2. RECOMMENDATIONS FOR FUTURE WORK

Some important areas for future research are:

- Different cathode materials should be tested.
- The arc should be driven by a gas vortex and the results compared with purely magnetically driven force.
- The work should be extended in all directions; different plasma gases, higher and lower arc currents, higher magnetic fields, more fundamental analysis of the current distribution on the electrode surface. A more complete study should be conducted on the determination of the work function due to the contamination of the cathode; this can be achieved through the use of controlled ion implantation.
- The heat transfer models must be improved to relax some of the assumptions made; most important are melting/volatilization assumptions. Also the heat

transferred to the cathode by the arc attachment (Joule heating and ion bombardment) must be determined in future works.

- A more complex and quantitative erosion model must include the electron emission characteristics of the cathode surface; the arc movement should be directly correlated with the cathode surface contamination (or electron emission) and then the erosion rates could be predicted more precisely.

### 3. CONTRIBUTIONS TO KNOWLEDGE

- a) A new formulation for the balance between Lorentz force and aerodynamic drag was proposed. A new force, the surface drag was identified.
- b) A correlation between surface drag and electron emission of the cathode was proposed.
- c) The effect of a slightly contaminated cathode surface on arc velocity, arc voltage and cathode erosion rates was shown.
- d) It was demonstrated that high speed filming is an equivalent diagnostic tool to arc current fluctuations for arc movement analysis.
- e) A new technique was developed for current distributions of the arc foot on the surface of the electrodes:
- f) The effect of surface contamination and magnetic field on the arc foot current distribution was shown. A relationship between cathode erosion rate and arc foot

current density was proposed.

g) Simple heat transfer analyses, which allowed the examination of the effect of arc velocity, current density and spacing among cathode spots on cathode erosion were carried out.

*- Watson, could you please get me those books over there?*

*Holmes has sat in front of that desk in his office for almost 3 weeks. He hardly eats or does anything else except writing, reading and thinking... He often coughs, but he refuses to take any medicine. Watson is concerned about his friend's health, but he also knows he shouldn't disturb Holmes... Watson sees now a good chance to talk to Holmes...*

*- Here they are, Holmes. So, how is your writing going? Is there something that I can do to help?*

*- Oh, thank you Watson. If everything goes well, in two hours we should be putting the final remarks in this erosion project. I know I haven't been too great of a company recently, but I hope you understand that I had no choice...*

*- It's all right, Holmes. I am just worried about you, you don't seem too well...But if you say you're fine, that's enough for me...*

*- Thank you again Watson... Thank you for being my friend, for all those years...*

*And saying this, Holmes goes back to the writing, just interrupting from time to time to consult something from the books. And Watson, happy for seeing his friend in a more friendly mood, moves to his favourite chair and starts reading the paper...*

*And a couple of hours later, Holmes finally drops the pen and breathes deeply. He turns to Watson.*

*- Well, dear friend, it is all done. We can now think about some vacations!!*

*- That's fantastic, Holmes! But what are you going to do with your notes now? Are you going to publish them?*

*- I don't think any editor would be interested in them, Watson. No, we cannot publish them but at the same time we have to tell the world about this project. As Dr. Bergman suspected, it really can be of great importance for everyone... I don't know Watson, I suspect that it will take some time for people to understand the whole idea of the project. Perhaps at the end of the century, 80 years from now, someone will find these notes and if he understands the importance of this work, he will try to publish them... Perhaps even in the form of a scientific work, a thesis maybe. I don't now, Watson, I'm too tired to think clearly... Why don't I make some tea and we discuss where we are going to spend the next few days?*

*And Holmes closes his notes, stands up, smiles to his friend and goes to the kitchen. Watson follows him, but stops in front of the desk. He looks at Holmes' notes and thinks to himself "I hope someday someone will be able to use this work..." And giving a last look at the title written on the cover of the notes, he wonders why Holmes chose it to*

*be "Erosion of Plasma Torch Electrodes"... And then letting his curiosity fade away, Watson moves to the direction of the kitchen, from where he can already smells mint tea...*

**APPENDICES**

APPENDICES

A) Three dimensional model

Fundamental heat transfer conduction equation:

$$\nabla^2 T = 1/\alpha \partial T/\partial t'$$

where  $\nabla^2 =$  Laplacien operator

$T =$  temperature

$\alpha =$  thermal diffusivity

$t' =$  time

Writing the equation in cylindrical coordinates,

$$1/r' \partial(r' \partial T/\partial r')/\partial r' + 1/r'^2 \partial^2 T/\partial \theta^2 + \partial^2 T/\partial z'^2 = 1/\alpha \partial T/\partial t' \quad 1$$

with the following boundaries and initial conditions,

$-k \partial T/\partial r' = q$	$r' = R_0, \theta' = w, t', z' = 0$
$h(T - T_\infty)$	$r' = R_0, \theta' = w, t', z'$
$\partial T/\partial z' = 0$	$z' = \pm L$
$T = T_0$	$r' = R_0$
$T _{\theta'} = T _{\theta'+2\pi}$	$r', z', t'$
$\partial T/\partial \theta' _{\theta'} = \partial T/\partial \theta' _{\theta'+2\pi}$	$r', z', t'$
$T _{t'} = T _{t'+2\pi/w}$	$r', \theta', z'$

where  $r', z', \theta'$  = cylindrical coordinates

$k$  = thermal diffusivity

$q$  = heat flux

$h$  = heat transfer coefficient

$w_r$  = radial frequency,  $Vel/R_1$

$T_0$  = external cathode temperature

$T_\infty$  = gas temperature

The fixed cylindrical coordinates are transformed into a system that travels tangentially with the arc. The two systems are then related;

$$r = r'/R_1$$

$$\theta = \theta' - w_r t'$$

$$z = z'/R_1$$

$$t = t'$$

and defining a non-dimensional temperature,

$$\phi = (T - T_\infty) k / qR_1$$

equation 1 becomes

$$1/r \partial(r \partial\phi/\partial r)/\partial r + 1/r^2 \partial^2\phi/\partial\theta^2 + \partial^2\phi/\partial z^2 = R_1^2/\alpha \partial\phi/\partial t - (Vel R_1 / \alpha) \partial\phi/\partial\theta \quad 2$$

The time term in equation 2 can be canceled because the temperature field stays constant for an observer travelling with the arc. Equation 2 is reduced to:

$$1/r \partial(r \partial\phi/\partial r)/\partial r + 1/r^2 \partial^2\phi/\partial\theta^2 + \partial^2\phi/\partial z^2 + a \partial\phi/\partial\theta = 0 \quad 3$$

with the boundary conditions,

$$\begin{array}{ll}
 \partial\Phi/\partial r = 1 & r = 1, \theta = 0, z = 0 \\
 b\Phi & r = 1, \theta = 0, z \\
 \partial\Phi/\partial z = 0 & z = \pm L/R_i \\
 \Phi = \Phi_0 & r = R_0/R_i \\
 \Phi|_{\theta} = \Phi|_{\theta+2\pi} & r, z \\
 \partial\Phi/\partial\theta|_{\theta} = \partial\Phi/\partial\theta|_{\theta+2\pi} & r, z
 \end{array}$$

where

$$\begin{aligned}
 a &= \text{Vel } R_i / \alpha \\
 b &= h R_i / k \\
 \Phi_0 &= (T_0 - T_{\infty}) / (q R_i / k)
 \end{aligned}$$

### B) Grid system for the 3D model

The grid system used in the 3D model was chosen to be very dense in the vicinities of the arc attachment. It is exponential (decreasing from the center of the attachment outwards) for the  $z$  and  $\theta$  directions and inversely proportional to the square of the grid number in the  $r$  direction (thickness of the cathode). In these simulations it was used a 16 grid spacing in the  $z$  and  $\theta$  directions and a 20 grid spacing in the  $r$  direction. This results on a first grid point located at 0.2 mm in the  $z$  and  $\theta$  direction and 0.01 mm in the  $r$  direction for an arc attachment of 1 mm diameter.

### C) Two dimensional model

The conduction heat equation in cylindrical coordinates was written as follows (for angular symmetry):

$$a(k r \partial T/\partial r)/\partial r + a(k r \partial T/\partial z)/\partial z + q r = \rho C_p r \partial T/\partial t$$

with boundary conditions as defined before in the thesis. The general equation that the PROTRAN program solves can be written as:

$$\partial A(x,y,U_x,U_y,U,t)/\partial x + \partial B(x,y,U_x,U_y,U,t)/\partial y + F(x,y,U_x,U_y,U,t) = C(x,y,U,t) \partial U/\partial t \quad 5$$

where  $x, y$  = coordinates

$t$  = time

$U_x$  =  $\partial U/\partial x$

$U_y$  =  $\partial U/\partial y$

$U$  = solution (vector)

$A, B, F, C$  = supplied functions (possibly vectors)

In order to use the PROTRAN program, the following substitutions were made (comparing equations 4 and 5).

$r = x$

$z = y$

$T = U$

$A = k_r \partial T/\partial r = k_x \partial U/\partial x$

$B = k_z \partial T/\partial z = k_y \partial U/\partial y$

$C = \rho C_p r = \rho C_p x$

$F = q_r = q_x$

#### D) Grid system for the 2D model

The grid system for the 2D model was chosen to be very dense in the vicinities of the cathode spot. For both directions,  $r$  and  $z$ , the grid density varies inversely with the square of the distance; this results in a very compact grid at the cathode spot, becoming less dense as moved away from the it. For a cathode spot of 1 micron

diameter, the first grid point is located at the surface ( $z = 0$ ), with  $r = 0.1$  micron.

**NOMENCLATURE**

NOMENCLATURE

$A$  = cross sectional area of the conductor

$\vec{B}$  = external magnetic field

$B$  = magnetic field strength

$C$  = concentration

$C_d$  = drag coefficient

$C_p$  = thermal capacity

$D$  = arc column diameter

$D_a$  = arc attachment diameter

$D_s$  = cathode spot diameter

$D_{eq}$  = minimum equivalent diameter

$E$  = erosion rate

$\vec{E}$  = external electrical field

$E_i$  = ionization potential

$F_d$  = aerodynamic drag force

$F_l$  = Lorentz force

Fourier<sup>-1</sup> = anti-transformation of Fourier

GFR = gas flow rate

$H(w)$  = transfer function

$I$  = arc current

$J$  = current density (peak current distribution)

$J_x$  = linear current distribution of the arc attachment in the x direction

$J_y$  = current density of the arc attachment

$L$  = cathode length in z direction

$L_w$  = cathode wall thickness

- $M$  = mutual inductance (cavity-coil)  
 $N$  = charge carriers per unit volume  
 $P_a$  = power input to the anode in percentage  
 $P_c$  = power input to the cathode in percentage  
 $Q$  = volumetric flow rate  
 $Q_i$  = ion bombardment heating  
 $Q_j$  = Joule heating  
 $Re$  = Reynolds number  
 $R_i$  = cathode internal radius  
 $S$  = surface drag force  
 $Spl$  = distance between spots (splitting)  
 $T$  = surface temperature  
 $U_c$  = cathode fall voltage  
 $V(t)$  = signal (voltage) from the coil  
 $Vel$  = arc velocity  
 $Vl$  = volume of the chamber  
 $Vol$  = arc voltage  
 $X_1$  = Fourier transformation of  $x_1$   
 $Y_1$  = Fourier transformation of  $y_1$   
 $Z$  = transfer impedance (cavity-coil)
- $a = Vel R_i / (\rho C_p)$   
 $b = h R_i / k$   
 $d = \text{arc length}$   
 $e = \text{particle charge}$   
 $h = \text{heat transfer coefficient on the inside cathode surface}$   
 $j_e = \text{electron emission current density}$   
 $j_+ = \text{positive ion current density}$

$k$  = thermal conductivity

$m$  = particle mass

$m_{\text{He}}$  = mass (helium) inside the chamber

$q$  = heat flux input

$q_0$  = power input

$r$  = radial coordinate

$r_i$  = cathode spot radius

$t$  = time

$\vec{v}$  = particle velocity

$v_x$  = arc velocity (x direction)

$w$  = frequency

$w_r$  = radial frequency,  $Vel / R_c$

$x_i$  = signal calibrated with the transfer function

$y_i$  = signal obtained from the no slit system for any condition

$z$  = z coordinate

$z_i$  = cathode spot depth

$\rho$  = gas density

$\mu$  = gas viscosity

$\phi$  = work function

$\xi$  = mean electrostatic potential across the metal surface

$\lambda$  = bulk chemical potential of the electrons

$\sigma$  = residence time of the arc attachment

$\eta$  = electrical resistivity of the metal

$\Phi$  = nondimensional temperature

$\theta$  = theta coordinate

